UNIVERSITY OF TECHNOLOGY SYDNEY

# THE ECO-PHYSIOLOGY OF TWO CONTRASTING ARID-ZONE WOODLANDS IN AUSTRALIA

**TONANTZIN TARIN TERRAZAS**

**Doctor of Philosophy – Science**

**PhD by Research**

**2019**

**UNIVERSITY OF TECHNOLOGY SYDNEY**

## *Certificate of Original Authorship*

I certify that the work in this thesis has not previously been submitted for a degree nor has it been submitted as part of requirements for a degree except as fully acknowledged within the text.

I also certify that this thesis has been written by me. Any help that I have received in my research work and the preparation of the thesis itself has been acknowledged. In addition, I certify that all information sources and literature used are indicated in the thesis.

Signature of Student:

Production Note:
Signature removed prior to publication.

Date: 10-January-2019

# *In memory of*

*Baltazar Terrazas Valdes (1956-2015), who had an incredible appreciation and passion for the natural world, and words cannot express how special he was for me.*

*Karla Nathaly Leon Velazquez (1987-2015), who was and will always be the best team I've ever had.*

*Jade Terrazas Bajo (2007-2018), I would much prefer it if you were alive and well.*

# *Acknowledgements*

I would like to acknowledge the support of the University Technology of Sydney (UTS) and the Consejo Nacional de Ciencia y Tecnología for the graduate fellowship (232184). This work was supported by an Australian Research Council grant awarded to Derek Eamus (DP14101150). A portion of the material present in this thesis is based upon work supported in part by OzFlux within the Terrestrial Ecology Research Network (TERN) and the Terrestrial Eco-hydrological Research Group at UTS.

I have been doubly privileged to call the stunning Sonoran Desert home and to complete a PhD on eco-physiology studying the spectacular semi-arid region in central Australia. For encouraging my interest on eco-hydrological studies and embracing my early career as a scientist, for all your support, guidance and endless advice, I will always be grateful to Dr. Jaime Garatuza-Payán and Dr. Enrico A. Yépez from The Sonoran Institute of Technology.

For all the exceptional guidance and support to make this thesis possible, I am extremely thankful for my supervisor Professor Derek Eamus who took the time to read many drafts of this thesis. Thanks Derek, for your patience and the many questions that helped to improve my reasoning in eco-physiology. I would like to thank my co-supervisor Dr. Rachael Nolan for her quality advice and dedication since the beginning of my PhD study. To Dr. James Cleverly, thanks for his insightful comments and for helping me to comprehend OzFlux data and many eco-physiological processes. I am also thankful to Professor Belinda Medlyn for supporting my research in central Australia and providing supervision through this thesis. I appreciated from all of you, your helpful suggestions, reviews and comments to improve my PhD thesis.

This thesis would also not have been accomplished without my family support. To my parents and sisters who were always there for me in the most difficult situations despite the distance between us. I am deeply grateful to all my family back in Mexico for the endless calls and the many motivational words that were a source of solace during the time I spent in Australia.

I would like to give a special thanks to Sheilla B. Syd Julian, Layla J.B., Deeni C. and Ivan C. who were my piece of México in a foreign country.

To my fellows at UTS, I thank you for sharing all your amazing stories, for all the good times and for making this journey the most enjoyable adventure. To my friends back in Mexico and across the world: Ann-Marie Rohlfs, Rachel Gray, Zulia Sánchez, Corina Quiroz, Asis Hallab, Fernando Castillo, Sammuel Villarreal, Laura Celis, An Tran, Marco Giardina, John Gallego, Rizwana Rummani, Carlos Ibarra, Sam Goyen, Rendy Ruvindy, Lorenzo Barolo, Marihta Harahap, Bojana Manojlovic, Alex Thomson, Qiaoyun Xie, Sofie Voerman, Kirsty Milner, Marco Alvarez, Paloma Matis, Divia Vinod, Tiziana Zingali, Eva Fernandez, Lia Barresi, Andrew Olivera, Oriana Cresta, Ewen Beard and Alistar Walsh. I greatly appreciated the innumerable supportive and motivating words you gave during my PhD studies and beyond.

# *Table of Contents*

# *List of Figures*

# *List of Tables*

# Abbreviations, acronyms and symbols

| | | |
|---|---|---|
| $A$ | Carbon assimilation | (μmol $m^{-2}$ $s^{-1}$) |
| AIC | Akaike information criterion | |
| $A_{max}$ | Maximum gross photosynthetic rates | (μmol $m^{-2}$ $s^{-1}$) |
| $A_n$ | Net photosynthetic carbon uptake | (μmol $m^{-2}$ $s^{-1}$) |
| $A_{n2000}$ | Net photosynthetic carbon uptake at PPFD= 2000 μmol photons $m^{-2}$ $s^{-1}$ | (μmol $m^{-2}$ $s^{-1}$) |
| ANN | Artificial neural network | |
| ANOVA | Analysis of variance | |
| BoM | Bureau of Meteorology | |
| C | Carbon | |
| $C_a$ | Atmospheric $CO_2$ concentration | (μmol $mol^{-1}$) |
| CFI | Comparative fit index | |
| $C_i$ | $CO_2$ concentration inside leaf air spaces | (μmol $mol^{-1}$) |
| CUE | Carbon-use-efficiency | (daily C gain *per* mol C fixed) |
| C3 | Carbon fixation pathway where $CO_2$ is fixed by Rubisco | |
| C4 | Carbon fixation pathway where $CO_2$ is fixed by PEP-Carboxylase | |
| $CO_2$ | Carbon dioxide | |
| $E$ | transpiration | (mol $m^{-2}$ $s^{-1}$) |
| EC | Eddy covariance | |
| ENSO | El Niño-Southern Oscillation | |
| ER | Ecosystem respiration | (gC $m^{-2}$ $d^{-1}$) |
| ET | Evapotranspiration | (mm) |
| $ET_0$ | Reference ET | (mm) |
| EVI | Enhanced vegetation index | |
| D | Vapour pressure deficit at the leaf surface | (kPa) |
| D2, D3 | Second and third drought, respectively | |
| DCG | Daily carbon gain | (mol C $m^{-2}$ $d^{-1}$) |
| G | Ground heat flux | (W $m^{-2}$) |
| $G_c$ | Canopy conductance | (mmol $m^{-2}$ $s^{-1}$) |
| GLSA | Global land sink anomaly | |
| GPP | Gross primary production | (gC $m^{-2}$ $d^{-1}$ or μmol $mol^{-1}$) |
| $g_0$ | Conductance when photosynthesis is zero | (mol $m^{-2}$ $s^{-1}$) |
| $g_1$ | Optimal stomatal model inversely related to $WUE_i$ | ($kPa^{0.5}$) |
| $g_s$ | Stomatal conductance | (mol $m^{-2}$ $s^{-1}$) |
| $g_c$ | Stomatal conductance for $CO_2$ | (mol $m^{-2}$ $s^{-1}$) |
| H | Sensible heat flux | (W $m^{-2}$) |
| $H_2O$ | Water vapour | |
| IRGA | Infrared gas analyzer | |
| LAI | Leaf area index | |
| LCP | Light compensation point | (μmol photon $m^{-2}$ $s^{-1}$) |
| LE | Latent heat flux | (W $m^{-2}$) |
| LMA | Leaf mass *per* area | (g $m^{-2}$) |
| LRC | Light response curve | |
| LSP | Light saturation point | (μmol photon $m^{-2}$ $s^{-1}$) |
| LUE | Light-use-efficiency | (mmol $CO_2$ $\mu mol^{-1}$ photon) |
| MAP | Mean annual precipitation | |
| MODIS | Moderate resolution imaging spectroradiometer | |
| N, $N_2$ | Nitrogen | |
| $N_a$ | Foliar N concentration *per* leaf area | (g N $cm^{-2}$) |
| NEE | Net ecosystem exchange | (gC $m^{-2}$ $d^{-1}$) |

| | | |
|---|---|---|
| NEP | Net ecosystem production | (gC $m^{-2}$ $d^{-1}$) |
| P | Precipitation | (mm) |
| PAR | Photosynthetically active radiation | (µmol $mol^{-1}$) |
| PDB | Pee Dee Belemnite | |
| PET | Monthly Penman-Monteith reference ET | |
| PFT | Plant functional type | |
| $P_{gross}$ | Gross photosynthesis | (mol C $m^{-2}$ $d^{-1}$) |
| $P_{net}$ | Net photosynthesis during the day | (mol C $m^{-2}$ $d^{-1}$) |
| PM | Penman-Monteith | |
| PNUE | Photosynthetic nitrogen-use-efficiency | ((µmol $CO_2$) *per* (g N)$^{-1}$ $s^{-1}$) |
| PPFD | Photosynthetic photon flux density | (µmol $mol^{-1}$) |
| PPT | Rainfall | (mm) |
| QA/QC | Quality assurance/control | |
| R | Project software® for language statistical computing and graphics | |
| $r_a$ | Aerodynamic resistance | (s $m^{-1}$) |
| $R_d$ | Dark respiration also $R_{dark}$ | (µmol $m^{-2}$ $s^{-1}$) |
| $R_{het}$ | Heterotrophic respiration | |
| $r_L$ | Leaf resistance | (s $m^{-1}$) |
| $R_n$ | Net radiation | (W $m^{-2}$) |
| $R_{night}$ | Nocturnal respiration | |
| $R_{plant}$ | Plant respiration | (µmol $m^{-2}$ $s^{-1}$) |
| $R_{sample}$ | Ratio of heavy to light isotopes in a sample | |
| $R_{standard}$ | Ratio of heavy to light isotopes in a standard | |
| RUE | Resource-use-efficiency | |
| SE | Standard error | |
| SEM | Structural equation modelling | |
| SPEI | Standardized precipitation-evapotranspiration drought index | |
| SOFM | Self-organizing feature map | |
| SOLO | Self-Organizing Linear Output | |
| SOM | Soil organic matter | (%) |
| SR | Solar radiation | (W $m^{-2}$) |
| SWC | Soil water content | ($m^3$ $m^{-3}$) |
| $T_{air}$ | Air temperature | (°C) |
| TERN | Terrestrial Ecosystem Research Network | |
| TDR | Time-domain reflectometry | |
| u* | Friction velocity | (m $s^{-1}$) |
| VPD | Vapour pressure deficit | (kPa) |
| VWC | Volumetric water content | (mm) |
| $w$ | Vertical wind velocity | |
| $WUE_i$ | Intrinsic water-use-efficiency | (µmol $mol^{-1}$) |
| eWUE | Ecosystem water-use-efficiency | (µmol $mol^{-1}$) |
| $_{int}$WUE | Instantaneous water-use-efficiency | (µmol $mol^{-1}$) |
| WW | Well-watered treatment | |
| WS | Water-stressed treatment | |
| $^{13}C$ | Carbon isotope with an atomic weight of 13 | |
| $^{12}C$ | Carbon isotope with an atomic weight of 12 | |
| $a$ | Fractionation during $CO_2$ diffusion through the stomata | (‰) |
| $b$ | Fractionation associated with reactions by Rubisco | (‰) |
| β | A function for a scalar reduction of a process | (normalized from 0 to 1) |
| $c_p$ | Heat capacity of moist air | |
| $q$ | A parameter to describe the non-linearity of β | |
| $q'$ | Mix concentration of $CO_2$ or $H_2O$ | (g $m^{-3}$) |
| γ | Psychrometric coefficient | |

| | | |
|---|---|---|
| $\Psi_{md}$ | Midday foliar water potential | (MPa) |
| $\Psi_{leaf}$ | Diurnal foliar water potential | (MPa) |
| $\Psi_{pd}$ | Pre-dawn foliar water potential | (MPa) |
| $\lambda$ | Marginal water cost of plant carbon gain | (mol $H_2O$ $mol^{-1}$ C) |
| $\Gamma^*$ | $CO_2$ compensation point | |
| $\phi$ | Quantum yield | (µmol $CO_2$ µmol $photons^{-1}$) |
| $\Delta$ | Stable isotope discrimination or $\Delta^{13}C$ | (‰) |
| $\delta$ | Delta-isotopic notation | (‰) |
| $\sigma$ | Standard deviation | |
| $\delta^{13}C$ | Ratio of $^{13}C$ to $^{12}C$ | (‰) |
| $\delta^{13}C_{air}$ | Carbon isotope ratio of the air | (‰) |
| $\delta^{13}C_{bulk\text{-}leaf}$ | Isotopic compositions of bulk-leaf tissue | (‰) |
| $\delta^{13}C_{sugars}$ | Isotopic compositions of leaf soluble sugars | (‰) |
| $Q_A$ | Difference between net radiation flux and ground heat flux | |
| $\rho_a$ | Density of moist air | (g $m^{-3}$) |
| $\chi^2$ | Chi-square test for goodness of fit | |

# *Abstract*

Semi-arid and arid ecosystems occupy 45 % of the Earth's land surface and approximately 40 % of the global population live in arid and semi-arid regions. Ecosystem productivity in these regions is constrained by water availability, which is in general erratic, spatially variable and confined to short periods during the wet season. Globally, semi-arid and arid ecosystems dominate the inter-annual variability of the global land carbon (C) sink. In particular, Australian semi-arid and arid regions were estimated to account for 60 % of the 2011 global land carbon sink anomaly (GLSA). Despite the importance of these Australian arid and semi-arid environments, mechanisms that explain variability in rates of C uptake (at regional- and global-scales) and trends are poorly understood, and these ecosystems remain little studied.

Australia is an extensive and flat continent, of which 70 % is arid or semi-arid land. Two biomes dominate the central semi-arid region: (1) Mulga woodland, dominated by species of the genus *Acacia* (shallow rooted $N_2$-fixing trees, from the Mulga complex of species)*;* and (2) open *Corymbia* savanna where the dominant cover is spinifex (a C4 grass) with widely spaced tall evergreen *Corymbia* trees. These two ecosystems are found within the Ti-Tree Basin, Northern Territory Australia, where two eddy covariance systems has been in operation for the past 4 and 7 years within a Mulga woodland and *Corymbia* savanna respectively. The main objective of this research was to investigate ecosystem functioning of the two semi-arid woodlands, in order to improve our understanding of the interaction of terrestrial semi-arid ecosystems with the atmosphere, through measurements of C and water fluxes at ecosystem- and leaf-scales. The overall hypothesis was that differences in ecosystem vegetation composition and structure would be significant factors explaining differences in C and water fluxes across two disparate ecosystems. To accomplish this general objective, C and water fluxes were evaluated at different temporal-scales (i.e., diurnal, seasonal, annual and inter-annual) and different spatial-scales (from plot- to leaf-scales) within a Mulga woodland and a *Corymbia* savanna. I employed three different approaches to evaluate C and water fluxes: i) eddy covariance data (at plot-scale); ii) a range of *in situ* eco-physiological investigations (at leaf-scale); and iii) glasshouse experimentation (at leaf- and whole-plant-scale).

In 2011 during the GLSA, the Mulga woodland captured 131 g C $m^{-2}$ $y^{-1}$ and total annual precipitation was 565 mm. The most recent hydrological year studied (August to July 2016-2017) had the largest annual rainfall recorded during my monitoring of ecosystem fluxes (713 mm) and net ecosystem production (NEP) was 217 gC $m^{-2}$ $y^{-1}$. In contrast to the Mulga woodland, the open *Corymbia*-savanna was a C source across most years (2012 to 2016), with

NEP ranging between -14 and -190 gC $m^{-2}$ $y^{-1}$, but was a C sink during 2016-2017 with NEP of 115 gC $m^{-2}$ $y^{-1}$. As a result of continuous monitoring of C fluxes, precipitation thresholds at which the two semi-arid woodlands switched from C source to C sink were identified for the first time. The pivot-point for the Mulga woodland was 262 mm $y^{-1}$ and 506 mm $y^{-1}$ for the *Corymbia* savanna.

The two semi-arid woodlands experience the same climatic conditions; hence, I observed that different climatic drivers (i.e., temperature, vapour pressure, soil water content) exerted similar influences over C and water fluxes across seasons. Intra-annual variability in C and water fluxes was mostly attributed to differences in SWC across seasons. However, different eco-physiological behaviours of co-occurring species within the Mulga woodland and *Corymbia* savanna contributed to explain differences in C and water fluxes between them. Dominant species at the Mulga woodland are highly adapted to periods of low water availability. Thus Mulga species were very water-use-efficient (WUE: trade-off between C gain *per* water loss) compared to species at the *Corymbia* savanna. This was demonstrated when evaluating responses of the $g_1$ parameter (as a proxy of intrinsic water-use-efficiency; $WUE_i$) to water availability. The Mulga woodland (at ecosystem- and leaf-scale) demonstrated large capacity for water consumption in wet periods and the plasticity to become highly WUE when experiencing water scarcity. In contrast, dominant species at the *Corymbia* savanna had larger water use (i.e., large stomatal conductance, at ecosystem-scale large rates of evapotranspiration) thus, smaller WUE compared to species at the Mulga woodland. The C4 spinifex grass can be highly productive at the *Corymbia* savanna during wet periods and, it is likely that the biomass produced during 2010-2011 was the fuel for photo-degradation of leaf litter, particularly of spinifex leaves in subsequent years, and this can explain the large negative NEP observed at the *Corymbia* savanna for much of the study period.

One of the novel aspects of the present research was to evaluate how soil water content drives WUE using the theory of the optimal stomata behaviour through the $g_1$ parameter (a normalized metric of intrinsic water-use efficiency: $_iWUE$) and compered $g_1$ values estimated from three different methods (leaf gas exchange, carbon isotopes and eddy covariance fluxes). Here my result showed discrepancies among methods and seasons. Thus, Seasonal and annual variation in *g1* derived from the three methods in this present study highlights the concern that the generic use of constant values of $g_1$ to describe stomatal functioning is not reliable when parameterizing global climate models (Medlyn *et al.*, 2017; Wolz *et al.*, 2017).

My research at a leaf-scale highlighted the importance of species-specific attributes in driving C fluxes in semi-arid Australia. Integrating plant eco-physiological responses of dominant species is an essential step for improving our understanding of C flux rates within a

Mulga woodland and *Corymbia* savanna. Comparing semi-arid ecosystems contributes to our understanding of ecosystem functioning and mechanisms underlying variability in rates of C and water flux within different ecosystems, which bring us closer to understanding global variability in C cycling in terrestrial ecosystems. The research at a leaf-scale highlighted the importance of species-specific attributes of co-occurring species driving C fluxes in central Australia. Understanding functional processes (i.e., C assimilation, stomatal behaviours plant water status) and the vegetation responses across different plant species and ecosystems is crucial for improving our ability to predict global change. There is now an opportunity to evaluate the inclusion of *in situ* observations and account for variations of C and water fluxes when applying earth systems models and terrestrial vegetation C models at regional- and global-scales.

# *Chapter I*

## General Introduction

## *1.1 Introduction*

Ecosystems are shaped by the different climate conditions which occur worldwide (Chapin, 2002). At the same time, ecosystem processes are important drivers of climate systems (Jung *et al.*, 2010; Newman *et al.*, 2006), through the continuous interchange of matter and energy between biosphere and atmosphere (Reichstein *et al.*, 2014). These interactions are frequently identified through the study of carbon and water fluxes as net ecosystem exchange (NEE) and evapotranspiration (ET), respectively. However, both climate and ecosystem functions respond to a range of processes across a large range of spatial-temporal-scales (Cubasch *et al.*, 2013), including those associated with the water and carbon cycles. Consequently, the study of ecosystem function is a complex challenge for the scientific community across a diverse range of disciplines (including ecology, hydrology, meteorology and plant physiology and eco-physiology).

Arid and semiarid zones receive less than 500 mm of rainfall per year (Allen *et al.*, 1998) and are represented across ~45 % of terrestrial ecosystems (Chapin, 2002; Poulter *et al.*, 2014). Approximately 40 % of the global population lives in arid and semi-arid regions. Arid ecosystems play an important role in the recirculation of large amounts of water through ET (ca. 80 to 100 % of the total annual site precipitation) (Wilson *et al.*, 2001), and also have a significant impact on global carbon (C) uptake from the atmosphere, especially during wetter-than-average years (Poulter *et al.*, 2014). In many, but not all, locations, some cases semi-arid ecosystems are strongly controlled by convective precipitation in pulse events; Mediterranean semi-arid ecosystems are an exception. Rates of ET tend to be larger during the wet season than the dry season and may contribute to future local precipitation (Dominguez *et al.*, 2009). Transpirational water flux is the loss of water from plants when the stomata open during

photosynthesis and stomatal opening links the water and C cycles in terrestrial ecosystems(Nobel, 2009). Globally, transpiration represents 61 % of total ET (Schlesinger and Jasechko, 2014), and is associated with large rates of C uptake (Huxman *et al.*, 2005; Yepez *et al.*, 2007).

Plants in arid and semi-arid regions have developed functional strategies in order to use efficiently use scarce water resources. Different plant traits have been identified across species that specifically relate to water uptake (rooting depth, mass and length), transport (hydraulic properties: xylem vessel diameter and architecture), storage (wood density, root mass), and loss (stomatal and cuticular conductance, leaf size, cuticular thickness, leaf hairs, sunken stoma) (Reichstein *et al.*, 2014). As a result, several studies argue that arid and semi-arid ecosystems are more efficient in their water-use than mesic ecosystems (Huxman *et al.*, 2004a; Ponce-Campos *et al.*, 2013; Tang *et al.*, 2014). Water-use-efficiency is the trade-off between C gain (through photosynthesis), and water loss (via transpiration). This efficiency can be also quantified as rain-use-efficiency (NEE/precipitation), generally expressed at ecosystem-scales over long periods of time (Gao *et al.*, 2014; Huxman *et al.*, 2004a) or as water-use-efficiency (WUE; the ratio of photosynthesis to transpiration or photosynthesis to stomatal conductance; see below for further discussion), at both ecosystem-and leaf-scales.

Carbon circulation between vegetation and the atmosphere is driven mainly by the photosynthetic capacity of vegetation, which produces organic carbon (Gross Primary Production, GPP). The net C accumulation in an ecosystem is termed net ecosystem production (NEP) derived as NEP= GPP - ER, where ER is ecosystem respiration from autotrophic and heterotrophic respiration. Thus, the water-use-efficiency of an ecosystem (eWUE) is quantified as the ratio of GPP to ET, because ET represents total ecosystem water-use (Troch *et al.*, 2009). At a leaf-scale, instantaneous water-use-efficiency ($_{int}$WUE) is the ratio of C assimilation ($A$) to water loss (E) by leaves, as $A/E$. Nevertheless, $E$ and $A$ not only determine $_{int}$WUE ($A/E$), but also influence stomatal conductance ($g_s$) *per se* because stomata respond to $C_i$ (the concentration of $CO_2$ inside the leaf air spaces) and $g_s$ is also responsive to transpiration rates (Eamus *et al.*, 2008; Seibt *et al.*, 2008). Stomatal conductance is a measure of the rate of flux of either water vapour or $CO_2$ through stomatal pores (Nobel, 2009). Therefore, another quantification of WUE, at the leaf-scale, is termed intrinsic $WUE_i$ (which is independent of evaporative demand) and is defined as the ratio of $A$ to stomatal conductance ($WUE_i = A/g_s$; Seibt *et al.*, 2008).

The application of different approaches to quantify water-use-efficiency (eWUE, $_{int}$WUE or $WUE_i$) at different spatial- and temporal-scales enable us to examine interactions among the C and water cycles and climate and hence the interactions between vegetation and climate

(Keenan *et al.*, 2013). WUE not only indicates the trade-off in water loss and carbon gain by plants, it also expresses changes in efficiencies arising from seasonal and inter-annual variation in water availability and other meteorological variables (e.g. vapour pressure deficit) at a site (Eamus *et al.*, 2008; Huxman *et al.*, 2004b). Furthermore, WUE is a useful indicator of ecosystem resilience because WUE increases with drought (Ponce-Campos *et al.*, 2013) and WUE can decline as an adaptation to some forms of land-use-change (Tang *et al.*, 2014). It is important to thoroughly evaluate changes in water-use-efficiencies in semi-arid ecosystems because these ecosystems dominate the high inter-annual variability in the global $CO_2$ sink (Ahlström *et al.*, 2015).

Ecosystem production is influenced by ecological attributes of the species present in the vegetation assemblage. Niche separation theory provides a framework to explain the co-occurrence of competing species (Silvertown *et al.*, 2015). Within ecosystems, different eco-hydrological niches exist and these are determined by competing strategies to maximize growth rate and resource-use efficiencies (i.e., light use, nutrient use and water use). These strategies are themselves determined by trade-offs and traits that enable species to survive and co-occur in a given ecosystem (Funk and Vitousek, 2007; Heberling and Fridley, 2013; Tarvainen *et al.*, 2015). Thus, different plant attributes, ecological niches and climatic factors influence resource-use efficiencies in both ecosystem-and leaf-scales (Eamus *et al.*, 2013; Huang *et al.*, 2015; Limousin *et al.*, 2015; Moreno-Gutierrez *et al.*, 2012; Shi *et al.*, 2014).

Current scenarios of likely future global climates predict an intensification of heavy precipitation events and increased frequency, intensity and geographic extent of heat waves may occur in the near-to-mid-term future, increasing the severity of natural extreme events (IPCC, 2014). Longer-lasting droughts produce the most significant effects in ecosystem carbon balance (Frank *et al.*, 2015). Globally, wetter-than average years induce large rates of carbon fixation and semi-arid ecosystems significantly contribute to the global land sink anomaly (GLSA) that occurred in 2010-2011 (Poulter *et al.*, 2014). Moreover, 60 % of this global land sink anomaly (GLSA) was attributed to semi-arid ecosystems in Australia (Ma *et al.*, 2016b; Poulter *et al.*, 2014). GLSA was primarily attributed to savannas and grasslands which cover ~50 % of the Australian continent (Fei *et al.*, 2017); although shrublands were the most efficient ecosystems in absorbing carbon (Ma *et al.*, 2016b). Thus, there is a need to understand how semi-arid ecosystems will respond to drier and warmer conditions and more intense rainfall events, in spite of their experience of long periods of low water input and high temperatures that characterize many arid and semi-arid regions.

As soil water availability declines, WUE generally increases in the short-term but may decrease under severe water stress (Manzoni *et al.*, 2011). A large WUE most often results from a reduction in plant water loss via *E*, through a reduction in stomatal opening (Manzoni *et al.*, 2011). Alternatively, a large WUE may indicate a significant increase in *A* during wet and favourable conditions, with a reduction in *E* arising because of the reduced vapour pressure deficit (VPD) associated with cooler temperatures arising from cloud cover and increased partitioning of incoming radiation to latent heat flux away from sensible heat flux (Duursma *et al.*, 2014; Yang *et al.*, 2015). Therefore, WUE can increase either by increased *A* at a constant *E*, or constant *A* and decreased *E* or both increased *A* and decreased *E* (Keenan *et al.*, 2013). Nevertheless, the mechanisms controlling WUE in response to fluctuations in soil water content in semi-arid and arid ecosystems represent a gap in our understanding of ecosystem plant-water carbon interactions.

The following sections aim to provide a comprehensive literature-based review of the overall concepts, processes and methodologies used in this research. It is followed by a description of the research questions, objectives, scope and structure of the thesis. Within this last section, the general hypotheses tested are presented following a brief description of the specific research data chapters.

### 1.1.1 Earth and climate system

Terrestrial landscapes at regional, continental and global-scales exert a strong influence on climate and variations in terrestrial vegetation carbon (C) and water cycles cause variability in global climate and *vice versa*. Annual solar radiation (short wave radiation: SWR) is the major driver of climate and this modulates temperatures over the troposphere (Fig.1.1). The sun delivers approximately 1368 W $m^{-2}$ SWR to the top of the atmosphere. On average across the globe, incoming solar radiation at the land surface is approximately 342 W $m^{-2}$. The tropics are more highly heated than the poles and this gradient in temperature between equator and poles determines the temperature, water cycle and ecosystem distribution globally (Chapin, 2002).

About 30 % of incoming solar radiation is reflected back to space by clouds and dust in the atmosphere and also from marine and terrestrial surfaces (known as albedo). The atmosphere absorbs approximately 20 % of incoming SWR (Cubasch *et al.*, 2013). Additionally the Earth's surface emits energy back to space as outgoing longwave radiation (LWR). A large fraction (96%) of the LWR is absorbed by certain atmospheric compounds (Cubasch *et al.*, 2013)

referred to as Greenhouse gases (GHGs) and including water vapour, carbon dioxide, methane and nitrous oxide.

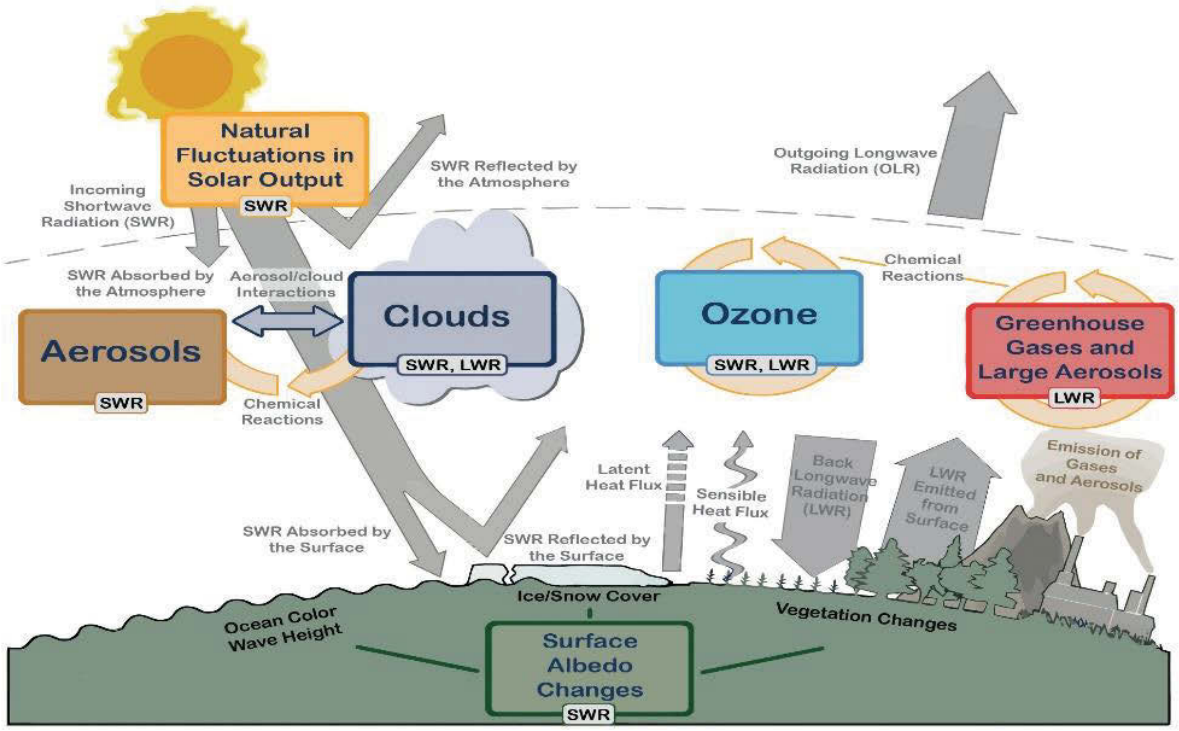


Figure 1.1 Representation of the Earth's energy balance. Source Cubasch *et al.* (2013).

The Earth's climate energy balances the incoming solar radiation and the outgoing energy, called the energy budget. Changes in net incoming solar radiation cause changes in the energy budget and affect the global hydrological cycle (Cubasch *et al.*, 2013; Jung *et al.*, 2010). For example, if there is an increase in global surface temperature, there is a positive feedback to atmospheric water vapour content, increasing the amount of water vapour in the atmosphere. This effect arises because more than half of the absorbed incoming radiation in the land surfaces is used to evaporate water as latent heat flux (LH). LH contributes to the regulation of surface temperatures, regional hydrological cycles, and regional climate characteristics (Dominguez *et al.*, 2009; Seneviratne *et al.*, 2006).

Anthropogenic emission sources of chemical compounds contribute to the increased greenhouse effect of the atmosphere, affecting both the energy and water budget of the planet by changing the relative distribution of energy between latent and sensible heat fluxes (Cubasch *et al.*, 2013). Increasing $CO_2$ concentration in the atmosphere has been observed in the last two

centuries because of increased fossil fuel consumption and deforestation associated with increased human population (Figure 1.2).

Recent models of future predictions of climate are more detailed and more accurately represent than those in the past, and more accurately represent current and recent past climate conditions (Cubasch *et al.*, 2013). These models require data inputs about atmospheric composition, land surface characteristics, ocean temperatures and circulation, carbon cycling, dynamic vegetation behaviour, and atmosphere-vegetation interactions. The lack of accurate data for parameterization of these models leads to significant errors and uncertainties in many state-of-the-art climate model projections (IPCC, 2012).

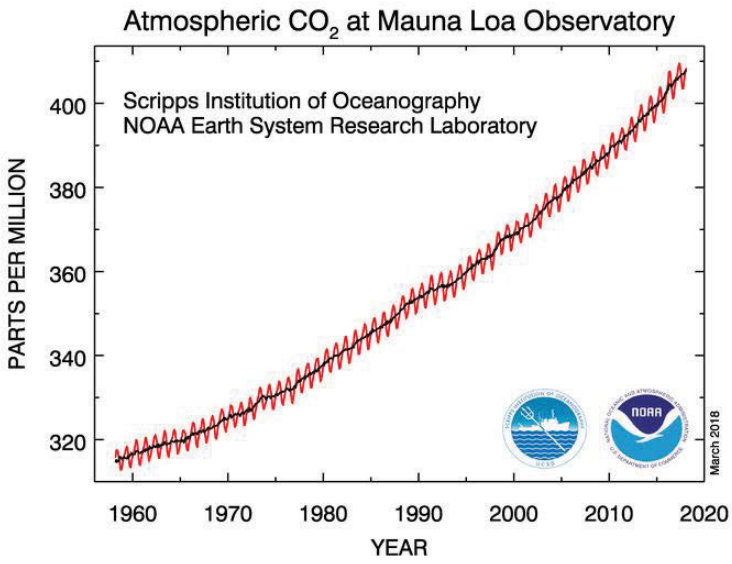


Figure 1.2 Atmospheric carbon dioxide increase observation at the Mauna Loa Observatory. Source: www.esrl.noaa.gov

In this context, new observations of the interactions among ecosystems, energy, carbon and water cycles are needed in order to reduce uncertainties in the models that have been developed in the last decade. A lack of cross-ecosystem comparisons and under-representation of ecosystems in remote locations represent a fundamental lack of information for ecosystem modelling (Baldocchi, 2014). Considering that fluxes of water and C integrate process occurring at different time-scales (e.g. days, seasons, years, decades) and space (from leaves to biome), understanding and quantifying processes at all of these scales is crucial (Baldocchi, 2014). This will contribute to the improvement of our understanding of how critical functional processes

control fluxes globally, particularly in relation to plant-atmosphere carbon-water interactions (Reichstein *et al.*, 2014).

### 1.1.2 Terrestrial ecosystem carbon and water fluxes

Both biotic and abiotic components of ecosystems influence the water and carbon cycles. Only vegetation is capable of assimilating $CO_2$ from the atmosphere through photosynthesis, whilst respiration from soil microorganisms, fauna and plants emit large amounts of C back to the atmosphere. Furthermore, plant roots determine the uptake and redistribution of soil water. These linkages and terms are now discussed in more detail.

Solar radiation drives the water cycle through the vertical transfer of water from the Earth (from soil, vegetation and oceans) to the atmosphere via ET (Chapin, 2002). Evaporation from the oceans in the Polar Regions is about 0.5 m $y^{-1}$, while 1.5 m $y^{-1}$ evaporates from tropical oceans (Eamus *et al.,* 2006). Eventually, evaporated water will precipitate into the ocean or precipitate inland. Precipitation (i.e., rainfall) is the major input of water into all ecosystems and exhibits great variability globally. Rainfall then has several fates: some is intercepted by vegetation canopies and results in stem flow, throughfall or is evaporated back to the atmosphere (Figure 1.3).

Of the rainfall reaching the soil surface, a fraction will infiltrate the soil profile and can then be transpired following root uptake, or flow laterally, contributing to river flow, or can percolate deeper and enter groundwater stores. This is an important process because the movement of water into terrestrial ecosystems contributes to groundwater stores (Eamus *et al.*, 2006; Gou *et al.*, 2015). Many plant species rely on groundwater and this can also be the major source of water for human consumption especially in arid and semi-arid regions. The amount of water remaining in the upper soil layers depends upon soil texture and root distribution. The amount of surface runoff is conditioned by the amount and intensity of rain events, soil surface conditions and local topography.

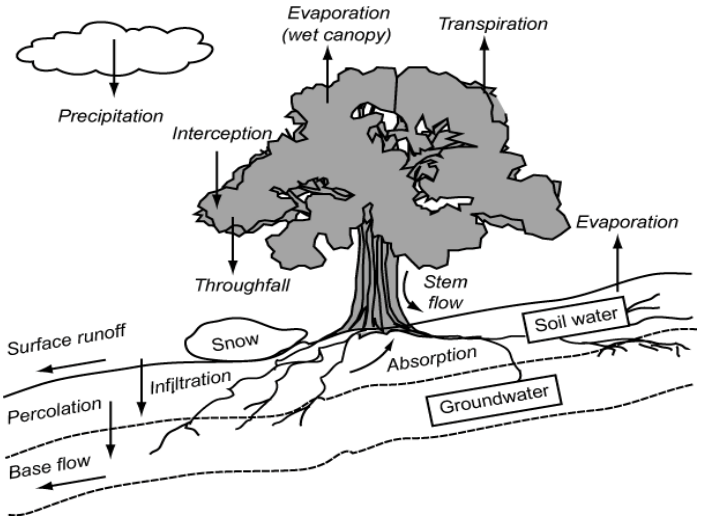


Figure 1.3 The water cycle in terrestrial ecosystems. Source Chapin (2002).

Annual precipitation is highly variable across the world: tropical wet forest may receive more than 4000 mm $y^{-1}$ but arid and semi-arid regions receive less than 500 mm $y^{-1}$ (Chapin, 2002; MEA, 2005; www.fao.org/). There is however, high variability in total annual precipitation across semi-arid regions and within a single semi-arid region (Biederman *et al.*, 2017; Fei *et al.*, 2017; Huang *et al.*, 2010; Wu *et al.*, 2015). For example, in semi-arid central Australia total annual rainfall has ranged from 97 to 751 mm in 1994 and 2010 respectively (1987-2017; www.bom.gov.au). Semi-arid Australia has been characterized as having the largest inter-annual variability in rainfall of any region (Fig. 1.4; Van Etten, 2009; Wischusen *et al.*, 2012).

The arid and semi-arid region in central Australia is influenced by the Australian monsoon, which occurs in the Austral summer (December-February; (Berry *et al.*, 2011). The Indian Ocean Dipole and El Niño-Southern Oscillation (ENSO) are also two natural systems that most influence weather patterns in central Australia (Cleverly *et al.*, 2016a), and both climatic systems are affected by greenhouse warming (Cai *et al.*, 2013; Cubasch *et al.*, 2013). Rainfall events for this region occur in episodes controlled by precipitation pulses.

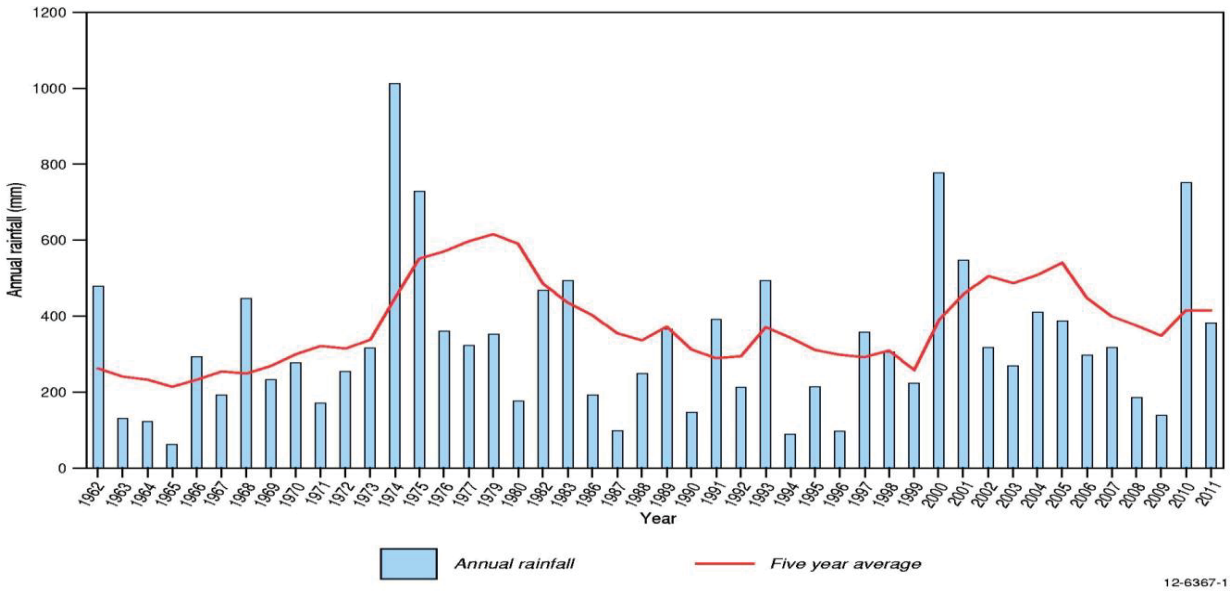


Figure 1.4 Total annual precipitation record from 1962 to 2011 in central Australia. Source Wischusen *et al.* (2012).

The sporadic and erratic availability of water in central Australia has a major influence on ecosystem function (Eamus *et al.*, 2016). Due to low rainfall conditions, vegetation has developed a range of strategies, reflected especially in their hydraulic traits, that allow them to use water efficiently and avoid reaching cavitation thresholds (Eamus *et al.*, 2013; Mitchell *et al.*, 2008; Nolan *et al.*, 2017a; Page *et al.*, 2016; Santini *et al.*, 2015). A cavitation threshold can be reached when bubbles form after hydraulic conductivity drops below a certain value (Shen *et al.*, 2002). Plants in central Australian ecosystems are able to withstand long periods of low soil water content and high temperatures (> 40 °C). A common behaviour in most, but not all, plant species co-occurring in central Australia is a decrease in pre-dawn and midday leaf water potentials and stomatal conductance during periods of low water availability (O'Grady *et al.*, 2009; O'Grady *et al.*, 2006; Page *et al.*, 2016).

Differences in soil moisture availability play an important role in determining plant hydraulic traits (Manzoni *et al.*, 2011; Mitchell *et al.*, 2008). The movement of water through plants can be described by application of the concept of the soil-plant-atmosphere continuum (SPAC; Fig. 1.5). The gradient in free energy needed to move the film of liquid water from the soil through the plant is termed water potential (measured in units of pressure: $\Psi$, MPa). The water potential needed to move water from plant to the atmosphere is controlled by the water vapour pressure deficit (VPD) in the atmosphere. There is a large gradient in VPD between the inside of the leaf and the atmosphere which drives water loss (as transpiration) from leaves to

the atmosphere. The loss of water from plants to the atmosphere drives the movement of water from the soil to replace the water lost as transpiration. Thus, a gradient in water potential occurs along the SPAC (Chapin, 2002; Sperry and Love, 2015).

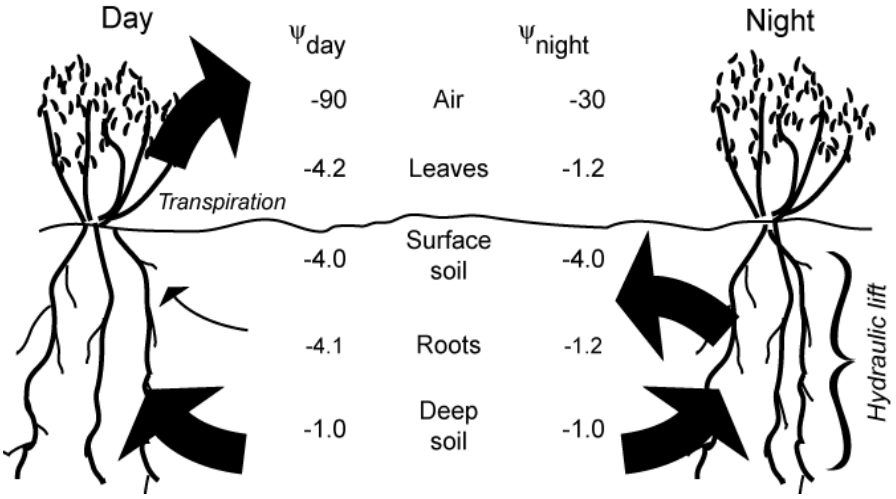


Figure 1.5 Water movement through the soil plant atmosphere continuum. Values indicate water potentials (MPa). Source Chapin (2002).

The movement of water along the SPAC varies temporally and spatially depending on water availability, rainfall events, temperature and soil properties of depth and texture and on transpiration rates. The gradient in water potential through the SPAC tends to be larger in arid and semi-arid ecosystems than in mesic ecosystems, due to lower soil water contents and larger atmospheric water vapour pressure deficits and higher temperatures occurring in semi-arid regions. Humidity in rainforests and mesic tropical regions tend to be high, hence atmospheric water potentials is closer to zero in rainforest, thus the water potential gradient is smaller. The largest drop in water potential occurs between leaf and air, and this difference is the main determinant of the size of the water potential gradient along the SPAC. During the day, solar radiation contributes to increasing temperatures, turning the atmosphere drier and therefore VPD increases relative to that of night-times (Fig. 1.5).

Plants use stomatal regulation to avoid excessive water loss from the canopy, thus stomatal conductance is strongly related to leaf water potential and VPD (Drake *et al.*, 2017; Manzoni *et al.*, 2011; McDowell *et al.*, 2004). However, we do not know the threshold at which leaf water potential triggers stomatal closure in the majority of plant species, nor the relationship between water potential and leaf carbon assimilation and transpiration in co-occurring species of central Australia. Additionally, the effect of drought on photosynthesis and stomatal conductance are still uncertain, especially in species that have the experience of long periods at low soil water

content. Therefore, evaluations on stomatal conductance and photosynthetic rates are crucial to understand how stomata behaves under stochastic water availability.

The opening of stomatal pores is necessary for $CO_2$ uptake during photosynthesis. This pathway of diffusion of $CO_2$ and water vapour provides the linkage between the water and C cycles, with implications for energy, water and C cycles at ecosystem-and global-scales.

Primary producers (both terrestrial and marine) are the only component of biota capable of removing $CO_2$ from the atmosphere through photosynthesis. Terrestrial ecosystems contribute more than 50 % of global carbon fixation (Le Quéré *et al.*, 2017). $CO_2$ present in the atmosphere diffuses through the stomatal pores in the leaves' surface. Primary producers convert inorganic C into organic C. Carbon is first assimilated and then transported, metabolized or stored as organic matter (i.e., carbohydrates, wood, leaves, roots, fruits, flowers). Environmental factors, such as solar radiation supply, soil water availability, VPD and nutrient availability limit plant function, particularly rates of C uptake. The photosynthetic process determines C and fixed energy inputs to terrestrial ecosystem (Fig. 1.6).

Photosynthesis at the leaf-and ecosystem-scale is termed gross primary production (GPP), given by the total amount of photosynthesis occurring in individual leaves. GPP is the largest flux in the carbon cycle (Yang *et al.*, 2015). Total carbon gain in terrestrial ecosystems is the result of the imbalance between GPP and C released from the ecosystem to the atmosphere by respiration (ER= ecosystem respiration = plant respiration, $R_{plant}$ + heterotrophic respiration, $R_{het}$). This net flux is defined as net ecosystem production (NEP= GPP - ER). Thus NEP is the difference between vegetation capacity to fix C through photosynthesis and plant (autotrophic) and heterotrophic (especially microbiological) respiration. NEP is influenced by ecological attributes of the species present in the vegetation assemblage and climatic drivers (Chu *et al.*, 2016; Michaletz *et al.*, 2014).

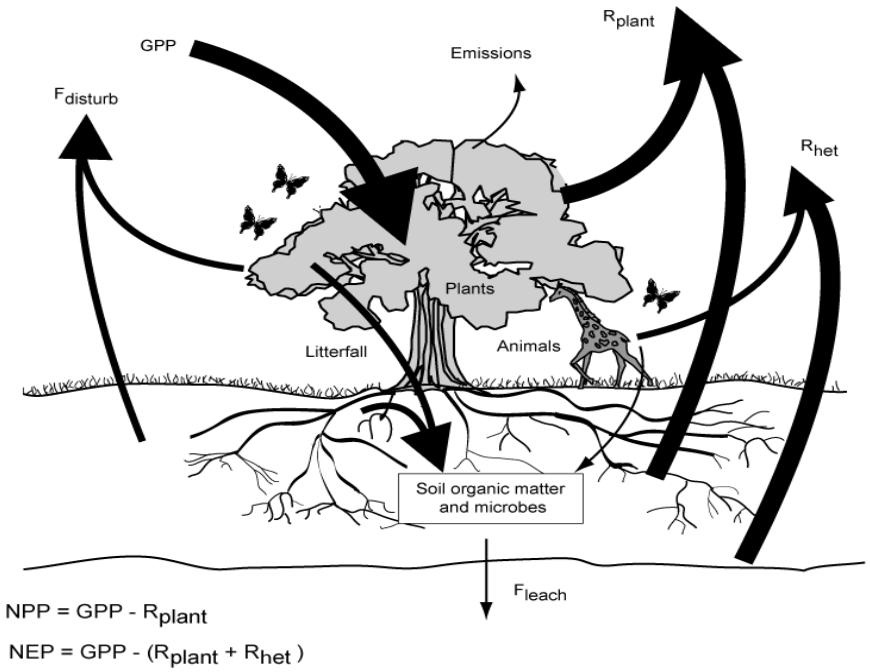


Figure 1.6 Plant carbon cycle. Source Chapin (2002).

Globally, drought is the most widespread climate extreme affecting the carbon cycle (Frank *et al.*, 2015; Reichstein *et al.*, 2014). Over the last decade (2000-2009), 70 % of the vegetated land area in the Southern hemisphere exhibited decreased net primary production (photosynthesis minus respiration; Chapin *et al.*, 2006) due to drought (Zhao and Running, 2010). However, little is known about how photosynthesis and respiration are being affected by extreme conditions such as drought (Frank *et al.*, 2015), particularly for arid and semi-arid zone species. All predictions are speculative and uncertain, whether they contain vegetation parameters or not, although in some we have greater confidence than others.

Different plant species and ecosystems have different maximum rates of C assimilation (*A*: leaf-scale) and respiration, and therefore GPP and NEP vary at ecosystem-scales (Chen *et al.*, 2015; Condon *et al.*, 2004). Photosynthesis is also linked to the solar energy that enters the ecosystem because of the requirement for light energy to reduce $CO_2$ and hence produce organic C. Measurements of GPP are therefore indicative of energy dynamics of an ecosystem (Baldocchi, 2014; Chapin, 2002; Chen *et al.*, 2015). Terrestrial plant species are classified into three groups depending on their photosynthetic pathways:

**C3 plants:** $CO_2$ from the atmosphere diffuses into leaves and is incorporated through the action of ribulose-1, 5-biorphophate carboxylase (the Rubisco enzyme) to yield two

molecules of a three-carbon compound: 3-phosphoglycerate. Over 90 % of plant species use this pathway (Nobel, 2009).

**C4 plants:** $CO_2$ in the form of $HCO^{3-}$ reacts with phosphoenol-pyruvate (PEP) via the enzyme PEP carboxylase to produce four-carbon organic acids. This process has higher photosynthetic water-use efficiency than C3 plants. C4 plants dominate many warm and high-light environments, including tropical grasslands and savannas.

**CAM** (Crassulacean Acid Metabolism): this pathway occurs in many succulent plant species in dry environments and epiphytes in tropical forests (Chapin, 2002). The initial C fixation step occurs at night, in contrast to C3 and C4 photosynthetic pathways where C fixation occurs during daylight hours. Some species using this pathway are able to switch between C3 and CAM under different climate conditions, depending mostly on water availability. CAM plants account for only a small portion of global carbon assimilation.

In all species, irrespective of which C fixation pathway is employed, climate drivers and diverse resources limit photosynthetic rates. Nutrients (especially, nitrogen and phosphorus), water availability, $CO_2$ concentration, temperature and light intensity are important factors that influence rates of photosynthesis. A better understanding of the trade-off between C gain and different resource availability will improve our understanding of daily, seasonal and annual patterns in resource-use-efficiency, and this is now discussed.

### 1.1.3 Resource-use-efficiencies

Understanding ecosystem productivity requires an investigation into resources-use-efficiency, from which ecosystem function can be evaluated. The leaf-economic theory predicts that plants should increase their efficiency in the acquisition of the most limited resource (Bloom *et al.*, 1985). The ability for the acquisition, capture, loss and cycling of energy and resources depends on different sets of physiological traits among plant species (Shipley *et al.*, 2016). Thus, the suite of traits in plant species ultimately determine the cycling of nutrients and energy at the ecosystem level.

Resource-use-efficiency (RUE) is defined as the C gain for a given unit of resource such as light, water or nutrients (i.e., nitrogen or phosphorous). RUE varies within and across ecosystems depending on vegetation composition and environmental drivers (Garbulsky *et al.*, 2010; Han *et al.*, 2016; Moreno-Gutierrez *et al.*, 2012). Light-use-efficiency (LUE) is quantified as

the ratio of the moles of $CO_2$ fixed in photosynthesis *per* mole of quanta (photons of light) absorbed (also called quantum yield). Apparent LUE is the ratio of moles of $CO_2$ fixed to the light flux density incident on a leaf. This determine the efficiency in which light is converted into fixed carbon. Light irradiance increases during the day but the maximum light level attained also changes across seasons. LUE is positively correlated with annual rainfall across different ecosystems because carbon assimilation is strongly controlled by water availability (Garbulsky *et al.*, 2010). At high-light intensities, the supply of other resources can limit photosynthetic rates, for example nitrogen (N) supply can limit maximum rates of photosynthesis because of the central role of N in electron transport and C fixation by Rubisco (Evans, 1989).

Photosynthetic nitrogen-use-efficiency (PNUE) is the ratio of photosynthetic carbon gain *per* unit of N contained *per* unit leaf area. $N_2$-fixing plant species tend to have a larger N content *per* unit of leaf area than non-$N_2$ fixing species. PNUE also correlates with leaf mass *per* area (LMA), the ratio of leaf dry weight to leaf area. LMA increases as rainfall decreases due to the influence of water availability on leaf expansion, which acts to reduce water loss (transpiration) to wilt less, thus affecting PNUE (Poorter *et al.*, 2009; Wright *et al.*, 2004). When plants have optimal conditions for growth, the ratio of assimilated carbon converted into structural biomass and not released by plant respiration is large and is termed carbon-use-efficiency (CUE; Bradford and Crowther, 2013). Depending on environmental conditions and the limited resources, CUE and PNUE vary seasonally and across species (Garbulsky *et al.*, 2010; Han *et al.*, 2016; Moreno-Gutierrez *et al.*, 2012).

In semi-arid and arid environments water is the resource that most limits photosynthesis (Eamus *et al.*, 2016; Schwinning and Sala, 2004). Although sunny warm conditions in arid and semi-arid regions are expected to favour high stomatal conductance, this would also result in large rates of transpiration, which would be unsustainable because water supply is generally limiting in these environments. There are multiple definitions of water-use-efficiency (Eamus, 1991) and I will now introduce different proxies and measures of water-use-efficiency in the following section.

### 1.1.4 Water-use-efficiencies

#### 1.1.4.1 Ecosystem water-use-efficiency

Water-use-efficiency (WUE) is the ratio of two processes and expresses ecosystem function and productivity through the ratio of C uptake to water loss (as transpiration or evapotranspiration at an-ecosystem scale). Ecosystems become more efficient in their water-use as water availability decreases (Huxman *et al.*, 2004a; Ponce-Campos *et al.*, 2013). However,

we lack a complete understanding of how vegetation responds at different spatial-temporal-scales in response to variability of water supply. Studies in WUE will ultimately improve our ability to predict changes in WUE in response to future climate conditions.

Arid and semi-arid regions have the largest slopes of the relationship between ecosystem productivity and precipitation (Huxman *et al.*, 2004a; Lieth, 1973; Ponce-Campos *et al.*, 2013). This slope is a direct measure of the ratio between net ecosystem productivity (NEP) and total annual precipitation in an ecosystem and is known as rain-use-efficiency. However, precipitation does not reflect the actual amount of water used by the ecosystem during C uptake. ET is recognized as a metric of water availability in semi-arid ecosystems and represents the water available for ecosystems due its relationship with soil moisture (Biederman *et al.*, 2016; Jung *et al.*, 2010). A better measure to study ecosystem water-use-efficiency (eWUE) is therefore the relationship between GPP and ET as eWUE= GPP/ET because ET represents total ecosystem water-use (Chen *et al.*, 2016; Huang *et al.*, 2015). Additionally, eWUE can account for the effect of environmental variables such as VPD, as the ratio of net ecosystem exchange (or GPP) × VPD to ET (Beer *et al.*, 2009; Eamus *et al.*, 2013; Zhou *et al.*, 2014)

The eddy covariance technique (EC) is a micrometeorological method that measures the instantaneous covariance between upward and downward motions of air and the concentration of gases contained within parcels of air (Fig. 1.7; Baldocchi *et al.*, 2001). EC allows the measurement of gases such as $CO_2$, $CH_4$ and water exchange between the terrestrial surface and the atmosphere. Micrometeorological towers equipped for the EC technique have the capability to sample a relatively large land surface area, thus representing a (albeit small of 100-2000 m) sample for an entire ecosystem. Although, the sampling area may change depending on site characteristics and vary at different times of the year, mainly due to wind direction and wind speed which influence the fetch-distance (Kljun *et al.*, 2004).

EC systems are continuously *in situ* monitoring the exchange of C and water fluxes across different biomes worldwide. A global network, FLUXNET project (http://fluxnet.ornl.gov/) is integrated by EC sites monitoring the land-atmospheric gas exchanges. EC sites in Australia are part of the OzFlux (http://www.ozflux.org.au/) within the Terrestrial Ecosystem Research Network (TERN).

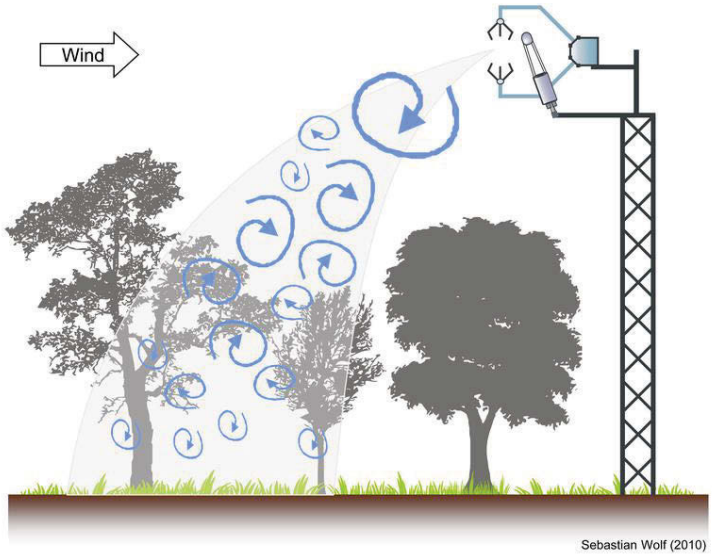


Figure 1.7 Eddy covariance (EC) technique used to measure carbon and water exchange between land surface and atmosphere. Edited from Wolf (2010). Swirls indicate the up and down motions of C and water fluxes measured by the sensors on top of the tower. The EC system is equipped with basic meteorological and sophisticated sensors to measure C and water concentrations.

This technique is able to measure the mass and energy fluxes over short and long time-scales from minutes, days, seasons and years (Baldocchi *et al.*, 2001). Net fluxes as carbon net ecosystem exchange (NEE) and ET are measured as follow:

$$F_N = \overline{p_a} \cdot \overline{w'c'} \qquad \text{(eq. 1.1)}$$

where net ecosystem flux ($F_N$) is estimated from high frequency measurements of the covariance between fluctuations in vertical wind velocity ($w$) and the mix ratio of a trace gas ($c$; i.e., $CO_2$ or $H_2O$) and $p_a$ is air density. Overbars denotes time averaging, generally at 30 or 60 min, and primes denote variations from the mean (Wolf, 2010). By definition, positive values of NEE (NEE= NEP) represent C uptake, when GPP exceeds ER; negative values of NEP represent C emissions from the ecosystem to the atmosphere (Chapin *et al.*, 2006). From NEP, GPP and ER are estimated by applying mathematical models, which are usually based on light and temperature thresholds (Cleverly *et al.*, 2013a; Scanlon and Kustas, 2010).

Continuous measurements of NEP and thus GPP and ET with the EC technique allow estimations of eWUE across different years and seasons. This is especially important in semi-arid ecosystems because of the large and erratic variability in precipitation pulses year-to-year and within seasons. Seasonal and inter-annual variability in rainfall, C and water flux represent

a challenge and contribute to the lack of consensus in how ecosystem productivity and functioning will be affected by a fluctuating environment. Therefore understanding changes in NEP, GPP and ET in semi-arid ecosystems associated with rainfall events is vital to forecast how water and C cycles will respond to change in rainfall patterns.

With EC data, it is possible to quantify instantaneous and time-integrated eWUE. It allows us to identify precipitation thresholds at which ecosystems switch from being C sources to C sinks (Scott *et al.*, 2015). However, once rainfall pulses occur (usually during the wet season), additional factors act to modulate the response of NEP and ET. For example, high temperatures are associated with a large atmospheric water demand, consequently decreasing soil moisture content and increasing soil evaporation, affecting both NEP and ET (Novick *et al.*, 2016). Therefore, understanding how meteorological variables such as solar radiation, temperature and relative humidity control NEP, GPP and ET across years and seasons is crucial for the development of a mechanistic understanding of eWUE.

#### 1.1.4.2 Leaf water-use-efficiency

Instantaneous WUE ($_{int}$WUE) is the ratio of C assimilation ($A$) to transpiration ($E$) ($_{int}WUE = A/E$; Seibt *et al.,* 2008). At short time periods $_{int}$WUE is studied with chambers that are able to measure the gas exchange of C and water fluxes in real time at the leaf-scale (Caemmerer and Farquhar, 1981). Measurements of leaf gas exchange help us understand plant responses to diurnal variation in micrometeorological variables (i.e., temperature, vapour pressure deficit, photosynthetically active radiation, (PAR)), and can be undertaken in parallel with studies of plant hydraulic traits (i.e., leaf water status through measurement of foliar water potentials). An alternate measure of WUE is termed intrinsic water-use-efficiency ($WUE_i = A/g_s$) and this has been used previously as a measure of WUE because it takes into account that fact that $E$ responds to changes in both VPD and $g_s$ while $A$ only responds to changes in $g_s$ (Eamus *et al.*, 2013; Seibt *et al.*, 2008).

Using stable isotopes (see below) of carbon ($^{12}C$ and $^{13}C$) is a useful tool to study $WUE_i$ (Farquhar *et al.,* 1984). Because the enzymatic and physical processes that occur during photosynthesis discriminate against the heavy isotope of carbon ($^{13}C$). Plants contain less $^{13}C$ as a proportion of the sum of $^{12}C$ and $^{13}C$ than the atmosphere. The model of carbon discrimination developed by Farquhar and Richard (1984), applies only at leaf-scales, and gives information about photosynthetic properties (Seibt *et al.*, 2008). The application of isotope analysis results in improved insight into plant C and water cycling and their interaction with the atmosphere.

Isotopes are atoms of the same element that differ in nuclear composition. This variation lies in the number of neutrons within the nucleus. Stable isotopes do not undergo radioactive decay. The stable isotopes of $^{12}C$ and $^{13}C$ account for 98.89% and 1.11% respectively, of all stable isotopes of C (Fry, 2006). $^{14}C$ is the unstable isotope of C that undergoes radioactive decay.

Isotopic values of any element are measured relative to standards. Isotopic composition of any source are expressed in delta notation (δ) and is a convent notation which magnify differences between the source sample and the standard (Fry, 2006). Due to the small fraction of the *R*-values (is the ratio of the heavy isotope to the light isotope for the element) all data are multiplied by one thousand, thus δ is reported as parts *per* mil (‰; Fry 2006) as follows:

$$\delta = \left[\left(\frac{R_{sample}}{R_{standard}}\right) - 1\right] \times 1000 \qquad \text{(eq. 1.2)}$$

where $R$ is the ratio of the heavy ($^{13}C$) to light ($^{12}C$) isotope of the element of interest ($^{13}C/^{12}C$ isotopes) in the sample and standard. The primary reference standard used in carbon isotope ratios is Pee Dee Belemnite (PBE), where $R_{standard}$ = 0.0112372 (Fry, 2006).

To study $WUE_i$ using the isotopic discrimination of the isotope $\delta^{13}C$, it is necessary to analyse the isotopic composition of plant tissue. For example, a time-integrated estimate of $WUE_i$ can be obtained through analysing bulk-leaf isotopic signatures, because bulk-leaf tissue values of $\delta^{13}C$ integrate the $WUE_i$ across the entire period in which the C was fixed (Brugnoli and Farquhar, 2000). In contrast, isotopic signatures of total sugars and specific compounds provide a better indication of the short-term changes in $^{13}C$-discrimination (Δ; eq. 1.3) and $WUE_i$ associated with changes in assimilation over the entire day (Brugnoli *et al.*, 1988; Brugnoli and Farquhar, 2000). The following model of isotopic discrimination was developed by Farquhar and Richard (1984):

$$\Delta = \frac{\delta^{13}C_a - \delta^{13}C_{plant}}{1+\delta^{13}C_{plant}} \qquad \text{(eq. 1.3)}$$

where Δ is the carbon discrimination against $^{13}C$, $\delta^{13}C_a$ is the isotopic signature of atmospheric $CO_2$ (-8 ‰), which is taken to be constant around the world due the strong mixing of the atmosphere and $\delta^{13}C_{plant}$ is the isotopic composition of plant organic material (i.e., bulk-leaf tissue, tree rings or specific chemical compounds such as sugars). The linearity between $^{13}C$-discrimination and $C_i/C_a$ is given by:

$$\Delta = a + (b' - a)\frac{C_i}{C_a} \quad \text{(eq. 1.4)}$$

where $a$ is the fraction during $CO_2$ diffusion through the stoma (4.4 ‰; Seibt *et al.,* 2008), and $b'$ is the fractionation associated with reaction by Rubisco and PEP carboxylase (27 ‰; Farquhar and Richards 1984). Thus, $C_i/C_a$ is used to approximate the assimilation of photosynthesizing leaves, which reflects the balance between net assimilation and stomatal conductance for $CO_2$ (Seibt *et al.,* 2008). According to Fick's law: $A = g_c(C_a - C_i)$, where stomatal conductance to water ($g_s$) and stomatal conductance for $CO_2$ ($g_c$) are related by the constant of 1.6 (i.e., $g_s = 1.6g_c$; 1.6 is used for converting from conductance to $CO_2$ to conductance to water vapour). This linear relationship allows the estimation of $WUE_i$ as:

$$\mathrm{WUE_i} = \frac{C_a}{1.6}\left(\frac{b'-\Delta}{b'-a}\right) \quad \text{(eq. 1.5)}$$

Alternatively, $WUE_i$ can be measured using the $g_1$ parameter derived by Medlyn *et al.* (2011) because $g_1$ is inversely related to $WUE_i$. The $g_1$ allows us to analyse the optimality of stomatal behaviour, which predicts that stomata should maximize C gain while regulating water loss ($\lambda = \partial E/\partial A$) (Cown and Farquhar 1977). The theory of optimal stomatal behaviour is explained through semi-empirical models widely used in global earth system models (Miner *et al.*, 2017; Wolz *et al.*, 2017). Medlyn *et al.* (2011) has demonstrated that the $g_1$ parameter predicts the optimal stomatal behaviour as:

$$g_s \approx g_0 + 1.6\left(1 + \frac{g_1}{\sqrt{\mathrm{D}}}\right)\frac{A}{C_a} \quad \text{(eq. 1.6)}$$

where D (kPa) is the vapour pressure deficit at the leaf surface, $A$ is the net assimilation rate (μmol $m^{-2}$ $s^{-1}$), $C_a$(μmol $mol^{-1}$) the atmospheric $CO_2$ concentration, $g_0$ is the leaf water vapour conductance when photosynthesis is zero (mol $m^{-2}$ $s^{-1}$) and, $g_1$ ($kPa^{0.5}$) is proportional to:

$$g_1 \propto \sqrt{\Gamma * \lambda} \quad \text{(eq. 1.7)}$$

where $\Gamma^*$is the $CO_2$ compensation point in the absence of mitochondrial respiration and λ (mol $H_2O$ $mol^{-1}$ C) is a parameter for the marginal water cost of plant carbon gain (Medlyn *et al.*, 2011). Therefore, the $g_1$ parameter is a normalized estimation of $WUE_i$, normalised to vapour

pressure deficit and atmospheric $CO_2$ concentration (Lin *et al.*, 2015; Medlyn *et al.*, 2017). Moreover, the $g_1$ parameter can be estimated from different datasets: at a leaf-scale (from carbon isotopic signatures and leaf gas exchange) and at an ecosystem-scale (using continuous flux measurements) by replacing $A$ and $g_s$ with GPP and canopy conductance ($G_c$) respectively in eq. 1.6 (Medlyn *et al.*, 2017). Thus, normalized $g_1$ values improve our ability to compare and contrast $WUE_i$ across ecosystems, plant species and plant functional types (Medlyn *et al.*, 2017).

Several studies have shown that $g_1$ varies among plant functional types and climates (Lin *et al.*, 2015; Medlyn *et al.*, 2017; Miner *et al.*, 2017). However, comparisons among co-existing species within the same ecosystem have been barely studied. The application of the $g_1$ parameter using three different datasets (carbon isotopes, leaf gas exchange and flux measurements with the EC system) from leaf-to ecosystem-scale has not been yet evaluated within a same ecosystem. Similarly, studies that have evaluated changes in stomatal behaviour and/or $WUE_i$, in response to environmental variables such as drought, using the $g_1$ parameter, are limited (Zhou *et al.,* 2013; Manzoni *et al.,* 2011; Miner *et al*., 2017). Understanding $WUE_i$ and stomatal responses to changing environment across different plant species and ecosystems is crucial to improve our ability to predict global changes in carbon and water cycles.

### 1.1.5 Two central Australian study sites

About 70 % of the Australian land surface is either semi-arid or arid land. The central Australian region is an extensive semi-arid land with sandy plains of low soil nitrogen content, low organic carbon content and low vegetation cover dominating the landscape. Consequently, vegetation in this region can be both nitrogen and water limited and are exposed to high levels of incident radiation and temperature. However, Australian semi-arid regions contributed to 60 % of the net C uptake during the global land sink anomaly that occurred in 2010-2011, when global land sink increased from the historical average of 2.6 Pg C $y^{-1}$ to 4.1 Pg C $y^{-1}$ (Poulter *et al.,* 2014). Thus semi-arid Australia has shown to be highly responsive to water availability with a high correlation between C assimilation and annual anomalies of high inputs of rainfall (Poulter *et al.,* 2014; Haverd *et al.,* 2017).

Two ecosystems dominate semi-arid central Australia: 1) Mulga woodland dominated by species of the genus *Acacia* ($N_2$-fixing Mulga species with shallow root systems) and 2) an open *Corymbia* savanna where the dominant cover is Spinifex (a C4 grass) and the tree cover is characterized by widely spaced tall *Corymbia* trees (a deep-rooted tree) and intermittent patches of Mulga. The Mulga woodlands covering ~20-25% of the continent (Cleverly *et al.*, 2016c; Eamus *et al.*, 2013), and *Corymbia* savanna over hummock grass (*Triodia* spp.) occupy

another 20-25 % (Bowman *et al.*, 2008). A site representing each of these dominante ecosystems was chosen and are located within the Ti-Tree Basin, 180 km NW of Alice Springs, in the Northern Territory of Australia (Fig. 1.8).

The Ti-Tree basin is characterized by narrow (< 10 m wide) riparian *Eucalyptus camaldulensis* (river red gum) forest, aligned with ephemeral rivers in alluvial zones. Although *E. camaldulensis* is not found within the footprint of the eddy covariance sites, *Eucalyptus* species represents one of the most iconic and important species in Australia. Both ecosystems are sites that contain micrometeorological towers equipped with eddy covariance sensor arrays operating since 2010 and 2012 for the Mulga woodland and the *Corymbia* savanna respectively. These two sites are part of the OzFlux Network (http://ozflux.org.au/) and the Terrestrial Ecosystem Research Network (TERN). Significant related eco-hydrological and eco-physiological studies have been conducted within the two semi-arid ecosystems of the Ti-Tree basin (Cleverly *et al.*, 2016a; Eamus *et al.*, 2013; O'Grady *et al.*, 2009).

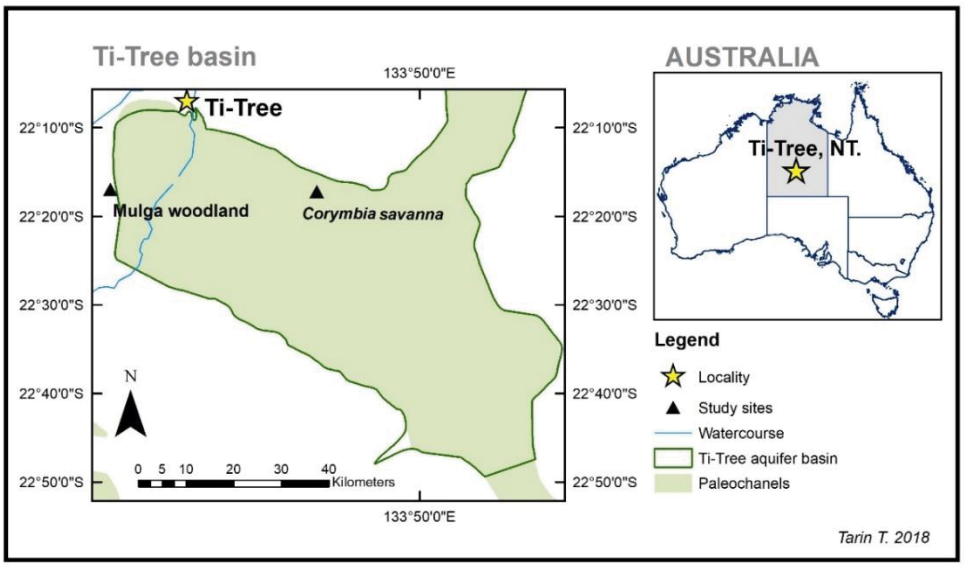


Figure 1.8 Research sites in semi-arid central Australia. The black triangles are the location of the two eddy covariance towers and the study sites. Shape files were taken from www.bom.gov.au/water/geofabric (Ti-Tree Palaeovalley site GIS; Geocat #74008).

## *1.2 Objectives*

The primary goal of this thesis is to investigate the ecosystem functioning of the two semi-arid central Australian ecosystems to improve our understanding of the interaction of terrestrial semi-arid ecosystems with the atmosphere, through measurement of C and water fluxes at ecosystem- and leaf-scales. The overall research questions that I answered were:

1. How do carbon and water fluxes of semi-arid ecosystems in central Australia compare across different time resolutions (daily, seasonally and yearly)?
2. How do climatic factors drive net ecosystem productivity and ET in semi-arid ecosystems in central Australia?
3. Are there significant differences in ecosystem WUE across seasons within ecosystems and within seasons? What drives these differences in ecosystem WUE and $WUE_i$?
4. How does soil water content influence ecosystem and leaf-scale water-use-efficiency?
5. How do different methodologies to estimate $WUE_i$ compare? What can different estimations of $WUE_i$ tell us about plant water-use across seasons?
6. How do co-occurring species diverge in resource-use-efficiency across seasons?
7. How do semi-arid tree species regulate their leaf gas exchange under drought? And how does preceding drought increase the range of tolerance to consecutive droughts across species?

This thesis answered the above questions by analysing C and water fluxes data, multiple meteorological variables and water availability at both ecosystem- and leaf-scales. Multiple intense fieldwork-campaigns were conducted during 2015 and 2016 in semi-arid central Australia. I measured leaf-scale fluxes of C and water in dominant co-existing species at each ecosystem: the Mulga woodland and *Corymbia* savanna. I collected plant tissue samples from dominant species to analyse their isotopic carbon composition and nitrogen content. At an ecosystem-scale, I analysed continuous data from both micrometeorological towers operating in central Australia. Finally, I conducted an experimental drought in a glasshouse to evaluate changes in leaf gas exchange and plant water status during repeated droughts in seedling of species that co-occur in central Australia.

## *1.3 Scope and structure of this thesis*

In this thesis I **first** hypothesized that the degree to which different climatic variables regulate carbon and water fluxes would vary seasonally and also year-to-year, due to the high intra- and inter-annual variability in rainfall in semi-arid Australia. **Second**, ecosystem vegetation composition would be a significant factor explaining differences in carbon and water fluxes across two disparate ecosystems, due to the particular eco-hydrological niches occupied by different species and because of their particular eco-physiological set of traits. **Third**, abiotic (i.e., light, soil water content) and biotic (i.e., plant water status, stomatal conductance) factors would influence resource-use-efficiencies, ecosystem WUE and $WUE_i$ within ecosystems and across species at different time-scales (i.e., diurnal and seasonal). **Fourth**, species that have a deep-root system and can access groundwater under field conditions will show less regulation in their leaf gas exchange under experimental drought conditions than species that have shallow root systems and depend on seasonal rainfall.

While the above hypotheses operate across the entire thesis, within each research chapter, specific research questions, objectives and hypotheses are presented in the four experimental chapters as now described:

This thesis encompasses six chapters including this introductory chapter (**Chapter I**), which provides the general background to terminologies and methodologies used in subsequent chapters (Table 1.1). Each research-data chapter embodies a prospective manuscript for submission to a journal, thus there is a degree of redundancy especially in introduction and methodologies when referring to the sites, data and sampling methods. Those chapters composed of fieldwork contain more redundancy in descriptions of sites and methodologies, although clear differences and research questions and hypotheses were addressed.

The focus of **Chapter II** was to evaluate relationships between NEP, ET, water availability (soil water content), meteorological variables (vapour pressure deficit, temperature, and solar radiation) and vegetation dynamics, specifically leaf area index. This study explored these relationships across different temporal-scales using multiple years of eddy covariance data and satellite observations of the two contiguous disparate ecosystems in central Australia: Mulga woodland and *Corymbia* savanna.

Table 1.1 Thesis structure.

| Chapters | Short description | Scale | Research type |
|---|---|---|---|
| **I** | General introduction | General | General |
| **II** | An evaluation of climatic drivers on NEP and ET | Ecosystem | Field data |
| **III** | An evaluation of resource-use-efficiencies across species in different seasons | Leaf | Field data |
| **IV** | Understanding $WUE_i$ from ecosystem to leaf-scale and how soil water availability influences $WUE_i$ | Ecosystem to leaf | Field data |
| **V** | Evaluating how plants of semi-arid regions respond to repeated droughts | Leaf | Experimental data |
| **VI** | General conclusion | General | General |

In **Chapter III**, I moved my focus to carbon and water exchange at the leaf-scale. The aim of Chapter III was to compare seasonal variability of carbon, nitrogen, water and light-use-efficiencies across multiple co-occurring tree species within the Mulga woodland and the *Corymbia* savanna. In **Chapter IV**, I aimed to evaluate seven continuous years of EC observations in the Mulga woodland in order to assess the response of $g_1$ (and thus, eWUE) to a metric of water availability. Additionally, this chapter evaluated $WUE_i$ with the $g_1$ parameter using three different approaches for calculating $g_1$: carbon stable isotope analyses, leaf gas exchange and eddy covariance fluxes within the same ecosystem to compare estimations of $WUE_i$ across special-scales.

The ability of co-occurring species of central Australia to respond to water availability depends in part of the rainfall regime. However, some species are deep rooted and can continually access groundwater (O'Grady *et al.,* 2009). Therefore, in **Chapter V,** seedlings of four dominant species of semi-arid Australia were studied in an experimental drought. The aim of this study was to compare the responses of leaf gas exchange as water stress increased in four co-occurring species during imposed repeated droughts. Finally, in **Chapter VI**, I provide a general discussion and conclusions of the achievements and main findings of this research.

# *Chapter II*

## Climatic drivers of divergence in carbon and water fluxes in two adjacent Australian semi-arid ecosystems

## *2.1 Introduction*

Semi-arid ecosystems can make a significant contribution to global terrestrial carbon uptake (carbon sink activity) (Poulter *et al.*, 2014). Furthermore, these ecosystems make the largest contribution to inter-annual variability in global carbon sink strength, accounting for 51 % of variability *versus* 24 % by tropical forests (Ahlström *et al.*, 2015; Biederman *et al.*, 2017). Net ecosystem production (NEP) is a measure of net carbon (C) accumulation by ecosystems, and is positive when gross primary production (GPP) exceeds ecosystem respiration (ER) and negative when respiratory loss exceeds GPP, assuming an absence of disturbance such as fire (Chapin *et al.*, 2006). In terrestrial ecosystems this difference (NEP= GPP – ER) determines whether an ecosystem is a net source or sink of atmospheric $CO_2$.

Semi-arid and arid regions account for 45 % of the terrestrial land surface (Chapin, 2002) receiving less than 500 mm of rainfall *per* year (FAO, 1989). These regions support many types of ecosystems, varying in vegetation composition and structure, e.g. evergreen and deciduous shrubs, perennial and annual species, C4 and C3 grasses. The timing and amount of rainfall is the primary limiting resource for ecosystem productivity in semi-arid regions. Rainfall and, to a smaller extent, temperature, are highly variable year-to-year and explain much of the inter-annual variation in carbon (Ahlström *et al.*, 2015; Haverd *et al.*, 2017; Schlesinger, 2017) and water fluxes (Chen *et al.*, 2013).

The second largest component of the water cycle after rainfall (Wilson *et al.,* 2001) in semi-arid ecosystems is evapotranspiration (ET), generally accounting for *ca.* 80 to 100% of annual precipitation. ET includes transpiration from plants and evaporation from soil and wet canopies (interception losses); transpiration from plants is an inherent cost of C assimilation (through stomata). ET may contribute to subsequent rainfall events and influences surface temperature

locally (Dominguez *et al.*, 2008; Jung *et al.*, 2010). Differences in the timing of peak rainfall (summer wet or winter wet ecosystems) and peak leaf area index (LAI) contribute to differences in the timing, magnitude and behaviour of ET and NEP across ecosystems (Richardson *et al.*, 2013). Vegetation greenness indices and LAI are widely used in monitoring dynamic spatiotemporal changes in ecosystems distribution, health and vegetation responses to rainfall (Chen *et al.*, 2010).

The point at which ecosystems shift from being an annual C source to an annual C sink can be identified from precipitation thresholds or pivot-points (Biederman *et al.*, 2016; Chen *et al.*, 2013; Ma *et al.*, 2016a; Scott *et al.*, 2015). The pivot-point is defined as the annual rainfall that results in an NEP of zero (Scott *et al.*, 2015). Various semi-arid ecosystems exhibit pivot-points of *ca.* 300 mm annual rainfall (Scott *et al.*, 2015). Although total annual rainfall can predict ecosystem productivity moderately accurately at inter-annual time-scales, this measure does not capture all inter-annual variability nor the intra-annual variability (Haverd *et al.*, 2017). Depending on the plant functional type and topography–runoff relations, annual rainfall may not always be an accurate indicator of ecosystem productivity (Bowling *et al.*, 2010), particularly when significant carry-over of rainfall as soil-stored water, from one hydrological year into the subsequent hydrological year, occurs (see below; Jia *et al.*, 2016; Shen *et al.*, 2016).

Water scarcity is a common feature of arid and semi-arid regions, where large inputs of total annual rainfall are rare (Haverd *et al.*, 2017; Huxman *et al.*, 2004b; Loik *et al.*, 2004). Vegetation in semi-arid regions is highly adapted to extended periods of low-to-zero rainfall. Legacy effects (or carry-over effects) from previous extreme events and inter-annual variability in rainfall play an important role in determining C and water fluxes in subsequent years (Chen *et al.*, 2013; Cleverly *et al.*, 2016b; Frank *et al.*, 2015; Reichstein *et al.*, 2013). For example, the storage of soil water from one hydrological year into the following hydrological year can mask the influence of annual rainfall on productivity and influence rates of ET (Jung *et al.*, 2010). Furthermore, some species may not respond to a rain event that is smaller than a specific threshold, while deciduous ecosystems may be unable to respond to rainfall outside of the growing season (Bowling *et al.*, 2010; Eamus *et al.*, 2016; Verduzco *et al.*, 2015). Likewise, access to groundwater for deep-rooted woody species may subsidize plant water requirements for maintaining C and water fluxes outside of the wet season, thereby causing disjunction between annual rainfall and total ET.

Semi-arid ecosystems can rapidly respond to wet periods, resulting in a positive dependency of productivity on rainfall in most, but not all, years (Haverd *et al.*, 2017; Lieth, 1973). This was evidenced in 2011, when the global land sink increased from the historical

average of 2.6 Pg C $y^{-1}$ to 4.1 Pg C $y^{-1}$ (Poulter *et al.*, 2014). Australian semi-arid regions contributed to 60 % of the net C uptake during this global land sink anomaly (Poulter *et al.,* 2014). Poulter *et al.* (2014) showed that additions of 100 mm of rainfall above the long-term average during the growing season led to a fourfold increase in net C uptake. Similarly, Haverd *et al.* (2017) found that 74 % of the Australian land surface had a positive response of GPP to annual anomalies of high inputs of rainfall.

Australia is a flat continent and *ca.* 70 % of its land surface is either semi-arid or arid. Dominant semi-arid ecosystems include: Mulga woodlands (*Acacia* spp.) covering ~20-25% of the continent (Cleverly *et al.*, 2016c; Eamus *et al.*, 2013), and *Corymbia* savanna over hummock grass (*Triodia* spp.) which cover another 20-25 % of the Australian continent (Bowman *et al.*, 2008). Using *in situ* observations with the eddy covariance method (Baldocchi, 2003), recent studies have shown that Mulga woodlands can oscillate between being a C sink and a C source (Eamus *et al.*, 2013; Eamus *et al.*, 2016) depending on variations in annual precipitation. Thresholds at which these ecosystems switch between C sink and C source have not been identified, and the degree in which climate variables such as temperature and solar radiation, in addition to rainfall, affect NEP and ET have only infrequently been examined. Such analyses are important for furthering our understanding of regional and global C and water cycles and to allow better modelling of future trajectories of vegetation behaviours.

The focus of this study was to evaluate relationships among NEP, ET, water availability (soil water content), meteorological variables (vapour pressure deficit, temperature, and solar radiation) and vegetation dynamics, specifically LAI. This study explored these relationships across different temporal-scales using multiple years of eddy covariance data and satellite observations of two contiguous disparate ecosystems in central Australia: Mulga woodland and *Corymbia* savanna. The overarching hypothesis tested was that the amount and timing of rainfall across years and between wet and dry seasons affects the relative importance of various meteorological variables. Differences in the relative importance of meteorological divers of water and C fluxes will explain intra-and-inter-annual variability in C and water fluxes in these two semi-arid ecosystems. Specifically, the following questions were addressed:

1. What are the daily, seasonal, annual and inter-annual patterns NEP and ET for a tall, open *Corymbia* savanna and closed Mulga woodland?
2. How do key abiotic drivers of NEP and ET explains the large differences in C and water fluxes between these two ecosystems seasonal and within each year?
3. Is there a carry-over effect between hydrologic years for either or both ecosystems?

4. Can this study identify thresholds of rainfall (pivot-points) at which each ecosystem switches from being a net source to a net sink of carbon?

## 2.2 Methods

### 2.2.1 Site descriptions

Two ecosystems were examined in central Australia in the Ti-Tree basin, 180 km NW of Alice Springs: Mulga woodland, dominated by *Acacia* species; and an open *Corymbia* savanna (Figure 2.1), characterized by few, tall, widely spaced *Corymbia opaca* trees and an understory of Spinifex (*Triodia schinzii,* a C4 grass) with occasional *Hakea* spp. (*Hakea macrocarpa* and *Hakea lorea*). Both sites are at the same latitude -22.28 S (133.25 E and 133.64 E; Mulga woodland and *Corymbia* savanna sites respectively at 553 m asl). These two Central Australian sites have eddy covariance (EC) towers installed and are part of the OzFlux Network (http://ozflux.org.au/) and the Terrestrial Ecosystem Research Network (TERN). Several related eco-hydrological and eco-physiological studies have been conducted in these ecosystems (Cleverly *et al.*, 2016a; Eamus *et al.*, 2013; O'Grady *et al.*, 2009; Santini *et al.*, 2015).

**a) Mulga woodland** **b) *Corymbia* savanna**

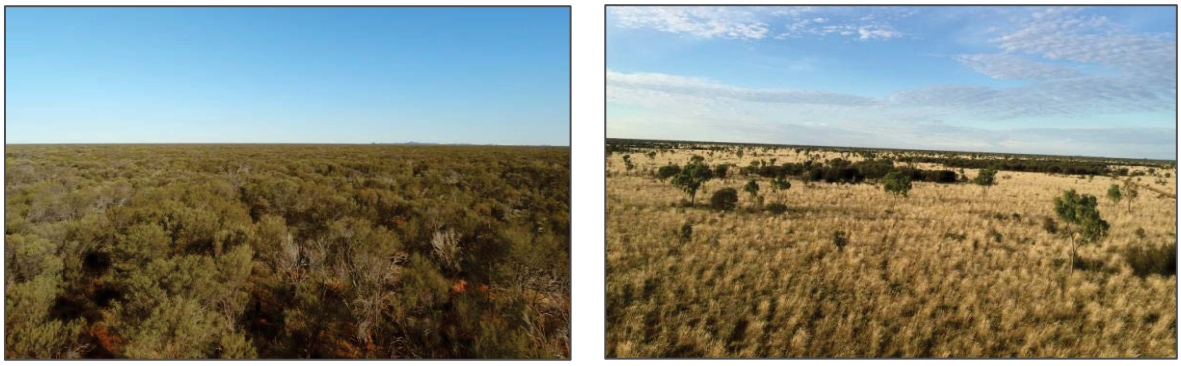

Figure 2.1 View of vegetation at the two sites of study. Photos taken at 25 m height.

The main landform in this region is an extensive floodplain and red sand plains located within the endorheic Ti-Tree basin. Depth to groundwater decreases from ~50 m in the southwest and southeast corners of the basin to less than 2 m in the north of the basin where groundwater discharges directly via evaporation and transpiration (Shanafield *et al.*, 2015). At the Mulga woodland the evergreen dominant species are part of the Mulga complex (12 *Acacia spp.*): *Acacia aptaneura* and *Acacia aneura* (Bowman *et al.*, 2007; Maslin and Reid, 2012) with a canopy height between 3 and 7 m; broad areas of bare soil are covered temporarily by grasses and herbs during favourable wet conditions. Previous surveys indicated *Acacia* spp. cover 74.5 % of the land area at the Mulga site (Cleverly *et al.*, 2016c). At the *Corymbia* savanna site located

40 km to the east, restricted small patches of Mulga can be found. Open widespread areas are dominated by *Triodia schinzii* (spinifex), with *Corymbia opaca* trees dispersed. *Acacia* is found through the savanna, but the Mulga are in patches (Nolan *et al.*, 2017a). *Corymbia opaca* is a deep-rooted tree (8-20 m), with access to groundwater (O'Grady *et al.*, 2006). More details of the Mulga site are found in Cleverly *et al.* (2013a) and Eamus *et al.* (2013).

At both sites, soil is characterized as a red kandosol (texture of 74:11:15 and 91:8:1 sand:silt:clay, Mulga woodland and *Corymbia* savanna, respectively). Soil organic matter (SOM) at the surface is 1.1 % and, porosity is 0.37 ± 0.01 and 0.30 ±0.03 at the surface and depth (1.41 ± 0.12 m) respectively (Eamus *et al.,* 2013). Annual average precipitation (1987-2017) at the nearest meteorological station to these two sites (the Territory Grape Farm, BoM station 015643, elevation 566 m), located 17 km south of the *Corymbia* savanna site is 324 mm (www.bom.gov.au). Inter-annual rainfall is highly variable in this region, and most of the annual precipitation (75 to 80 %) falls during the summer months of November to February inclusive (Eamus *et al.,* 2013). Hot and windy conditions are common in summer with temperatures above 40 °C. Mean historical maximum temperatures oscillate between 34 to 37 °C in wet months (November to March) and between 22 to 30 °C in dry season (April to October). Mean minimum temperatures vary ranged from 20 °C to 9 °C (wet and dry season. respectively; www.bom.gov.au).

### 2.2.2 Instrumentation

Both sites contain micrometeorological towers equipped with EC sensor arrays as described in Eamus *et al.* (2013) and Cleverly *et al.* (2016a, b). Briefly, one tower is 13.7 m tall (Mulga woodland: 7.2 m above canopy) and the second is 10 m tall (*Corymbia* savanna: 4.4 m above canopy; Table S.2.1). Water flux (ET) and net ecosystem exchange (NEE) were measured simultaneously at 10 Hz using a LI7500 open-path infrared gas analyser (LI7500, LI-COR, Lincoln, Nebraska; LI7500A at the *Corymbia* savanna site) while wind speed and wind direction were measured with a three-dimensional sonic anemometer (CSAT3, Campbell Scientific, Logan, UT, USA), also at 10 Hz. For the Mulga woodland the three-dimensional EC system was mounted 11.6 m above ground (canopy height 6.5 m) and facing into the predominant SE wind direction. For the *Corymbia* savanna site the system was mounted at 9.8 m (average canopy height 4.85 m), also facing SE. All data were logged at 30 min intervals using a CR3000 datalogger (Campbell Scientific Australia, Townsville, QLD, AU).

Sensors were installed at each site to measure additional variables, including net radiation with a four-way radiometer, CNR1 at the Mulga woodland and CNR4 at the *Corymbia* savanna

site (Kipp & Zonen, Delft, The Netherlands). The constant fraction (c= 0.45) of solar radiation (in energetic units W $m^{-2}$) was used to calculate photosynthetically active radiation (PAR) fluxes (Yang *et al.*, 2015). Air temperature ($T_{air}$) and relative humidity were measured using HMP45C sensors (Vaisala, Helsinki, Finland) at 11.6 m and 9.8 m (Mulga woodland and *Corymbia* savanna sites, respectively). Precipitation was measured with a tipping bucket rain gauge CS7000 at each flux tower (Hydrologic services, Warwick, NSW, Australia). Atmospheric pressure was measured 1.0 m above the ground using a Vaisala CS106 barometric pressure sensor. Direction and horizontal wind speed were measured in a profile at height increments of 2.5 m up at the Mulga woodland (Wind Monitor, R.M. Young, MI USA). Temperature and humidity profiles were measured at both towers. These data were averaged at 30 min intervals, except for precipitation (half-hour sums), and were logged using a CR3000 datalogger.

Soil moisture content was measured using soil water reflectometers (CS616 and CS610, Campbell Scientific, Logan, UT, USA). An array of sensors was installed under three plots at each site: 1) under Mulga canopy, under bare soil and, under the understory (at 0-10 cm depth) at the Mulga site; 2) under Mulga canopy, under *Triodia schinzii* grass and combination Mulga-grass (at 0-10 cm depth) at the *Corymbia* savanna site. Averages across all sensors and depths of these arrays were computed to obtain soil water content (SWC: $m^3$ $m^{-3}$) at each site. Ground heat flux plates (CN3, Middleton Solar, Melbourne, AU) were buried 8 cm below the surface; averaging soil thermocouples (TCAV, Campbell Scientific, Townsville, AU) were buried at 4 and 6 cm deep. Soil moisture was also measured in two vertical arrays using time-domain reflectometry (TDR) system probes inserted at a 45° angle (CS610, Campbell Scientific, Townsville, AU) at the Mulga woodland and a frequency-domain reflectometer (CS16) at the *Corymbia* savanna. Insertions were at 10, 60, and 100 cm. All soil measurements were collected on a separate CR1000 data-logger and stored on the CR3000 via PakBus communications (Eamus *et al.*, 2013).

### 2.2.3 Eddy covariance processing

#### 2.2.3.1 QA/QC and gap filling

OzFlux sites follow the quality assurance/control (QA/QC) procedures established by Isaac *et al.* (2017). The OzFluxQC Simulator (version 2.9.5) was used to: 1) detect and correct electronic spikes; 2) exclude fluxes within a 90° arc behind the sonic anemometers and tower (10% of the observations; Cleverly *et al.*, 2016c); 3) filter measurements when excessive humidity from rainy half hours was in the IRGA; 4) apply 2-dimensional coordinate rotation (Wesely, 1970); 5) apply frequency-response corrections (Massman and Clement, 2004); 6)

convert virtual-to-actual sensible heat flux (Schotanus *et al.*, 1983); 7) correct for air density (which accounts the density effect arising from heat and water vapour fluxes; (Webb *et al.*, 1980); and 8) account for storage of heat in the soil above the heat flux plates (Malek, 1993; Prueger *et al.*, 1996). Absolute humidity from the HMP45C sensors and Li7500/Li500A were regressed to discard outliers in the measurements.

Gap filling of fluxes was performed using the Self-Organizing Linear Output (SOLO) that is trained on a self-organizing feature map (SOFM) of meteorological and soil measurements as described in Eamus *et al.* (2013). SOLO is a statistical artificial neural network (ANN) which provides resistance to overtraining and has the ability to simulate fluxes (Abramowitz *et al.*, 2006; Hsu *et al.*, 2002). Learning sensitivity of the ANN was set to minimize root mean square error following stepwise procedures (Cleverly *et al.*, 2016c; Eamus *et al.*, 2013). Gaps were 30-300 min in length and occurred at different times for either site. Gaps were filled from one-minute averages (usually from 26 to 29 one-minute values), linear interpolation, replacement of measurements from the companion tower (Cleverly *et al.*, 2016c) or SOLO-SOFM trained on measurements with the paired tower. Gap filling data accounted for 20 to 30 % of annual half-hour measurements, except in 2016 with 31 % and 33 % for the Mulga woodland and *Corymbia* savanna datasets, respectively.

#### 2.2.3.2 Footprint, energy balance and carbon flux partitioning

Footprint calculations demonstrated that the towers measured fluxes occurring within 200 to 300 m to the southeast under turbulent conditions at both towers (Cleverly *et al.*, 2016c; Kljun *et al.*, 2004). The *Corymbia* savanna was more heterogeneous than the Mulga woodland, with 75 % of the footprint corresponding to the small Mulga patch mixed with *Corymbia opaca* trees, and 25 % to the combination of open grassland and widely spaced *Corymbia* trees (Cleverly *et al.*, 2016c). The energy balance ratio as $(H+LE)/(R_n-G)$ was calculated yearly using daily averages of the energy fluxes (Table 2.1). The Mulga woodland flux time series covers the period from Sep-2010 to Dec-2016 (6.3 years); for the *Corymbia* savanna ecosystem the data stream covers the period from Jul-2012 to Dec-2016 (4.5 years).

Table 2.1 Energy balance statistics coefficients. Years are hydrological years from August to July. Acronym for Mulga woodland is M and *Corymbia* savanna is C (n= number of daily averages used). Fluxes are: latent heat (LE), sensible heat (H), ground heat (G) and, net radiation ($R_n$). Parameters estimated from the energy balance equation (LE+H= m($R_n$-G)+b) were: slope and intercept with 95 % confidence. Adjusted $r^2$ of the regression model. The last two columns are the energy balance ratio for each site.

| Year | n | | Slope | | Intercept | | $r^2$ | | Σ(LE + H)/ Σ ($R_n$ - G) | |
|---|---|---|---|---|---|---|---|---|---|---|
| | M | C | M | C | M | C | M | C | M | C |
| 2010-2011 | 329 | | 0.74 | | 18.1 | | 0.89 | | 0.87 | |
| 2011-2012 | 348 | | 0.73 | | 22.6 | | 0.85 | | 0.87 | |
| 2012-2013 | 365 | 365 | 0.68 | 0.98 | 23.2 | 3.2 | 0.83 | 0.92 | 0.87 | 1.01 |
| 2013-2014 | 365 | 365 | 0.77 | 0.96 | 11.3 | 1.3 | 0.86 | 0.92 | 0.87 | 0.98 |
| 2014-2015 | 365 | 365 | 0.45 | 0.56 | 55.1 | 34.7 | 0.51 | 0.75 | 0.94 | 0.84 |
| 2015-2016 | 366 | 366 | 0.73 | 0.88 | 13.9 | 6.0 | 0.91 | 0.82 | 0.83 | 0.93 |
| 2016-2017 | 153 | 153 | 0.73 | 0.85 | 18.6 | 13.3 | 0.82 | 0.76 | 0.86 | 0.96 |
| All years | 2309 | 1628 | 0.67 | 0.77 | 25.7 | 19.0 | 0.79 | 0.79 | 0.87 | 0.94 |

Carbon flux partitioning of NEE into GPP and ER for the Mulga site followed Cleverly *et al.* (2013a). ER was first calculated and then GPP was estimated (from -NEE=GPP-ER) for the Mulga woodland. ER was estimated from responses of NEE under three different conditions when GPP can be assumed to be zero: (i) at night; (ii) at the *y*-intercept of a light-response curve of NEE *versus* solar radiation (SR); (iii) or on rare occasions when complete stomatal closure could be reasonably assumed under midday light levels. Nocturnal respiration ($R_{night}$) was assumed equal to the average of NEE on nights without gaps in the data set. Nights with gaps used thermal sensitivity curves ($Q_{10}$ exponential model) developed from $R_{night}$ and average nocturnal soil temperature in three SWC classes to estimate $R_{night}$. Dark respiration ($R_{dark}$) and maximum NEE were regressed into temperature classes and plotted as double exponential functions (Cleverly *et al.*, 2013a). $R_{dark}$ was obtained from the intercept of NEE *versus* SR when SR was < 500 W $m^{-2}$. When SR was > 500 W $m^{-2}$ maximum NEE was identified within a given temperature class, thus accounting for those annual and seasonal periods when NEE greatly exceeded 0 µmol $m^{-2}$ $s^{-1}$ and GPP was assumed to be negligible. Total daily ecosystem respiration (ER) was calculated as follows:

$$ER = \sum R_{night} + \sum R_{dark} + \sum NEE_{max(SR>500\ W\ m^{-2})} \quad \text{(eq. 2.1)}$$

Due to the strong influence of abiotic decomposition and photo-degradation in the *Corymbia* savanna, standard methods of partitioning NEE produced physically meaningless values of GPP (Cleverly *et al.,* 2016c). For this reason, NEE partitioning into GPP and ER was undertaken only at the Mulga woodland. By definition, positive values of NEP (NEE= -NEP) represent C uptake, when GPP exceeds ER; negative values of NEP represent C emissions from the ecosystem to the atmosphere (Chapin *et al.*, 2006).

### 2.2.4 Time series processing

Due to the meteorological characteristics of these sites, hydrological years (August-July) were used instead of calendar years for total C and water flux budgets. To simplify the analyses for seasonal comparisons data were divided into two major seasons based on rainfall records: 1) wet (~Oct-April) seasons were defined to have started when rainfall > 5 mm $d^{-1}$ occurred and SWC was > 0.05 $m^3$ $m^{-3}$ and, when the first major excursion to negative values in NEP after the dry season were observed; 2) dry seasons (~May-Sep) were deemed to have started when 10 consecutive days without rain occurred at the end of April or May, and SWC dropped below 0.05 $m^3$ $m^{-3}$. Thus, the duration of wet and dry seasons varied each year based on rainfall and soil moisture. For seasonal and annual analyses, daily sums for ET and NEP, and daily averages of VPD, SWC, $T_{air}$ and SR were used and for diurnal analyses, 30 min data were used.

### 2.2.5 Multivariate SPEI index analysis

To characterize the relative severity of seasonal variations in water supply, the standardized precipitation-evapotranspiration drought index (SPEI) was used (Vicente-Serrano *et al.*, 2010). SPEI is based on the climatic water balance using precipitation, temperature and potential evapotranspiration (PET) to calculate changes in evaporative demand caused by temperature fluctuations (eq. 2.2):

$$D = P - PET \qquad \text{(eq. 2.2)}$$

where D is the climatic water balance, P is monthly precipitation (mm) and monthly PET (mm) was represented by Penman-Monteith reference ET ($ET_0$) from Allen *et al.* (1994). SPEI was computed using the SPEI-package in R (Vicente-Serrano *et al.*, 2010) at monthly intervals, then averaged for each wet and dry season. Positive SPEI indicates wet conditions and negative SPEI values indicate dry conditions, based on the supply and demand concept of the water-balance (eq. 2.2).

### 2.2.6 Remote sensing observations of vegetation indices

The enhanced vegetation index (EVI) correlates well in Australia with phenology (Ma *et al.*, 2013; Restrepo-Coupe *et al.*, 2016) and minimizes the effect of bare soil on the calculation of the index (Huete *et al.*, 2002) and consequently this was used in the present study to asses vegetation phenology. EVI and LAI were obtained at 16-day and 8-day intervals respectively from the moderate resolution imaging spectroradiometer (MODIS) sensor (MOD13Q1 for EVI and MOD15A2 for LAI; ORNL DAAC. 2008). Composites of 9 x 9 pixel (250 m pixel spatial resolution) centered on each tower (2.25 km box) were linearly interpolated to obtain daily values to allow for a gradual progression of vegetation changes (Cleverly *et al.*, 2016c). In addition, a smoothing technique that included the combination of weighted local regression and a second degree polynomial model (with a span of 5 %) was applied to the raw data to minimize noise (Méndez-Barroso *et al.*, 2014).

### 2.2.7 Statistical analyses

Path analysis was used to evaluate the dependence of NEP, GPP (GPP only applies for the Mulga woodland) and ET to several climate parameters. Path analysis is a statistical analysis to test causal hypotheses (Chen *et al.*, 2015; Huxman *et al.*, 2003). In this study path analyses were built based on structural equation modelling (SEM) to explore the mechanistic interactions among environmental parameters and a target variable using daily data. Three days were removed after each precipitation pulse, including the day with rain and two consecutive days to reduce contributions from soil and wet canopy evaporation. Path analysis was tested in four different subsets: 1) all wet seasons combined (for 6.3 and 4.5 years of data; *ca.* Oct-April) at each site to obtain a broad view of the growing season; 2) dry seasons (*ca.* May-Sep); and finally wet seasons were sub-divided into 3) early and 4) mid-to-end of the wet season, which began when NEP became positive after sufficient rainfall had accumulated. The subdivision of the wet season was needed due to the contrasting behaviour of carbon and water fluxes at the start of the rainy season *versus* the end of the wet season. Note that wet and dry seasons do not necessarily match the end and start of hydrological years (August to July).

Statistical analyses were performed in R 3.2.1 Project software® (R Development Core Team 2016). First, multiple linear regressions were applied to identify significant regressions among variables. The minimum adequate models were selected using the Akaike information criterion (AIC), with forward and backward stepwise selection. Parameter estimates were obtained under maximum-likelihood estimation using standardized partial coefficients based on

the coefficient matrix (Pearson method). Path strengths generated the following analyses: 1) NEP regressed on ET, LAI, SWC and $T_{air}$; 2) ET regressed on SWC, LAI, $T_{air}$ and VPD; 3) VPD regressed on $T_{air.}$ For the Mulga woodland, GPP was regressed with PAR, LAI and $T_{air}$. The models were designed to evaluate seasonal shifts in primary factors that were controlling C and water fluxes. The goodness-of-fit were assessed by chi-square ($\chi^2$) test and comparative fit index (CFI). A non-significant $\chi^2$ ($p$>0.05) and CFI ≥ 0.95 indicated a good fit (Shipley, 2000). In R, the Lavaan-package (Yves, 2012) was used to produce the SEM and its fitting; semPlot-package (Epskamp, 2017) was used to generate path diagrams and visual analyses of SEM.

Additionally, linear regressions were applied using ordinary least squares regression to identify precipitation thresholds (pivot-points) between total annual rainfall and total NEP. To improve such regressions, in the last period of editing this research, complete observations for the hydrological year 2016-2017 (Aug-Jul) were used for both sites.

## *2.3 Results*

### 2.3.1 Weather conditions

The wettest hydrologic year was in 2010-2011 (565 mm of rainfall recorded at the Mulga woodland; Table 2.2). Rainfall in this year was 74 % larger than the long-term average of 324 mm (Australian met. station 015643). The following four years at the Mulga woodland, (2011 to 2015) and the two first years of measurements recorded at the *Corymbia* savanna (2012-2013 and 2013-2014) had lower rainfall than the historical average (Table 2.2; Fig. 2.2a). From 2015 to 2016, annual rainfall was above the historical annual average at both ecosystems. The hydrologic year 2016-2017 received almost as much rainfall as the extreme year of 2010-2011 (496 mm; Table 2.2).

The difference in annual rainfall at the two sites ranged between 2 mm (2012-2013) and 96 mm (2014-2015) but averaged only 18 mm. Wet season rain accounted for > 90 % of total annual rainfall at both sites, with two exceptions (2012-2013 and 2015-2016 at the *Corymbia* savanna; Table 2.2). The majority of rain pulses (> 60 %) were between 1 and 5 mm $d^{-1}$ and 10 % between 6 and 10 mm $d^{-1}$, across all years in the two ecosystems. Larger rain pulses, between 11 and 20 mm $d^{-1}$, accounted for 11 % of the total rain pulses in both ecosystems. Rain pulses > 20 mm accounted for 8 % and 12 % of the total rain events for Mulga woodland and *Corymbia* savanna respectively (Fig. 2.2a, 2.3a).

In the *Corymbia* savanna average maximum daily temperatures were 34.4 ± 1.2 and 30.6 ± 4.3 °C during wet and dry seasons, respectively, and average minimum temperatures were 16.3 ± 2.8 and 9.3 ± 1.1 °C during wet and dry seasons, respectively (Fig. 2.3b). In the Mulga woodland average daily maximum temperatures were 34.2 ± 1.1 and 29.8 ± 3.8 °C during wet and dry seasons, respectively, and average minimum temperatures were 13.2 ± 1.5 and 8.5 ± 1.1 °C during wet and dry seasons, respectively (Fig. 2.2b). Mean annual VPD was 2 ± 0.3 kPa in both ecosystems; but mean daily values of VPD reached up to 5 kPa in the summer of 2013-2014 at the two ecosystems. Seasonally, the Mulga woodland had an average VPD of 2.4 ± 0.4 and 1.7 ± 0.4 kPa in wet and dry seasons respectively. The *Corymbia* savanna had an average VPD of 2.6 ± 0.4 and 2.0 ± 0.4 kPa (wet and dry seasons respectively; Fig. 2.3b).

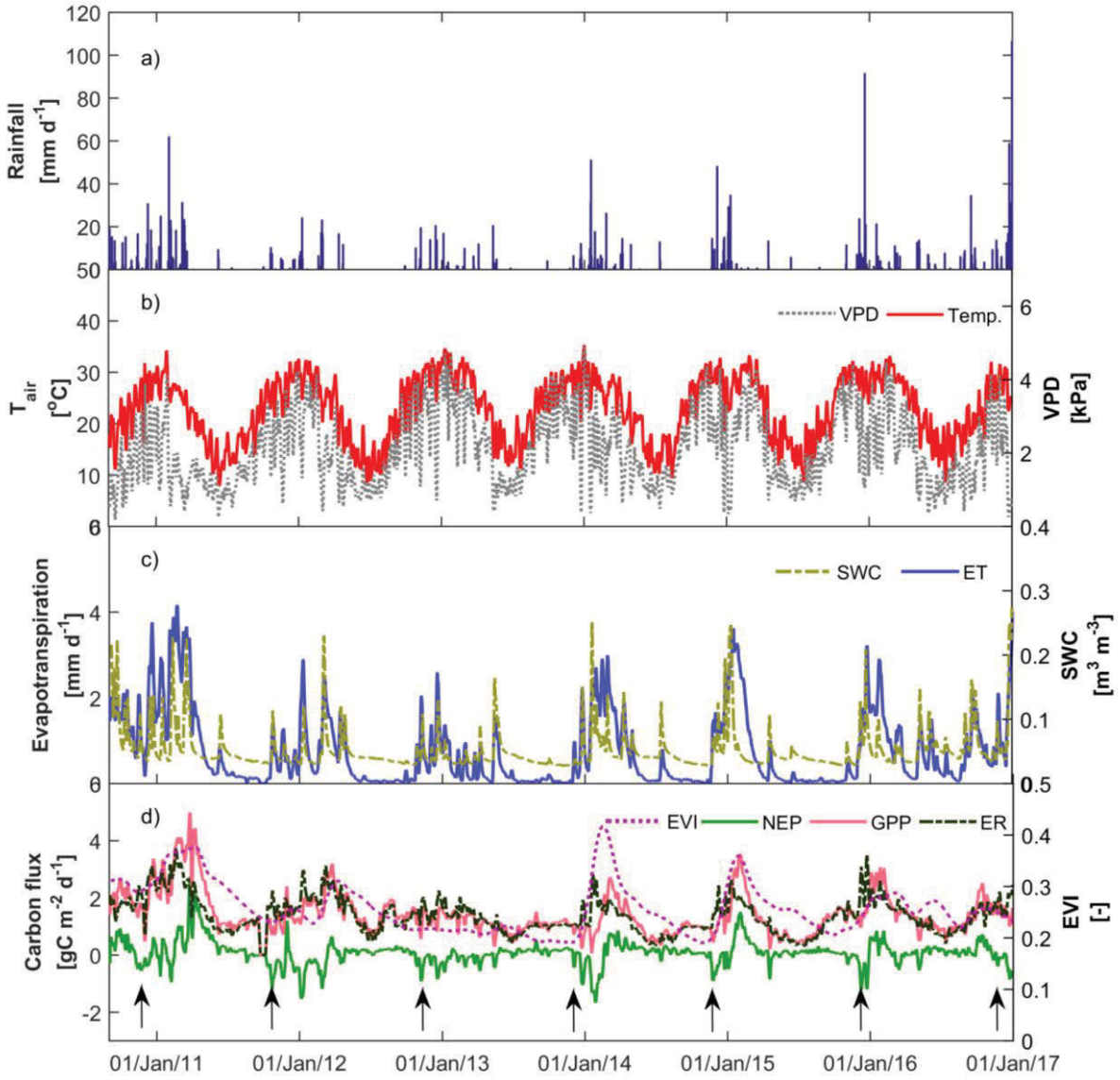


Figure 2.2 Climatic conditions of SWC, ET, EVI and carbon budget for 6.3 hydrological years in the Mulga woodland. Rainfall, carbon fluxes (GPP, ER, and NEP) and evapotranspiration are daily totals. Air temperature, VPD and SWC are daily averages. EVI values were interpolated to a daily time-step from 16-day MODIS data. Arrows indicate the start of the wet seasons.

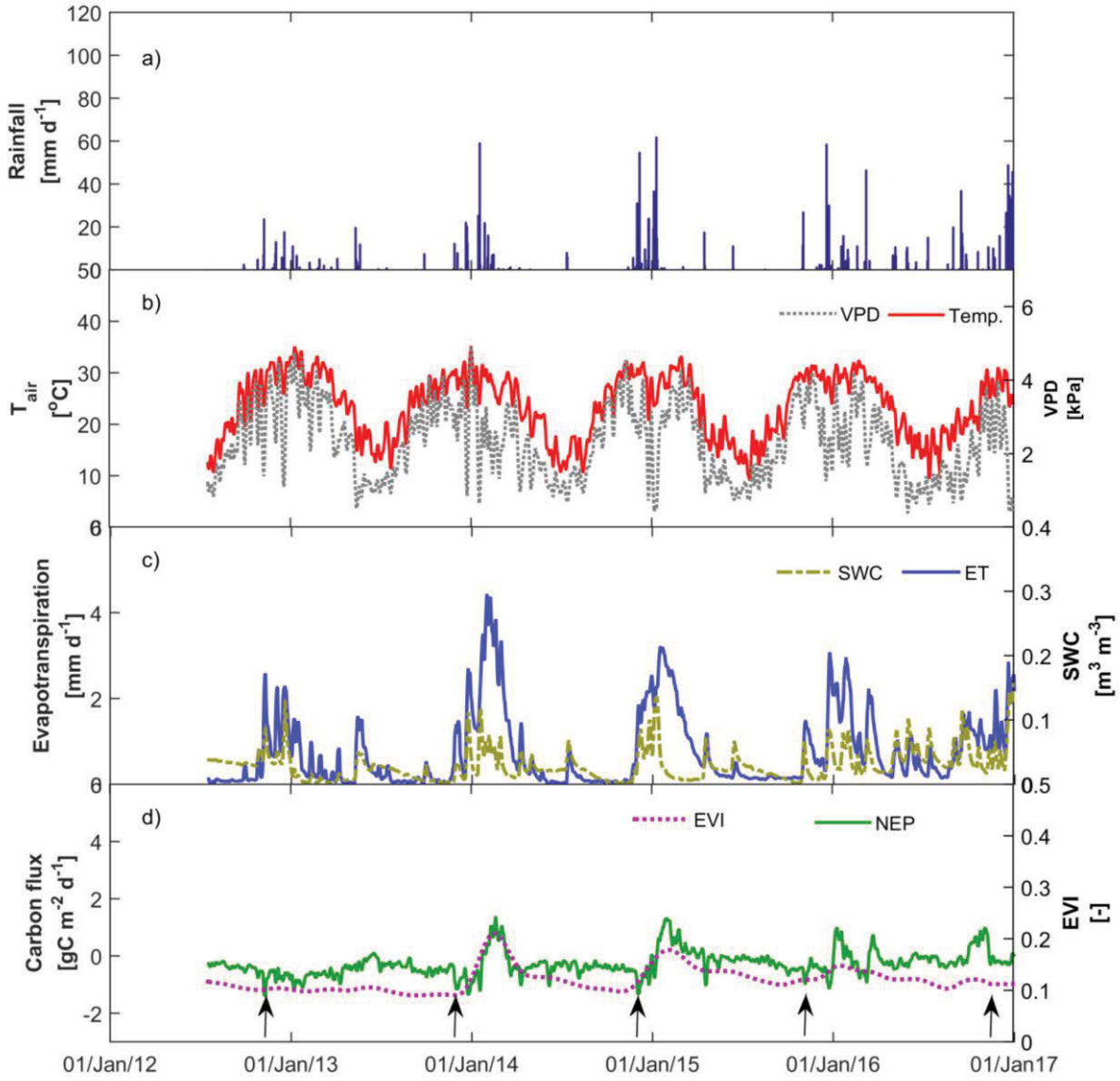


Figure 2.3 Climatic conditions of SWC, ET, EVI and carbon budget for 4.5 hydrological years in the *Corymbia* savanna. Rainfall, NEP and evapotranspiration are daily totals. Air temperature, VPD and SWC are daily averages. EVI values were interpolated to a daily time-step from 16-day MODIS data. Arrows indicate the start of the wet seasons.

### 2.3.2 Soil water content and EVI

Daily and seasonal patterns in soil water content (SWC) closely followed daily and seasonal patterns in rainfall at both sites. SWC ranged between 0.04 and 0.3 $m^3$ $m^{-3}$ at the Mulga woodland (Fig. 2.2c) and 0.01 to 0.17 $m^3$ $m^{-3}$ at the *Corymbia* savanna (Fig. 2.3c). The Mulga woodland showed larger wet season maximum values in SWC across all years: 0.26 ± 0.02 $m^3$ $m^{-3}$, compared with 0.14 ± 0.01 $m^3$ $m^{-3}$ in the *Corymbia*-savanna. EVI of the Mulga increased during

the early wet season and typically peaked in January of each year, with minima recorded in the mid-to-late dry season of each year (Fig. 2.2d).

Average EVI from 2010 to 2017 of the Mulga woodland was 0.26 ± 0.04, in which wet seasons averaged 0.27 ± 0.04 and dry season 0.24 ± 0.03. During the growing season of hydrologic year 2010-2011, EVI reached 0.4 at the Mulga woodland, and remained high throughout dry season of 2011 (~May-Sep). Only two maxima in EVI were observed in the *Corymbia* savanna (wet season 2013-2014; 2014-2015; Fig. 2.3d). Maximum EVI of the *Corymbia* savanna site occurred during the wet season of 2013 -2014 (EVI = 0.2). Mean EVI for the *Corymbia* savanna was 0.12 ± 0.02 across all years (2012–2016), and averaged for the wet season was 0.13 ± 0.02 and dry season 0.11 ± 0.01. EVI had much less seasonal and inter-annual variation at the *Corymbia* savanna than the Mulga woodland.

### 2.3.3 Water and carbon fluxes

#### 2.3.3.1 Inter-annual and seasonal patterns

Annual ET was consistently larger (by 9–23 %) from the *Corymbia* savanna than from the Mulga woodland for all 4.5 years for which data were available for both sites (Table 2.2). Annual ET ranged between 73 % (2015-2016) and 90 % of annual rainfall for the Mulga site and between 73 % (2014-2015) and 106 % (2013-2014) at the *Corymbia* savanna. Average daily ET at the Mulga woodland was 1.6 ± 0.82 mm $d^{-1}$ during the wet year 2010-2011 and <0.9 mm $d^{-1}$ in the following years (Fig. 2.2c). Average daily ET of the *Corymbia* savanna ranged between 0.4 and 1 mm $d^{-1}$ across the five years of study (Fig. 2.3e). ET maxima during the wet season were similar at both sites (ET across all years was 4.2 ± 0.8 mm $d^{-1}$ in the Mulga woodland and 4.2± 0.9 mm $d^{-1}$ *Corymbia* savanna respectively; Fig. 2.2c and 2.3c).

Maximum SPEI values were 0.9 at the Mulga woodland and *Corymbia* savanna, while minimum SPEI was -1.1 at the Mulga and -0.7 in the *Corymbia* savanna (Table 2.2). Seven dry periods were identified across all years by their negative SPEI at the Mulga woodland, along with four dry periods at the *Corymbia* savanna. Three of six dry periods (negative SPEI) at the Mulga woodland were during wet seasons (~Oct-April). The *Corymbia* savanna had negative or zero SPEI in the same negative SPEI wet seasons as in the Mulga woodland, except for the wet seasons of 2013-2014 (SPEI= 0.5).

Table 2.2 Annual and seasonal carbon and water budgets at the Mulga woodland and the *Corymbia* savanna. Annual sums of rainfall (PPT) and ET using hydrological years (August to July). The percentage of rain (% rain) is a function of annual rainfall. SPEI values are monthly averages and, σ is the standard deviation. Seasonal sums are also showed for rainfall, ET, NEP, GPP and ER. Note that the duration of wet and dry seasons varied each year based on rainfall and soil moisture and, in some cases, a season might overlap the following hydrological year.

| Year | PPT | ET | Season | | | SPEI | | PPT | ET | NEP | | GPP | ER |
|---|---|---|---|---|---|---|---|---|---|---|---|---|---|
| | (mm) | (mm) | | (days) | (% Rain) | (avg.) | σ | (mm) | (mm) | (gC $m^{-2}$ *per* season) | | | |
| ***1) Mulga Woodland*** | | | | | | | | | | | | | |
| **2010-2011** | 565 | 512 | Wet | (n=221) | 97 | 0.9 | ±0.33 | 549 | 458 | 70 | (sink) | 569 | 504 |
| | | | Dry | (n=172) | 3 | 0.6 | ±0.51 | 16 | 60 | 62 | (sink) | 242 | 184 |
| **2011-2012** | 239 | 207 | Wet | (n=213) | 98 | 0.2 | ±0.53 | 238 | 189 | -60 | (source) | 342 | 402 |
| | | | Dry | (n=178) | 2 | -0.1 | ±0.57 | 4 | 18 | 27 | (sink) | 242 | 213 |
| **2012-2013** | 193 | 153 | Wet | (n=213) | 97 | -0.4 | ±0.68 | 187 | 136 | -37 | (source) | 257 | 311 |
| | | | Dry | (n=182) | 3 | -1.1 | ±1.5 | 6 | 18 | 29 | (sink) | 184 | 164 |
| **2013-2014** | 295 | 249 | Wet | (n=172) | 94 | -0.1 | ±0.85 | 272 | 227 | -11 | (source) | 232 | 255 |
| | | | Dry | (n=191) | 6 | 0.2 | ±0.79 | 18 | 25 | 22 | (sink) | 157 | 140 |
| **2014-2015** | 301 | 251 | Wet | (n=159) | 98 | -0.5 | ±0.74 | 295 | 232 | 29 | (sink) | 260 | 251 |
| | | | Dry | (n=185) | 2 | -0.5 | ±0.62 | 7 | 14 | 19 | (sink) | 166 | 150 |
| **2015-2016** | 336 | 247 | Wet | (n=223) | 96 | -0.3 | ±0.93 | 322 | 225 | 2 | (sink) | 360 | 370 |
| | | | Dry | (n= 70) | 4 | 0.7 | ±0.06 | 13 | 18 | 10 | (sink) | 63 | 53 |
| **2016-2017** | 496 | 150 | Wet | (n=133) | 100 | 0.8 | ±1.2 | 496 | 149 | 8 | (sink) | 206 | 206 |
| ***2) Corymbia savanna*** | | | | | | | | | | | | | |
| **2012-2013** | 191 | 186 | Wet | (n=175) | 71 | 0.1 | ±1.0 | 134 | 129 | -124 | (source) | | |
| | | | Dry | (n=211) | 28 | -0.5 | ±0.73 | 54 | 55 | -76 | (source) | | |
| **2013-2014** | 290 | 307 | Wet | (n=154) | 92 | 0.5 | ±0.34 | 267 | 275 | -42 | (source) | | |
| | | | Dry | (n=207) | 6 | -0.4 | ±0.61 | 16 | 28 | -80 | (source) | | |
| **2014-2015** | 396 | 292 | Wet | (n=158) | 97 | -0.7 | ±1.0 | 383 | 261 | 9 | (sink) | | |
| | | | Dry | (n=233) | 15 | -0.2 | ±0.62 | 60 | 72 | -63 | (source) | | |
| **2015-2016** | 340 | 281 | Wet | (n=175) | 78 | 0.0 | ±0.46 | 266 | 209 | -24 | (source) | | |
| | | | Dry | (n= 80) | 8 | 0.9 | ±0.49 | 29 | 28 | -11 | (source) | | |
| **2016-2017** | 478 | 164 | Wet | (n=123) | 99 | 0.9 | ±1.0 | 474 | 156 | 10 | (sink) | | |

Mean NEP was 0.1 ± 0.1 gC $m^{-2}$ $d^{-1}$ across the 6.3 years of study at the Mulga woodland (Fig. 2.2d) and -0.3 ± 0.2 gC $m^{-2}$ $d^{-1}$ across the 4.5 years of study at the *Corymbia* savanna (Fig. 2.3d). Average NEP was 0.01 ± 0.2 gC $m^{-2}$ $d^{-1}$ for the seven wet seasons at the Mulga woodland and was 0.2 ± 0.1 gC $m^{-2}$ $d^{-1}$ for six dry seasons. The *Corymbia* savanna showed an average of -0.2 ± 0.3 gC $m^{-2}$ $d^{-1}$ across all wet seasons and -0.3 ± 0.1 gC $m^{-2}$ $d^{-1}$ across all dry seasons (Fig. 2.3d). Mean

seasonal maximum values of NEP were 1.5 ± 0.9 gC $m^{-2}$ $d^{-1}$ and 0.8 ± 0.8 gC $m^{-2}$ $d^{-1}$ for wet and dry seasons respectively at the Mulga woodland (Fig. 2.2d). The *Corymbia* savanna had an average of maxima NEP of 1.3 ± 0.8 gC $m^{-2}$ $d^{-1}$ and 0.1 ± 0.2 gC $m^{-2}$ $d^{-1}$ for wet and dry seasons respectively (Fig. 2.3d).

Average seasonal maximum GPP was 3.4 ± 1.0 gC $m^{-2}$ $d^{-1}$ for the wet season and 2.1 ± 1.1 gC $m^{-2}$ $d^{-1}$ during the dry season at the Mulga woodland. Maximum GPP of 5.2 gC $m^{-2}$ $d^{-1}$ occurred during the wet season 2010-2011 and minimum GPP of 1.8 gC $m^{-2}$ $d^{-1}$ during the dry season of 2012-2013. Seasonal average GPP of the Mulga woodland was 1.6 ± 0.4 gC $m^{-2}$ $d^{-1}$ and 1.1 ± 0.3 gC $m^{-2}$ $d^{-1}$ in the wet and dry seasons respectively. Average seasonal maximum ER was 3.4 ± 1.0 gC $m^{-2}$ $d^{-1}$ in the wet season and 1.6 ± 0.5 gC $m^{-2}$ $d^{-1}$ in the dry season.

#### 2.3.3.2 Comparing a wet and a dry year

To describe fluxes with a finer temporal resolution than seasonal or annual, this section focuses on two contrasting hydrological years: 2012-2013 and 2015-2016 for which data are available for both sites.

Rainfall was considerably lower in the hydrological year 2012-2013 than in the wet-year 2015-2016 (Table 2.2). This had implications for carbon fluxes in both ecosystems (Figs. 2.4 and 2.5). Neither ecosystem showed large variations in carbon fluxes following precipitation pulses, which were < 20 mm $d^{-1}$ (Figs. 2.4b and 2.5b). This was the case for 2012-2013, in which NEP oscillated between 0.33 and -0.92 gC $m^{-2}$ $d^{-1}$ at the Mulga woodland (Fig. 2.4b), or between 0.11 and -1.41 gC $m^{-2}$ $d^{-1}$ at the *Corymbia* savanna (Fig. 2.5b). Conversely, larger precipitation pulses in the wet-year (2015-2016) had major implications for carbon flux variability of 2015-2016 (Figs. 2.4d and 2.5d).

NEP was lower (i.e., more negative) with the arrival of the rain during the wet months (*ca*. November to December) than during previous months (August to October) at both sites. Negative extremes of NEP occurred when at least 10 mm of rain were accumulated in November or December. These negative NEP values were correlated with a fast response of ER to the first rainfall events (Fig. 2.4b-d). In contrast, GPP showed a slow response to rainfall. GPP increased from ~Jan-Feb when it was 20 % larger than ER and this was maintained for up to four consecutive months (to mid-June). Consequently, NEP was positive during this period. Positive peaks of NEP in both ecosystems correlated well with the increase in EVI during this period. Maxima in EVI corresponded to maxima in NEP (positive values) observed across all years (Fig. 2.2d, 2.3d).

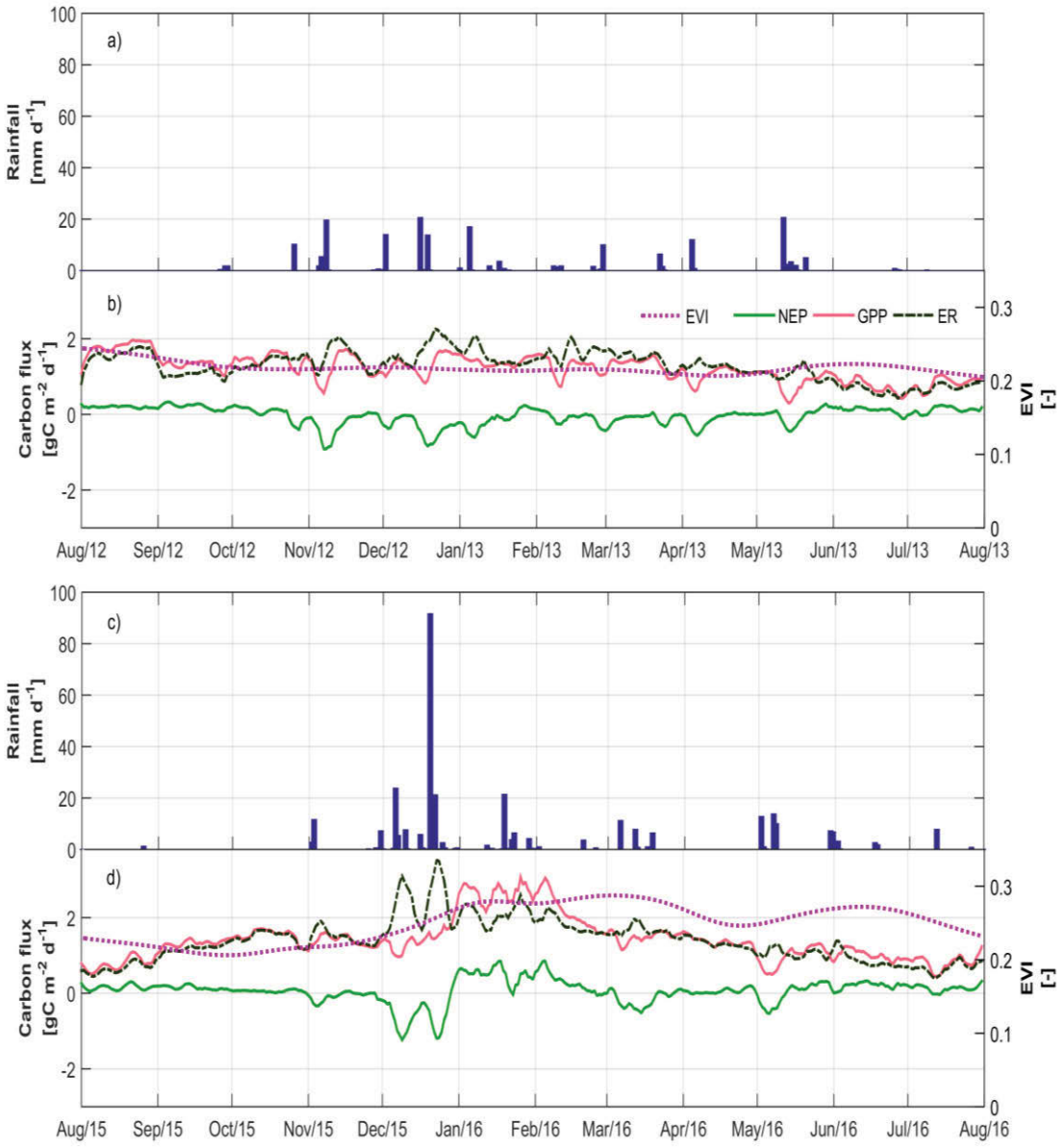


Figure 2.4 Comparison of rainfall, EVI and carbon budgets in a dry hydrologic year (August 2012-July 2013; panels a-b) and a wet hydrologic year (2015-2016; panels c-d) in the Mulga woodland. Carbon fluxes, rainfall and EVI are daily values as in figure 2.2. Months indicate the first day of the month.

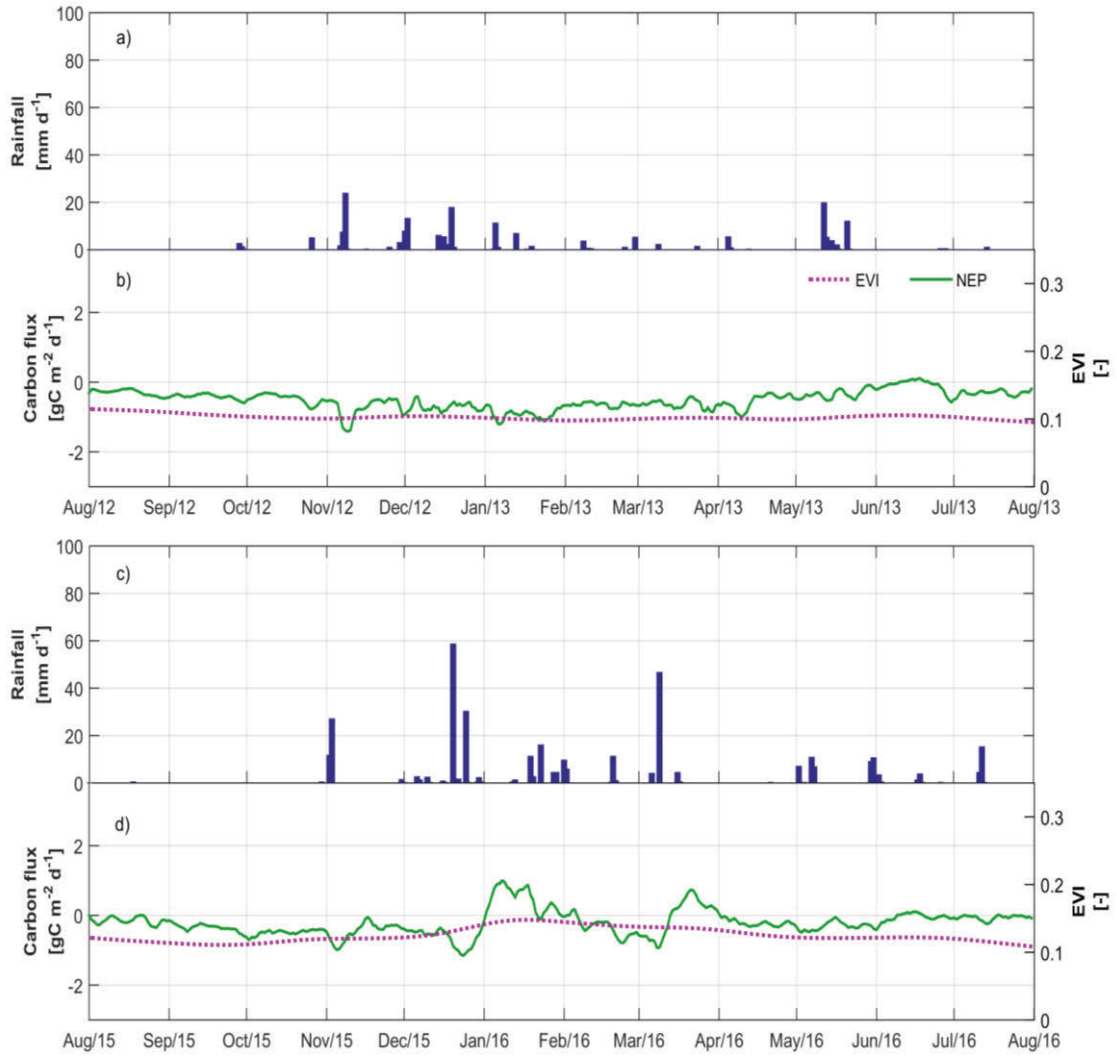


Figure 2.5 Two hydrological years: dry-year (2012-2013; panels a-b) and wet-year (2015-2016; panels c-d) for the *Corymbia* savanna. Carbon fluxes are daily totals as in figure 2.3. Months indicate the first day of the month.

#### 2.3.3.3 Carbon budgets and precipitation thresholds (pivot-points)

In four of seven wet seasons the Mulga woodland was a C sink and, therefore in three wet seasons, Mulga was a C source (Table 2.2). Source strength varied between NEP of -60 and -11 gC $m^{-2}$ *per* season and sink strength varied between 2 and 70 gC $m^{-2}$ *per* season for the Mulga woodland. In contrast, three of five wet seasons the *Corymbia* savanna was a C source and hence it was a C sink in 2 wet seasons (2014-2015 and 2016). In four dry seasons, the *Corymbia* savanna was a C source. Source strength varied between -124 and -11 gC $m^{-2}$ *per* season while sink strength was 9-10 gC $m^{-2}$ *per* season.

During seasons in which Mulga was a C source, ER was larger than GPP by 10-21 % (Table 2.2). In all other seasons GPP was >10 % larger than ER and, up to 24 % larger in the dry seasons of 2010-2011. GPP varied from 63 to 569 gC $m^{-2}$ *per* season (wet 2010-2011 and dry season 2015-2016, counter-respectively). Similarly, ER ranged from 53 to 504 gC $m^{-2}$ *per* season. The average GPP/ER ratio for the Mulga woodland was 1.1 ± 0.1 across all years

Annual total budgets of NEP and rainfall allowed me to estimate the precipitation values at which ecosystems changed from being a C source to a C sink (precipitation thresholds). This occurred when rainfall reached 262 mm $y^{-1}$ (Fig. 2.6; $r^2$= 0.93, $p$<0.05, CI: 95 %) at the Mulga woodland. In contrast, the *Corymbia* savanna had a precipitation threshold of 506 mm $y^{-1}$ ($r^2$= 0.63, $p$<0.05, CI: 95 %). The last year 2017 was the first year since the eddy covariance system has been operational at the *Corymbia* savanna site in which annual NEP was positive (115 gC $m^{-2}$ $y^{-1}$) and the Mulga woodland had larger NEP (217 gC $m^{-2}$ $y^{-1}$) than in the global land sink anomaly year (2010-2011) .

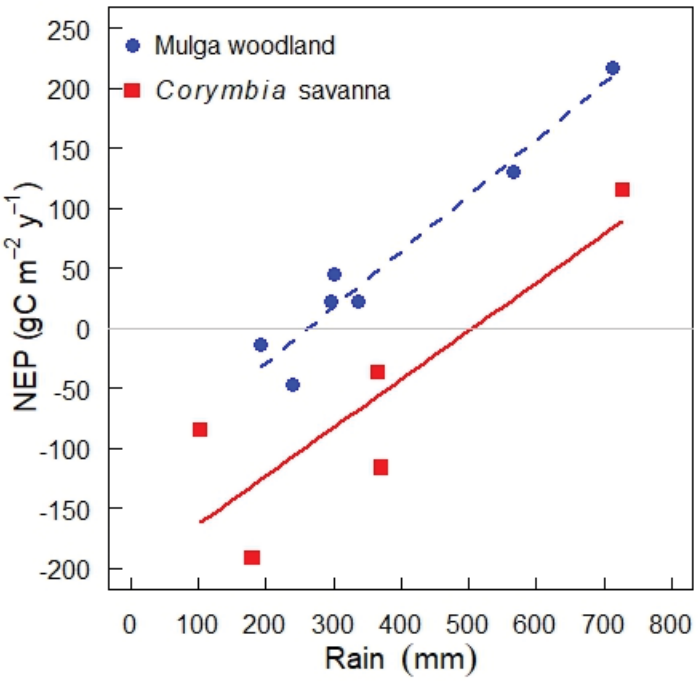


Figure 2.6 Net ecosystem production and total annual precipitation. The data points are the total annual net ecosystem production for the Mulga woodland ($r^2$= 0.93, $p$-value <0.05, CI: 95 %), and *Corymbia* savanna ($r^2$= 0.63, $p$-value <0.05, CI: 95 %).

### 2.3.3.4 Monthly and diurnal comparisons of water and carbon fluxes

Monthly averages for daily C and water fluxes are presented in figure 2.7, these reveal the inter-annual variability of both fluxes in both ecosystems. The largest NEP value in the Mulga

woodland was observed during the hydrological year 2010-2011 whilst the largest NEP for the *Corymbia* savanna occurred in 2013-2014 and 2014-2015 (Fig. 2.7a, b). Maximum mean daily NEP occurred between January and March in both sites. There were three exceptions in which NEP had negative instead of positive values during the wet season: January 2012 and 2014 in the Mulga woodland and January 2013 in the *Corymbia* savanna. The year with the largest mean daily GPP was 2010-2011 at the Mulga woodland, in which GPP was > 4 gC $m^{-2}$ $d^{-1}$ from September to May (Fig. 2.7c).

The driest hydrological year 2012-2013 exhibited the lowest variability in NEP in both ecosystems (Fig. 2.7a, b). In that dry year, NEP was positive in 5 months (0.1 ± 0.07 gC $m^{-2}$ $d^{-1}$) and negative in the remaining seven months (-0.2 ± 0.11 gC $m^{-2}$ $d^{-1}$) at the Mulga woodland. By contrast, there were no months when NEP in the *Corymbia* savanna was positive that year.

Average daily ET increased as expected during the wet season in both ecosystems and declined during the dry season (Fig. 2.7d, e). Maximum mean daily ET was observed in ~Jan-Mar (>1.4 mm $d^{-1}$) in all years except 2012-2013, when maximum ET occurred in December 2012 (1.2 ± 0.8 mm $d^{-1}$ at the Mulga woodland and 1.8 ± 0.8 mm $d^{-1}$ at the *Corymbia* savanna).

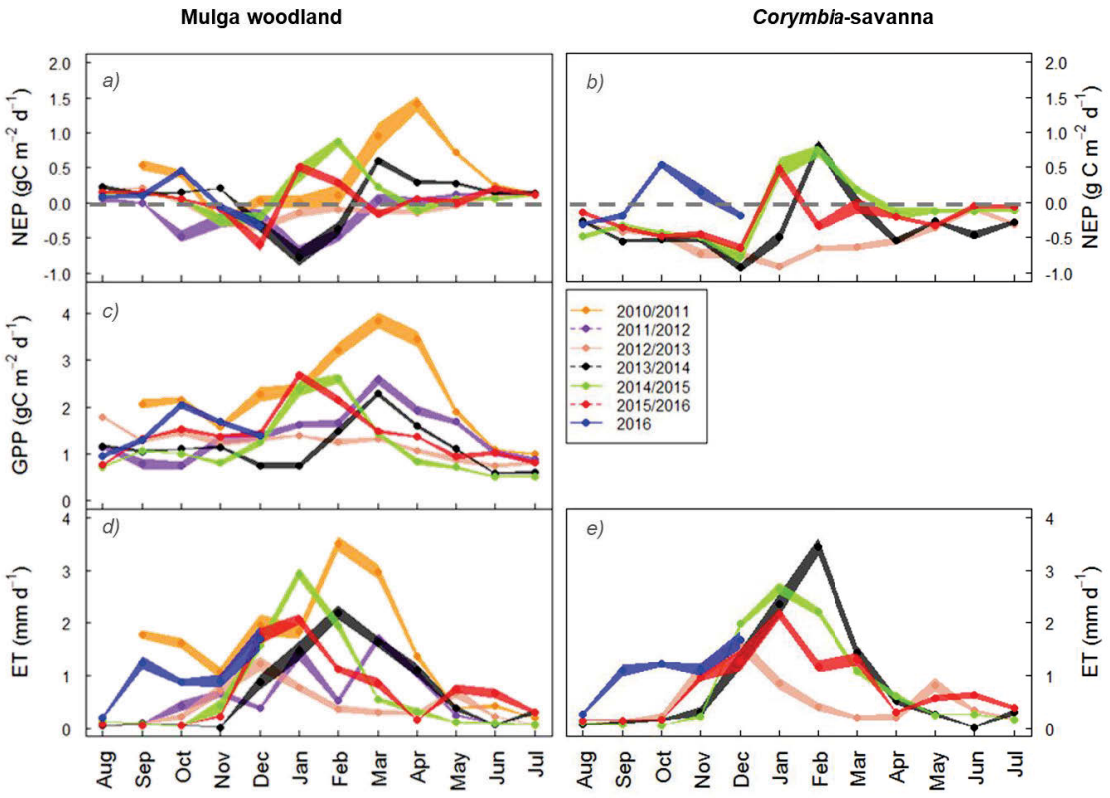


Figure 2.7 Seasonal cycles of NEP, ET and, GPP across hydrological years. Dots are daily averages of daily sums averaged across all days for each month. Thickness of shadow lines illustrates ± 1SE.

Figure 2.8 shows diurnal cycles of mean C and water fluxes (example wet and dry hydrological years are presented). There was minimal variation in NEP across the day in the two ecosystems in the dry year (2012-2013), with values close to zero throughout the day and night (Fig. 2.8e, m), whereas in a wet year (2010-2011) monthly average NEP reached *ca*. 8 and 4 μmol $m^{-2}$ $s^{-1}$ for the Mulga and *Corymbia* savanna respectively (Fig. 2.8a,i). To some extent, ET showed variability even during the dry year between 10:00 h and 15:00 h, ET was <0.10 mm $h^{-1}$ compared to the wetter year, when ET > 0.1 mm $h^{-1}$. Both NEP and ET had maximum values in the middle of the day between 10:00 h and 15:00 h in both ecosystems during the wet season. NEP and ET declined after 15.00 h as $T_{air}$ and VPD reached their mid-afternoon maxima (~14:00-15:00 h).

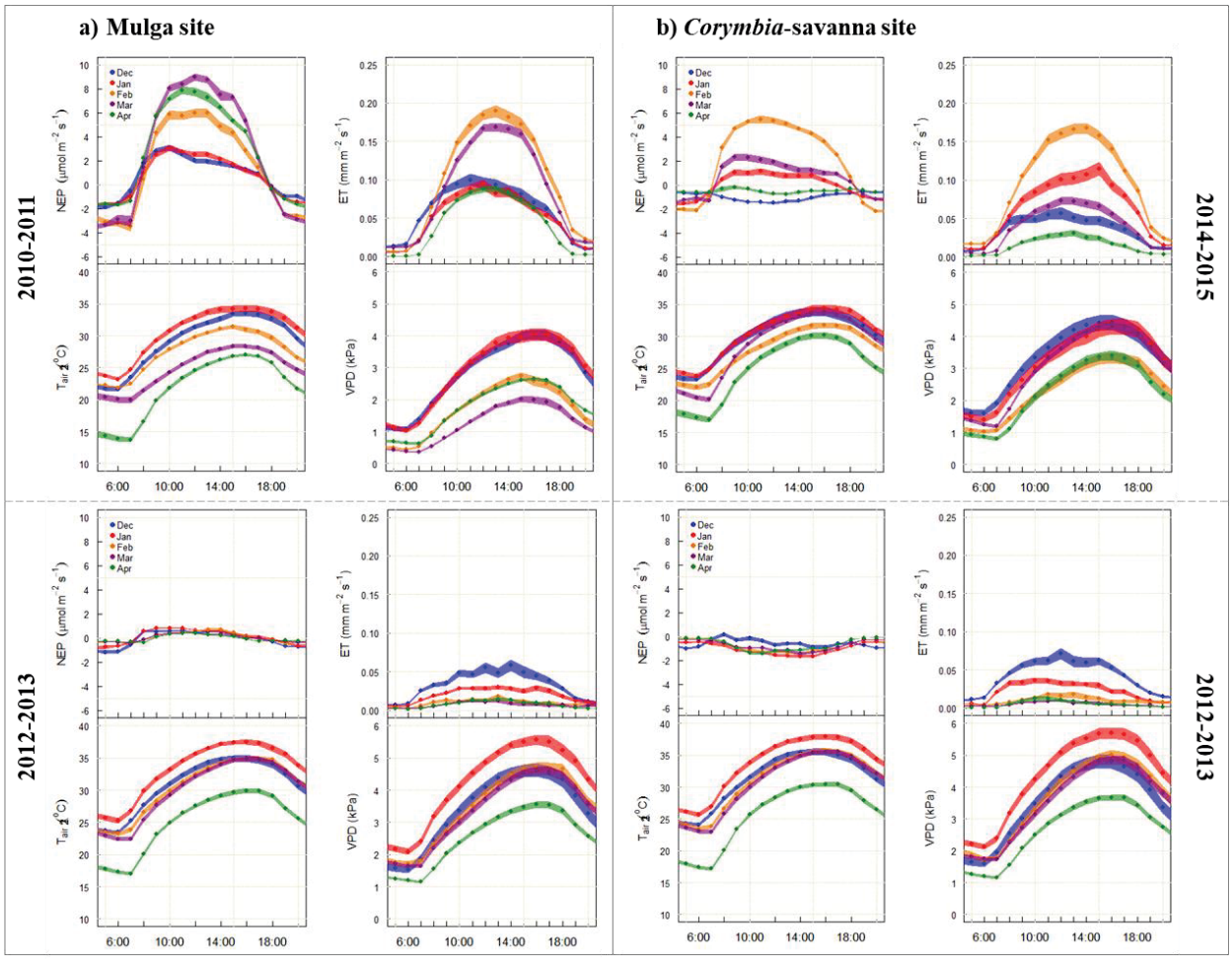


Figure 2.8 Diurnal cycle of NEP (μmol $m^{-2}$ $s^{-1}$), ET (mm $h^{-1}$), air temperature (°C) and, VPD (kPa) during wet months (Dec-Apr). Left set of panels correspond to the Mulga woodland (a very wet-year in the upper panel, a representative dry-year in the lower panel). The right sets of panels correspond to the *Corymbia* savanna. Data points are hourly averages for days at each month. Thickness of shadow lines illustrates ±1SE.

### 2.3.4 Responses of NEP, GPP and ET to climatic factors and SWC

Path analysis revealed correlations of NEP, GPP and ET with meteorological variables in both ecosystems (Figs. 2.9 and 2.10). To have an overview of the growing season, an analysis of all wet seasons (~Oct – May) are presented in figure 2.9. Within the Mulga woodland, ET was most strongly and positively correlated with SWC and LAI while NEP was most strongly and positively correlated with LAI and ET (values > 0.5; Fig. 2.9a). NEP of Mulga was negatively correlated with both SWC and $T_{air}$. VPD was strongly and positively correlated with $T_{air}$. GPP was positively and most strongly correlated with ET; it was also positively but less strongly correlated with LAI and PAR (Fig. 2.9b). GPP of the Mulga woodland was negatively and weakly (-0.11) correlated with $T_{air}$.

The standardized partial correlation coefficients for the Mulga woodland and *Corymbia* savanna sites for three different periods are shown in figure 2.10: dry seasons (D), early wet seasons (S) and mid-to-late (M) wet seasons for the 6.3 and 4.5 years of available data. By differentiating between these three periods, changes in the effect of the various drivers (e.g. LAI, SWC, $T_{air}$ and PAR) on ET, GPP and NEP were identified.

Within the *Corymbia* savanna NEP was most strongly and positively correlated with ET, and positively but less strongly correlated with LAI (Fig. 2.9c). As was observed in the Mulga, NEP in the *Corymbia* savanna was negatively correlated with SWC and $T_{air}$ ET of the *Corymbia* savanna was positively and strongly correlated with LAI and SWC but in contrast to the Mulga, ET of the *Corymbia* site was positive correlated with $T_{air}$ (0.36).

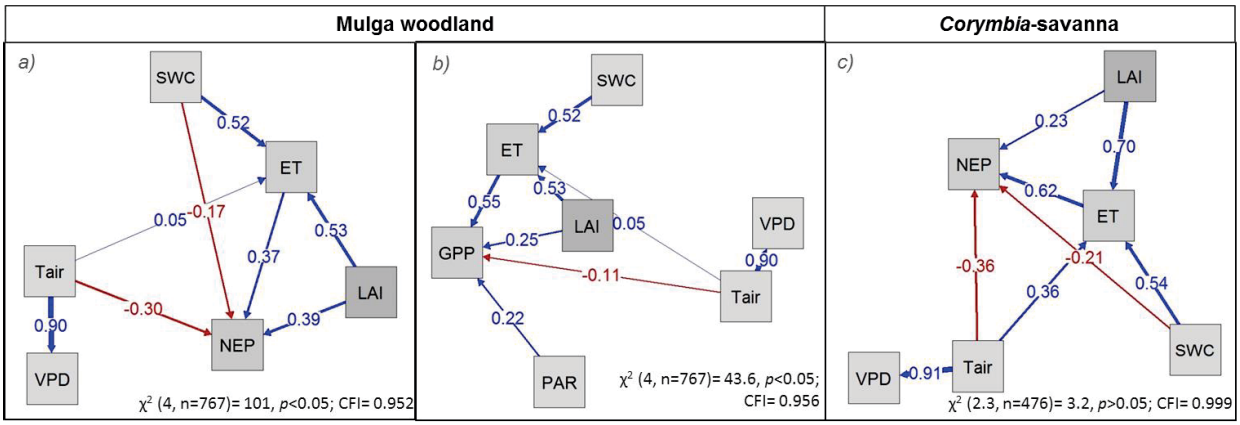


Figure 2.9 Path diagrams illustrate the effect of different climatic variables and SWC on a) NEP, ET and b) GPP at the Mulga woodland and, c) NEP and ET at the *Corymbia* savanna. The path strengths were plotted with the standardized correlation coefficients, where blue arrows are positive correlations and, negative correlations in red ($p$<0.001). Data represent the ecosystem behaviour using daily measurements only during the wet seasons (~Oct-May) across all years.

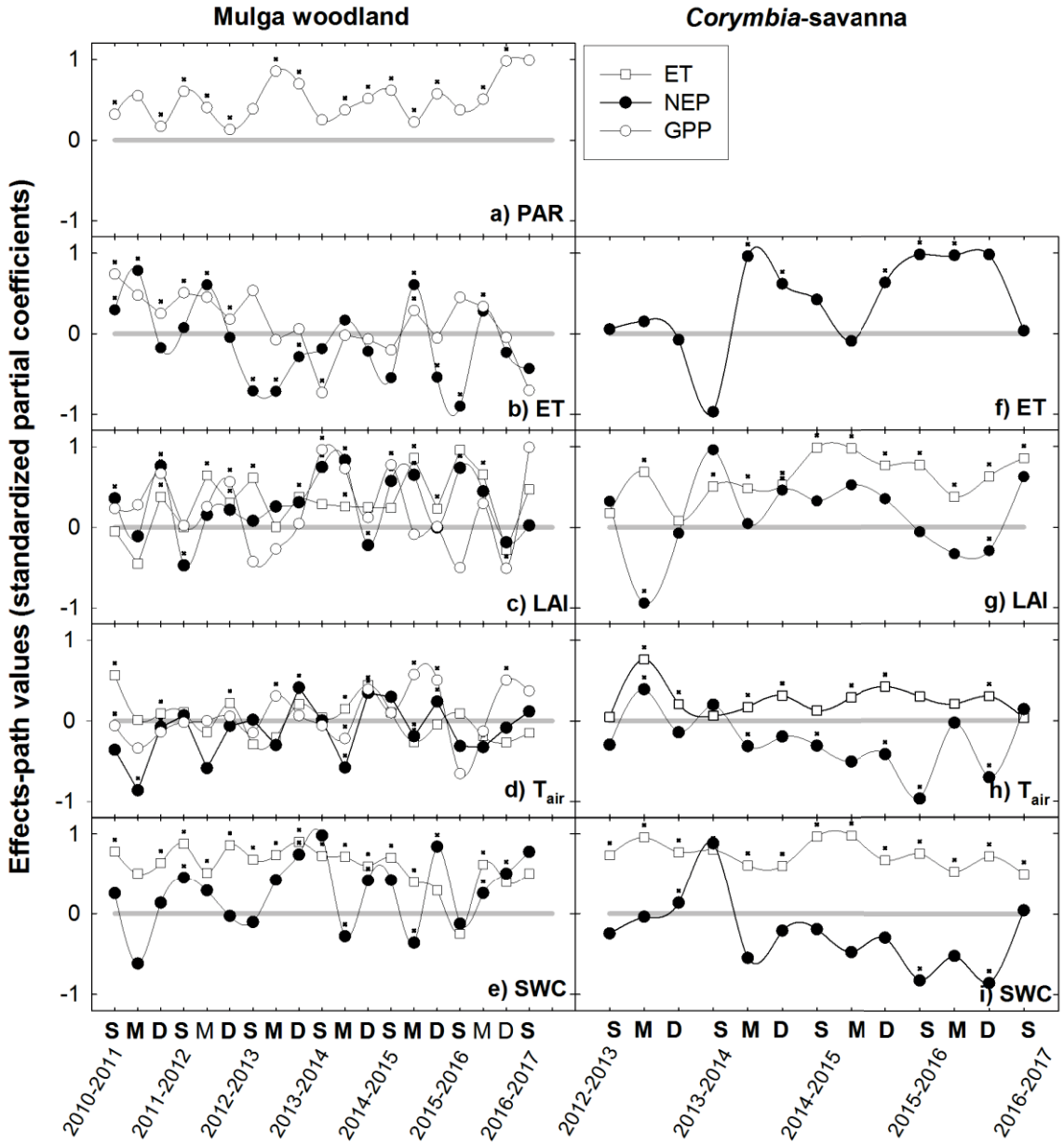


Figure 2.10 Standardized partial correlation coefficients of SWC, $T_{air}$, PAR, LAI and ET, from path analysis. Large positive or negative values represent strong sensitivity on the target flux (ET, NEP or GPP). In the *x*-axis, S indicates the early wet seasons, M mid-to-end of the wet season and, D is the dry season (bold, highlighted letters S, D and M on the *x*-axis indicate that path-models were statistically significant by $\chi^2$ (*p*-value >0.05) and CFI ≥ 0.95. Dots above individual symbols indicate significant correlations (*p*-value < 0.05).

For the Mulga woodland, GPP was consistently and positively correlated with PAR across all three periods (Fig 2.10a) and all years. Similarly ET was consistently and positively correlated with SWC across 18 of the 19 periods (Fig. 2.10e). In addition, GPP, ET and NEP in the Mulga woodland were all predominantly positively correlated with LAI, with occasional non-correlation or moderate negative correlations observed at different periods (early wet season,

mid-to-late, dry) in different years for each of the three fluxes (ET, GPP, NEP). $T_{air}$ tended to have little explanatory power for ET (standardized partial coefficients close to zero) and its impact on NEP and GPP was also small-to-moderate and varied between having a positive and negative correlation across the 19 time-periods.

For the *Corymbia* savanna, ET and NEP tended to be strongly and positively correlated, although one period (early wet season of 2013-2014) showed a strongly negative correlation (Fig. 2.10f). ET was predominantly positively and strongly correlated with LAI across all three time-periods across all years. However, the effect of LAI on NEP varied between strongly negative and strongly positive at different periods in different years (Fig. 2.10g). As was observed for the Mulga woodland, $T_{air}$ tended to have little explanatory power for ET (standardized partial coefficients close to zero), although occasionally (4 of 13 time-periods) moderate-to-large negative correlations between $T_{air}$ and NEP were found in the *Corymbia* savanna. As was observed for the Mulga woodland, SWC had a strong and positive impact on ET in the *Corymbia* savanna (Fig. 2.10i), but unlike the Mulga woodland, SWC had a predominantly (9 of 13 time-periods) negative impact on NEP of the *Corymbia* savanna.

## *2.4 Discussion*

Climatic drivers play an important role in determining the magnitude of carbon and water fluxes in terrestrial ecosystems (Cubasch *et al.*, 2013). This study evaluated the effect of climatic drivers on NEP and ET for all years of observed data, derived from the eddy covariance method. The two disparate central Australian ecosystems, the Mulga woodland and the *Corymbia* savanna, exhibited large differences in patterns and rates of NEP and ET year-to-year and seasonally (Figs. 2.2, 2.3; Table 2.2), and showed large inter-annual variability, particularly in NEP during the 6.6 and 4.5 years of observed data (Fig. 2.6). Seasonal and inter-annual variability in the carbon budgets are linked to different climatic drivers such as temperature, VPD, solar radiation, and water availability. Here, it was found that the effect on NEP and ET caused by several climatic drivers varied year-to-year and across different dry and wet seasons (Fig. 2.10). These effects will be discussed in detail in the following sections.

### 2.4.1 Carbon and water fluxes compared across ecosystems

Semi-arid ecosystems have been gaining attention due to their important contribution to inter-annual variability of the global carbon cycle (Poulter *et al.,* 2014; Ahlström *et al.,* 2015). Annual NEP ranged from 217 to -47 gC $m^{-2}$ $y^{-1}$ in the Mulga woodland and 115 to -190 gC $m^{-2}$ $y^{-1}$ at the *Corymbia* savanna (Fig. 2.6). The Mulga woodland switched inter-annually from C source to C sink and the *Corymbia* savanna was for two seasons a C sink and closed with a positive NEP budget for the first time of observed data in 2017 (Table 2.2; Fig. 2.6). Semi-arid ecosystems worldwide have shown this ability to switch from C source to C sink (Biederman *et al.*, 2016; Jia *et al.*, 2016; Ma *et al.*, 2016a). In the Southwest semi-arid region in North America the NEP of various biomes oscillate from -355 ± 108 to 326 ± 75 gC $m^{-2}$ $y^{-1}$ (Biederman *et al.*, 2017) and the semi-arid shrubland in China, NEP ranges from 77 to -22 gC $m^{-2}$ $y^{-1}$ (Jia *et al.*, 2016).

This study has identified, for the first time, the precipitation-threshold (pivot-point) at which the two ecosystems switched from a C source to a C sink (Fig. 2.6). The pivot-point for the Mulga woodland (262 mm $y^{-1}$) is in the range observed in other semi-arid ecosystems. Scott *et al.* (2015) reported pivot-points of <300 mm annual rainfall for a grassland ecosystem and >300 mm for a savanna ecosystem, values that are similar to that observed for a grassland in China with *ca.* 300 mm as a pivot point (Chen *et al.*, 2013). In contrast, the *Corymbia* savanna (which behaved as a C source for 4 out of 5 years) had a larger pivot-point (506 mm $y^{-1}$) than the Mulga woodland (262 mm $y^{-1}$). Negative NEP at the *Corymbia* savanna may be explained by the large influence of solar radiation and high temperature on photo- and thermal-degradation of

senescent dried vegetation accumulated during the wet year of 2010–2011. These processes play an important part in the decomposition of accumulated litter, especially that derived from spinifex grass (Cleverly *et al.,* 2016c; Fig. 2.1b). Further studies are needed to conclusively establish the effect of photo- and thermal-degradation at the *Corymbia* savanna.

The semi-arid region of central Australia experiences long dry seasons in autumn/winter and regular summer wet seasons (Figs. 2.2a, 2.3a). The start of the wet season most frequently occurred in October or November. Variations in annual rainfall were large because of the influence of the wet hydrological year (2010-2011, 565 mm) and the subsequent dry years with 60 % less annual rainfall (2012-2013 <193 mm). This variability in rainfall is the result of the interactions of three different climate modes: the ENSO (El Niño-Southern Oscillation), the Indian Ocean dipole and the southern annual mode (Cleverly *et al.*, 2016a), all of which are affected by climate change (Cai *et al.*, 2013; Cubasch *et al.*, 2013).

In the present study, ET accounted for >70 % of annual rainfall at the Mulga woodland and up to 106 % at the *Corymbia* savanna (Table 2.2). Due to the negligible slope across the landscape, and the fact that rainfall was generally of low intensity (90 % of rainfall events were of < 20 mm per event), runoff from the EC sites was unlikely to be significant. However, the excess of rainwater presumably contributed to the groundwater recharge, although it has been shown this occurs only after intense rainfall events >100 to 200 mm/month (Harrington *et al.*, 2002). The *Corymbia* savanna showed larger annual rates of ET (9-23 % larger than Mulga-woodland). This difference may be attributed to the larger extent of bare soil at the *Corymbia* savanna than the Mulga woodland and because of access to groundwater by *Corymbia opaca* trees at the savanna site (but no access by vegetation to groundwater at the Mulga site; Cleverly *et al.*, 2016c; O'Grady *et al.*, 2006). Year-round access to groundwater by *Corymbia opaca* may partially explain the extra evapotranspiration (307 mm) in 2013-2014 compared with total annual precipitation (290 mm). The potential for a carry-over of rainfall from the previous hydrologic year is presumably small given that 2012-2013 received less than the long-term average annual rainfall.

### 2.4.2 Vegetation responses to water availability

Initially, rainfall triggered increased carbon and water fluxes at the start of the wet seasons (Figs. 2.2, 2.3) but additional factors (i.e., SWC, temperature and VPD) acted to moderate NEP and ET. Water availability is determined by SWC within the rooting zone (assuming no input from groundwater or from below the hardpan; Cleverly *et al.,* 2016b). SWC was highly variable depending on the amount of rain and the size and frequency of individual rainfall events (Figs.

2.2c, 2.3c). SWC tended to be slightly larger at the Mulga woodland than the *Corymbia* savanna and several factors may contribute to explaining this. Rainfall events between 6–20 mm were 16 % more frequent at the Mulga woodland (Fig. 2.2a) than at the *Corymbia* savanna. These size of events are more likely to be either intercepted by the canopy, litter layer and lost to evaporation (Owens *et al.*, 2006) than infiltrate down through the soil profile. However, stem flow, which can contribute significantly to SWC at the base of trees, depending on canopy and leaf morphology (Eamus *et al.*, 2006; Pressland, 1973), concentrates water in the soil at the base of Mulga. This occurs because of Mulga generally vertical morphology and long and narrow phyllodes, and the canopy area exposed to interception of water is large (Pressland, 1973). The canopy of individual trees at the Mulga woodland is wider and more closed than that at the *Corymbia* savanna (Fig. 2.1a), and soil texture is slightly higher in clay at the Mulga than at the *Corymbia* savanna (Cleverly *et al.,* 2016c). All these factors might explain the larger SWC values recorded at the Mulga woodland with the *Corymbia* savanna.

Path analyses showed a strong positive effect of SWC on ET at both sites (Fig. 2.10e, i). SWC and ET increased immediately with the arrival of rainfall (Figs. 2.2, 2.3), even when data were excluded for the 2 days immediately following rainfall. At the start of the wet season, NEP decreased (i.e., ER> GPP) following early rains due to the influence of large rainfall events on SWC and increased ER (Figs. 2.2, 2.3). Therefore, when using the entire wet season data for all years in path analyses there was a negative effect of increasing SWC on NEP on average across all growing seasons (Fig. 2.9a, c). However, when wet seasons were divided into two periods: the start and the mid-to-end of the wet season; there was much more variability in the effect of SWC on NEP (Fig. 2.10e, i), which is now discussed.

The large ER as SWC increased at the Mulga woodland with the arrival of rainfall following the dry season was associated with increased growth (as evidenced through increased EVI) and and therefore increased growth respiration as vegetation responded to the increased availability of soil water. Much of this growth was the result of large increases in grass and herb cover in the understory (Eamus *et al.,* 2013). The efflux of C (-NEP) into the atmosphere via ecosystem respiration (a combination of soil respiration and growth respiration) and microbial breakdown of litter, and degassing of $CO_2$ from the soil profile (Chapin *et al.,* 2006), explains the negative effect of SWC on NEP. Carbon efflux upon the arrival of the earliest rainfall events was consistent in both ecosystems (Figs. 2.2d, 2.3d; see arrows). Increases in soil moisture causing an increase in soil $CO_2$ efflux has been observed among different ecosystems, including arid grasslands (Thomey *et al.*, 2011; Vargas *et al.*, 2012), temperate deserts (Wu *et al.*, 2015) and deciduous semi-arid ecosystems (Perez-Ruiz *et al.*, 2010).

Following large rainfall events, SWC remained large and this supported large rates of understory and overstory photosynthesis. Concomitant increases in heterotrophic respiration (Thomey *et al.*, 2011), combined with a possible re-degassing of soil $CO_2$ may explain peaks in ER during the wet season (Fig. 2.4). Vargas *et al.* (2012) found in arid grassland that high soil $CO_2$ efflux was influenced by rainfall event size rather than rainfall frequency. However, further and more sophisticated studies with automated measurements of soil $CO_2$ efflux such as respiration chambers or isotopic methods are needed to better characterise the various components of $CO_2$ efflux (Cueva *et al.*, 2015; Kuzyakov and Gavrichkova, 2010; Pataki *et al.*, 2003), especially in the *Corymbia* savanna which has been a persistent carbon source, except for 2017.

The wettest year observed at the Mulga woodland (2010-2011) that induced high biomass production as suggested with EVI (Fig. 2.2d) was followed by a year with lower-than-average rainfall in 2011-2012. The effect from a wetter-year to a lower-than-average rainfall was likely to induce heterotrophic respiration, thus negative NEP or large values of ER were observed in 2011-2012, because of the breakdown of stored litter that was accumulated in the wetter-than-average year (2010-2011). Larger heterotrophic respiration rates likely occurred following the productive year, when the above-average GPP triggered an accumulation of litter (Shen *et al.*, 2016). The legacy effect from year-to-year has been observed in other semi-arid ecosystems (Shen *et al.*, 2016).

In contrast to the transition from a wetter-than-average year to a drier-than average-year (as discussed above when comparing 2010-2011 with 2011-2012), the comparison of a drier-year-than-average year (2012-2013) with a wetter-than-average year (2015-2016; Fig. 2.4c), demonstrates the resilience and large capacity of the ecosystem. The Mulga woodland had a rapid and positive response to the larger-than-average rainfall of 2015-2016 despite the drier-than-average year preceding this hydrological year. Between this two wetter- and drier- years (2012-2013 and 2015-2016), the hydrological years 2013-2014 and 2014-2015 had lower-than average annual rainfall 295 mm $y^{-1}$ and 301 mm $y^{-1}$ respectively, thus NEP was -14 gC $m^{-2}$ $y^{-1}$ for the former and 23 gC $m^{-2}$ $y^{-1}$ for the hydrological year 2014-2015.

As ecosystems transited from wet to dry seasons, and depending on the volume of accumulated rainfall, soil moisture content declined relatively smoothly (see SWC values from May to Aug months in figures 2.2c and 2.3c). A slow dry-down of soil water lead to a short-legacy of the wet season into the dry season, resulting in the maintenance of a positive NEP. For example, NEP was positive even during periods when there was no rainfall for up to *ca.* 4 months (2011-2012) and *ca.* 2 months (2014-2015) at the Mulga woodland (Fig. 2.2c, d).

Similarly, this was observed at the *Corymbia* savanna, but only for *ca.* 2 months during the two years when the *Corymbia* savanna behaved as a C sink (2014–2015 and 2016–2017; Fig. 2.3c, d; Table 2.2). This legacy effect allowed both ecosystems to maintain positive NEP into the start of the dry season. This extended production after the end of the wet season has similarly been observed in other semi-arid ecosystems, including temperate semi-arid shrublands in northern China (Jia *et al.*, 2016).

NEP can remain positive with decreasing SWC after the wet season because plant species dominating these two Australian ecosystems are highly adapted to low SWC. Although Mulga species have shallow roots that mainly draw from SWC at <1.2 m soil depth (Cleverly *et al.*, 2016b; O'Grady *et al.*, 2009); leaf-scale studies have demonstrated that Mulga are very anisohydric and can maintain open stomata despite experiencing low water potentials (see Chapter III; Nolan *et al.*, 2017a) and due to foliar osmotic adjustments as SWC declines (O'Grady *et al.*, 2009; Warren *et al.*, 2011). The adaptations of Mulga species to arid conditions may explain sustained productivity in the Mulga woodland, even as SWC declined at the end of the wet season. By contrast, the *Corymbia* savanna is dominated by spinifex (a C4 grass) and *Corymbia opaca* trees which invest in a deep roots to access deep soil water and groundwater (O'Grady *et al.*, 2009). Likewise, spinifex is a highly drought tolerant grass which maintains low levels of photosynthetic activity through the winter dry season (Grigg *et al.,* 2008). However, the efflux of $CO_2$ through photo- and thermal-degradation of leaf litter, especially spinifex litter, significantly influenced NEP and consequently NEP was rarely positive at the *Corymbia* savanna.

Contrasting vegetation composition at the two sites resulted in significant differences not only in rates and patterns of carbon and water fluxes, but also for EVI (Figs. 2.2d, 2.3d). Seasonal peaks in vegetation greenness coincided with periods of increased temperature and SWC in both ecosystems. Consequently, ET and NEP were positively correlated with LAI in both ecosystems and also with GPP at the Mulga woodland (Fig. 2.9). Enhancements in vegetation greenness are correlated with increased vegetation biomass, particularly through increased leaf area index (Huete *et al.*, 2002). During the wet season, LAI increased because leaves of trees become fully expanded and because there is a growth of new foliage (Richardson *et al.*, 2013; Xu *et al.*, 2016), and herbs and grasses underwent significant rapid germination and growth in the understory (Eamus *et al.*, 2013). Many studies have demonstrated that increasing soil water in arid and semi-arid regions has a positive impact on plant growth, in particular, increases in LAI and EVI that can be observed from MODIS-satellite data (Flanagan and Adkinson, 2011; Peng *et al.*, 2017; Shi *et al.*, 2017).

### 2.4.3 Temperature and VPD influence ecosystem productivity

Ecosystem productivity through gross primary production (total photosynthesis of an ecosystem) is not only limited by water availability; temperature and VPD can also exert strong influences on photosynthesis through the temperature dependency of carboxylation and electron transport (Farquhar *et al.*, 1980) and through effects on stomatal conductance (Duursma *et al.*, 2014). Similarly, ecosystem respiration (ER) is strongly dependent on temperature when not limited by water availability (Adair *et al.*, 2011; Janssens *et al.*, 2001). The link between GPP and ER to changes in temperature determines the strength of the effect of $T_{air}$ on NEP (NEP = GPP – ER). The effect of $T_{air}$ on NEP varied from positive to negative effect of at the start of the wet seasons and during the dry seasons (Fig. 2.10d, h). The two semi-arid ecosystems had mainly a positive response in NEP to the increase in temperature from winter to summer (i.e., during the early wet season and the dry season; Figs. 2.2, 2.3). However, high temperature generally caused negative effects on NEP during the wet season in both ecosystems (Fig. 2.9a, c). Although temperate ecosystems are more sensitive to increasing temperatures than tropical and semi-arid ecosystems (Huxman *et al.*, 2003; Keenan *et al.*, 2014; Wang *et al.*, 2016), the reduction in NEP as temperature increased might reduce the C sink strength of these two Australian ecosystems in response to future climate change-induced increase in mean daily temperatures. Similar results of warm temperatures causing a negative effect on NEP were found in semi-arid southwestern North America (Biederman *et al.*, 2017), and modelling studies have forecast a decrease of NEP with climate warming, resulting from a shortening of the growing season (Grant *et al.*, 2012).

Diurnal analyses of water and carbon fluxes showed a strong decline in ET and NEP once maxima of VPD and $T_{air}$ were reached (Fig. 2.8). Air temperature was positively correlated with VPD and ET because VPD increases as a fourth-power of temperature at a constant humidity (Breshears *et al.*, 2013) and soil temperature increases soil evaporation. Both soil moisture supply and VPD affect ET and vegetation productivity (Novick *et al.*, 2016; Zhou *et al.*, 2017). For example, stomata respond to transpiration rates known as the apparent 'feed-forward response', implying that transpiration strongly decreases at high VPD (Duursma *et al.*, 2014). However, transpiration increases with VPD due to increase of evaporative atmospheric demand, but as VPD and transpiration continue to increase, this causes a decline in leaf water potential and induces stomatal closure. When stomata close, vegetation no longer assimilates C, and this is when semi-arid Australian ecosystems are more likely to switch from a C sink to a C source.

## *2.5 Conclusions*

The aim of this study was to compare and contrast patterns and controls of carbon and water fluxes at different time-scales in two semi-arid ecosystems of central Australia. The precipitation threshold at which these ecosystems switched from C source to C sink were also identified. Additionally, this study contributes to our understanding of the effect of the key drivers of patterns in GPP, NEP and ET and how these varied within-and-between seasons across two disparate ecosystems.

Path analysis was a valuable tool to identify the relative importance of different drivers affecting carbon and water fluxes in the two central Australian ecosystems. Due to the arid conditions of these sites, rainfall was the first major driver that triggered changes in GPP, NEP and ET as observed with the influence of SWC on these fluxes. Summer rainfall along with high temperature and low VPD at the end of the wet season, all contribute to the observed increase in NEP during the wet season. However, a negative effect of higher temperatures on NEP was identified within the wet season, with warmer conditions negatively affecting NEP in both ecosystems.

Slow-controls of the C cycle (i.e., photo and thermal-degradation) are likely to considerably affect the carbon balance of the *Corymbia* savanna, and this may explain the C source behaviour evidenced from application of the EC method to this site. Although, an exceptional year was observed in 2017 in which NEP closed with 115 gC $m^{-2}$ $y^{-1}$ with 728 mm of annual rainfall, this allowed the estimation of the precipitation-threshold at which the *Corymbia* savanna switched from C source to C sink. Further studies are needed in order to partition ET and C fluxes, especially $CO_2$ efflux (i.e., partitioning of $CO_2$ efflux into abiotic decomposition and ecosystem respiration, which is further separated into heterotrophic and autotrophic respiration, and partitioning of ET into transpiration from plants and soil evaporation). The final conclusion of this study was that differences in vegetation composition, and the timing, amount and size of rain events affecting SWC, were the major determining factors that explain the contrasting differences in NEP and ET among the two ecosystems.

# *Chapter III*

## Seasonal changes in resource-use-efficiencies in five semi-arid co-occurring species of central Australia

## *3.1 Introduction*

An adequate supply of light, $CO_2$, water and optimization of the amount and activity of photosynthetic enzymes (for example Rubisco and the electron transport chain proteins within chloroplasts) can result in high photosynthetic rates (carbon gain). However, this comes at the "cost" of both investment of nitrogen and the "expenditure" of water as transpiration (Nobel, 2009). Resource-use-efficiency (RUE) can be used as a proxy to evaluate how plant species invest available resources to make more "profit" (i.e., C gain), at leaf-scales (Funk and Vitousek, 2007). RUE is analogous to the economic theory of "cost-benefit" analyses (Bloom *et al.*, 1985). RUE varies seasonally and spatially across ecosystems and plant functional types depending on the nature of the limiting resource (i.e., nutrients, light and water) and climate conditions (Garbulsky *et al.*, 2010; Han *et al.*, 2016; Moreno-Gutierrez *et al.*, 2012).

The wet season is usually considered a period of relatively high resource abundance in arid and semi-arid ecosystems (compared to the dry season; Austin *et al.*, 2004; Schwinning and Sala, 2004). A cascade effect occurs when water becomes more readily available, typically in the summer season in northern and central Australia. This is because moisture stimulates ecological processes, including nutrient release by microbial activity followed by nutrient uptake by roots, in plant communities and soil (Cleverly *et al.*, 2016b; Huxman *et al.*, 2004b). In wet periods plants increase carbon (C) assimilation (*A*) through photosynthesis; simultaneously, transpiration rates are larger because soil water contents are larger (Scott *et al.*, 2006), and therefore stomatal conductance is larger.

One may hypothesize that when water is relatively abundant in semi-arid environments, plants will become more productive, but other resources may become limiting, (i.e., light or nutrient supplies). During wet seasons, for example, increased levels of clouds reduce the amount of light reaching the top of canopies (Ryu *et al.*, 2008) and plants have to maximize the

efficiency of use of the most limiting resource (Bloom *et al.*, 1985). Within ecosystems, different plant species have evolved with contrasting physiological strategies to access resources and these allow different plant species to co-occur (Alvarez-Yepiz *et al.*, 2017; Nolan *et al.*, 2017a; Santini *et al.*, 2015). Niche separation theory provides a framework to explain the co-occurrence of competing species (Silvertown *et al.*, 2015). Species in semi-arid Australia have been shown to occupy different eco-hydrological niches, allowing species to co-occur (Nolan *et al.*, 2017a; O'Grady *et al.*, 2009).

A leaf with adequate supply of water will fix more $CO_2$ than a water-stressed leaf with closed stomata. Stomata play an important role in controlling rates of *A*, *E* and plant water status (i.e., foliar water potentials) in response to environmental conditions, including atmospheric water vapour pressure, light availability and soil water content (Duursma *et al.*, 2014; Eamus *et al.*, 2008; Sperry and Love, 2015). Water stress influences plant water potentials, thus leaf gas exchange and foliar water potentials are often correlated (McDowell *et al.*, 2008). Two physiological behaviours explain stomatal responses to declines in leaf water potential: isohydric and anisohydric behaviour. Isohydric species use rapid and early declines in $g_s$ to tightly regulate leaf water potentials in the early stages of soil desiccation, resulting in decreasing $A_n$ (Limousin *et al.*, 2013; Meinzer *et al.*, 2009; Nolan *et al.*, 2017a). In contrast, anisohydric species tolerate a larger decline of leaf water potentials, thereby allowing the maintenance of $g_s$ and $A_n$ further into very low values of soil water content. These two contrasting behaviours are two extremes in the water potential regulation through stomatal conductance, but in reality species fall along a continuum of behaviours (Klein, 2014).

Water-use-efficiency (WUE) defines the relationship between carbon uptake and water use by plants and ecosystems. At a leaf-scale, WUE explains the trade-off between photosynthesis and water loss (transpiration; *E*) through stomata. Instantaneous water-use-efficiency ($_{int}$WUE) is thus defined as the ratio of carbon assimilation to transpiration: *A/E* (Seibt *et al.*, 2008). Nevertheless, transpiration and photosynthesis are not the only determinants of $_{int}$WUE, because both *A* and *E* are influenced by stomatal conductance ($g_s$). Stomatal responses to the concentration of $CO_2$ inside the leaf air spaces ($C_i$) affect *A*, but $g_s$ also responds to transpiration rates (Eamus *et al.*, 2008, 2013). Consequently, another quantification of WUE, at the leaf-scale, is termed intrinsic ($WUE_i$) and is defined as the ratio of assimilation to stomatal conductance ($A/g_s$; Seibt *et al.,* 2008).

$WUE_i$ has been widely evaluated using different approaches, including analyses of carbon stable isotopes in plant tissue (i.e., leaf tissue, plant compartments, tree rings, organic and inorganic compounds) and direct gas exchange measurements with leaf chambers (Brienen *et*

*al.*, 2017; Cernusak *et al.*, 2013a; West *et al.*, 2007). While gas exchange measurements provide a real-time observation of $WUE_i$, analyses of carbon stable isotope content integrate at different time-scales depending on the plant tissue analysed. However, it is not clear which approach is most appropriate to predict seasonal variability of $WUE_i$ in semi-arid ecosystems with intermittent rainfall. Different evaluations of $WUE_i$ may contribute to understanding strategies of plant water-uptake, especially in co-occurring species that occupy different eco-hydrological niches (Rumman *et al.*, 2018). Previous studies have reported that moderate water stress increases $WUE_i$ but it decreases under severe water stress in a concave function (Limousin *et al.*, 2015; Manzoni *et al.*, 2011). Moderate declines in water availability can thus promote $WUE_i$, but this may not increase plant productivity and this may be exacerbated by decreases in the availability of other resources.

The relationship between net assimilation ($A_n$) and incident photosynthetically active radiation (PAR) can be represented in light response curves (Fig. 3.1; Chapin, 2002; Whitehead and Gower, 2001). Increasing light intensities from low-to-moderate levels increase net carbon assimilation ($A_n$) rates. At high light levels $A_n$ reaches an asymptote or may decline at light levels approaching full sunlight because of photo-inhibition/photo-oxidation. The threshold of low light intensity at which photosynthesis is equal to leaf respiration and, therefore $A_n$ is zero, is termed the light compensation point (LCP). Low light intensities below the LCP result in larger rates of $CO_2$ loss by respiration than carbon gain by photosynthesis, assuming that stomata are still open. Leaf dark respiration ($R_d$) is approximated as the *y*-intercept when $A_n$ is negative and light intensity is zero. Light saturation of photosynthesis occurs at intermediate-to-large rates of light supply and in practice, photosynthesis is limited by the supply of $CO_2$ rather than the supply of light. The quantum yield ($\phi$; μmol $CO_2$ $\mu mol^{-1}$ photons) of photosynthesis is the ratio of the moles of $CO_2$ fixed in photosynthesis *per* mole of quanta (photons of light) absorbed, and is a measure of the efficiency in which light is converted into fixed carbon.

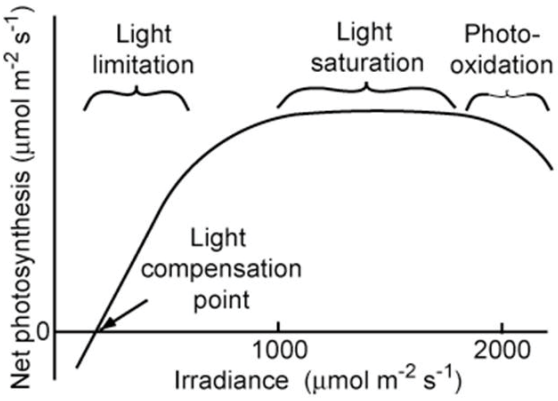


Figure 3.1 Light response curve. Relationship between net carbon assimilation ($A_n$) and, incident irradiance. Source, Chapin (2002)

The demand for carbon for growth and hence biomass allocation depends of the supply of carbohydrates and is limited by the balance between photosynthesis and plant respiration (Brandes *et al.*, 2006). Carbon-use-efficiency (CUE) is the ratio of assimilated carbon to structural biomass (Fernández-Martínez *et al.*, 2014; Frantz and Bugbee, 2005). When plants have optimal conditions for growth (i.e., water and nutrients), CUE is increases, this is that the C gained is allocated to growth (*per* unit C acquired) instead of the C that is lost as respiration (Bradford and Crowther, 2013). CUE is highly temporally variable depending on environmental conditions, ecosystem composition and stand age (DeLucia *et al.*, 2007). For example, high temperatures increase rates of plant respiration (when excluding thermal acclimation; Atkin, 2003) and this results in reduced CUE. In contrast, a large foliar nitrogen content (N) can increase CUE (Bradford and Crowther, 2013).

Foliar N is required to produce photosynthetic enzymes such as Rubisco, which accounts for *ca.* 25 % of all foliar nitrogen (Chapin, 2002). $N_2$-fixing species generally have large foliar N contents and foliar N is positively correlated with leaf mass *per* area (LMA= leaf dry weight/leaf area; Poorter *et al.*, 2009). A worldwide meta-analysis showed that LMA increases with decreasing rainfall (Wright *et al.*, 2004). LMA can decreases during periods of low water availability as a mechanism to reduce water loss (Poorter *et al.*, 2009). Additionally, a lack of N and subsequently low rates of photosynthesis leads to an accumulation of total non-structural carbohydrates, which may increase LMA, thus there is a covariation between leaf N and LMA (Poorter *et al.*, 2009; Wright *et al.*, 2004). Therefore, $A_n$, leaf area and foliar N concentration (as N *per* unit of leaf area ($N_a$; g N $cm^{-2}$)) define the photosynthetic nitrogen-use-efficiency (PNUE) which is the photosynthetic carbon gain *per* unit of N invested *per* unit leaf area (PNUE= $A_n/N_a$). PNUE generally declines with increasing leaf $N_a$ (Funk and Vitousek, 2007).

Analyses of resource-use-efficiencies (RUE= carbon assimilation *per* unit of resource) such as WUE, CUE, PNUE, and the efficiency in which light is converted into fixed carbon (quantum yield) contribute to our understanding of plant and ecosystem function. Moreover, RUE may be a determinant of plant survival and adaptation, since some species may be more efficient in using a specific limited resource than others (Ehrenfeld, 2003; Funk and Vitousek, 2007; Heberling and Fridley, 2013). The evaluation of RUE across different ecosystems and within ecosystems will lead to a better estimation of carbon budgets in terrestrial ecosystems and increase our understanding of the eco-physiological strategies employed by co-occurring species.

Semi-arid Australia is characterized by low mean annual rainfall with high inter-annual variability, high light intensity, nutrient-poor soils and low vegetation cover. These conditions limit several physiological functions of semi-arid vegetation to a short period year-to year. Consequently, plant species adapt their physiological traits in response to large seasonal changes in water availability (Gleason *et al.*, 2013). Several plant functional traits, such as leaf area and LMA, and several plant variables, such as pre-dawn and midday leaf water potentials and stomatal conductance, decrease during periods of low water availability (O'Grady *et al.*, 2009; O'Grady *et al.*, 2006; Page *et al.*, 2016). Indeed, declining pre-dawn water potential *per se* negatively impacts on stomatal conductance and rates of carbon and water fluxes (McDowell *et al.*, 2015).

Semi-arid Australia represent 70 % of the entire land surface, with dominant ecosystems including woodlands and savannas (Cleverly *et al.*, 2016c; Eamus *et al.*, 2013). Acacias dominate the woodland ecosystems, which cover 20-25 % of the continental land (Bowman *et al.,* 2008). Acacias may also occupy small patches in the savanna ecosystem (Cleverly *et al.*, 2016c). *Acacia spp.*, including the Mulga complex, have the ability to fix atmospheric $N_2$ (Cook and Dawes-Gromadzki, 2005; Page *et al.*, 2011). *Acacia* spp., along with *Hakea* spp., have shallow root systems, and possess specific features to withstand high light and low water availability (Groom *et al.*, 1994; Lamont, 1993; Page *et al.*, 2011).

Grasses dominate the understory in both Mulga woodland and savanna biomes, with *Triodia* spp. (a C4 grass) occupying extensive areas throughout the savanna ecosystems (Bowman *et al.*, 2007). Dominant tall trees are from the family *Myrtaceae* (i.e., *Eucalyptus spp.* and *Corymbia spp.*); both are tall deep-rooted trees known for accessing groundwater (O'Grady *et al.*, 2009; Rumman *et al.*, 2018). A set of contrasting physiological strategies allow these species to co-occur by occupying different eco-hydrological niches in semi-arid Australia (Nolan *et al.*, 2017a; O'Grady *et al.*, 2009; Santini *et al.*, 2015). Several studies on these genera in mesic northern

Australia have demonstrated that seasonality exerts control over plant physiological behaviour, including leaf gas exchange (Eamus *et al.*, 2000; Kelley *et al.*, 2007; Prior *et al.*, 2005). However, little is known about how resource-use-efficiencies differ and between co-occurring species in central Australia.

Previous studies on carbon assimilation and additional plant physiological traits have been conducted in semi-arid Australia, predominantly during the wet season, with few studies undertaken during the dry season (Nolan *et al.*, 2017a; O'Grady *et al.*, 2009). However, dry seasons occupy a large fraction of each year and hence a complete understanding of the ecophysiology of co-occurring species throughout the year is lacking. Furthermore, the majority of tree species in central Australia are evergreen, retaining leaves throughout the dry season. Consequently, the absence of detailed information concerning dry-season behaviour is particularly pertinent. In particular, we have limited information on resource-use-efficiencies across an entire annual cycle. Therefore, the aim of the present study was to compare seasonal variability of carbon, nitrogen, water and light-use-efficiencies across multiple co-occurring tree species in central Australia. In particular, I examined the following hypotheses:

1. During periods of declining soil moisture content (i.e., the dry season), $WUE_i$ will increase for all species examined and this will negatively correlate with leaf pre-dawn water potentials.
2. Assessing different evaluations of $WUE_i$ (such as carbon isotope discrimination and gas exchange) will reveal contrasting insights into plant $WUE_i$ depending on strategies of plant water uptake across species.
3. During wet seasons differences in light-use-efficiency and carbon-use-efficiency among species will be driven by contrasting physiological traits; species that have specific traits to tolerate high light intensities and low soil moisture content will be more efficient in their resource-use-efficiencies than species experiencing less exposure to water limitation and fewer adaptations to semi-arid conditions.
4. Variations in PNUE will be correlated with differences in LMA between species and $N_2$-fixing species that have large nitrogen content *per* leaf area and will have smaller PNUE compared with species that are not $N_2$-fixing.
5. Anisohydric species and isohydric species will exhibit contrasting carbon and stomatal conductance behaviours.

## *3.2 Methods*

### 3.2.1 Site and co-occurring species description

This study encompassed two sites at which four tree species and a grass species were examined. The sites are located in central Australia within the Ti-Tree basin, 180 km NW of Alice Springs (Figure 3.2). These two sites are representative of two major biomes of semi-arid Australia: 1) Mulga woodland; and 2) open savanna (*Corymbia* savanna). Both sites have eddy covariance (EC; Baldocchi, 2014) towers installed and are part of the OzFlux Network (http://ozflux.org.au/) and the Terrestrial Ecosystem Research Network (TERN). Both sites are at the same latitude -22.28 S (133.25 E and 133.64 E; Mulga woodland and *Corymbia* savanna sites respectively at 553 m asl). Several related eco-hydrological and eco-physiological studies have been conducted in these ecosystems (Cleverly *et al.*, 2016a; Eamus *et al.*, 2013; Nolan *et al.*, 2017a; O'Grady *et al.*, 2009; Santini *et al.*, 2015).

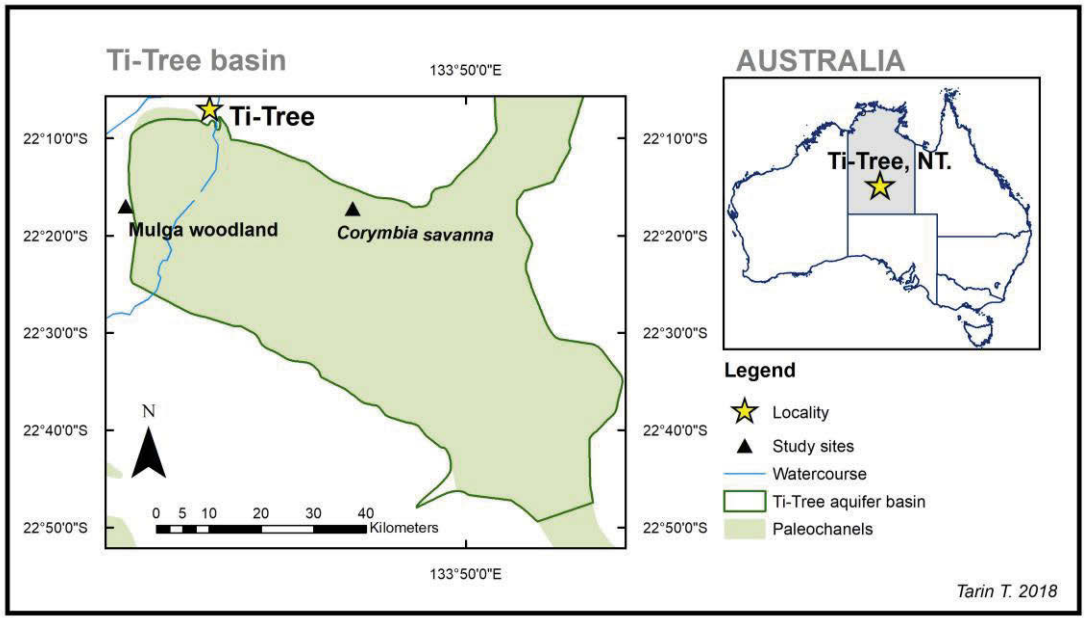


Figure 3.2 Study sites in semi-arid central Australia (shape files were taken from www.bom.gov.au/water/geofabric; Ti-Tree Palaeovalley site GIS; Geocat #74008). The black triangle is the location of the two eddy covariance towers and the study sites.

Annual average precipitation (1987-2017) at the nearest meteorological station (the Territory Grape Farm, BoM station 015643, elevation 566 m), located 17 km south of the *Corymbia* savanna site is 324 mm (www.bom.gov.au). Inter-annual rainfall is highly variable in this region and most of the annual precipitation (75 to 80%) falls during the Summer months of

November to February inclusive (Eamus *et al.*, 2013). Mean historical maximum temperature is 35 °C and 27 °C (wet and dry season respectively); mean minimum temperature varies from 20 °C to 9 °C (wet and dry season respectively; www.bom.gov.au). More details of the Mulga site are found in Cleverly *et al.* (2013a) and Eamus *et al.* (2013) and for the *Corymbia* savanna site in Cleverly *et al.* (2016c).

Sandy plains with low soil N and low organic carbon content dominate in central Australia. Climatic conditions are extremely similar at these two sites. However, vegetation composition and depth to the water table are dissimilar. Depth to groundwater decreases from ~50 m in the southwest and southeast corners of the Ti-Tree basin to less than 2 m in the north of the basin where groundwater discharges directly via evaporation and transpiration (Cook and Dawes-Gromadzki, 2005; Shanafield *et al.*, 2015). In the Mulga woodland, *Acacia aptaneura* and *Acacia aneura* (3 to 7 m tall) are the dominant species and are part of the Mulga complex (Maslin and Reid, 2012). At the Mulga woodland, depth to the water table is *ca.* 49 m. At the *Corymbia* savanna site depth to the water table is *ca.* 8-10 m and dominant species are: *Corymbia opaca* trees (8 to 20 m tall) and there is an understory of spinifex grass (*Triodia schinzii)* with occasional *Hakea* spp. (*H. macrocarpa* and *H. lorea*) and infrequent and widely dispersed *Acacia aptaneura* patches.

Three field campaigns were undertaken to sample across the annual cycle of dry and wet seasons: i) March-2015 (late wet season: 46 days after last precipitation event > 5 mm $d^{-1}$); ii) October-2015 (late dry season, 185 days since last precipitation event > 5 mm $d^{-1}$); and iii) February-2016 (middle of wet season: 7 days after last precipitation event > 5 mm $d^{-1}$). During all three campaigns leaf gas exchange and additional plant physiological measurements were made across four dominant tree species and one grass species. Phyllodes and leaf samples were collected (see below for details) for *Acacia* spp. (*A. aptaneura* and *A. aneura*), *C. opaca*, *H. macrocarpa* and *T. schinzii*. Meteorological conditions reported in this study were obtained from the eddy covariance tower located at the Mulga woodland.

### 3.2.2 Leaf water potentials

Predawn ($\Psi_{pd}$) and solar midday ($\Psi_{md}$) foliar water potentials were measured during the three field campaigns (n= 6 leaves *per* 4 trees *per* species). Additionally, diurnal foliar water potentials ($\Psi_{leaf}$; n= 4 leaves *per* 4 trees *per* species) were measured in March-2015 and February-2016 at 2 hour intervals to synchronize with diurnal surveys of leaf gas exchange (rates of photosynthesis, transpiration and stomatal conductance) measurements (see details below). For pre-dawn measurements, fully expanded healthy leaves / phyllodes were excised

before sunrise, between 05:00 h and 06:00 h and immediately placed in Ziploc bags, sealed, and stored in the dark. Leaves were measured within one hour of excision using a Scholander-type pressure chamber (PMS Instruments, Albany, OR, USA).

### 3.2.3 Leaf gas exchange

Diurnal surveys of leaf gas exchange were made from 07:00 to 16:00 h in summer (Mar-2015 and Feb-2016), but to 14:00 h in Oct-2015, at 2 hour intervals. An infrared gas analyser (IRGA) system (Li-6400XT, Li-Cor Inc., Lincoln, NE, USA) coupled to a 2 x 3 cm broadleaf chamber (6400-02B LED Light Source; Li-Cor Inc.) was used. For each measurement, one leaf / phyllode from four plants *per* species were measured. Due to differing sizes of the leaves / phyllodes, a different number of leaves / phyllodes were inserted into the gas exchange chamber at each measurement period (n= 1 in *C. opaca* and *H. macrocarpa*, n≈ 5 in *A. aptaneura* and *T. schinzii*). All leaf gas exchange values were area-corrected following each measurement. Each leaf / phyllode was measured for *ca.* 5 to 10 min until stomatal conductance reached steady-state conditions. Inside the cuvette, temperature and vapour pressure deficit were set to equal the environmental conditions at the time of measurement. Light flux density was kept constant at 1500 μmol $m^{-2}$ $s^{-1}$ and $CO_2$ concentration was set to 400 μmol $mol^{-1}$.

Photosynthetic responses to incident irradiance (photosynthetic photon flux density (PPFD)) were measured in the mornings between 06:00 to 8:00 h only for the wet season (Febraury-2016), when soil water availability was large and, along with temperature and VPD was least likely to be limiting gas exchange. Cuvette temperature (30 ± 0.3 °C) and VPD (2 ± 0.1 kPa) were constant for all measurements across all species. PPFD in the leaf cuvette declined from a maximum of 2000 to a minimum of 0 μmol photons $m^{-2}$ $s^{-1}$, with 6 intermediate values (2000, 1000, 500, 100, 60, 40, 20 and 0 μmol photons $m^{-2}$ $s^{-1}$). $CO_2$ concentration within the cuvette was maintained at 400 μmol $mol^{-1}$. Values of $A_n$ were logged at 3 min intervals at each PPFD until stability was achieved. Light response curves were fitted following Heberling and Fridley (2013). In brief, a non-linear least squares regression (non-rectangular hyperbola) was fitted to estimate parameters using the following equation:

$$A_n = \frac{\phi PPFD + A_{max} - \sqrt{(\phi PPFD + A_{max})^2 - 4\theta\phi PPFD(A_{max})}}{2\theta} - R_d \qquad \text{(eq. 3.1)}$$

where $A_n$ and $A_{max}$ are the net and maximum gross photosynthetic rates (μmol $CO_2$ $m^{-2}$ $s^{-1}$) respectively; $\phi$ is the apparent quantum yield (μmol $CO_2$ μmol photons$^{-1}$) defined by the slope of the curve above the LCP; $R_d$ the day-time dark respiration rate (equal to $A_n$ when light flux density is zero); $\theta$ is the curve convexity parameter (unitless). Light compensation point (LCP) was calculated when $A_n$ (equal to zero) intercepts the *x*-axis. The light saturation point (LSP) was estimated at the point where 75 % of $A_{max}$ was reached (model asymptote).

### 3.2.4 Leaf structure and chemical characteristics

Leaves/ phyllodes used for diurnal measurements were collected and placed in a darkened container at the end of each day of measurements to determine LMA and foliar N concentration. Projected leaf area was measured using an image analysis system (WinDIAS 3, Delta-T Devices, Cambridge UK) followed by oven-drying at 65°C for 72 h then dry weight obtained. Leaf mass *per* unit area (LMA) was calculated with the oven-dry leaf weight (g) and leaf area ($m^{-2}$). Leaves were subsequently ground for analyses of leaf N content with an Elemental Analyser (Model PE2400 CHNS/O; PerkinElmer, Shelton, CT, USA) gas chromatograph. Foliar N concentration ($N_a$) was then calculated as N content (g) *per* unit leaf area ($cm^{-2}$) as $N_a$; g N $cm^{-2}$.

### 3.2.5 $^{13}C$ Isotope analyses

Carbon isotopic compositions were measured on leaf soluble sugars ($\delta^{13}C_{sugars}$) and bulk-leaf tissue ($\delta^{13}C_{bulk\text{-}leaf}$). The same ground leaf tissue that was used for determination of foliar N content was used for $\delta^{13}C_{bulk\text{-}leaf}$. Adjacent leaves from the same branch to those leaves used for gas exchange were collected at 17:00 h for $\delta^{13}C_{sugars}$ analyses. Leaves / phyllodes were immediately immersed in liquid-$N_2$ to suppress enzymatic activity. Soluble carbohydrates were extracted from the leaves using the modified protocol from Brugnoli *et al.* (1988) (West *et al.*, 2007). Leaves were first oven-dried at 65°C for 72 h, then ground to a fine powder. A sample of 150 mg tissue was placed in a 50 ml centrifuge tube with 35 $cm^3$ of de-ionized water. The centrifuge tube was boiled in a water bath for 30 min, left to cool and shaken for 3 min at room temperature. After centrifugation at 12,100 *g* for 15 min, the supernatant was collected using a syringe. Subsequently, the supernatants were passed through a C-18 Sep-Pak cartridge (Water, Milford, Mass.) to remove large organic molecules. Samples were passed through an ion-exchange column, of Dowex-50 and Dowex-1 (Sigma-Aldrich, St. Louis, Mo.) and filtered. The sugar-containing fractions were freeze-dried and stored dry for carbon isotope analyses.

Both bulk-leaf tissue and total-sugars were weighed in tin capsules (~ 2 mg of leaf sample). Isotopic signature analyses were performed using a standard Cavity Ring-Down Spectrometer with combustion module (CM-CRDS; model G212i, Picarro Inc. Sunnyvale CA, USA). The measuring error of the CM-CRDS system was 0.5 ± 0.1 ‰ and two laboratory internal standards (Acetanilide -33.77 ‰ and, Atropine -21.45 ‰ (Costech Analytical Technologies, Valencia, CA, USA)) were used to calibrate the CM-CRDS. Corrected $\delta^{13}C$ values are expressed relative to the international standard, Pee Dee Belemnite (PDB).

### 3.2.6 Metrics of leaf resource-use-efficiencies

#### 3.2.6.1 Water-use-efficiency

In this study intrinsic water-use-efficiency ($WUE_i = A/g_s$) was estimated using two different approaches: carbon isotope ratios (bulk-leaf and total sugars) and leaf gas exchange measurements. The carbon isotopic discrimination ($\Delta^{13}C$) is linearly related to the ratio of the intercellular and ambient $CO_2$ concentration ($C_i/C_a$, respectively), which reflects the balance between $A_n$ and $g_s$ for $CO_2$ ($g_c$) (Farquhar *et al.*, 1989). Bulk-leaf $\delta^{13}C$ is a proxy of long-term $WUE_i$, whereas sugar $\delta^{13}C$ provides a proxy of short-term changes in $\Delta^{13}C$, because measurements of carbohydrates better reflect the faster turnover rate of assimilated carbon (Page *et al.*, 2016; Scartazza *et al.*, 2013). According to Fick's law: $A = g_c(C_a - C_i)$, where water stomatal conductance ($g_{sw}$) and $g_c$ are related by the constant of 1.6 ($g_{sw} = 1.6\, g_c$). This linear relationship allows the estimation of intrinsic water-use-efficiency using stable isotope measurements ($WUE_i$; eq. 3.2):

$$WUE_i = \frac{C_a}{1.6}\left(\frac{b' - \Delta}{b' - a}\right) \qquad \text{(eq. 3.2)}$$

The relationship between $WUE_i$ and $\delta^{13}C$ of leaf tissue is calculated from following equation 3.3:

$$WUE_i = \frac{C_a}{1.6(b-a)}(b - \delta^{13}C_{air} + \delta^{13}C_{leaf}) \qquad \text{(eq. 3.3)}$$

where $a$ is the fractionation during $CO_2$ diffusion through the stomata (4.4 ‰; O'Leary, 1981), $b$ is the fractionation associated with reactions by Rubisco and PEP carboxylase (27 ‰; Farquhar and Richards 1984), $\delta^{13}C_{air}$ is the carbon isotope ratio of the air (-8 ‰), $\delta^{13}C_{leaf}$ is either

$\delta^{13}C_{bulk\text{-}leaf}$ or $\delta^{13}C_{sugars}$. Higher $\delta^{13}C_{leaf}$ values indicate larger time-integrated $WUE_i$. Note that this isotopic discrimination theory to estimate $WUE_i$ does not apply to C4 species because of bundle sheath leakiness (Cernusak *et al.*, 2013a). Thus, *Triodia schinzii* was excluded in the carbon isotopic analyses.

### 3.2.6.2 Photosynthetic nitrogen and carbon-use-efficiencies

Instantaneous PNUE was calculated using daily maximum net assimilation rate ($A_{max}$) from diurnal surveys (n≈ 5 leaves *per* 4 individuals *per* species) divided by the amount of nitrogen *per* unit leaf area (PNUE= $A_n/N_a$).

Leaf-scale CUE was calculated as the carbon incorporated into plants divided by the total amount of carbon fixed in photosynthesis following Frantz and Bugbee (2005):

$$\text{CUE} = \frac{DCG}{P_{gross}} \quad \text{(eq. 3.4)}$$

were $P_{gross}$ is gross photosynthesis and DCG is daily carbon gain. Using the sum of $A_n$ from diurnal surveys $P_{net}$ was calculated (net photosynthesis, mol C $m^{-2}$ $d^{-1}$) and this was combined with $R_n$ (night-time respiration) to allow calculation of DCG as:

$$\text{DCG} = P_{net} - R_n \quad \text{(eq. 3.5)}$$

In theory $P_{gross}$ should incorporate both C fixed ($P_{net}$) and C that is respired. However, it is difficult to accurately measure daytime respiration ($R_d$), here it was assumed that the rate of $R_d$ and $R_n$ were equal (Frantz and Bugbee, 2005; Limousin *et al.*, 2015). Although $R_d$ was not measured, $R_d$ was estimated from the light response curves and assumed constant for the same wet season. $P_{gross}$ was calculated as:

$$P_{gross} = P_{net} + R_d \quad \text{(eq. 3.6)}$$

### 3.2.5 Statistical analyses

To test for differences between seasons and within species, statistical analyses were undertaken using the R 3.2.1 Project software® (R Development Core Team 2016). The normality of the data was verified with the Shapiro-Wilk test. One and two-way ANOVAs with Tukey's HSD *post-hoc* were undertaken to test differences between species and the effect with seasons as species × date (seasons). Three-way ANOVAs was used to test for significant

differences between $WUE_i$ methods as species × date × method (leaf gas exchange *versus* stable isotope approach, bulk-leaf and total sugar). Linear mixed models with replicates (individuals *per* species) as random factor were applied followed by a Tukey's honestly significant difference *post-hoc* test for significant differences between species within the same sample dates and differences within species across dates. Linear regressions were applied to determine relationships between: diurnal leaf water potential (diurnal $\Psi_{leaf}$) and $A_n$, $g_s$ and $WUE_i$. Slope differences were tested using a standardized major axis method in the SMATR package in R and multiple comparison pair-wise test comparisons among species (Warton *et al.*, 2012).

## *3.3 Results*

### 3.3.1 Climate conditions during the study period

Total precipitation measured for two consecutive months immediately prior to each field campaign ranged between 0 mm in the dry season (Sep and Oct-2015) to 44 mm during the early wet season of the 2016 (Jan and Feb-2016) field campaign (Table 3.1). During the late dry season (Feb –Mar 2015) 3 mm of rainfall was received in the 2 months prior to the field study (Table 3.1). Mean daily temperature and maximum temperatures were largest during wet seasons of 2015 and 2016 (summer) and smallest during the dry season (winter; Table 3.1). Similarly, the largest VPDs occurred during the early or late wet seasons and the smallest VPD was recorded in the dry season (Sep-Oct-2015). During the day, maximum temperatures and VPD exceeded 40 °C and 6 kPa respectively. During sunlight hours, VPD ranged between 2.7 and 6.8 kPa in Feb-Mar-2015, 1.5 to 6.0 kPa in Sep-Oct-2015 and 2.5 to 7.2 in Jan-Feb-2016.

Table 3.1 Climate conditions during the three field campaigns. 1) Late wet season; 2) dry season and, 3) early wet season. Daily averages (±1SE), average minima and maxima of temperature ($T_{air}$) and vapour pressure deficit (VPD) and total rainfall amount for the two consecutive months, one month preceding each field campaign and the month of the field campaign.

| | Date | Rain (mm) | $T_{air}$ mean (°C) | $T_{air}$ max (°C) | $T_{air}$ min. (°C) | VPD mean (kPa) | VPD max (kPa) |
|---|---|---|---|---|---|---|---|
| 1) | Feb-Mar-2015 | 3 | 29±0.7 | 35±0.8 | 24±0.1 | 3.3±0.1 | 4.8±0.3 |
| 2) | Sep- Oct-2015 | 0 | 24±3.8 | 29.6±1.1 | 20±4.0 | 2.7±0.6 | 3.7±0.3 |
| 3) | Jan-Feb-2016 | 44 | 30±0.6 | 34.7±0.8 | 25±0.4 | 2.9±0.3 | 4.7±0.3 |

### 3.3.2 Leaf water potential

Leaf water potentials (both pre-dawn and midday) were highly variable across species in the three periods of study (Table 3.2). Both pre-dawn water potential ($\Psi_{pd}$) and midday water potential ($\Psi_{md}$) were consistently lower for the two *Acacia* species than the remaining three species across all three sampling periods. The largest (closest to zero) $\Psi_{pd}$ and $\Psi_{md}$ were observed for *C. opaca* trees and *H. macrocarpa* shrubs. The difference between $\Psi_{pd}$ and $\Psi_{md}$ was on average 1.6 ± 0.2 MPa across all species and dates.

The interaction between species × date was statistically significant for both pre-dawn water potentials and midday water potentials ($p$-value < 0.001; Table S.3.1). In the dry season (Oct-2015), both *Acacia* spp. from the Mulga woodland had the lowest values of both pre-dawn and

midday water potentials (< -9 MPa). In contrast, for the same dry season, both pre-dawn water potential ($\Psi_{pd}$= -5.6 ± 0.27) and midday water potential ($\Psi_{md}$= -6.5 ± 0.23) of *A. aptaneura* sampled from within the *Corymbia* savanna was significantly larger (closer to zero) than the two *Acacia* spp. sampled in the Mulga woodland. Seasonal variability with significant differences between dates was observed in $\Psi_{pd}$ and $\Psi_{md}$ from *Acacia* spp. from both sites.

Table 3.2 Mean of foliar water potentials (± 1SE; n= 6): pre-dawn ($\Psi_{pd}$), midday ($\Psi_{md}$) and the difference between $\Psi_{pd}$ $\Psi_{md}$ ($\Delta\Psi$). **A. aptaneura* located in the *Corymbia* savanna site. Within columns, different letters indicate that means were significantly different at *p*-value < 0.05 among species and dates assessed with two-way ANOVAs and the Tukey's HSD *post-hoc* tests for significant differences between species.

| Species | Date | $\Psi_{pd}$ | $\Psi_{md}$ | $\Delta\Psi$ |
|---|---|---|---|---|
| | | (MPa) | | |
| *Acacia aptaneura* | Mar-2015 | -3.9±0.2 be | -5.6±0.19 ab | 1.7 |
| | Oct-2015 | -9.3±0.21 g | -9.3±0.13 g | 0.1 |
| | Feb-2016 | -3.4±0.1 ab | -5.8±0.09 ab | 2.4 |
| *Acacia aneura* | Mar-2015 | -4.6±0.19 e | -7.3±0.3 f | 2.7 |
| | Oct-2015 | -9.1±0.19 g | -10.0±0.25 g | 0.9 |
| | Feb-2016 | -3.1±0.18 a | -5.2±0.19 a | 2.2 |
| *Corymbia opaca* | Mar-2015 | -0.7±0.05 c | -2.5±0.17 cd | 1.8 |
| | Oct-2015 | -0.4±0.02 c | -2.2±0.18 d | 1.7 |
| | Feb-2016 | -0.8±0.02 c | -2.7±0.09 cd | 2.0 |
| *Hakea macrocarpa* | Mar-2015 | -1.9±0.13 d | -3.2±0.12 ce | 1.3 |
| | Oct-2015 | -0.8±0.05 c | -2.7±0.14 cd | 1.9 |
| | Feb-2016 | -1.6±0.11 d | -2.7±0.13 cd | 1.1 |
| *A. aptaneura** | Mar-2015 | -1.8±0.09 d | -4.0±0.12 e | 2.2 |
| | Oct-2015 | -5.6±0.27 f | -6.5±0.23 bf | 0.9 |
| | Feb-2016 | -3.4±0.05 ab | -5.4±0.09 a | 2.0 |
| *Triodia schinzii* | Feb-2016 | -0.7±0.06 c | -2.4±0.11 cd | 1.7 |

Maximum values of foliar water potential occurred in the wet season (Feb-2016) for two of the four species, with the exceptions being *C. opaca* and *H. macrocarpa*. There were no significant differences in foliar water potential over time for *C. opaca.* The range in water potentials across sampling periods was smaller in *C. opaca* and *H. macrocarpa* than the remaining species. Average $\Psi_{pd}$ across seasons were -0.6 ± 0.23 MPa and -1.5 ± 0.6 MPa, for *C. opaca* and *H. macrocarpa* respectively. Similarly, averaged $\Psi_{md}$ were -2.5 ± 0.3 and -2.9 ± 0.3 MPa, *C. opaca* and *H. macrocarpa* respectively. It was not possible to measure leaf water potential in *Triodia schinzii* (spinifex grass) outside of the wet season due to leaf browning. However, in Feb-2016 *T. schinzii* did not show significant differences from *C. opaca* in both $\Psi_{pd}$

(-0.7 ± 0.06 MPa) and $\Psi_{md}$ (-2.4 ± 0.11 MPa), but these were significantly different from the remaining species.

### 3.3.3 Seasonal and diurnal survey of leaf gas exchange

Net assimilation rates ($A_n$), stomatal conductance ($g_s$), and intrinsic water-use-efficiency ($WUE_i$) differed across species and seasons (Fig. 3.3; Table S.3.1). The highest photosynthetic rates occurred for all species between 07:00 h and 10:00 h across seasons, except for *T. schinzii* and *C. opaca* which showed large values of $A_n$ until midday in Feb-2016. In the early morning (at 7:00 and 8:00 h), $A_n$ varied between 8 and 20 μmol $m^{-2}$ $s^{-1}$ in both Mar-2015 and Feb-2016 across all species. In contrast, in the dry season (Oct-2015), *Acacia* spp. at the Mulga woodland had low values of $A_n$ (< 3 μmol $m^{-2}$ $s^{-1}$), but the $A_n$ of *A. aptaneura* at the *Corymbia* savanna varied between 0.34 and 6.9 μmol $m^{-2}$ $s^{-1}$.

Across all species, $A_n$ declined to below 5 μmol $m^{-2}$ $s^{-1}$ and $g_s$ reached values close to 0 mol $m^{-2}$ $s^{-1}$ after 15:00 h during March and October 2015. The largest $A_n$ values in March and October 2015 were observed in *H. macrocarpa* (> 15 μmol $m^{-2}$ $s^{-1}$) at 7:00 h. *T. schinizii* and *C. opaca* had the largest $A_n$ during the wet season (Feb-2016) which occurred between 10:00 and 12:00 h (Fig. 3.3c). During March and October-2015 campaigns all species maintained $g_s$ values below 0.2 mol $m^{-2}$ $s^{-1}$ across the day. Similarly, in February-2016 species had $g_s$ values below 0.2 mol $m^{-2}$ $s^{-1}$, except for *C. opaca*, which had the largest $g_s$ (0.36 mol $m^{-2}$ $s^{-1}$).

Large diurnal variation in $WUE_i$ was observed for most species in March 2015 (Fig. 3.3g); the exception was *C. opaca*, which exhibited minor variation across the day. During Oct 2015 and Feb 2015 $WUE_i$ tended to increase from a minimum early in the morning to a maximum around midday, with small declines later in the afternoon for many species (Fig. 3.3h, i).

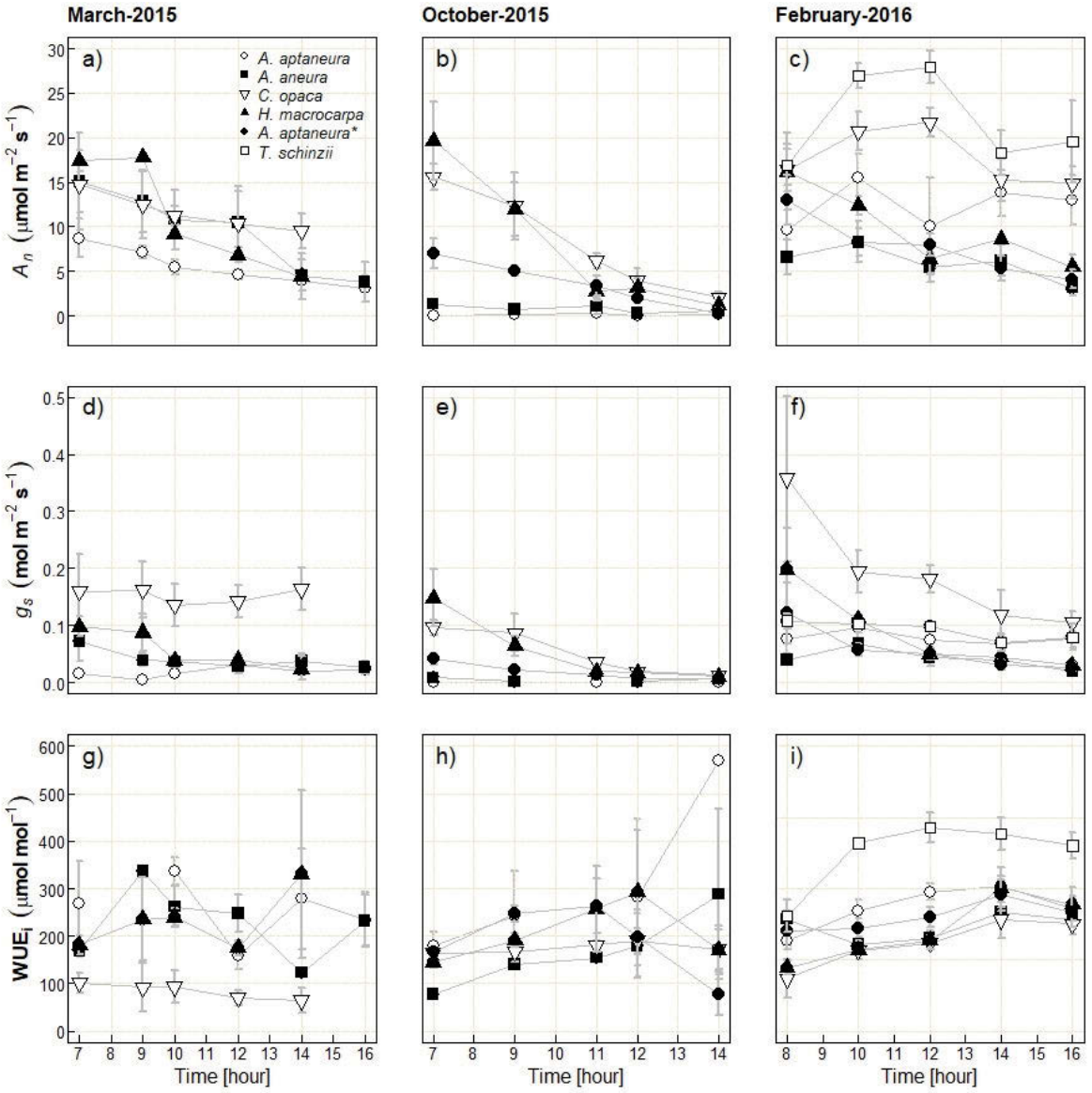


Figure 3.3 Diurnal variation of stomatal conductance ($g_s$), net assimilation ($A_n$) and intrinsic water-use-efficiency (WUE$_i$) across 3 different periods. (*) *A. aptaneura* located in the *Corymbia* savanna site. Error bars represent ± 1SE (n= 4).

### 3.3.3.1 Photosynthetic response to light intensity

All species showed a non-rectangular hyperbolic response of $A_n$ to increasing photosynthetic photon flux density (PPFD). Net assimilation rates at PPFD= 2000 μmol m$^{-2}$ s$^{-1}$ were calculated from the light response curves (Fig. 3.4) and compared across species as $A_{n2000}$ (Table 3.3; Table S.3.1 for differences between species). The largest $A_{n2000}$ values were observed in *A. aptaneura* (19.6 ± 1.3 μmol m$^{-2}$ s$^{-1}$), *H. macrocarpa* (19.7 ± 2.4 μmol m$^{-2}$ s$^{-1}$), and *T. schinizii* (21.2 ± 2.7 μmol m$^{-2}$ s$^{-1}$), with no significant differences among these species. There were no

significant differences in $A_{n2000}$ between *C. opaca* (14.4 ± 1.5 μmol $m^{-2}$ $s^{-1}$) and *H. macrocarpa*. The lowest $A_{n2000}$ value was observed in *A. aneura* (7.7 ± 0.5 μmol $m^{-2}$ s-1) and this was significantly lower than the remaining species.

The largest maximum gross photosynthetic ($A_{max}$) rates were observed for *A. aptaneura* (25.4 ± 2.2 μmol $m^{-2}$ $s^{-1}$, Table 3.3), *H. macrocarpa* (25.2 ± 3.5 μmol $m^{-2}$ $s^{-1}$), and *T. schinizii* (27.5 ± 3.3 μmol $m^{-2}$ $s^{-1}$), with no significant differences among these species (Table 3.3). *A. aneura* had the smallest $A_{max}$ value (12.6 ± 0.4 μmol $m^{-2}$ $s^{-1}$) and this was not significantly different from that of *C. opaca* (16.6 ± 1.8 μmol $m^{-2}$ $s^{-1}$) and *A. aptaneura* (17.6 ± 2.6 μmol $m^{-2}$ $s^{-1}$) from the *Corymbia* savanna site.

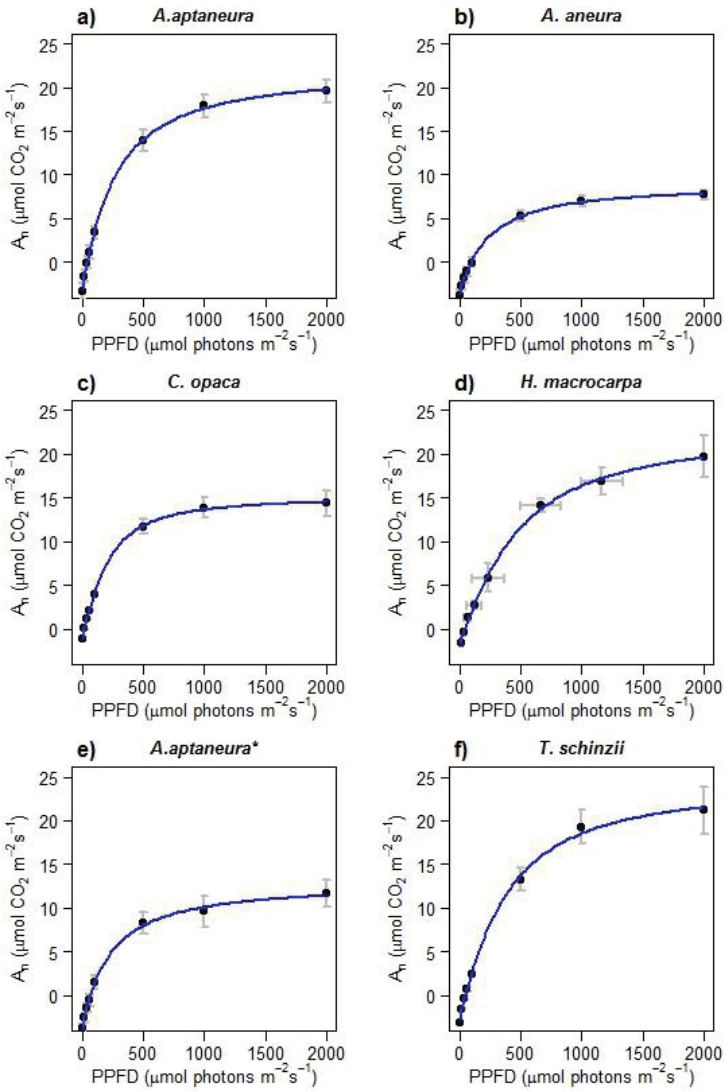


Figure 3.4 Modelled light response curves and field data *per* species. Measurements represent net photosynthetic rates net photosynthetic rates ($A_n$) at different irradiances (photosynthetic photon flux density; PPFD). (*) *A. aptaneura* located at the *Corymbia* savanna site. Error bars represent ± 1SE (n= 4).

The light compensation point (LCP) ranged between 19 μmol photons $m^{-2}$ $s^{-1}$ (*C. opaca*) and 101 μmol photons $m^{-2}$ $s^{-1}$ (*A. aneura*), and this difference was significant. There were few significant differences among the remaining comparisons across species. The species with the lowest $A_{max}$ value (*A. aneura*) had the highest LCP (101 ± 17.1 μmol photons $m^{-2}$ $s^{-1}$) and this was significantly different from the LCP of *A. aptaneura* (44 ± 10.8 μmol photons $m^{-2}$ $s^{-1}$) from the same Mulga woodland site. There were no significant differences among species in the apparent quantum yield ($\phi$; Table 3.3). Averaged $\phi$ for all species was 0.064 ± 0.03 μmol $CO_2$ $\mu mol^{-1}$ photons.

Table 3.3 Summary of mean values (±1SE; n= 4) of light compensation point (LCP), light saturation point (LSP), maxima rate of gross assimilation ($A_{max}$, model asymptote), net assimilation $A_{n2000}$ at PPFD= 2000 μmol $m^{-2}$ $s^{-1}$, the day-time dark respiration rate ($|A_n|$ at no light) and apparent quantum yield ($\phi$). All these parameters where estimated from light response curves (Fig. 3.4). (*) *A. aptaneura* located at the *Corymbia* savanna site. Within columns, letters indicate that means were significantly different ($p$-value<0.05) as tested with one-way ANOVAs with Tukey's HSD *post-hoc* tests for significant differences across species.

| **Species** | $A_{max}$ | $A_{n2000}$ | $R_d$ | **LCP** | **LSP** | $\phi$ |
|---|---|---|---|---|---|---|
| | (μmol $CO_2$ $m^{-2}$ $s^{-1}$) | | | (μmol photons $m^{-2}$ $s^{-1}$) | | (μmol $CO_2$ $\mu mol^{-1}$ photons) |
| *A. aptaneura* | 25.4±2.2 cd | 19.6±1.3 cd | 3.2±0.9 b | 44±10.8 ab | 244±41.7 a | 0.080±0.011 a |
| *A. aneura* | 12.6±0.4 a | 7.7±0.5 a | 3.7±0.5 b | 101±17.1 c | 945±279.3 a | 0.050±0.003 a |
| *C. opaca* | 16.6±1.8 ab | 14.4±1.5 bc | 1.1±0.1 a | 19±1.6 a | 958±458.1 a | 0.058±0.002 a |
| *H. macrocarpa* | 25.2±3.5 bd | 19.7±2.4 cd | 1.9±0.2 ab | 44±20.8 ab | 503±145.9 a | 0.062±0.017 a |
| *A. aptaneura** | 17.6±2.6 abc | 11.7±1.6 ab | 3.9±0.5 b | 75±17.2 bc | 584±131.9 a | 0.073±0.008 a |
| *T. schinzii* | 27.5±3.3 d | 21.2±2.7 d | 2.8±0.1 ab | 51±3.6 ac | 469±111.3 a | 0.060±0.006 a |

### 3.3.4 Relationship between leaf gas exchange and leaf water potential

The relationships between diurnal leaf gas exchange parameters ($A_n$ and $g_s$) and diurnal leaf water potential ($\Psi_{leaf}$) were evaluated in two study periods: Mar-2015 and Feb-2016 (Fig. 3.5). Diurnal leaf water potential was excluded in the dry season (Oct-2015), due to very low values in $\Psi_{pd}$ (< -10 MPa) which exceeded my capacity to measure them with the pressure chamber available (limit of -10 MPa). In the other two periods of study (Mar-2015 and Feb-2016) *C. opaca* and *H. macrocarpa* had the largest (closest to zero) mean diurnal $\Psi_{leaf}$ and both were significantly different from *Acacia* species ($p$-value < 0.001), but *H. macrocarpa* was not significantly different from *T. schinizii* in Feb-2016 (Table 3.4).

Table 3.4 Summary of mean values (±1SE n= 4) of leaf / phyllode diurnal water potentials ($\Psi_{leaf}$) measured at 2 hour intervals. (*) *A. aptaneura* located at the *Corymbia* savanna site. Within columns, letters indicate that means were significantly different ($p$-value<0.05) as tested with linear mixed models with observations as random factor and, the Tukey's HSD *post-hoc* tests for significant differences within dates across species.

| Species | Date | $\Psi_{leaf}$ (MPa) |
|---|---|---|
| *Acacia aptaneura* | Mar-2015 | -5.6±0.23 a |
| | Feb-2016 | -5.1±0.11 a |
| *Acacia aneura* | Mar-2015 | -6.4±0.32 a |
| | Feb-2016 | -4.9±0.17 a |
| *Corymbia opaca* | Mar-2015 | -2.4±0.43 b |
| | Feb-2016 | -2.9±0.12 b |
| *Hakea macrocarpa* | Mar-2015 | -3.0±0.18 b |
| | Feb-2016 | -2.6±0.10 bc |
| *A. aptaneura** | Feb-2016 | -4.6±0.10 a |
| *Triodia schinzii* | Feb-2016 | -2.2±0.14 c |

Both $A_n$ and $g_s$ were significantly and positively correlated with foliar water potentials during the days of measurement (Fig. 3.5). For $A_n$ there was significant increase in slope (m; $p$-value= 0.012) between Mar-2015 (m= 1.1, $r^2$= 0.14; $p$-value= 0.070; Fig. 3.5a) and Feb-2016 (m= 2.9, $r^2$= 0.32; $p$-value<0.001; Fig. 3.5d). Similarly, for $g_s$ there was significant increase in slope (m; $p$-value= 0.02) between Mar-2015 (m= 0.02, $r^2$= 0.51; $p$-value< 0.001; Fig. 3.5b) and Feb-2016 (m= 0.03, $r^2$= 0.25; $p$-value= 0.002; Fig. 3.5e). There were positive relationships for $A_n$ and $g_s$ with foliar water potential, and there was a significant negative correlation between $WUE_i$ and $\Psi_{leaf}$ in March-2015 ($r^2$= 0.23; $p$-value= 0.03) for all species combined (Fig. 3.5c). In Feb-

2016 the negative correlation was statistically significant when *T. schinizii* was excluded from the regression ($r^2$= 0.15; *p*-value= 0.03; Fig. 3.5f). There was, however no difference in slope of $WUE_i$ and $\Psi_{leaf}$ between March-2015 and Feb-2016 (*p*-value= 0.06).

Consistently in both periods *Acacia* spp., at the Mulga woodland were the extreme values in the regression of $\Psi_{leaf}$ *versus* $WUE_i$, with the smallest values of $\Psi_{leaf}$ and maximum values of $WUE_i$. The $\Psi_{leaf}$ value at which $WUE_i$ reached its maxima in Mar-2015 was < -6.0 MPa in *Acacia* spp. at the Mulga woodland. In contrast, in Feb-2016 maximum $WUE_i$ values across species were reached by *T. schinizii* with $\Psi_{leaf}$ of -2.75 MPa. During the late wet season (Mar-2015), Mulga species had the largest $WUE_i$ of 200 to 350 μmol $mol^{-1}$ (Fig. 3.5c).

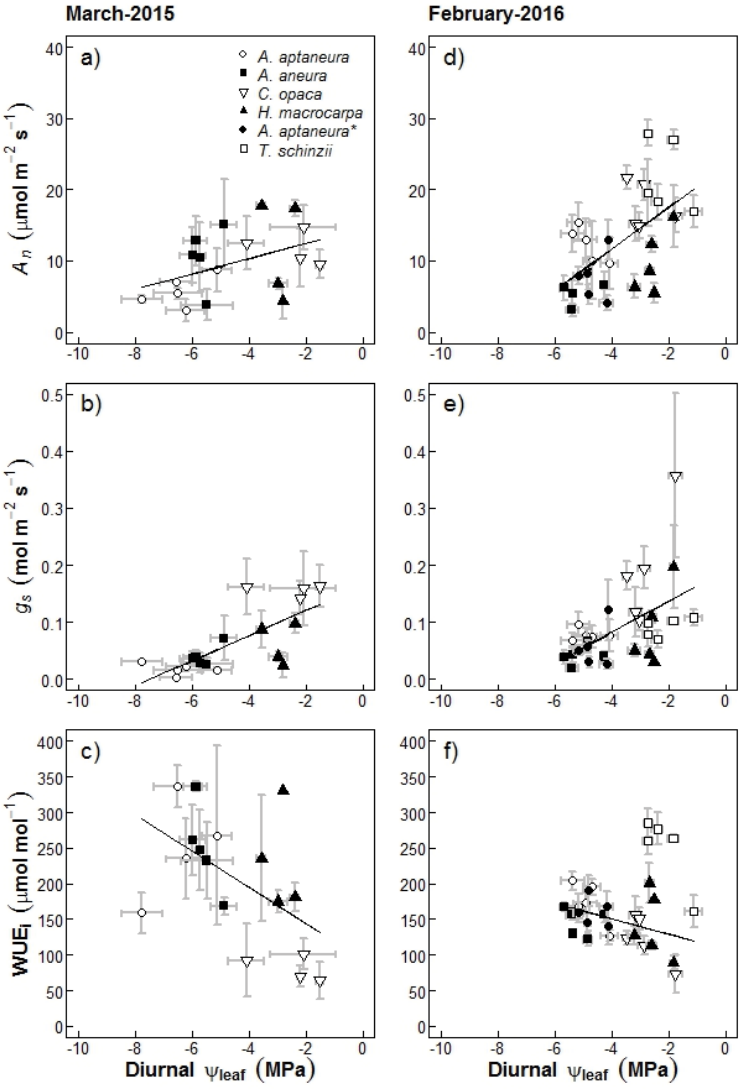


Figure 3.5 Relationship between diurnal leaf water potentials and net assimilation ($A_n$; a and d), stomatal conductance ($g_s$; b and e) and intrinsic water-use-efficiency ($WUE_i$; c and f). (*) *A. aptaneura* was sampled in the *Corymbia* savanna site. Error bars represent ± 1SE (n= 4). *T. schinzii* was excluded from the regression in panel f).

### 3.3.5 Leaf carbon isotope ratios

The ratio of intercellular to ambient $CO_2$ concentration ($C_i/C_a$) and $\delta^{13}C$ isotopic composition for bulk leaf and leaf total sugars are presented in Fig. 3.6 (see also Table S.3.2 and S.3.3). The mean $C_i/C_a$ ratio calculated from the bulk leaf isotopic compositions ranged from 0.63 to 0.73 (Fig. 3.6a), whereas mean $C_i/C_a$ from total sugar isotopic composition ranged from 0.40 to 0.78 (Table S.3.3). The interaction species × date of $C_i/C_a$ from bulk leaf isotopic compositions did not show significant differences ($p$-value= 0.09). There were, however, significant differences in the $C_i/C_a$ for bulk-leaf isotopic compositions in *H. macrocarpa* compared to both *A. aptaneura* ($p$-value= 0.003) and *C. opaca* ($p$-value= 0.05) (see supplementary information Table S.3.2 for bulk-leaf).

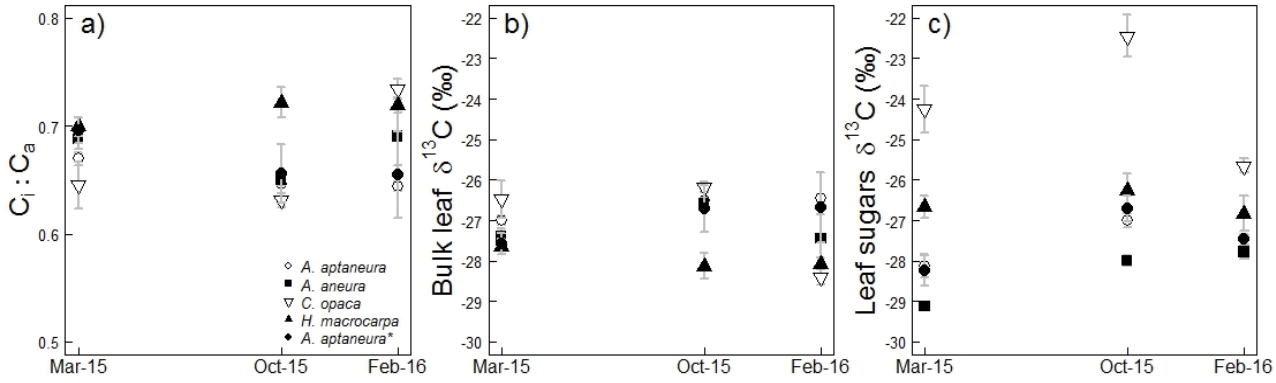


Figure 3.6 Ratio of the intercellular and ambient $CO_2$ concentration ($C_i$/ $C_a$) derived from bulk-leaf isotopic composition (a), $\delta^{13}C$ isotope ratio for bulk leaf (b) and total sugars (c). (*) *A. aptaneura* located at the *Corymbia* savanna site. Error bars represent ±1SE (n= 4).

Mean carbon isotopic compositions ($\delta^{13}C$) for all tree species examined ranged between -28.4 to -26.2 ‰ (Fig. 3.6b) for bulk leaf and -29.12 to -22.45 ‰ in leaf-total sugars (Fig. 3.6c). *C. opaca* showed some seasonal variability in both isotopic compositions of bulk-leaf ($\delta^{13}C_{bulk-leaf}$) and soluble sugars ($\delta^{13}C_{sugars}$) across the three months of analysis (Table S.3.2 and S.3.3). For example, values for $\delta^{13}C_{bulk-leaf}$ and $\delta^{13}C_{sugars}$ of Mar-2015 ($\delta^{13}C_{bulk-leaf}$= -26.5 ± 0.47 ‰ and $\delta^{13}C_{sugars}$= -24.3 ± 0.58 ‰) were statistically different ($p$-value<0.05; Table S.3.2) from values measured in Oct-2015 ($\delta^{13}C_{bulk-leaf}$ = -26.2 ± 0.14 ‰ and $\delta^{13}C_{sugars}$ = -22.5 ± 0.52 ‰), but no significant differences were observed between Mar-2015 and Feb-2016 ($\delta^{13}C_{bulk-leaf}$ = -28.4 ± 0.20 ‰ and $\delta^{13}C_{sugars}$ = -22.7 ± 0.17 ‰). *A. aptaneura* at the *Corymbia* savanna showed significant differences in $\delta^{13}C_{sugars}$ between Oct-2015 ($\delta^{13}C_{sugars}$ = -26.7 ± 0.32 ‰) and Feb-2016

($\delta^{13}C_{sugars}$ = -27.5 ± 0.13 ‰; Table S.3.3). These two species also showed significant differences in parameters estimated from isotopic composition such as $\Delta^{13}C$ and $C_i/C_a$.

### 3.3.6 Resource-use-efficiencies

#### 3.3.6.1 Water-use-efficiencies: a comparison

Intrinsic water-use-efficiencies ($WUE_i$) at a leaf-scale derived from leaf gas exchange and carbon isotopic methods are presented in Table 3.5. Intrinsic water-use-efficiency derived from leaf-gas exchange ($WUE_{i(leaf\text{-}gas)}$) varied from 84.1 ± 7.2 to 266.3 ± 64.8 μmol $mol^{-1}$, for *C. opaca* and *A. aptaneura* respectively. $WUE_i$ derived from bulk-leaf isotopic compositions ($WUE_{i(bulk\text{-}leaf)}$) varied from 66.4 ± 3.2 to 92.2 ± 1.6 μmol $mol^{-1}$ in *C. opaca*. In contrast, $WUE_i$ values estimated from total-leaf sugars ($WUE_{i(total\text{-}sugars)}$) were from 58.0 ± 1.2 to 135 ± 5.9 μmol $mol^{-1}$ in *A. aptaneura* and *C. opaca* respectively.

The interaction species × method × date was not statistically significant for $WUE_i$ (*p*-value = 0.3551; Table S.3.1), but was statistically significant (*p*-value< 0.05) for the interaction species × method (Table S.3.1). The average of $WUE_i$ by method across all species and dates was of 187.2 ± 5.1 μmol $mol^{-1}$ for $WUE_{i(leaf\text{-}gas)}$, 80 ± 1.4 μmol $mol^{-1}$ for $WUE_{i(bulk\text{-}leaf)}$ and, 85.4 ± 2.7 μmol $mol^{-1}$ for $WUE_{i(total\text{-}sugars)}$. $WUE_{i(leaf\text{-}gas)}$ was generally larger than $WUE_i$ derived from the isotopic approach. Note, that this difference was small in *C. opaca* when comparing $WUE_{i(leaf\text{-}gas)}$ *versus* $WUE_{i(total\text{-}sugars)}$.

Cross-species comparison of $WUE_i$ within the same measurement dates showed significant differences (*p*-value< 0.001; Table 3.5; Table S.3.1). In Mar-2015 $WUE_{i(leaf\text{-}gas)}$ of *C. opaca* was significantly smaller than the remaining species ($WUE_{i(leaf\text{-}gas)}$= 84.1 ± 7.2 μmol $mol^{-1}$). The pattern in $WUE_{i(total\text{-}sugars)}$ showed that *C. opaca* had significantly larger means when compared with the other species across all dates, except for Feb-2015. *A. aptaneura* from the two sites did not show significant differences in $WUE_{i(total\text{-}sugars)}$.

Table 3.5 Summary of mean values of resource-use-efficiencies. Intrinsic water-use-efficiency derived from leaf gas exchange ($WUE_{i(leaf\text{-}gas)}$) measurements and carbon isotopic compositions: bulk-leaf ($WUE_{i(bulk\text{-}leaf)}$) and leaf total-sugars ($WUE_{i(total\text{-}sugars)}$). Means from leaf gas exchange were taken from diurnal surveys (n= 4 at 2 h intervals), foliar nitrogen content ($N_a$), leaf mass *per* area (LMA), photosynthetic nitrogen-use-efficiency (PNUE), carbon-use-efficiency (CUE) and light-use-efficiency (LUE) derived from apparent quantum yield (errors are ±1SE; n= 4 individual *per* plant species). Within columns, letters indicate that means were significantly different (*p*-value<0.05) as tested with two-way ANOVAs with Tukey's HSD *post-hoc* tests for significant differences across species.

| Species | Month | $WUE_{i(leaf\text{-}gas)}$ (mmol $mol^{-1}$) | | $WUE_{i(bulk\text{-}leaf)}$ (mmol $mol^{-1}$) | | $WUE_{i(total\text{-}sugars)}$ (mmol $mol^{-1}$) | | PNUE ((µmol CO2) *per* (g $N)^{-1}$ $s^{-1}$) | | $N_a$ (g N $m^{-2}$) | | LMA (g $m^{-2}$) | | CUE (daily C gain *per* mol C fixed) | | LUE (mmol $CO_2$ $mmol^{-1}$ photon) | |
|---|---|---|---|---|---|---|---|---|---|---|---|---|---|---|---|---|---|
| *A. aptaneura* | March | 253.7±30.7 | a | 82.7±1.5 | abc | 69.5±3.4 | df | 2.5±0.14 | cef | 5.1±0.29 | bcdf | 296.6±18.1 | abc | | | | |
| | October | 266.3±64.8 | ab | 88.5±2.3 | ab | 82.7±2 | cef | 0.2±0.02 | g | 6.6±0.89 | def | 451.2±59.0 | bcde | | | | |
| | February | 173.5±8.0 | abcde | 89.0±1.0 | ab | 74.5±3.1 | def | 2.5±0.1 | cef | 9.2±0.38 | e | 548.2±21.7 | e | 0.89±0.03 | ab | 80±11 | a |
| *A. aneura* | March | 227.6±20.8 | abd | 78.0±2.4 | abc | 58.0±1.2 | d | 4.7±0.91 | bcdef | 6.9±1.34 | cdef | 345.2±57.8 | abcde | | | | |
| | October | 179.2±42.9 | abcde | 87.6±1.3 | abc | 71.1±1.5 | def | 0.7±0.11 | g | 5.4±0.75 | bcdf | 297.6±46.4 | abc | | | | |
| | February | 146.4±5.1 | bcde | 77.4±6.8 | abc | 73.7±1.2 | def | 1.7±0.04 | ef | 8.5±0.22 | ef | 472.2±21.3 | bcde | 0.72±0.11 | b | 50±3.0 | a |
| *C. opaca* | March | 84.1±11.7 | c | 88.7±5.4 | ab | 114.4±6.7 | b | 6.6±1.94 | bcd | 3.1±0.72 | abcd | 309.5±31.3 | abcd | | | | |
| | October | 175.1±9.8 | abcde | 92.2±1.6 | a | 135.1±5.9 | a | 6.0±0.47 | bcd | 3.3±0.25 | abcd | 334.6±13.1 | abcd | | | | |
| | February | 123.6±10.3 | ce | 66.4±2.3 | c | 98.3±1.9 | bc | 6.8±0.94 | bd | 4.1±0.56 | abcd | 397.9±24.2 | abcde | 0.98±0.01 | a | 58±2.0 | a |
| *H. macrocarpa* | March | 232.6±35.2 | abde | 75.1±2.1 | abc | 86.5±3.2 | ce | 3.7±0.65 | bcdef | 5.5±0.88 | cdf | 409.8±44.8 | abcde | | | | |
| | October | 206.2±29.9 | abde | 69.6±3.5 | bc | 91.3±4.8 | cef | 7.5±0.22 | b | 4.2±0.13 | abcd | 484.5±51.7 | bde | | | | |
| | February | 141.6±11.9 | cde | 70.2±1.7 | bc | 84.6±5 | cef | 5.3±1.52 | bcdf | 6.2±1.23 | cdef | 495.8±61.6 | de | 0.92±0.01 | ab | 62±17 | a |
| *A. aptaneura** | March | NA | | 76.0±2.9 | abc | 68.2±4.3 | df | NA | | 5.5±0.84 | cdf | 285.6±36.1 | ac | | | | |
| | October | 208.1±20.3 | abde | 86.1±6.7 | abc | 86.1±4.3 | cef | 1.6±0.19 | ef | 6.5±0.77 | cdef | 414.6±47.0 | bcde | | | | |
| | February | 160.6±8.9 | abcde | 86.4±10 | abc | 77.2±1.5 | ef | 2.9±0.28 | cdef | 6.3±0.56 | cdef | 456.7±39.4 | bcde | 0.80±0.03 | ab | 73±8.0 | a |
| *T. schinzii* | February | 249.6±12.9 | a | | | | | 15.9±0.82 | a | 2.1±0.11 | ab | 229.5±4.6 | a | 0.95±0.00 | a | 60±6.0 | a |

### 3.3.6.2 Nitrogen, carbon and light-use-efficiencies

Carbon and light-use-efficiencies were evaluated in the wet season (Feb-2016; Table 3.5). *C. opaca* exhibited the largest CUE (0.98 ± 0.00 daily C gain *per* mol C fixed) while *A. aneura* exhibited the smallest CUE of 0.72 ± 0.11 daily C gain *per* mol C fixed and, this was significantly smaller than the CUE of *C. opaca*. *H. macrocarpa* and *T. schinzii* were the only two species that did not have CUE mean values different from *C. opaca*. Mean values of the photosynthetic light-use-efficiency (LUE) were not significantly different among species and ranged between 50 and 80 mmol $CO_2$ $\mu mol^{-1}$ photons.

The mean values of instantaneous PNUE occasionally differed significantly among species (*p*-value<0.001) within sample dates (Table 3.5). Averaged PNUE across species and dates was 3.92 ± 1.60 μmol $CO_2$ $(g\ N)^{-1}\ s^{-1}$, ranging from 0.1 ± 0.01 to the very extreme value of 15.9 ± 0.82 μmol $CO_2$ $(g\ N)^{-1}\ s^{-1}$ from *T. schinzii.* PNUE in Mar-2015 did not show significant differences among species with an average value of 3.68 ± 0.63 μmol $CO_2$ $(g\ N)^{-1}\ s^{-1}$ across all species. In contrast, PNUE values in *Acacia* spp. (from both sites) were significant smaller than those of *H. macrocarpa* (4.5 ± 1.53 μmol $CO_2$ $(g\ N)^{-1}\ s^{-1}$) and *C. opaca* (6.0 ± 0.47 μmol $CO_2$ $(g\ N)^{-1}\ s^{-1}$). The PNUE did not differ significantly among these two species. A similar pattern was observed in Feb-2016 with the exception of *T. schinzii, which* was significantly larger than the remaining species.

PNUE had a negative exponential decay correlation function with leaf mass *per* area (LMA) across all species (Fig. 3.7) such that as LMA increased, PNUE decreased exponentially. Lower PNUE values were observed in C3 species, compared to high PNUE and low LMA in the C4 grass (*T. schinzii*). LMA for C3 species ranged from 247.1 g $m^{-2}$ in *C. opaca* to extremely high values > 500 g $m^{-2}$ in *H. macrocarpa* and *A. aptaneura*. The C4 species (*T. schinzii*) had the lowest LMA values averaging 229.4 ± 2.42 g $m^{-2}$.

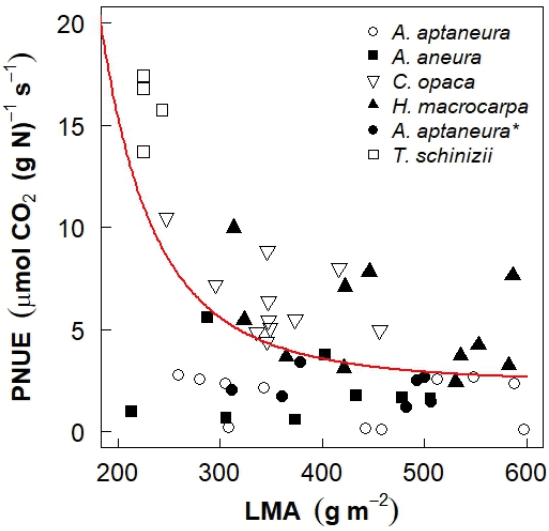


Figure 3.7 Photosynthetic nitrogen-use-efficiency (PNUE) as a function of leaf mass per area (LMA). The relationship PNUE *vs.* LMA displayed with a negative power function ($y = a^* x^{-b} + c$; $r^2 = 0.38$; $p$-value<0.05 for parameters estimated). Points are individuals as replicates *per* species.

## *3.4 Discussion*

In this study, I evaluated seasonal variability of resource-use-efficiencies (RUE) in co-occurring species of two semi-arid ecosystems in central Australia. At leaf-level, resources such as water and nitrogen were examined in three contrasting periods (late wet season, dry season and wet season), while light and carbon-use efficiencies were evaluated only in the wet season when water was not limiting. Additionally, two different evaluations of intrinsic water-use-efficiency ($WUE_i$; gas exchange and carbon isotope discrimination) were compared.

### 3.4.1 Relationships among plant water status with leaf gas exchange

A determining feature of seasonality in central Australia is that of variation in soil water content (Cleverly *et al.*, 2016b; Eamus *et al.*, 2016), with low values in the dry season and larger values in the wet season. Seasonal variations in $\Psi_{pd}$ provided insights about plant-water availability, and was especially useful in highlighting the different eco-hydrological niches occupied by the *Acacia* spp., compared to *C. opaca* and *H. macrocarpa*. Variability in soil water content ultimately depends on the magnitude and timing of rainfall, which triggers plant productivity in the Mulga woodland and *Corymbia* savanna species that depend on shallow soil water content.

Here it was observed that *Acacia* spp., at both sites (Mulga woodland and *Corymbia* savanna), had significantly lower foliar pre-dawn ($\Psi_{pd}$) values than those observed for *C. opaca* and *H. macrocarpa*, across the three study periods (Table 3.2). Extreme negative $\Psi_{pd}$ (< -9 MPa) values were observed in *Acacia* spp. during the dry season (Oct-2015) in agreement with values observed in previous studies (Nolan *et al.*, 2017a; O'Grady *et al.*, 2009; Page *et al.*, 2016). In contrast, *C. opaca* and *H. macrocarpa* maintained relatively high $\Psi_{pd}$ values, even at the end of the dry season (Table 3.2). Previous studies have demonstrated that *C. opaca* has access to ground water (O'Grady *et al.*, 2009; Rumman *et al.*, 2018), and this explains the high $\Psi_{pd}$ values observed throughout the year and is a key determinant of the eco-hydrological niche occupied by this species. Likewise, *H. macrocarpa* is highly likely to produce root clusters, which are common across *Hakea* spp. (Lamont, 2003). Root clusters have three beneficial effects on plant water relations: they increase the surface area of roots by a large factor (up to 140 fold); increase the soil volume explored by a factor of up to 300; and release deeply sourced water at night for subsequent uptake the following day through the process of hydraulic lift (Lamont, 2003). All three features are likely to contribute to the improved water status of *H. macrocarpa* compared to the co-occurring *Acacia* spp.

Pre-dawn water potential impacts on stomatal conductance ($g_s$) and the regulation of carbon and water fluxes (McDowell *et al.*, 2015). Across the three study periods, species with the highest $\Psi_{pd}$ values (i.e., *C. opaca* and *H. macrocarpa*; Table 3.2) also maintained the largest $g_s$ (Fig. 3d, f). Conversely, the two *Acacia* spp., which maintained the lowest $\Psi_{pd}$ and also exhibited low $g_s$ values across all seasons (< 0.15 mol $m^{-2}$ $s^{-1}$). Although $\Psi_{pd}$ is a useful indicator of plant water availability, other factors such as temperature and water vapour pressure deficit influence $g_s$ (Eamus *et al.*, 2008; Sperry and Love, 2015). Therefore, plants have to regulate their water transport within the soil-plant-water-atmosphere continuum in order to survive both large changes in soil water availability and atmospheric evaporative demand.

A large change in environmental conditions (light, temperature, water vapour pressure deficit, soil water content) occurred during the day between the early morning and late afternoon in the Mulga woodland and *Corymbia* savanna (see Chapter II). Consistently, all species exhibited large declines in foliar water potentials from $\Psi_{pd}$ to $\Psi_{md}$ (Table 3.2). *T. schinizzi* displayed significantly more negative water potentials from $\Psi_{pd}$ (-0.7 MPa) to $\Psi_{md}$ (-2.4 MPa) and these values were comparable to those reported by Grigg *et al.* (2008). The largest differences between $\Psi_{pd}$ and $\Psi_{md}$ were usually (but not always) observed in *Acacia* spp. (> 2.0 MPa). There were, however, significant differences in $\Psi_{md}$ between *A. aptaneura* and *A. aneura* in all three-study periods (Table 3.2). Page *et al.* (2016) argued that differences within *A. aptaneura* (most terete phyllodes) and *A. aneura* (sub-terete) are due to differences in Huber values (the ratio of sapwood to leaf area) and phyllode types, since large phyllodes can transpire more water and experience lower phyllode water potentials than small phyllodes (Page *et al.*, 2016). Thus, this may partially explain the differences in $\Psi_{md}$ found within the two *Acacia* spp. The systematic variation from $\Psi_{pd}$ to $\Psi_{md}$ demonstrates how environmental conditions can influence plant water potentials. The very negative values of water potential experienced by the *Acacia* spp. confirmed the reliance of these species on rainwater in the upper soil profile. This arises because of the shallow root system of *Acacia* spp., and the presence of a shallow (< 1.2 m) hardpan at the Mulga site (Cleverly *et al.*, 2016b).

Although differences from $\Psi_{pd}$ to $\Psi_{md}$ in *C. opaca* were almost 2.0 MPa, water potentials were still higher (less negative) than those of either *Acacia* spp. (Table 3.2). Thus, *C. opaca* maintained relative high $g_s$ (> 0.15 mol $m^{-2}$ $s^{-1}$) from early morning to midday except for the late dry season (Oct-2015), at which time $g_s$ approached zero (Fig. 3.3). Similarly, $\Psi_{pd}$ and $\Psi_{md}$ values of *H. macrocarpa* were in the range of those observed in *C. opaca* except for the transition between wet and dry season (Mar-2015). These different behaviours among species revealed an important insight into regulation of leaf water potentials through stomatal regulation and assist in classification of these species into one of two strategies: isohydric or anisohydric (Martinez-

Vilalta *et al.*, 2014). Isohydric species use rapid declines in $g_s$ to tightly regulate leaf water potentials in the early stages of soil desiccation, resulting in decreasing $A_n$ (Limousin *et al.*, 2013; Meinzer *et al.*, 2009; Nolan *et al.*, 2017c). In contrast, anisohydric species tolerate a larger decline of leaf water potentials, thereby allowing the maintenance of $g_s$ and $A_n$ during the latter stages of soil drying despite large declines in soil and xylem water potential. Therefore, my results support the conclusion that *Acacia* spp. utilized an anisohydric strategy, during the three study periods relative to the more isohydric species (Fig. 3.5; *C. opaca* and to some extent *H. macrocarpa*) (Nolan *et al.*, 2017a, b; O'Grady *et al.*, 2009).

I now discuss relationships among diurnal foliar water potentials, $g_s$ and $A_n$ and therefore intrinsic WUE ($WUE_i$).

### 3.4.2 Diurnal trends in $\Psi_{leaf}$, $g_s$, $A_n$ and $WUE_i$

Significant positive relationships were observed between diurnal foliar water potentials ($\Psi_{leaf}$) and diurnal leaf gas exchange. In both Mar 2015 and Feb 2016, $A_n$ and $g_s$ increased linearly with increasing foliar water potential (Fig. 3.5a, b, d, e), with species being described by a single regression, indicating significant convergence in behaviour across species. Furthermore, there was a significant negative correlation between $WUE_i$ and foliar water potential (Fig. 3.5c, f). This is in agreement with the hypothesis that during periods of declining foliar water potential (i.e., moving into the dry season), $WUE_i$ will increase for all species examined and this will negatively correlate with leaf pre-dawn water potentials, due to the positive influence of pre-dawn water potentials on $g_s$ and hence $A_n$. The two extremes in the regressions for Mar-2015 (Fig. 3.5a, c) were *A. aptaneura* and *C. opaca. A. aptaneura* had the most negative $\Psi_{leaf}$ (average < -5 MPa; Table 3.4) with the lowest $g_s$ values, reflecting this species' reliance on soil moisture in the upper soil profile. In contrast, *C. opaca* had highest $\Psi_{leaf}$ (average > -3 MPa; Table 3.4) with largest $g_s$ during the day, reflecting its year-long access to groundwater. *A. aneura* and *H. macrocarpa* maintained intermediate $\Psi_{leaf}$ and $g_s$ values in the regression, with *H. macrocarpa* displaying values of $A_n$ and $g_s$ closer to *C. opaca,* and *A. aneura* was most similar to *A. aptaneura* (Table 3.4). However, earlier in the wet season (Feb-2016) *A. aneura* exhibited the most negative $\Psi_{leaf}$ and the lowest $g_s$.

Similarly, there was a positive and significant relationship between $\Psi_{leaf}$ and $A_n$, in which extreme large $A_n$ and highest $\Psi_{leaf}$ values were observed for *T. schiinizii* (a C4 grass) and *C. opaca* along with *H. macrocarpa.* The year-long water supply from groundwater in *C. opaca* can explain the maintenance of large values of both $A_n$ and $g_s$ (in both periods Mar-2015 and Feb-2016),

despite large values of VPD and temperature during these periods. In contrast, *T. schiinizii*, which maintained large values of $A_n$ with moderate-low $g_s$, which arises from the fact that this grass is a C4 species which can maintain large photosynthetic rates because of the $CO_2$ concentrating mechanism inherent in the Kranz anatomy of C4 grasses, especially if the atmospheric water demand is being satisfied, such as was the case Feb-2016 when soil moisture content was large. Here, *T. schiinizii* had significant large $g_s$ (< 0.4 mol $m^{-2}$ $s^{-1}$ or 1.7 mmol $g^{-1}$ $s^{-1}$) compared with that observed by Grigg *et al.* (2008) of *ca.* 1.3 mmol $g^{-1}$ $s^{-1}$. This difference may be due to differences in local topography, since *T. schiinizii* within the *Corymbia* savanna occurs in a flat floodplain, whilst in the Grigg *et al.* (2008) study, *T. schiinizii* occurred in dunes.

In addition to the relationships of $\Psi_{leaf}$ with $A_n$ and $g_s$, I observed that $WUE_i$ was significantly and negatively correlated with $\Psi_{leaf}$ (Fig. 3.5), in agreement with a five-species comparison of north Australian tropical trees (Thomas *et al.*, 1999b). $WUE_i$ increased linearly among species as $\Psi_{leaf}$ decreased due to changes in both $g_s$ and $A_n$. *C. opaca* exhibited the smallest $WUE_i$ and simultaneously the highest $\Psi_{leaf}$ values. The small $WUE_i$ is a consequence of the maintenance of a large $g_s$, which will support large rates of transpiration during periods of large VPD throughout the day (Fig. 3a, d). Although *C. opaca* were sampled in this study in a semi-arid environment, previous studies have concluded that *C. opaca* behaves similarly to species growing in mesic environments, due to its low variability in leaf water potential (Nolan *et al.*, 2017a), large rates of sap flow and gas exchange (Nolan *et al.*, 2017b; O'Grady *et al.*, 2009), low water-use-efficiency observed with large carbon isotope discrimination (Rumman *et al.*, 2018) and high hydraulic conductance and wide xylem vessel diameter (Santini *et al.*, 2015). A recent study by Rumman *et al.* (2018) has shown that there were no differences in xylem water and bore water (i.e., groundwater) isotopic compositions of water and no differences between wet and dry seasons in *C. opaca*. Thus, the results of $\Psi_{leaf}$, $A_n$ and $g_s$, and $WUE_i$ indicated that *C. opaca* was not sensitive to changes in diurnal conditions (i.e., increasing temperature and VPD, declines in upper soil water content) nor changes across seasons and this can be ascribed to year-long access to groundwater by this tall, deep rooted tree (Rumman *et al.*, 2018).

The large $WUE_i$ observed in *Acacia* spp. can be explained by their low $g_s$, even during wet seasons (Fig. 3.3, see at Mar-2015 and Feb-2016). *Acacia* spp., as previously observed with the stable isotopes approach (Rumman *et al.*, 2018) and several plant physiological trait relationships (Nolan *et al.*, 2017a; Page *et al.*, 2016) exhibits an “opportunistic” strategy of water-use when water is available. Several important bivariate trait relationships have been identified in *Acacia* spp., from central Australia, including relationships among high wood density (Santini *et al.*, 2017), narrow xylem vessels (Page *et al.,* 2011), large leaf mass *per* area (Nolan *et al.,* 2017b) and high root and branch xylem vessel resistance to implosion (Santini *et*

*al.*, 2015; Santini *et al.*, 2017). These traits confer a large capacity to withstand periods of very low soil moisture content and very low canopy water potentials (Nolan *et al.*, 2017c) that may contribute to any explanation of the low stomatal conductance observed in *Acacia aptaneura*.

Significantly larger slopes in the regressions of $\Psi_{leaf}$ *versus* $A_n$ and $\Psi_{leaf}$ *versus* $g_s$ were observed when comparing Feb 2016 with March-2015. This may arise because larger rainfall in the preceding 2 months (44 mm compared to 3 mm) in Feb-2016 and smaller mean VPD allowed a larger $A_n$ to be expressed when foliar water potential was high, but simultaneously had a steeper decline in $A_n$ as foliar water potentials declined as soil became drier. Such an effect was discussed in Thomas *et al.* (1999b) in an analysis of the response of a north Australian savanna eucalypt to VPD. Because of the larger variation in $WUE_i$ observed across species (especially for *A. aptaneura*) in Mar-2015 the slopes of $WUE_i$ *versus* diurnal water potentials did not differ across the two sampling periods. However, if one outlier for *A.aptaneura* in Fig. 3.5c is omitted, the larger slope that arises in Mar-2015 is consistent with the smaller values of $A_n$ and the fact that far less rain was received in the two months prior to field sampling in Mar-2015 than Feb-2016 and similar values of $g_s$ observed between Mar-2015 and Feb-2016 and consistent with the conclusions drawn by Eamus *et al.* (2013).

### 3.4.3 Resource-use-efficiencies and trait combinations across species

Despite expectations of large and significant variation in resource-use-efficiencies (RUE) among species, arising from the different foliar water status (as evidenced by $\Psi_{pd}$ and $\Psi_{md}$), leaf forms, $N_2$-fixing/non $N_2$-fixing habits, cluster roots of *Hakea macrocarpa* and shallow *versus* deep-rooted habits of *Acacia* spp. *versus Corymbia opaca*, there were surprisingly few significant differences in non-water RUEs, and what differences were apparent were relatively small. Table 3.6 summarizes some of the key differences, similarities and relationships among species. I speculate that the minor differences in RUE among species are indeed the result of divergent plant physiological traits and distinct eco-hydrological niches occupied by the species selected for this study (Nolan *et al.*, 2017a; O'Grady *et al.*, 2009). Thus, whilst occupying specific ecological niches, and having distinct WUE, species convergence to similar RUE across key resources is apparent in central Australia, in particular, CUE, LUE and PNUE. I will now explain my main findings in CUE, LUE and PNUE across species, while WUE is explained further in the following section.

Table 3.6 Summary of key differences, similarities and relationships among woody-species of leaf traits and resource-use-efficiencies (RUEs). Traits are: midday and diurnals foliar water potential ($\Psi_{md}$ and $\Psi_{leaf}$, respectively), net assimilation ($A_n$) and $A_n$ at PPFD= 2000 μmol $m^{-2}$ $s^{-1}$ ($A_{n2000}$), maxima rate of gross assimilation ($A_{max}$, model asymptote), light saturation point (LSP), light compensation point (LCP), stomatal conductance ($g_s$), maxima $g_s$ ($g_{s\text{-}max}$) and leaf mass *per* area (LMA). RUEs are: plant nitrogen-use-efficiency (PNUE), carbon-use-efficiency (CUE) and light-use-efficiency (LUE). (*) *A. aptaneura* located at the *Corymbia* savanna site.

| | Variables | *Acacia aptaneura* | *Acacia aneura* | *Corymbia opaca* | *Hakea macrocarpa* | *Acacia aptaneura** |
|---|---|---|---|---|---|---|
| **Species trait combinations** | **Dry season $\Psi_{md}$** | very low | lowest | highest | high | low |
| | $A_{n2000}$ | very low | lowest | moderate | high | low |
| | $A_{max}$ | high | lowest | moderate | high | moderate |
| | **LSP** | No species differences | No species differences | No species differences | No species differences | No species differences |
| | $\Psi_{leaf}$ ***vs*** $A_n$ | all species converge to one regression | all species converge to one regression | all species converge to one regression | all species converge to one regression | all species converge to one regression |
| | $\Psi_{leaf}$ ***vs*** $g_s$ | all species converge to one regression | all species converge to one regression | all species converge to one regression | all species converge to one regression | all species converge to one regression |
| | $g_{s\text{-}max}$ | smallest | small | largest | second largest | small |
| **Resources-use-efficiencies** | **PNUE** | very low (dry season) to moderate (wet season) | very low (dry season) to moderate (wet season) | largest | large | very low (dry season) to moderate (wet season) |
| | **CUE** | Moderate | smallest | largest | large | small |
| | **LUE** | No species differences | No species differences | No species differences | No species differences | No species differences |
| | **PNUE *vs.* LMA** | all species converge to one regression | all species converge to one regression | all species converge to one regression | all species converge to one regression | all species converge to one regression |

Species that have a set of traits to withstand semi-arid condition such as *A. aptaneura, H. macrocarpa* and *T. schinzii* (Grigg *et al.*, 2008; Groom *et al.*, 1994; O'Grady *et al.*, 2009; O'Grady *et al.*, 2006; Page *et al.*, 2016) had the largest $A_{n2000}$ and this may reflect a large investment of available resources to photosynthetic processes or much larger RUE or a combination of both strategies. Similarly, these species had the largest values in maximal rates of assimilation ($A_{max}$) under light saturated conditions, which again represents a large return on resources invested in leaves (Cernusak *et al.*, 2011). Because photosynthesis is the fuel for respiration, these species had also the largest $R_d$ (Table 3.3). Sufficient water (as measurements were only made in the wet season), high light intensities and a C4 photosynthetic pathway resulted in *T. schinizii* attaining high rates of carbon assimilation, consistent with Grigg *et al.* (2008). *A. aptaneura* is a species with high tolerance to low soil moisture content values but, perhaps most importantly, is a $N_2$-fixing species. Resource substitution (substituting $N_2$ for water) allows *Acacias* to maintain low $g_s$ but a large $A_n$ during dry periods (Taylor and Eamus, 2007). Large rates of $A_{max}$ and $A_{n2000,}$ a large $WUE_i$, resource substitution and extreme tolerance to low soil moisture contents may explain the high abundance and large distribution of *Acacia* spp. across the semi-arid and arid regions of Australia.

In order to maximize LUE a large investment in N is required (Chapin, 2002). Although, this study only evaluated LUE during the wet season, LUE varies across seasons (Shi *et al.*, 2014) and among different vegetation types (Ma *et al.*, 2014). In a remote sensing study, Shi *et al.* (2014) found that differences in LUE and WUE between wet and dry seasons in Australia were due to changes in soil water content and leaf area index. To my knowledge there has not been LUE reported at leaf-scales for these species. Therefore, my results may contribute to parameterization of remote sensing algorithms that can reduce uncertainties in the estimation of gross primary productivity at ecosystem-scales (Running *et al.*, 2004).

In order to maximize LUE a large investment in N is required. Across all seasons, *C. opaca* exhibited the largest PNUE values and were statistically larger than *Acacia* spp. (Table 3.5). Here, it was also found that *C. opaca* had the lowest $R_d$ of all species examined (Table 3.3). Therefore, *C. opaca* had the largest CUE values (Table 3.6). Large CUE may be due to *C. opaca* having a large demand for C to support its (presumably genetically defined) large stature, which in turn requires a large rate of maintenance respiration, because plant respiration is an inherent component in plant growth and a key component in the estimation of CUE (DeLucia *et al.*, 2007). Therefore, *C. opaca* had moderate $A_{n2000}$ and $A_{max}$ values (Fig. 3.4 and Table 3.3). It may be that *C. opaca* is limited by its carboxylation capacity which may be limited by N supply (Evans 1989) as this species is not an $N_2$-fixer. The year-long water supply from groundwater and upper soil water, and high PNUE by *C. opaca* likely explain its success in semi-arid Australia.

*Acacia* spp. showed seasonal variability in PNUE, with low values in the dry season and high values in the wet season. Because PNUE is a ratio, seasonal differences can be explained by the two components of PNUE ($A_n/N_a$). First, the abrupt decay $A_n$ during dry seasons due to low soil water content, explains the very low PNUE values observed in *Acacia* spp. in the dry season when compared with wet seasons (Table 3.5). Second, foliar N content usually changes little over the year, however changes in $N_a$ can be attributed to fluctuations in leaf area (as N *per* unit of leaf area ($N_a$; g N $cm^{-2}$)), where a shrinkage in the leaves / phyllodes might cause lower values of leaf area. Nonetheless, seasonal changes in PNUE observed in *A. aptaneura* and *A. aneura* were attributed only to $A_n$. To conclude, *Acacia spp.* had marginal returns of carbon gain *per* unit of N used as the supply of N increases (low PNUE, especially during the dry season when $N_a$ increases). Clearly, *Acacia* spp. have superior efficiency in water use ($WUE_i$) but *C. opaca* has a larger PNUE and CUE compared with the Acacias.

There was an inverse correlation between PNUE and LMA in which all species converged to one regression (Fig. 3.7). The inverse relationship between PNUE and LMA support the hypothesis that predicted that variations in PNUE will be correlated with differences in LMA among species and $N_2$-fixing species that have large N content *per* leaf area and will have smaller PNUE compared with species that are not $N_2$-fixing. This result is in agreement with similar relationships observed between LMA and attributes of leaf N content (Lamont *et al.*, 2002).

### 3.4.4 How does $WUE_i$ estimated with different methods predict seasonal variability of plant water uptake?

This study aimed to evaluate two different approaches to estimate $WUE_i$ at the leaf-scale using: i) leaf gas exchange and ii) carbon isotope signatures ($\delta\ ^{13}C$), to test the hypothesis that different evaluations of $WUE_i$ will disclose contrasting insights into plant water uptake. While leaf gas exchange measures the real time $WUE_i$, $\delta^{13}C$ calculates $WUE_i$ based on the carbon discrimination ($\Delta^{13}C$) by the Rubisco enzyme and carbon diffusion across the stomatal pathway (Farquhar *et al.*, 1989). $WUE_i$ estimated using stable isotopes from bulk leaf and leaf total sugars did not show significant differences across the three study periods and related isotopic parameters ($\Delta^{13}C$ and $C_i/C_a$; Table S.3.2, S.3.3) except for *C. opaca.* These results are in the same range of values observed in *Corymbia spp.* that occur in northern Australia under 500 mm (Cernusak *et al.*, 2011). It is likely that *C. opaca* combines the use of groundwater and upper soil water derived from rain and therefore water availability was not limiting during the wet period (i.e., Feb-2016), resulting in low $WUE_i$ in the wet season as observed with the large $\Delta^{13}C$ and

therefore. This can be confirmed with the large $g_s$ and $A_n$ observed with leaf gas exchange measurements (Fig. 3.3c, f). $WUE_i$ was reduced during wetter conditions causing a depletion of $\delta^{13}C$ (-28.4 ± 0.20 ‰; Feb-2016) in leaves and increased $\Delta^{13}C$. Consistently, $\Delta^{13}C$ decreased during dry periods (Mar-2015 and Oct-2016) in *C. opaca* and it was not statistically different from $\Delta^{13}C$ observed in *Acacia* spp. (Table S.3.2), converging in the long-term $WUE_{i(bulk\text{-}leaf)}$ among these species (Table 3.5). Previous studies have demonstrated that $\Delta^{13}C$ varies with mean annual precipitation (Cernusak *et al.*, 2005; Miller *et al.*, 2001; Rumman *et al.*, 2017; Turner *et al.*, 2010). Here, I observed that $\Delta^{13}C$ responded to seasonality of rainfall and this result contributes to our understanding of the contrasting $WUE_i$ observed across seasons.

The $\Delta^{13}C$ of bulk leaf tissue has been widely used to estimate $WUE_i$, since leaves are more exposed to environmental conditions of variations in temperature, VPD and hence $g_s$ (via changes in soil moisture content) (Bowling *et al.*, 2008). Bulk-leaf isotopic signature (as $\delta^{13}C_{bulk\text{-}leaf}$) encompassed the entire period in which the carbon was fixed. Consequently, $\Delta^{13}C$ represents an integrated assimilation-weighted estimate of intercellular and atmospheric water vapour pressures ratios (Brugnoli and Farquhar, 2000). Here, $\Delta^{13}C$ estimated in *Acacia spp.* and *H. macrocarpa* did not show changes for bulk leaf tissue across seasons (Table S.3.2). This indicates a steady $\Delta^{13}C$ and therefore $WUE_i$ observed in *Acacia spp.,* and *H. macrocarpa.* It is likely that carbon isotopic signatures (hence, $\Delta^{13}C$ and $WUE_i$) observed in *Acacia spp.,* and *H. macrocarpa* was strongly influenced by the average environmental conditions of the long dry periods (i.e., low soil moisture, high VPD, high solar radiation) rather than the short-term conditions extant during the wet season (i.e., high soil moisture, low VPD and low solar radiation) that are extremely variable year-to-year in semi-arid regions (Van Etten, 2009).

The carbon signal in total leaf sugars ($\delta^{13}C_{sugars}$) should provide a better indication of the short-term changes in $\Delta^{13}C$ and $WUE_i$ associated with changes in assimilation over the entire day (Brugnoli *et al.*, 1988; Brugnoli and Farquhar, 2000). However, in this study, similar $\Delta^{13}C$ values were observed between estimations from $\delta^{13}C_{sugars}$ and $\delta^{13}C_{bulk\text{-}leaf}$ in *Acacia spp.*, and *H. macrocarpa* and no significant differences across seasons (Table S.3.3). These results are in agreement with other studies in which small seasonal changes in $\delta^{13}C_{sugars}$ were attributed to slow turn-over rates of photo-assimilates or due to the significant storage carbon components (Page *et al.*, 2016; Scartazza *et al.*, 2004). In agreement with Page *et al.,* 2016, my results suggested that *Acacia spp.* and *H. macrocarpa* maintained low photo-assimilate turnover times across the entire annual cycle. Because $\delta^{13}C_{sugars}$ is an approximation of the new photo-assimilate (Brugnoli *et al.*, 1988); my results showed that $\delta^{13}C_{sugars}$ in *Acacia spp.,* and *H. macrocarpa* reflect the long-term assimilation (as $\delta^{13}C_{bulk\text{-}leaf}$) and not new photo-assimilation. Hence, total sugars analyses were not reliable estimates of short-term assimilation, at least for

*Acacia spp.,* and *H. macrocarpa*. Other factors influencing leaf carbon balance and hence carbon isotopic signal, include mesophyll conductance and photorespiration which are not integrated in the $\Delta^{13}C$ model (Seibt *et al.*, 2008). Specifically, measurements of $A_n$ in *Acacia* spp., during the late dry season (Oct-2015) were extremely low or negative (Fig. 3.3b) and this can explain the unrealistic short-term $WUE_i$ estimated using $\delta^{13}C_{sugars}$. Further studies in *Acacia* spp. should be conducted using phloem sap soluble sugars, which is the substrate for plant respiration as this can reveal information about seasonal changes in $\delta^{13}C$ (Scartazza *et al.*, 2004).

In contrast to *Acacia spp., H. macrocarpa* and *C. opaca* had low $\Delta^{13}C$ (estimated from $\delta^{13}C_{sugars}$) values which were statistically smaller from the remaining species (Table S.3.3). The low $\Delta^{13}C$ observed in the late dry season (Oct-2015) in *C. opaca* indicates a significant shift in $\Delta^{13}C$ (and therefore in $WUE_i$) compared to Mar-2015 and Feb-2016. This raises the question: why did *C. opaca* have low $\Delta^{13}C$ (and hence increased $WUE_i$) during the dry season (Oct-2015), if *C. opaca* relies on groundwater supply? This question can be addressed in two ways and the first is based on the same discussion made for $\Delta^{13}C$ estimated from $\delta^{13}C_{bulk\text{-}leaf}$. If *C. opaca* has the capability to use both groundwater and water from the upper soil profile, then both isotopic compositions (from bulk leaf and leaf total sugars) reflect the influence of two sources of water, with one source (the upper soil water content) declining significantly in the dry season. Second, this capacity to use both groundwater and water from the upper soil profile has implications for xylem hydraulic conductance since the path length from where the water is absorbed differs. Gleason *et al.* (2013) found that xylem hydraulic conductance is correlated with plant height, whereas McDowell *et al.* (2011) has reported that as tree height increased, $\Delta^{13}C$ declined (hence, increases in $WUE_i$) across a wide range of habitats and species because of the gravitational constraints upon hydraulic conductance. Similarly, Rumman *et al.* (2018) found that $\Delta^{13}C$ was negatively correlated with leaf vein density (LVD) and LVD is related to leaf hydraulic conductance which is proportional to the length of the hydraulic path (Brodribb *et al.*, 2007).

Different approaches of estimating $WUE_i$ at leaf-scale showed a broad view into plant water uptake strategies at different time resolutions. The conclusions are: (i) to observe changes in $WUE_i$ in shallow-rooted species, $WUEi_{(leaf\text{-}gas)}$ was best captured using temporal changes in $WUE_i$ (both seasonally and diurnally; Fig. 3.3g, i), (ii) $WUE_i$ estimated from isotopic signatures (both, $\delta^{13}C_{sugars}$ and $\delta^{13}C_{bulk\text{-}leaf}$) was able to detect seasonal shifts in *C. opaca* but not in *Acacia* spp. and *H. macrocarpa*. This indicates that both $\Delta^{13}C$ (and hence $WUE_i$) from leaf sugars and bulk-leaf values revealed long-term trends in $WUE_i$ in *Acacia* spp. and *H. macrocarpa,* because isotope signatures did not detect seasonal differences (Table S.3.2, S.3.3). In contrast, total sugars and bulk-leaf estimates of $WUE_i$ from isotopic analyses provided important information about water-use strategies (water uptake and $WUE_i$) in the deep-rooted species *C. opaca*. These results

confirmed that $\Delta^{13}C$ reveal insights into groundwater dependency of vegetation (Moreno-Gutierrez *et al.*, 2012; Rumman *et al.*, 2018).

## *3.5 Conclusions*

The aim of this study was to compare variation of carbon, nitrogen, water and light-use-efficiencies across multiple co-occurring species in central Australia. I found that although the five species of this study (4 tree species and 1 grass species) occupy specific eco-hydrological niches and they diverged in WUE; species converged to similar RUE across key resources, particularly CUE, LUE and PNUE. Seasonal variations in foliar water potential and carbon isotopic discrimination provided insights about plant-water availability and water sources, and was especially useful in highlighting the different eco-hydrological niches occupied by the *Acacia* spp., compared to *C. opaca* and *H. macrocarpa*.

Due to large changes in environmental conditions (light, temperature, water vapour pressure deficit and soil water content) which drives plant transpiration rates, all species exhibited large declines in foliar water potentials from pre-dawn to midday ($\Psi_{pd}$ to $\Psi_{md}$ respectively). This variation demonstrated how environmental conditions influenced diurnally plant water status. The very negative values of water potential experienced by the *Acacia* spp. across seasons, confirmed the reliance of these species on rainwater in the upper soil profile. In contrast, I observed large water potentials (less negative values) in *C. opaca* reflecting its year-long access to groundwater, and *H. macrocarpa* possibly because of the possession of root clusters.

Carbon assimilation and stomatal conductance increased linearly with increasing foliar water potential. These different behaviours among species revealed an important insight into regulation of leaf water potentials through stomatal regulation and assisted in the classification of these species into isohydric and anisohydric. Furthermore, there was a significant negative correlation between $WUE_i$ and foliar water potential, species being described by a single regression, indicating significant convergence in behaviour across species.

# *Chapter IV*

## An evaluation of how changes in soil moisture content drive changes in intrinsic water-use-efficiency via optimal stomatal behaviour

## *4.1 Introduction*

Stomata are tiny pores in the leaf surface that allow plants to photosynthesize and transpire. Thus diffusion through stomata is the pathway through which carbon and water fluxes are linked. Evapotranspiration (ET) is an important component of the water budget in terrestrial ecosystems, with transpiration representing *ca.* 61 % of total ET (ET: soil evaporation, wet canopies and plant transpiration; Schlesinger and Jasechko, 2014) and more than 50 % of carbon fixation worldwide occurs in terrestrial ecosystems via photosynthesis (Le Quéré *et al.*, 2017). Therefore, an understanding of stomatal functioning is crucial to improving our understanding of the global carbon (C) and water fluxes and budgets, and to improve water and ecosystem management (Keenan *et al.*, 2013; Tang *et al.*, 2014).

Stomata respond to biotic (e.g. plant hormone concentration, leaf water potential) and abiotic (e.g. soil water content, vapour pressure deficit (VPD), light flux density) factors (Nobel, 2009; Sperry and Love, 2015). Stomata have the ability to control the loss of water transpired for the $CO_2$ that plants need for photosynthesis (Berry *et al.*, 2010). This trade-off is defined as water-use-efficiency, for which there are multiple definitions (Eamus, 1991), including the ratio of carbon assimilation ($A$) to transpiration ($E$) as WUE= $A/E$ (Seibt *et al.*, 2008). It is predominantly (though not exclusively) via changes in stomatal conductance ($g_s$) that changes in environmental factors (i.e., abiotic factors) result in changes in WUE. An alternate measure of water-use-efficiency is termed intrinsic water-use-efficiency ($WUE_i = A/g_s$) and this is a commonly used measure of WUE because it takes into account the fact that $E$ responds to changes in both VPD and $g_s$ while $A$ responds to changes in $g_s$ but not VPD (Eamus *et al.*, 2013; Seibt *et al.*, 2008).

Optimization theory, as applied to transpiration and photosynthesis (Cowan and Farquhar, 1977) states that stomata should behave such that the C gained through photosynthesis is maximized *per* unit water transpired, that is, there is a coordination between $A$ and the marginal cost of water use (λ) as $\lambda = \partial E/\partial A$, which defines an optimal behaviour of stomata (Medlyn *et al.*, 2011). The theory of optimal stomatal behaviour is described with semi-empirical models, parameters of which are used in global earth system models (Miner *et al.*, 2017; Wolz *et al.*, 2017). The widely used empirical Ball-Berry model (Ball and Berry, 1987) evaluates the relationship between $g_s$ and $A$ as a function of environmental conditions (Miner *et al.*, 2017).

Models related to the Ball-Berry model describe stomatal conductance as a function of the rate of net photosynthetic carbon uptake ($A_n$), and vary in complexity, assumptions and required parameters to determine optimal stomatal functioning (Damour *et al.*, 2010; Thomas *et al.*, 1999a; Wolz *et al.*, 2017). Consequently, several issues associated with the implementation of these different models have been identified (Thomas *et al.*, 1999a). For example, an apparent increase of $\partial$E/$\partial$A with increasing VPD or an incorrect representation of stomatal response to atmospheric $CO_2$ concentration (Medlyn *et al.*, 2011; Thomas *et al.*, 1999b) make it difficult to compare values of the optimal stomata behaviour across different ecosystems, plant species or vegetation growing under different abiotic conditions.

Medlyn *et al.* (2011) derived a semi-empirical optimal stomatal model closely analogous to the empirical Ball-Berry model, but taking into account VPD and $CO_2$ concentration, with the following form:

$$g_s \approx g_0 + 1.6\left(1 + \frac{g_1}{\sqrt{\mathrm{D}}}\right)\frac{A}{C_a} \qquad \text{(eq. 4.1)}$$

where D (kPa) is the vapour pressure deficit at the leaf surface, $A$ is net assimilation rate (μmol $m^{-2}$ $s^{-1}$), $C_a$ (μmol $mol^{-1}$) the atmospheric $CO_2$ concentration, $g_0$ is the leaf water vapour conductance when photosynthesis is zero (mol $m^{-2}$ $s^{-1}$) and, $g_1$ ($kPa^{0.5}$) is given by:

$$g_1 \propto \sqrt{\Gamma * \lambda} \qquad \text{(eq. 4.2)}$$

where $\Gamma^*$is the $CO_2$ compensation point in the absence of mitochondrial respiration and λ (mol $H_2O$ $mol^{-1}$ C) is a parameter for the marginal water cost of carbon gain (Medlyn *et al.*, 2011). From equation 4.2, the parameter $g_1$ should increase with $\Gamma^*$and the marginal water cost of carbon. Therefore, $g_1$ is inversely related to intrinsic water-use-efficiency, $WUE_i$ (Lin *et al.*, 2015; Medlyn *et al.*, 2011). Thus, large $g_1$values indicate low $WUE_i$, and *vice versa*.

$WUE_i$ can be measured across different temporal and spatial scales. At a leaf-scale, measurements of leaf gas exchange can provide real time estimations of $WUE_i$ in an

environmentally controlled leaf chamber (Caemmerer and Farquhar, 1981). Additionally, stable isotope discrimination theory allows estimation of $WUE_i$ using carbon isotopic compositions ($\delta^{13}C$) of whole leaves or sugars within leaves (Seibt *et al.*, 2008). Commonly, $WUE_i$ calculated from bulk-leaf tissue provides an estimate of the average $WUE_i$ estimated over the entire period during which the carbon was fixed (Brugnoli and Farquhar, 2000). In contrast, the carbon isotope signal in total leaf sugars should provide an indication of the short-term changes in isotopic discrimination ($\Delta^{13}C$) and $WUE_i$ associated with changes in assimilation over the day rather than the lifetime of the leaf (Brugnoli *et al.*, 1988). One problem with the isotopic discrimination theory is that it partially incorporates mesophyll conductance, which determines $CO_2$ diffusion inside the leaf and chloroplasts. At ecosystem-scales, the eddy covariance technique (EC) allows the measurement of carbon and water fluxes between the terrestrial surface and atmosphere (Baldocchi, 2014). From EC, calculated gross primary production (GPP: total photosynthesis by the ecosystem) and evapotranspiration (ET) can be used to estimate ecosystem WUE (eWUE= GPP/ET) (Ponton *et al.*, 2006; Tang *et al.*, 2014). All of these different approaches to estimate WUE have been used worldwide to evaluate vegetation performance, but multiple methods have not been applied to a single ecosystem.

A key problem with $WUE_i$ is its sensitivity to vapour pressure deficit and atmospheric $CO_2$ concentration. Therefore, the $g_1$ parameter represents a suitable alternative to compare $WUE_i$ among different plant functional types (PFT) in a constantly changing environment, because $g_1$ normalizes to VPD and $CO_2$ concentration (Lin *et al.*, 2015; Medlyn *et al.*, 2017). Recent work by Medlyn and colleagues (2017) compared global datasets of different estimations derived from different methods (i.e., stable isotopes, leaf gas exchange and eddy covariance) of $WUE_i$ across a range of plant functional types (PFT) using the $g_1$ parameter as a standardized proxy of $WUE_i$. Results of this study revealed that $WUE_i$ was not consistent among different datasets (i.e., different methodologies for calculating $WUE_i$) within a single PFT, thereby highlighting the difficulties in reconciling these different methodologies.

Knauer *et al.* (2018) evaluated physical and physiological mechanisms that could explain uncertainties in estimates of eWUE across different forests. They demonstrated that there are large uncertainties associated with derived GPP, partly arising from physiological variability in leaves within canopies and this leads to errors in estimations of eWUE. However, comparing data from different datasets is also difficult due to differences in data collection, data processing and standardized calibration protocols. Knauer *et al.* (2018) and Medlyn *et al.* (2017) focused on comparing $WUE_i$ (through the $g_1$ parameter) among PFT, rather than comparing different estimations of $WUE_i$ within a single site with more controlled protocols for data acquisition.

Moreover, it is not entirely clear which other environmental factors exert control over $g_1$ (hence, $WUE_i$) after it has been normalized by VPD and atmospheric $CO_2$ concentration.

Water availability is the most limiting resource in arid and semi-arid ecosystems (Huxman *et al.*, 2004b; Schwinning and Sala, 2004) and is a key factor driving optimization of the marginal cost of water, λ (Manzoni *et al.*, 2011). Water availability for plants is controlled by soil moisture content. As soil moisture content declines, water tension increases within plants and this has significant implications for leaf gas exchange (McDowell *et al.*, 2008). Thus, soil moisture content exerts a major control on ET (Jung *et al.*, 2010) and, consequently affects eWUE (i.e., GPP/ET). Soil moisture content is highly variable spatially and temporally, depending on the amount of rain, size and frequency of rain events, temperature, topography and changes in VPD and vegetation structure (Huxman *et al.*, 2004b; Loik *et al.*, 2004; Mascaro and Vivoni, 2016). The responses of leaf, whole-tree and ecosystem processes (i.e., photosynthesis, phenology, decomposition, $WUE_i$) to changes in water availability (i.e., rainfall or soil moisture) can be described with a scalar, β (Smith *et al.*, 2014). This empirical scalar ranges from 0 to 1 and describes the response of $g_1$ to a metric of water availability to simulate the process of stomatal closure during drought or periods of low levels of water availability (Drake *et al.*, 2017).

Semi-arid Australia is characterized by low mean annual rainfall with high inter-annual variability and consequently, water resources available to plant roots are highly variable and frequently limiting to gas exchange (Cleverly *et al.*, 2016c). Following cessation of the annual dry season (typically 5 months or more in duration), increased soil water availability triggers increased rates of carbon uptake and ET (Eamus *et al.*, 2016). Poulter *et al.* (2014) used modelling to conclude that additions of 100 mm of rainfall above the long-term average during the growing season led to a fourfold increase in net C uptake in semi-arid Australia. Thus, semi-arid Australia is an ideal location to evaluate the response of $eWUE_i$ to water availability.

One of the dominant ecosystems in semi-arid Australia is the Mulga woodlands, which occupy ~20-25% of the continent of Australia (Cleverly *et al.*, 2016c; Eamus *et al.*, 2013). Mulga is a complex of 12 closely related *Acacia* species (Maslin and Reid, 2012). The Mulga woodlands are relatively homogenous, and are typically dominated by one or two species. Mulga demonstrates high tolerance to arid and hot conditions, despite their shallow root systems. While Mulga can tolerate extended dry periods, they are also quick to respond to pulses of rain. For example, Cleverly *et al.* (2016c) demonstrated with field observations (EC data) that the Mulga woodland in the Ti-Tree Basin in central Australia exhibited an increase in annual NEP during the 2010-2011 global land sink anomaly when rainfall was almost double the long-term

average (Chapter II, this thesis). Likewise, Haverd *et al.* (2017) found that 74 % of the Australian land surface (including semi-arid regions) had a positive response of GPP to annual anomalies of large-than-average of rainfall. This demonstrates the resilience and large capacity of Mulga to respond rapidly and positively to larger-than-average rainfall. Therefore, the Mulga woodland offers an ideal opportunity to evaluate $WUE_i$ in a highly water dependent ecosystem with a relatively simple composition and simple vertical structure to the vegetation.

Mulga woodlands experience long periods of low levels of soil moisture content, an analysis of stomatal sensitivity to periods of both low and high values of soil moisture content is crucial to enable an understanding of whether stomata do maximize carbon gain (through *A* or GPP; leaf to ecosystem-scales respectively) while regulating water loss (through $g_s$) throughout the year. Additionally, evaluating the response of $WUE_i$ to changes in soil moisture content represents an opportunity to quantify ecosystem-scale responses to changes in soil moisture content, thereby providing valuable insights to potential responses to droughts (Frank *et al.*, 2015).

This represents the first example of the application of three different approaches to estimate $g_1$ and hence $WUE_i$ from leaf to ecosystem-scales within the same ecosystem. The specific objectives of this study were: 1) to evaluate seven continuous years of EC observations in a Mulga woodland in order to assess the response of $g_1$ (and thus, eWUE) to a metric of water availability; and 2) to evaluate $WUE_i$ with the $g_1$ parameter using three different approaches: carbon stable isotope analyses, leaf gas exchange and eddy covariance within the same ecosystem. The hypotheses to test are:

1. $g_1$ will decline as soil water content declines across the wet-dry seasons, because soil water content sustains ecosystem productivity of the Mulga woodland.
2. $g_1$ estimates from EC will be larger than $g_1$ derived from leaf gas exchange because of the contribution of evaporation from wet soil and canopies.
3. $g_1$ will be a reliable indicator of the rapid response by the Mulga woodland to stochastic rainfall events.
4. $g_1$ estimates from EC will tend towards the value of $g_1$ from Medlyn *et al.* (2017) for angiosperm trees as you move from wet season to dry season because the contribution from C4 grasses will disappear as the grasses die-off.
5. $g_1$ estimated from isotopes will be smaller than $g_1$ from gas exchange, because the contribution of mesophyll conductance is partially included in the isotopic discrimination model, but not in gas exchange measurements.

## *4.2 Methods*

### 4.2.1 Site description

The Mulga woodland is located in central Australia within the Ti-Tree basin, 180 km NW of Alice Springs (-22.28 S, 133.25 E) at 600 m asl. The evergreen dominant species are part of the Mulga complex (12 related *Acacia* spp.): *Acacia aptaneura* and *Acacia aneura* (Maslin and Reid, 2012) with a canopy height between 3 and 7 m. Patches of bare soil are covered temporarily by short grasses and herbs during favourable wet conditions (Cleverly *et al.*, 2013a). Previous surveys indicated *Acacia* spp. cover 74.5 % of the land area (Cleverly *et al.*, 2016c). In this site an eddy covariance (EC) system has been installed since September 2010. The site is part of the OzFlux Network (http://ozflux.org.au/) and the Terrestrial Ecosystem Research Network (TERN). Several related eco-hydrological and eco-physiological studies have been conducted in this Mulga woodland (Cleverly *et al.*, 2016a; Eamus *et al.*, 2013; O'Grady *et al.*, 2009).

Soil is characterized as a red kandosol (texture of 74:11:15, sand:silt:clay). Soil organic matter (SOM) at the surface is 1.1 % and porosity is 0.37 ± 0.01 and 0.30 ±0.03 at the surface and at a depth of 1.41 ± 0.12 m respectively (Eamus *et al.*, 2013). Annual average precipitation is 324 mm (1987-2017), obtained from the nearest meteorological station (the Territory Grape Farm, BoM station 015643, elevation 566 m; www.bom.gov.au; 43 km distance from the study site). Inter-annual rainfall is highly variable in this region (Van Etten, 2009) and most of the annual precipitation (75 to 80 %) falls during the summer months of November to February inclusive (Eamus *et al.,* 2013). Hot and windy conditions are common in summer with daytime temperatures frequently above 40 °C. Mean historical maximum temperatures oscillate between 34 to 37 °C in the wet months (November to March) and between 22 to 30 °C in the dry season (April to October). Mean minimum temperatures ranged from 20 °C to 9 °C (wet and dry seasons respectively; www.bom.gov.au).

### 4.2.2 Micrometeorological and soil measurements

The eddy covariance tower is at 13.7 m, which is *ca.* 7.2 m above the canopy. A detailed description of the instrumentation and the eddy covariance system can be found in Eamus *et al.* (2013) and Cleverly *et al.* (2016a, b). In brief, water flux (ET) and net ecosystem exchange (NEE) were measured simultaneously at 10 Hz using a LI7500 open-path infrared gas analyser (LI7500, Li-Cor, Lincoln, Nebraska) while wind speed and wind direction were measured with a three-dimensional sonic anemometer (CSAT3, Campbell Scientific, Logan, UT, USA), also at 10 Hz. The three-dimensional EC system was mounted at 11.6 m above ground (canopy height 6.5

m) and facing into the predominant southeast wind direction. All data were logged at 30 min intervals using a CR3000 datalogger (Campbell Scientific Australia, Townsville, QLD, AU).

Measurements of additional variables included net radiation with a four-way radiometer, CNR1 (Kipp & Zonen, Delft, The Netherlands). Air temperature ($T_{air}$) and relative humidity were measured using HMP45C sensors (Vaisala, Helsinki, Finland) at 11.6 m. Precipitation was measured with a tipping bucket rain gauge CS7000 (Hydrologic services, Warwick, NSW, Australia). Atmospheric pressure was measured 1.0 m above the ground using a Vaisala CS106 barometric pressure sensor. Direction and horizontal wind speed were measured in a profile at height increments of 2.5 m (Wind Monitor, R.M. Young, MI USA). These data were averaged at 30 min intervals, except for precipitation (half-hour sums), and were logged using a CR3000 datalogger.

Soil moisture content was measured using soil water reflectometers (CS616 and CS610, Campbell Scientific, Logan, UT, USA). An array of sensors was installed at different depths 0-10, 10-30, 60-80 and 100-130 cm from which volumetric water content (VWC, mm) was estimated. In the present study, values below 100 cm depth were excluded because Mulga species have been shown not to have access below the hard pan which is located at 100 cm depth (Cleverly *et al.*, 2016c). Ground heat fluxes plates (CN3, Middleton Solar, Melbourne, AU) were buried 8 cm below the surface; averaging soil thermocouples (TCAV, Campbell Scientific, Townsville, AU) were buried at 4 and 6 cm depth. Soil moisture was also measured in two vertical arrays using time-domain reflectometry (TDR) system probes inserted at a 45° angle (CS610, Campbell Scientific, Townsville, AU). All soil measurements were collected on a separate CR1000 data-logger and stored on the CR3000 (Eamus *et al.*, 2013).

### 4.2.3. Eddy covariance and QA/QC

The quality assurance/control (QA/QC) procedures for the eddy covariance data followed the OzFlux protocol established by Isaac *et al.* (2017). The OzFluxQC Simulator (version 2.9.5; Cleverly and Isaac 2016) was used to: 1) detect and correct electronic spikes; 2) exclude fluxes within a 90$^{o}$ arc behind the sonic anemometers and tower (10 % of the observations); 3) filter measurements when humidity from rainy half-hours affected the IRGA; 4) apply 2-dimensional coordinate rotation (Wesely 1970); 5) apply frequency-response corrections (Massman and Clement, 2004); 6) convert virtual-to-actual sensible heat flux (Schotanus *et al.*, 1983); 7) correct for flux-density (which accounts the density effect arising from heat and water vapour fluxes; (Webb *et al.*, 1980); and 8) account for storage of heat in the soil above the heat flux

plates (Malek, 1993; Prueger *et al.*, 1996). Absolute humidity from the HMP45C sensor and LI7500 were regressed to discard outliers in the measurements.

Gap filling of fluxes was performed using the Self-Organizing Linear Output (SOLO) that is trained on a self-organizing feature map (SOFM) of meteorological and soil measurements as described in Eamus *et al.* (2013). SOLO is a statistical artificial neural network (ANN), which provides resistance, to overtraining and has the ability to simulate fluxes (Abramowitz *et al.*, 2006; Hsu *et al.*, 2002). Learning sensitivity of the ANN was set to minimize root mean square error following stepwise procedures (Cleverly *et al.*, 2016c; Eamus *et al.*, 2013). Gaps were 30-300 min in length and occurred at different times. Gaps were filled from one-minute averages (usually from 26 to 29 one-minute values), linear interpolation, replacement of measurements from a companion tower (Cleverly *et al.*, 2016c) or SOLO-SOFM trained on measurements with the paired tower (located 40 km East in the same latitude). Gap filling data accounted for 20 to 30 % of annual half-hour measurements.

### 4.2.4 Ecosystem flux measurements

Carbon flux partitioning of NEE (into GPP and ecosystem respiration, ER) and canopy conductance were calculated according to Cleverly *et al.* (2013a, b). In brief, ER was first calculated and then GPP was estimated (from -NEE=GPP-ER). ER was estimated from responses of NEE under three different conditions when GPP can be assumed to be zero: (i) at night; (ii) at the *y*-intercept of a light-response curve of NEE *versus* solar radiation (SR > 500 W $m^{-2}$); (iii) or on rare occasions when complete stomatal closure could be reasonably assumed under midday light levels (SR > 500 W $m^{-2}$). Nocturnal respiration ($R_{night}$) was assumed equal to the average of NEE on nights without gaps in the data set. Dark respiration from light-response curves ($R_{dark}$) and maximum midday NEE were binned into temperature classes and regressed as double exponential functions around a peak (optimal) temperature (Cleverly *et al.*, 2013a). Total daily ER was calculated as the sum of $R_{night}$ + $R_{dark(SR>500\ Wm^{-2})}$ + $NEE_{max(SR>500\ Wm^{-2})}$.

The Penman-Monteith inverted equation (eq. 4.3) was used to estimate canopy conductance ($G_c$) following Cleverly *et al.* (2013b). The Penman-Monteith equation includes the aerodynamic resistance ($r_a$) to gas exchange as:

$$G_c^{-1} = r_a \left\{ \left[ \left( \frac{\Delta Q_A + \rho_a c_p D r_a^{-1}}{\lambda \overline{w'q'}} - \Delta \right) \gamma^{-1} \right] - 1 \right\} \qquad \text{(eq. 4.3)}$$

where $Q_A$ is the difference between net radiation flux and ground heat flux, $\rho_a$ is the density of moist air, $c_p$ is the heat capacity of moist air, $D$ is the vapor pressure deficit, Δ is the slope of the saturation vapour pressure curve against temperature, $\lambda$ is the latent heat of water vapour, $\gamma$ is the psychrometric coefficient and $\overline{w'q'}$ is the kinematic vapour flux. $r_a$ was estimated by assuming a long profile of wind speed in the surface layer (Allen *et al.*, 1998; Cleverly *et al.*, 2013b; see also Chapter II). $G_c$ is assumed to be a function of individual leaf resistance and leaf area index (Allen *et al.*, 1998; Cleverly *et al.*, 2013b).

### 4.2.5 Leaf gas measurements

Three field campaigns were undertaken to sample across the annual cycle of dry and wet seasons: i) March-2015 (late wet season: 46 days after last precipitation event > 5 mm $d^{-1}$); ii) October-2015 (late dry season, 185 days since last precipitation event > 5 mm $d^{-1}$); and iii) February-2016 (middle of wet season: 7 days after last precipitation event > 5 mm $d^{-1}$). During all three campaigns leaf gas exchange was measured in the dominant tree species.

Diurnal surveys of leaf gas exchange were made from 07:00 to 16:00 h in summer, but to 14:00 h in winter at 2-hour intervals. An infrared gas analyser (IRGA) system (Li-6400XT, Li-Cor Inc., Lincoln, NE, USA) coupled to a 2 x 3 cm broadleaf chamber (6400-02B LED Light Source; Li-Cor Inc.) was used. Phyllodes (n≈ 5) of *A. aneura* and *A. aptaneura* from four plants *per* species were measured at the top of the canopy. Each measurement was made for *ca.* 5 to 10 min until stomatal conductance reached steady-state conditions. Inside the cuvette, temperature and vapour pressure deficit were set to equal the environmental conditions at the time of measurement. Light flux density was kept constant at 1500 μmol $m^{-2}$ $s^{-1}$ and $CO_2$ concentration was set to 400 μmol $mol^{-1}$. Leaf gas exchange values were area-corrected following each measurement.

### 4.2.6 $^{13}C$ Isotope analyses

Phyllodes used during diurnal gas exchange measurements were collected and placed in a darkened container at the end of each day for estimation of carbon isotopic ratio. Carbon isotopic compositions were measured on leaf soluble sugars ($\delta^{13}C_{sugars}$) and bulk-leaf tissue ($\delta^{13}C_{bulk\text{-}leaf}$). Phyllodes were oven-dried at 65°C for 72 h, and then ground to a fine powder. Adjacent phyllodes from the same branch to those phyllodes used for gas exchange were collected at 17:00 h for $\delta^{13}C_{sugars}$ analyses. At the time of collecting the sample, phyllodes were immediately immersed in liquid-$N_2$ to suppress enzymatic activity. Soluble carbohydrates were

extracted from the leaves using the modified protocol from Brugnoli *et al.* (1988) (West *et al.*, 2007). More details about foliar sugar extraction can be found in Chapter III section 3.2.5 of this thesis.

Both bulk-leaf tissue and total-sugars were weighed in tin capsules (~ 2 mg of leaf sample). Isotopic signature analyses were performed using a standard Cavity Ring-Down Spectrometer with combustion module (CM-CRDS; model G212i, Picarro Inc. Sunnyvale CA, USA). The measuring error of the CM-CRDS system was 0.5 ± 0.1 ‰ and two laboratory internal standards (Acetanilide -33.77 ‰ and, Atropine -21.45 ‰ (Costech Analytical Technologies, Valencia, CA, USA)) were used to calibrate the CM-CRDS. Corrected $\delta^{13}C$ values are expressed relative to the international standard, Pee Dee Belemnite (PDB).

### 4.2.7 Semi-empirical optimal stomatal model

Primarily the slope (m) of the linear regression of $g_s$ *versus* $A/C_a\sqrt{D}$ was used to visualize the fit of the empirical model developed by Ball and Berry (1987), and therefore to visualize the empirical $g_1$ model (Medlyn *et al.*, 2011). The optimal stomatal conductance model for $g_1$ was calculated following Medlyn *et al.* (2011) using three different data sets: 1) $g_1$ values derived from ecosystem-scale flux measurements, 2) $g_1$ values derived from direct leaf gas exchange measurements and, 3) $g_1$ values derived from carbon isotopic ratios (bulk-leaf and total leaf sugars).

For the estimation of the $g_1$ parameter at an ecosystem-scale, continuous eddy covariance data from Sep-2010 to July-2017 were used. First, hourly $g_1$ values were calculated manually by solving equation 4.1. GPP replaced carbon assimilation ($A$) to determine $g_1$ at an ecosystem-scale ($g_{1\text{-EC-flux}}$). Hourly $g_{1\text{-EC-flux}}$ were plotted against time since last rainfall events in order to minimize non-transpiration fluxes in the further calculation of daily $g_1$ values. Segmented linear regressions were applied in R 3.2.1 (R Development Core Team, 2016) to identify the break point at which $g_1$ values stabilized after rainfall events.

The plantecophys R package (Duursma 2015) in R was used to estimate $g_1$ values by fitting equation 4.1 to data for leaf gas exchange and eddy covariance fluxes. A 3-day period following each rainfall event was excluded in the calculation of daily $g_{1\text{-EC-flux}}$. Canopy conductance replaced stomatal conductance in eq. 4.1 and GPP replaced carbon assimilation to determine daily $g_{1\text{-EC-flux}}$. Thus, the $g_1$ parameter allowed for the estimation of both ecosystem-scale $WUE_i$ ($eWUE_i$) and leaf-scale $WUE_i$ ($WUE_i$).

The carbon isotopic discrimination ($\Delta^{13}C$) by leaves is linearly related to the ratio of the intercellular and ambient $CO_2$ concentration ($C_i/C_a$, respectively), which reflects the balance between $A_n$ and $g_s$ for $CO_2$ ($g_c$) (Farquhar *et al.,* 1989). The ratio $C_i/C_a$ was estimated with carbon isotopic composition (bulk-leaf and total-sugars) following Farquhar *et al*. (1989) for C3 species as:

$$\frac{C_i}{C_a} = \frac{\Delta^{13}C - a}{b - a} \qquad \text{(eq. 4.4)}$$

where $a$ is the fractionation during $CO_2$ diffusion through the stomata (4.4 ‰; O'Leary, 1981), $b$ is the fractionation associated with reactions by Rubisco and PEP carboxylase (27 ‰; Farquhar and Richards 1984). Then, values of $g_1$ were estimated for isotopic compositions as Medlyn *et al.* (2017):

$$g_1 = \frac{\left(\frac{C_i}{C_a}\sqrt{D}\right)}{\left(1 - \frac{C_i}{C_a}\right)} \qquad \text{(eq. 4.5)}$$

Where values of D were taken from diurnal leaf gas exchange measurements and averaged for each species.

### 4.2.8 Relationship of $g_1$ with volumetric water content

Fitting the β model was used to evaluate the relationship of $g_1$ with volumetric water content (VWC) following Drake *et al.* (2017). In brief, an empirical scalar (β) was calculated with the following equation:

$$\beta = \left[\frac{X - X_l}{X_h - X_l}\right]^q \qquad \text{(eq. 4.6)}$$

where β represents the scalar reduction of a process (i.e., $g_1$), $X$ is a measurement of soil water content (here VWC), $X_l$ is the low value of $X$ (β= 0) and $X_h$ is the high limit value of $X$ (β= 1), and $q$ is the parameter describing the non-linearity of β as a function of $X$ between $X_l$ and $X_h$. $g_1$ values were normalized yearly relative to the maximum $g_1$ value which relates to $X_l$. A nonlinear least squares "nls" function in R 3.2.1 was used to apply equation 4.6. Confidence intervals (CI= 95 %) were obtained via bootstrapping using the bootCase function with the car package (Fox and Weisberg, 2011) as described by Drake *et al.* (2017).

### 4.2.9 Statistical analysis

All statistical analyses were undertaken using the R 3.2.1. The normality of the data was verified with the Shapiro-Wilk test. Two-way analysis of variance (ANOVA) was used to test for differences between species among methods used to estimate the $g_1$ parameter with the interaction of method × date (study periods). Pair-wise student's t-test was used for *post hoc* comparisons of species with a Bonferroni correction to discriminate specific differences among species. Similarly, Tukey's honest *post hoc* test was used to identify differences when the interaction term (method x date) was significant. Slope differences were tested using a standardized major axis method in the SMATR package in R (Warton *et al.*, 2012).

## *4.3 Results*

### 4.3.1 Carbon and water budgets at the Mulga woodland

Semi-arid ecosystems such as the Mulga woodland have the ability to switch between being a C sink and a C source depending on annual rainfall (Table 4.1; see also Chapter II of this thesis). During seven continuous years of observation of carbon and water fluxes, the Mulga woodland was an annual C sink for five years and a C source for two years (2011-2012 and 2013-2013). The driest year observed was in 2012-2013 with 193 mm of annual rainfall. This was 40 % less than the historical mean annual precipitation of 324 mm. Consequently, the Mulga woodland was a small source (-14 gC $m^{-2}$ $y^{-1}$) in this hydrologic year. In favourable years such as 2010-2011 with extremely large rainfall inputs (565 mm $y^{-1}$), the Mulga woodland behaved as a C sink (NEP= 131 gC $m^{-2}$ $y^{-1}$) with a GPP of 752 gC $m^{-2}$ $y^{-1}$.

Table 4.1 Annual rainfall and carbon and water budgets at the Mulga woodland for seven hydrological years (2010-2017), defined from August to July. Annual budgets for net ecosystem production (NEP), gross primary production (GPP), rainfall (PPT), evapotranspiration (ET), ecosystem water-use-efficiency (eWUE) and the ratio ET:PPT.

| Hydrological year | PPT | ET | NEP | | GPP | eWUE | ET:PPT |
|---|---|---|---|---|---|---|---|
| | (mm $y^{-1}$) | | (gC $m^{-2}$ $y^{-1}$) | | | (gC $mm^{-1}$ $H_2O$ $y^{-1}$) | |
| 2010-2011 | 565 | 512 | 131 | (sink) | 752 | 1.47 | 0.91 |
| 2011-2012 | 239 | 207 | -47 | (source) | 512 | 2.47 | 0.87 |
| 2012-2013 | 193 | 153 | -14 | (source) | 443 | 2.89 | 0.79 |
| 2013-2014 | 295 | 249 | 23 | (sink) | 414 | 1.66 | 0.85 |
| 2014-2015 | 301 | 251 | 45 | (sink) | 420 | 1.67 | 0.83 |
| 2015-2016 | 336 | 247 | 22 | (sink) | 515 | 2.08 | 0.74 |
| 2016-2017 | 713 | 530 | 217 | (sink) | 835 | 1.58 | 0.74 |

Evapotranspiration was larger in wetter-than average years than drier-than-average years. For example, in the hydrological year, 2010-2011 total annual rainfall was 565 mm and ET accounted for 512 mm. Thus, in 2010-2011 ET was 91 % of total rainfall. The ratio ET: PPT was consistently above 0.70 for all years. Ecosystem water-use-efficiency (eWUE= GPP/ET) increased as rainfall decreased. The maximum eWUE value was observed in the driest hydrological year (2012-2013). Annual variability in rainfall had implications in eWUE and leaf

water-use-efficiency, which I will explore in detail in the following sections using $g_1$ as a proxy of intrinsic water-use-efficiency ($WUE_i$).

### 4.3.2 Stomatal conductance and photosynthesis relationship

There was large variation in the relationship between $G_c$ and $\mathrm{GPP}/C_a\sqrt{\mathrm{VPD}}$ within a single year as observed in the period Jan-2015 to April-2016 (Fig. 4.1a). Both terms $G_c$ and $\mathrm{GPP}/C_a\sqrt{\mathrm{VPD}}$ varied across a large range of values across the entire annual cycle. $G_c$ was consistently low and close to zero for most of the dry season. For example, in Oct-2015 (Fig. 4.1c) $G_c$ was very low (< 0.025 mol $m^{-2}$ $s^{-1}$) for the entire range of $\mathrm{GPP}/C_a\sqrt{\mathrm{VPD}}$ values. Consequently, the linear regression ($G_c$ *versus* $\mathrm{GPP}/C_a\sqrt{\mathrm{VPD}}$) was insignificant and could not predict a relationship. In contrast, Mar-2015 and Feb-2016 showed larger values of $G_c$ compared with the very dry period of Oct-2015. There were no significant differences in slopes m, ($p$-value= 0.09) between Mar-2015 (m= 0.080 ± 0.006; $r^2$= 0.23, $p$-value<0.001) and Feb-2016 (m= 0.085 ± 0.008; $r^2$= 0.22, $p$-value<0.001). Therefore, there were seasonal differences between wet and dry seasons but not between late wet season (Mar-2015) and early wet season (Feb-2016). The slope value for the entire period Jan-2015 to Apr-2016 included was m= 4.99 ± 0.11 ($r^2$= 0.24; $p$-value< 0.001; Fig. 4.1a).

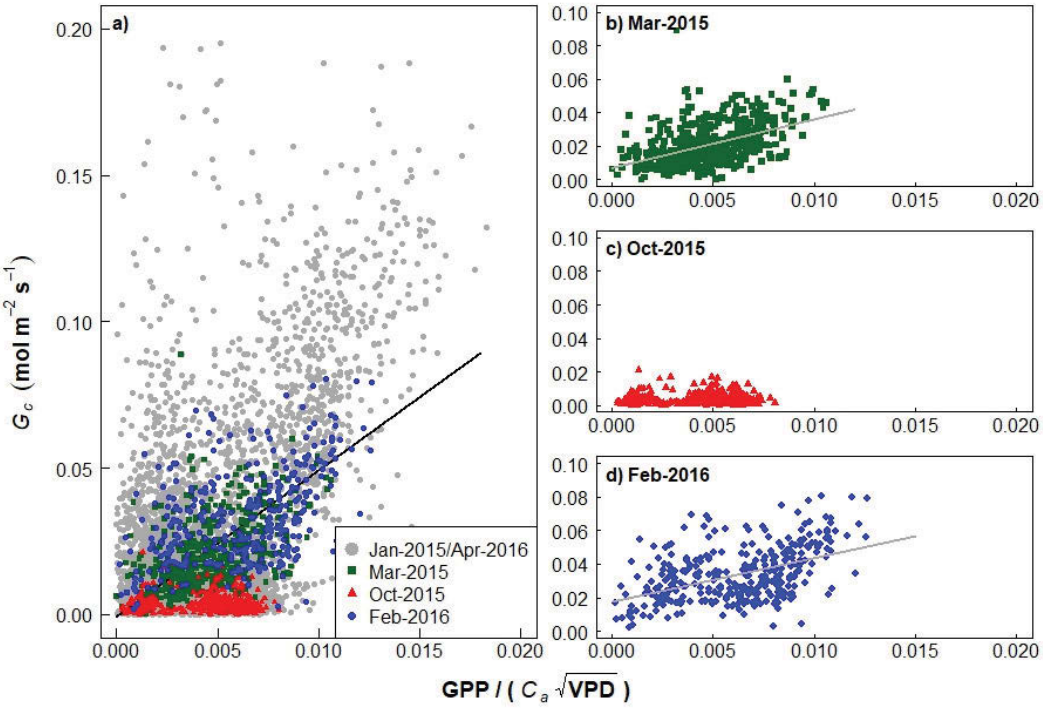


Figure 4.1 Canopy conductance ($G_c$) plotted as a function of GPP/$C_a\sqrt{\mathrm{VPD}}$. a) All months included from Jan-2015 to Apr-2016; b) Mar-2015, late wet season; and, c) Oct-2015 dry season and d) Feb-2016, early/mid wet season. Note that the grey points in (a) are months other than Mar-2015, Oct-2015 and Feb-2016. All points are at 30 min resolution. Slope differences were tested using a standardized major axis method.

At the leaf-scale, significant linear regressions of the relationship $g_s$ *versus* $A/C_a\sqrt{\mathrm{D}}$ were observed in the two dominant species of the Mulga woodland: *A. aneura* and *A. aptaneura* (Fig. 4.2). All measurements *per* species across all seasons converged to one regression. For both species, measurements conducted in Oct-2015 (dry season) were the extreme low values in the regression, consistent with ecosystem-scale observation based on EC data (i.e., low $g_s$ and low $G_c$; Fig. 4.1c). In contrast, measurements conducted in Mar-2015 and Feb-2016 resulted in large values for $g_s$ and $A/C_a\sqrt{\mathrm{D}}$ consistent with ecosystem-scale observations. Distinct separation of the leaf-scale observations for the three sampling periods (Mar, Oct, Feb) was apparent for *A. aptaneura* (Fig. 4.2a) but this was less apparent for *A. aneura* (Fig. 4.2b). There were significant differences in the slopes between species ($p$-value= 0.006). *A. aptaneura* had the largest slope (m= 4.77 ± 0.23; $r^2$= 0.92; $p$-value< 0.001) compared with *A. aneura* (m= 3.33 ± 0.29; $r^2$= 0.74, $p$-value< 0.001). Both ecosystem (Fig. 4.1) and leaf-scale measurements (Fig. 4.2) confirm the strong linear relationship observed between $G_c$ and GPP/$C_a\sqrt{\mathrm{VPD}}$ and, $g_s$ and $A/C_a\sqrt{\mathrm{D}}$.

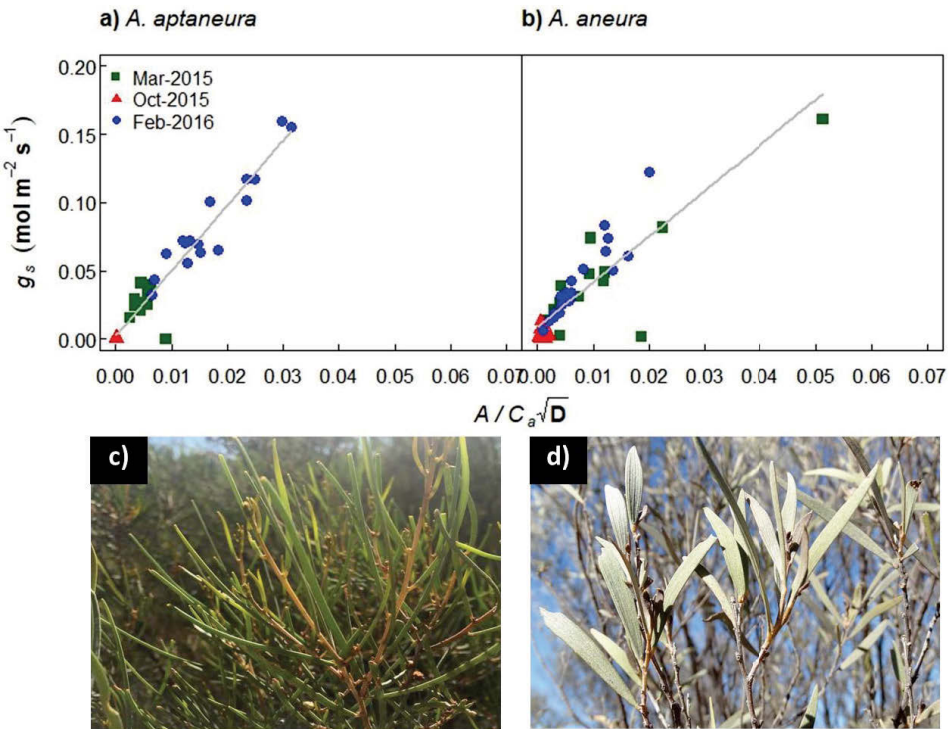


Figure 4.2 Instantaneous values of stomatal conductance ($g_s$) plotted as a function of light saturated net photosynthesis ($A$; μmol m$^{-2}$ s$^{-1}$) against the combined term as $A/C_a\sqrt{D}$. D is the vapor pressure deficit (kPa) and $C_a$ is the atmospheric $CO_2$ at the leaf surface (μmol mol$^{-1}$). Each point represents one measurement to a set of phyllodes (n= 4 trees). Photos show phyllodes shapes for c) *Acacia aptaneura* needle shape and d) *Acacia aneura* sub-terete at similar height (3 to 5 m). Slope differences were tested using a standardized major axis method.

Estimated values of $g_1$ derived from leaf-scale measurements for each species are presented in Table 4.2. There were no significant differences across species in all three-study periods for either method (carbon isotopes and leaf gas exchange approach; supplementary Table S.4.1). However, there were some differences between study periods (i.e., seasons) within *A. aneura*. There were significant differences in *A. aneura* $g_1$ values derived from total-sugar isotopic composition ($g_{1\text{-sugars}}$) from late wet season (Mar-2015) and the other remaining two periods. There were however, no differences in $g_1$ values derived from bulk-leaf isotopic composition ($g_{1\text{-bulk-leaf}}$) between seasons and within each species. In contrast, $g_1$ values derived from leaf gas exchange ($g_{1\text{-leaf-gas}}$) were larger in the dry season (Oct-2015) than the early and late wet season (Feb-2016), but wet seasons (late wet season and early wet season) were similar for *A. aneura*.

Table 4.2 Species comparison of the $g_1$ parameter ($kPa^{0.5}$ ± SE) across different periods and methods. $g_{1\text{-leaf-gas}}$ represent the $g_1$ derived from leaf gas exchange, whereas $g_{1\text{-sugars}}$ and $g_{1\text{-bulk-leaf}}$ are the isotopic derived $g_1$ values. Within columns, different letters indicate that means were significantly different at $p$-value < 0.05 among species and dates assessed with two-way ANOVAs and pair-wise student's t-test was used for *post hoc* comparisons of species with Bonferroni correction.

| Dates | $g_{1\text{-leaf-gas}}$ | $g_{1\text{-bulk-leaf}}$ | $g_{1\text{-sugars}}$ |
|---|---|---|---|
| 1. *Acacia aptaneura* | | | |
| Mar-15 | 1.42±0.28 b | 4.59±0.12 a | 5.93±0.49 ab |
| Oct-15 | 2.98±2.25 ab | 5.12±0.21 a | 5.67±0.21 b |
| Feb-16 | 1.15±0.14 b | 3.86±0.07 a | 5.05±0.33 b |
| 2. *Acacia aneura* | | | |
| Mar-15 | 1.43±0.29 b | 4.65±0.19 a | 6.98±0.19 a |
| Oct-15 | 4.84±1.29 a | 4.14±0.09 a | 5.62±0.19 b |
| Feb-16 | 1.53±0.12 b | 4.81±0.65 a | 4.99±0.11 b |

### 4.3.3 The response of $g_1$ to rainfall events

The calculation of the $g_1$ parameter at an ecosystem-scale relied on the assumption that non-transpiration fluxes are included in equation 4.1. Therefore, average hourly $g_1$ values for 7 consecutive years of eddy covariance fluxes were plotted in intervals of hours since last rainfall events (Figure 4.3). This visualization allowed me to evaluate the stability of $g_1$ after rainfall events (Knauer *et al.*, 2018). Although $g_1$ had in general a smooth decline after each rainfall event; the first and most abrupt decline in $g_1$ occurred in the first 76.5 ± 3.2 h (or 3.2 days) as suggested by segmented regression analysis (95 % CI 70.3 to 82.7; $p$-value<0.001). In that period (76.5 h) estimated $g_1$ values dropped *ca. 3.*5 $kPa^{0.5}$ (from 7.5 to 4 $kPa^{0.5}$), while beyond the break point, $g_1$ changed more gradually, *ca.* 2 $kPa^{0.5}$ for up to 10 consecutive days.

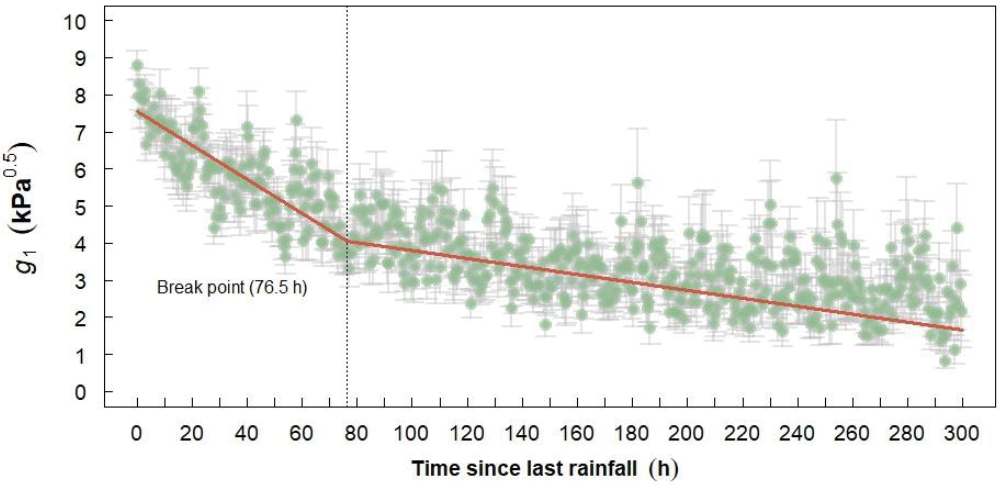


Figure 4.3 Hourly $g_1$ values at the time since last rainfall events. The break point at 76.5 h was estimated with segmented regression analysis.

Estimated values of $g_1$ using eddy covariance fluxes for the period January 2015 to July 2016 (including months of leaf gas exchange measurements) are shown in figure 4.4. Large rainfall events resulted in large increases in $g_1$ (and hence a decline in $eWUE_i$) in the days following rain until a new large rainfall event. Thus, there was a maximum value of $g_1$ (smallest $eWUE_i$) observed immediately after each rainfall event and exponential declines to a minimum value of $g_1$ (increasing $eWUE_i$) that occurred just before the next rainfall event.

At the beginning of 2015, during the first 12 days of January the Mulga woodland received a total of 116 mm of rainfall (Fig. 4.4). That large amount of rainfall (note that it was *ca.* 30 % of the historical annual rainfall in just 12 days) resulted in a mean over five days of maximum of $g_1$ values of 9.8 ± 0.3 $kPa^{0.5}$ (at VWC= 142 ± 5.8 mm), representing the peak of both VWC and $g_1$ values prior to a subsequent exponential decline. It is important to note that mean values of $g_1$ were calculated after excluding the 3-day period following each rainfall event to avoid inclusion of evaporation of water from wet canopies and soil in the calculation of $g_1$ (Fig. 4.3). Thus, the above average values (VWC and $g_1$) represented the end of the subsequent week after the last rainfall event. Following the 116 mm of total rainfall during the last week of March 2015, $g_1$ values declined to a minimum of 1.2 ± 0.5 $kPa^{0.5}$ when VWC was 48 ± 0.1 mm by mid-March-2015. Following the 13 mm rainfall event in mid-March, $g_1$ increased (meaning reduced $eWUE_i$) to 7.3 ± 1.3 $kPa^{0.5}$ (at VWC= 54 ± 0.4 mm).

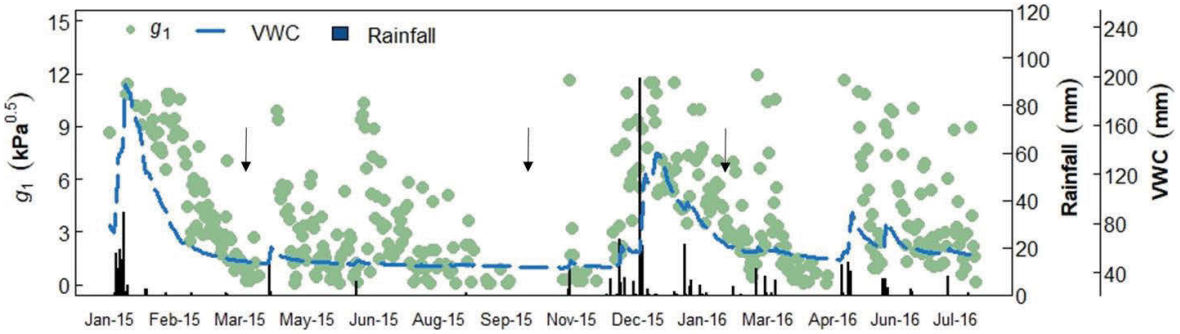


Figure 4.4 Total daily rainfall events and estimated $g_1$ values from eddy covariance fluxes from January-2015 to July-2016. Arrows indicate leaf-scale sampling dates (Mar, Oct and Feb). Bars represent rainfall events (mm), dots are daily $g_1$ values derived from eddy covariance fluxes and dashed line represents volumetric water content (VWC, mm).

Similar responses of $g_1$ to each pulse of rainfall were observed in the subsequent wet season (Dec-2015 to Apr-2016; Fig. 4.4). While $g_1$ was 0.6 ± 0.17 kPa$^{0.5}$ (at VWC of 46 ± 0.10 mm) at the end of Nov-2015; consecutive rainfall events resulted in accumulated rainfall of 180 mm in Dec-2015 leading to a 17-fold increase in $g_1$ values (10.6 ± 0.2 kPa$^{0.5}$). Note that the accumulated rainfall that occurred in Dec-2015 and Jan-2016 caused an increase of VWC (136 ± 0.4 mm). However, VWC and $g_1$ consistently declined until the end of April-2016 when sufficient rain was received again and $g_1$ increased and $eWUE_i$ was reduced. Consistently, $g_1$ reached a plateau between consecutive storms during March and April of 2016.

Continuous monitoring of carbon and water fluxes at the Mulga woodland allowed a continuous estimation of $g_1$ derived from eddy covariance fluxes for 7 consecutive years (Fig. 4.5). Estimated $g_1$ responded to rainfall events across each hydrological year (August to July). This was especially evident at the end of the wet season (*ca.* April-May) and moving into the dry season in 2010-2011, 2014-2015, and 2016-2017 (Fig. 4.5a, e and g respectively). However, during drier-than-average years such as 2011-2012 (Fig. 4.5b) and 2012-2013 (Fig. 4.5c), the $g_1$ response to rainfall was less pronounced than during wetter-than-average years. Likewise, there was much noisy data at the end of the hydrological years of 2014-2015 and 2015-2016.

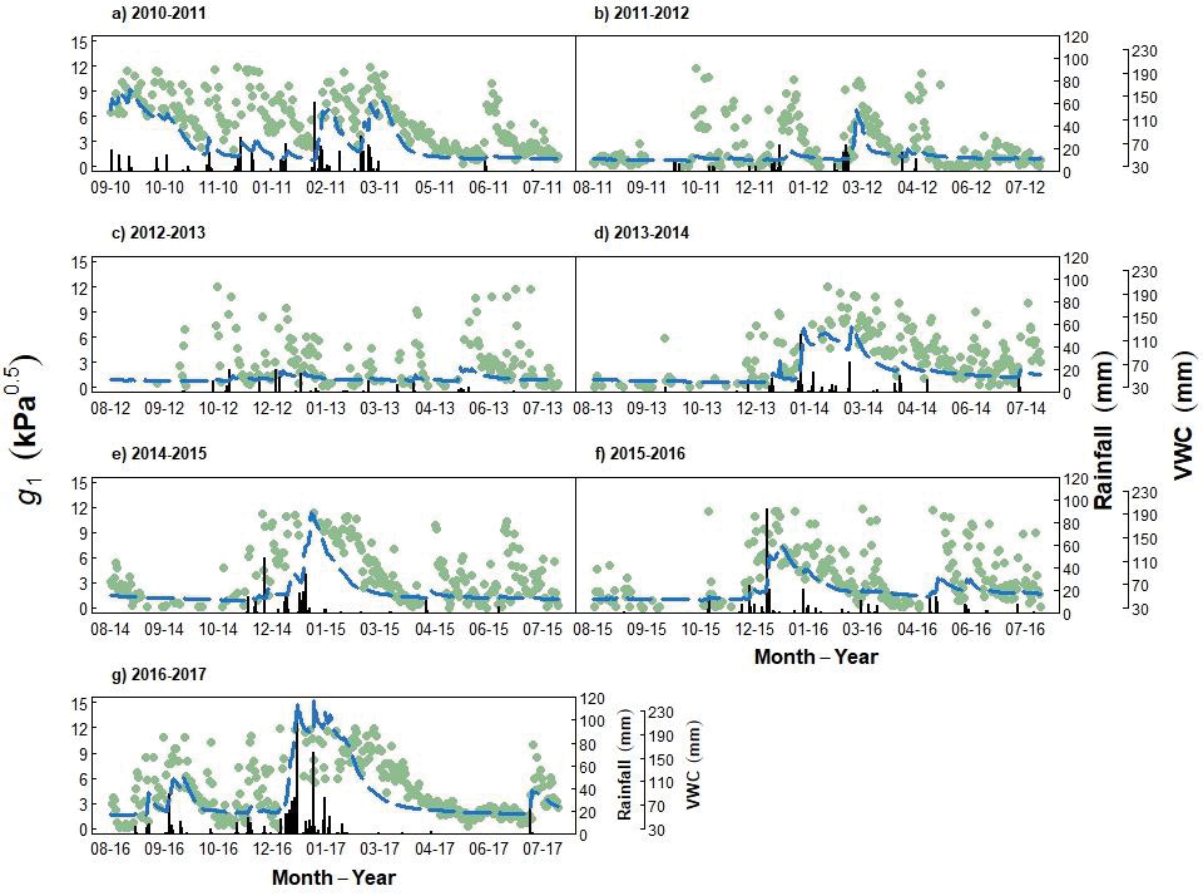


Figure 4.5 Daily rainfall events and estimated $g_1$ values from eddy covariance fluxes for seven consecutive years at the Mulga woodland. Bars represent rainfall events, dots calculated daily $g_1$ values and dashed line represents volumetric water content (VWC, mm).

### 4.3.4 Fitting functional relationships with volumetric water content

In order to evaluate the $g_1$ response to volumetric water content, data collected during the 76 h following each rainfall event were excluded in the analysis of $g_1$ at ecosystem-scale. By excluding data from the first 76 h, $g_1$ is expected to more closely represent the behaviour of transpiration from the canopy, and to reduce the impact of evaporation from wet canopies or wet soil (see Fig. 4.3). The β-function described the reductions in normalized $g_1$ (from 0 to 1 using minimum and maximum values of VCW, eq. 4.6) as VWC decreased. For all years of study, $g_1$ declined (and hence $eWUE_i$ increased) with decreasing VWC (Fig. 4.6).

Across all seven years VWC had a minimum of 38 mm and a maximum of 207 mm. The driest hydrological year (2012-2013; excluded from Fig. 4.6) had an average of 44 ± 0.2 mm with a maximum VWC of 56 mm. Thus, the β-function was unable to fit the relationship between $g_1$ and VWC due to the low variability in VWC values in this year.

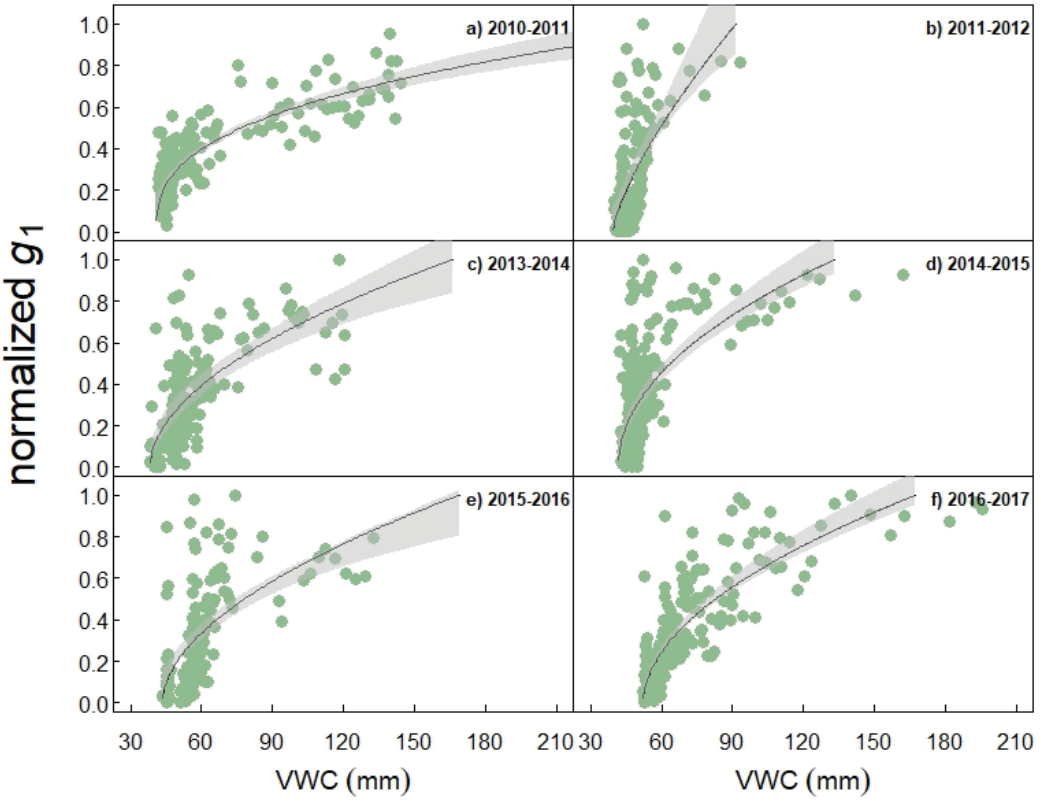


Figure 4.6 Daily-normalized $g_1$ values regressed with total volumetric water content (VWC). 76 h since last rainfall event were excluded. Lines represent the β-function (eq. 6) and shaded areas reflect 95 % confidence intervals. Note that the hydrological year 2012-2013 is missing in the figure because the model was unable to resolve a fit to the data due to the small range in VWC values (see total rainfall in 2012-2013; Table 4.1 and Fig. 4.5c).

Fitting coefficients estimated with the β-function (see figure 4.6) are presented in Table 4.3. I found that $g_1$ responded to a range of VWC values with $q$ parameters below 1.0. This $q$ parameter defines the concave relationship (Smith *et al.*, 2014) between $g_1$ and VWC. The average $q$ for all years was *ca.* 0.52 indicating that the rate of change in normalized $g_1$ *per* unit of change as VWC declined. Similarly, $X_l$ and $X_h$ covered a full range of values of observed VWC. $X_l$ fluctuated between 38 and 52 mm across all hydrological years. In contrast, $X_h$ ranged from 91.36 mm in 2011-2012 to 282.03 mm in the wettest year 2010-2011.

Table 4.3 β-function parameters (± SE) for normalized $g_1$ as a function of volumetric water content (VWC). A nonlinear least squares "nls" function was used to apply equation 4.6.

| Hydrological year | $X_l$[a] | $X_h$[b] | $q$[c] | $p$- value[d] |
|---|---|---|---|---|
| 2010-2011 | 40.74 (1.08) | 282.03 (34.14) | 0.37 (0.03) | <0.001 |
| 2011-2012 | 39.41 (1.52) | 91.36 (7.59) | 0.72 (0.12) | <0.001 |
| 2012-2013 | NA | NA | NA | |
| 2013-2014 | 38.15 (0.79) | 166.08 (18.36) | 0.53 (0.05) | <0.001 |
| 2014-2015 | 41.85 (1.65) | 133.01 (12.87) | 0.49 (0.06) | <0.001 |
| 2015-2016 | 43.48 (1.19) | 169.13 (24.28) | 0.54 (0.07) | <0.001 |
| 2016-2017 | 52.27 (0.54) | 167.44 (8.23) | 0.52 (0.03) | <0.001 |

X-variable = VWC (mm)

Y-variable = normalized $g_1$

[a] The low-limit value of VWC (mm), below which β= 0.

[b] The high-limit value of VWC (mm), below which β= 1.

[c] The shape parameter that describes the rate of change in β (Smith *et al.*, 2014)

### 4.3.5 How does $g_1$ estimated at leaf- and ecosystem-scales compare?

Estimated $g_1$ values with the three methods (carbon isotopes, leaf gas exchange and eddy covariance fluxes) differed significantly across the three study periods (Fig. 4.7; $p$-value< 0.001; supplementary Table S.4.1). The largest temporal variation was observed using EC data to calculate $g_1$ while the smallest temporal variation was observed using bulk-leaf values of carbon isotopes to calculate $g_1$. In general, there was a trend for the median value of $g_1$ to increase in the following sequence:

$$g_{1\text{-sugars}} > g_{1\text{-bulk-leaf}} > g_{1\text{-EC-fluxes}} > g_{1\text{-leaf-gas}}$$

where $g_{1\text{-sugars}}$ is the $g_1$ isotope-derived value from total-sugars, $g_{1\text{-bulk-leaf}}$ is the $g_1$ value derived from bulk-leaf isotopic compositions, $g_{1\text{-EC-fluxes}}$ is the $g_1$ derived from eddy covariance data and

$g_{1\text{-leaf-gas}}$ is the $g_1$ value from leaf gas exchange measurements. This trend was significant in March 2015, significant for the leaf *versus* EC data comparison in Feb 2016 and leaf *versus* total-sugar comparison in Oct-2015 (Fig. 4.7). Overall, it was not possible to unambiguously discern a seasonal pattern in change in $g_1$ from isotopic-derived values. From leaf gas exchange and EC flux data, $g_1$ increased significantly from the dry season (Oct-15) to the wet season (Feb-16).

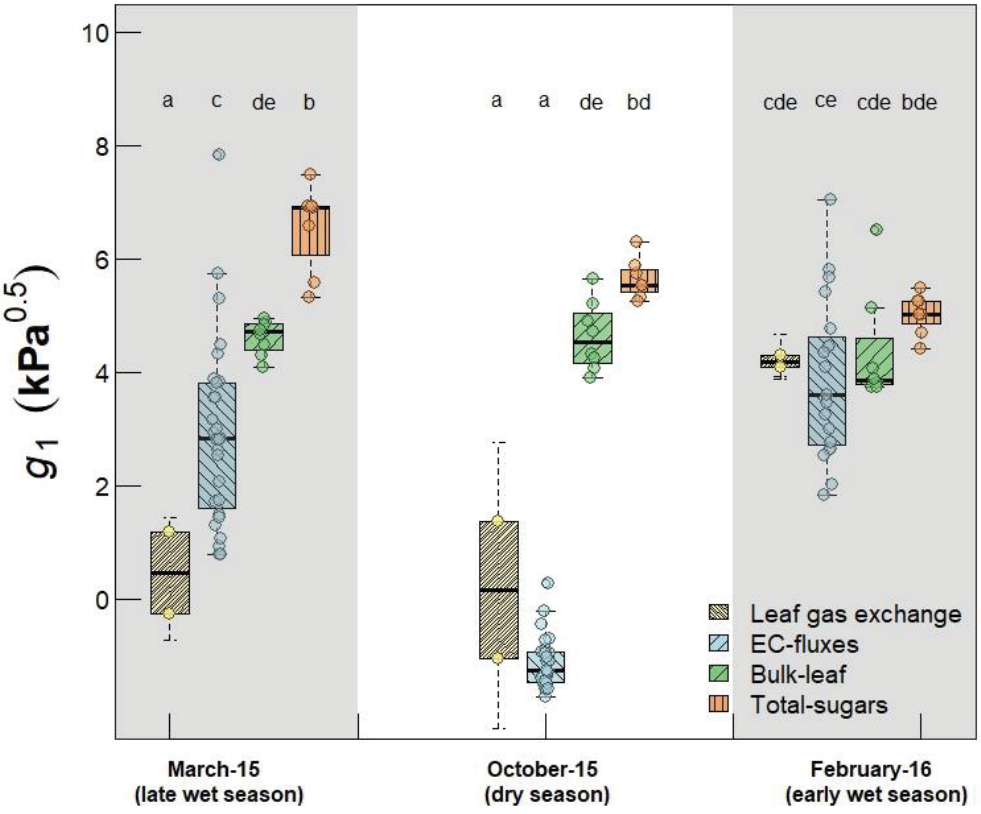


Figure 4.7 Estimated $g_1$ values from leaf gas exchange, leaf isotopes and eddy covariance data per period of measurements along a hydrological year cycle (2015-2016). Box and whisker plot (line, median; box, interquartile range); dots outside of the whiskers show outliers. Leaf gas exchange represent all measurements from diurnal surveys for each species (*Acacia aneura* and *Acacia aptaneura*). Stable isotopes are n= 4 trees *per* specie. Eddy covariance (EC) data encompassed daily $g_1$ estimations for the entire month where leaf-scale measurements where conducted. Letters indicate that means were significantly different ($p$-value<0.05) as tested with linear mixed models with observations as random factor and, the Tukey's HSD *post-hoc* tests for significant differences between methods and dates.

## *4.4 Discussion*

The aim of this study was to evaluate stomatal sensitivity to a metric of water availability and to compare different approaches to estimate the $g_1$ parameter as a proxy of intrinsic water-use-efficiency ($WUE_i$) in a semi-arid ecosystem: a Mulga woodland. The three methods used (carbon isotopes, leaf gas exchange and eddy covariance fluxes) in this study allowed an estimation of $g_1$ for the first time in the same ecosystem across three study periods within a hydrological year (late wet season, dry season and early wet season). Several years of eddy covariance observations showed that estimated $g_1$ values increased as volumetric water content increased (Fig. 4.6). This pattern of increased $g_1$ was not apparent in the $g_1$ derived from carbon isotopic composition across the three study periods (bulk-leaf and total leaf sugars; Fig. 4.7). Estimated $g_1$ values derived from leaf gas exchange and eddy covariance fluxes showed more variability across seasons than $g_1$ derived values from isotopic compositions (Fig. 4.7). I will now discuss these findings in detail in the following sections.

### 4.4.1 Ecosystem response to water availability

This study identified large variation in $g_1$ values across seven hydrological years of carbon and water fluxes in a semi-arid ecosystem (Fig. 4.5). I observed that when water becomes available (usually during the wet season ∽Oct-Mar) the Mulga woodland had large $g_1$ values (low $eWUE_i$). This indicates a rapid rate of response to changes in water availability and water-use by the Mulga woodland. In contrast, as days progressed into the dry season (∽May-Oct), $g_1$ decreased significantly. The Mulga woodland is characterized by low mean annual rainfall with high inter-annual variability (Eamus *et al.*, 2016). This characteristic limits ecosystem productivity to a short period of each year. Thus, Mulga trees are highly adapted to low soil water content values that occurs across much of each year but the ecosystem rapidly responded to high levels of soil water content, in agreement with the positive response to rainfall by semi-arid ecosystems reported in a continental study by Haverd *et al.* (2017). A clear example of this response was observed in the hydrological year 2010-2011 when the Mulga woodland received 74 % more rainfall than the historical mean annual precipitation (Table 4.1). This amount of rainfall increased $g_1$ values in Mulga 10-fold, compared with subsequent hydrological years when rainfall was closer to the long-term mean. Interestingly, the latest hydrological year (2016-2017) received 148 mm more rainfall than in 2010-2011. The Mulga response to wetter-than-average years allowed to significantly increasing NEP for up to 217 gC $m^{-2}$ $y^{-1}$; this is the largest NEP observed at the Mulga woodland to-date. These results are consistent with global-

scale studies, which show that semi-arid ecosystems can be highly resilient to low rainfall and be highly responsive to favourable periods of abundant water (Huxman *et al.*, 2004a; Ponce-Campos *et al.*, 2013).

Immediately following periods of heavy rain (i.e., >30 % of annual rainfall; Fig. 4.4), when the upper soil profile attained field capacity, the Mulga woodland reached peak productivity and exhibited a much smaller $eWUE_i$ (large $g_1$-values). This result of small $eWUE_i$ as water availability increases differ from those presented by Scott *et al.* (2015) and Hu *et al.* (2008) in semi-arid ecosystems, possible because of the different methods normalizing $eWUE_i$ (Beer *et al.*, 2009). As the soil profile dried-down, $eWUE_i$ increased and productivity declined. With negligible slope and a hardpan at shallow depth, water storage in the upper profile was significant and runoff was minimal. The first rainfall events saturated the soil to ∽10 cm depth, with subsequent rainfall events infiltrating deeper into the soil profile. In an earlier study at the Mulga woodland, Eamus *et al.* (2013) concluded that the Mulga woodland responded to small rainfall events (< 20 mm) within 3 days, and for a prolonged period (> 6 days) even when the Mulga woodland had preceding periods of 80 days without water. My study supports this conclusion: estimated $g_1$ values changed from 0.6 ± 0.17 $kPa^{0.5}$ to 10.6 ± 0.2 $kPa^{0.5}$ within 15 days, supporting the rapid response by the Mulga woodland to rainfall (Fig. 4.4).

Because plant functioning closely follows soil water dynamics as a strategy to maintain ecosystem productivity, I was able to describe stomatal responses to volumetric water content (VWC, as a metric of soil water availability) using the β-function (Smith *et al.*, 2014). The $g_1$ values estimated at the Mulga woodland closely followed changes in VWC in 6 of 7 years of eddy covariance observations. That is, the Mulga woodland had a strong positive relationship between VWC and $g_1$, which was observed in six of the seven years (Fig. 4.6). This finding supports my hypothesis that $g_1$ values would increase (i.e., $eWUE_i$ would decrease) as soil water content increased usually during the wet season. Similarly, Lu *et al.* (2016) proposed an extended combined model for optimal stomatal behaviour under stochastic rainfall regimes and pointed out the importance of understanding stomatal functioning with changes in soil water content. My study represents the first study of $g_1$ derived from three methods of analyses and supports the optimality model of stomatal behaviour in response to changes in VWC. Omitting such stomatal responses to different VWC levels in ecosystem models will result in substantial errors and inaccuracy when estimating C and water budgets.

### 4.4.2 Species comparisons of stomatal response

The Mulga woodland has shown large capacity for water consumption in wet periods and the plasticity to become highly water-use-efficient (low $g_1$ values) when experiencing water scarcity (i.e., during the dry season). Plant species with aggressive water use may displace other species with different or low water-use strategies and this might explain the partially homogenous ecosystem occupied by the majority Mulga species. Dominant species of the Mulga woodland studied are *Acacia aptaneura* and *Acacia aneura,* which together cover 74.5 % of this semi-arid ecosystem (Cleverly *et al.*, 2016c). These species from the Mulga complex are close relatives, which share a combination of morphological attributes (Maslin and Reid, 2012). Consequently, similar $g_1$ values derived from the three methods were observed across species (Table 4.2). Results of $g_1$ values derived from leaf gas exchange measurements for the Mulga species ($g_1$ values ranged from 1.15 to 4.84) are in the same range of values as the most important hardwood species of the United States forest such as the tulip tree ($g_1$= 1.11), Osage orange ($g_1$=1.18) and sycamore ($g_1$= 1.61) (Wolz *et al.*, 2017). *Acacia aptaneura* and *Acacia aneura* $g_1$ values were close to those of evergreen needle leaf forest ($g_1 \approx 2.2$) and C4 grasses ($g_1 \approx 1$) reported by Medlyn *et al.* (2017). In contrast, $g_1$ isotopic derived values of these species were considerably larger than any of the isotopic values reported by Medlyn *et al.* (2017). Mulga species have $g_1$ isotopic values closer to those of tropical rain forests ($g_1 \approx 4$) and the combined savannas ($g_1 \approx 3.8$) of Medlyn *et al.* (2017).

The relationship between $g_s$ and the combination of terms $A/C_a\sqrt{\mathrm{D}}$ allowed a visualization of the empirical model proposed by Ball and Berry (1987), where the slope is proportional to the $g_1$ parameter (Medlyn *et al.*, 2011). My results showed significant differences in the slope between the two Mulga species when leaf gas exchange observations from the three study periods were combined (Fig. 4.2). *A. aneura* had the smallest slope (m= 3.33, meaning larger water-use-efficiency) compared with *A. aptaneura* (m= 4.77). Surprisingly, the slope of *A. aneura* was in the same range for evergreen broadleaf forest (m= 3.75) and *A. aptaneura* had a slope value towards the deciduous broadleaf forest (m= 4.89; Medlyn *et al.,* 2017) at least for $g_1$ derived from leaf gas exchange data. Both slope values for *A. aneura* and *A. aptaneura* are considerably lower (thus, there is a large $WUE_i$) than the Mediterranean deciduous blue oak (m= 8.88) that inhabit the grassland of the Sierra Nevada in California (Xu and Baldocchi, 2003).

Although both species (*ca.* 3 to 7 m tall) are known for being highly tolerant to very low soil moisture contents (Page *et al.*, 2011); *A. aneura* exhibited less variation in $g_s$ values (Fig. 4.2b) and this may be attributed to its leaf morphology. Larger phyllodes (sub-terete; Fig. 4.2d) in *A. aneura* can transpire more water and thus experience lower phyllode water potentials than small phyllodes in *A. aptaneura* (Fig. 4.2c; Page *et al.*, 2011; Page *et al.*, 2016). Foliar water potentials of these species for the same study periods are presented in Chapter III. Thus *A.*

*aneura* had the smallest slope (meaning largest $WUE_i$) compared with *A. aptaneura*. This contrasting response can be interpreted as an extreme anisohydric strategy to tolerate a larger decline of leaf water potentials, thereby allowing the maintenance of $g_s$ and $A_n$ during the latter stages of soil drying despite large declines in soil and xylem water potential (Martinez-Vilalta *et al.*, 2014; Nolan *et al.*, 2017a). Although, Mulga are highly resistant to cavitation, pushing plant species of the Mulga woodland to operate at minima soil water content values to maintain their leaf gas exchange values increases the risk of embolism and cavitation (McDowell *et al.*, 2015; Page *et al.*, 2011; Santini *et al.*, 2015; Sperry and Love, 2015). Several studies have reported considerable variation in $g_1$ values and the slope parameter among different plant species worldwide. For example, Heroult *et al.* (2013) found that under drought conditions, some species of *Eucalyptus* reduced the slope but other species did not. Similarly, Zhou *et al.* (2013) found that $g_1$ values can remain constant in sclerophyll tress, but $g_1$ declined in several species with water stress. Therefore, my results support the previous conclusion that variation in stomatal functioning is large among species and within plant functional types (Lin *et al.*, 2015; Medlyn *et al.*, 2017; Wolz *et al.*, 2017).

### 4.4.3 Seasonal comparison of leaf and ecosystem $WUE_i$

This study presents, for the first time, a comparison of three methods to estimate $WUE_i$ with the normalized $g_1$ parameter in the same ecosystem within a single hydrological year (2015-2016), including wet and dry seasons. The largest temporal variation was observed in $g_1$ values derived from EC data ($g_{1\text{-EC-fluxes}}$), while the smallest temporal variation was observed in $g_1$ derived from isotopic compositions ($g_{1\text{-sugars}}$ and $g_{1\text{-bulk-leaf}}$). I found inconsistencies between the three methods since leaf-scale measurements and stable isotopes did not agree with flux data at the ecosystem-scale (Fig. 4.7). The one exception for all three methods was during the wet season, when $g_1$ values converged to similar medians. Conversely, only $g_{1\text{-leaf-gas}}$ and $g_{1\text{-EC-fluxes}}$ medians agreed during the dry season (Oct-2015) and late wet season (Mar-2015). Overall, the magnitude of the differences in the three methods presented in this work are in agreement with differences among methods observed in the global synthesis of the $g_1$ parameter analysed by Medlyn *et al.* (2017). It is possible that discrepancies among data sets relate to theoretical assumptions behind each approach and I will now discuss this in the following paragraphs.

My results showed that $g_{1\text{-EC-fluxes}}$ values were larger than $g_{1\text{-leaf-gas}}$ during the late wet season but not significantly different during the early wet season (Feb-2016; Fig. 4.7). This partially supports my hypothesis that $g_{1\text{-EC-fluxes}}$ values would be larger than $g_{1\text{-leaf-gas}}$ due to the influence of evaporation from wet soil and canopies. The water flux measurement (ET) with the eddy

covariance technique accounts for evaporation from wet soil, canopy, and transpiration from plants (Wilson *et al.*, 2001). However, in an attempt to exclude non-transpiration fluxes, 76.5 hours of flux measurements were removed after each rainfall event before calculating $g_{1\text{-EC-fluxes}}$ (Fig. 4.3). I suspect that this rough approach to exclude non-transpiration fluxes is not 100 % effective and I now discuss this.

Evapotranspiration usually represents a large portion of total annual precipitation in semi-arid ecosystems (Reynolds *et al.*, 2000; Yaseef *et al.*, 2010). For example, in the hydrological year 2010-2011, ET represented 90 % of the total annual rainfall (Table 4.1), but I did not account for relative contributions of fluxes from transpiration or soil and canopy evaporation. It is difficult and expensive to accurately separate the ratio of these water fluxes (Schlesinger and Jasechko, 2014; Wilson *et al.*, 2001). However, there is a trend for transpiration to dominate ET (T/ET), especially in semi-arid ecosystems, where T/ET > 80 % (Reynolds *et al.*, 2000; Yaseef *et al.*, 2010; Yepez *et al.*, 2007) and worldwide T/ET= 60 % (Jasechko *et al.*, 2013). Yet, transpiration is the pathway that links with GPP and inconsistencies between $g_{1\text{-EC-fluxes}}$ and $g_{1\text{-leaf-gas}}$ could possibly be attributed to an inability to estimate T/ET. Therefore, a thorough estimation of $g_1$ at the ecosystem-scale (hence $eWUE_i$) should include a more robust and detailed estimation of transpiration. A method of suitably partitioning ET would increase our understanding of biological water *per se* demand and vegetation feedback into the hydrological cycle (Newman *et al.*, 2006). Failure in accurate partitioning of ET can have a medium-to- large effect on $g_{1\text{-EC-fluxes}}$ of up to 50 % (Knauer *et al.*, 2018).

Carbon partitioning from net ecosystem exchange into GPP and ecosystem respiration (ER) has been widely conducted with mathematical models based on u* (low friction velocity) thresholds (Reichstein *et al.*, 2005; Scanlon and Kustas, 2010). Thus, GPP does not represent net photosynthesis since leaf respiration is not excluded in the calculation. Knauer *et al.* (2018) found that uncertainties associated with carbon partitioning led to errors in $g_{1\text{-EC-fluxes}}$ for up to 20 %. However, this uncertainty may vary depending on site-specific characteristics and time-scales used. For example, in the Mulga woodland during the wet season, $g_{1\text{-EC-fluxes}}$ will include a contribution from carbon fluxes arising from the abundance of C4 grasses, whereas this effect is absent in the dry season. However, measurements made during the dry season in the Mulga woodland may include the contribution of other e-fluxes ($CO_2$ emission from the ecosystem to the atmosphere) arising from photo-and-thermal degradation of leaf litter (Cleverly *et al.*, 2016c; Eamus *et al.*, 2013), that may alter the overall net gas exchange observed at the site. Adding $CO_2$ from reuptake of respired $CO_2$ by grasses and their associated photosynthetic rates directly influence the overall NEE, hence GPP; thus $g_{1\text{-EC-fluxes}}$ represented a combination of C4 and C3 species, especially during the wet season.

In this study, daily $g_{1\text{-EC-fluxes}}$ values during dry seasons (~May to Oct; Fig. 4.4) were as low as values reported by Medlyn *et al.* (2017) for C4 grasses, but as high as values for evergreen needleleaf forest and evergreen broadleaf forest during the wet seasons (~Oct-Apr) in the same study of Medlyn *et al.* (2017). Thus, differences photosynthetic pathways from C4 and C3 species may explain inconsistences found between $g_{1\text{-EC-fluxes}}$ and $g_{1\text{-leaf-gas}}$ since the leaf gas exchange measurements were conducted only for Mulga. However, the C4 represents only *ca.* 0.2 to 0.3 of the total vegetation fraction during the wet season at the Mulga woodland and it is not clear to what extent C4 grasses influenced the carbon and water fluxes at the ecosystem-scale and therefore the extent to which these affected my estimated $g_{1\text{-EC-fluxes}}$ values. Although Medlyn *et al.* (2017) did not find any evidence for the C4 fraction influencing $g_{1\text{-EC-fluxes}}$, a proper accounting of the relative contribution of C3 and C4 vegetation to carbon and water fluxes (NEP and ET) may reduce the gap between differences in $g_{1\text{-EC-fluxes}}$ and $g_{1\text{-leaf-gas}}$. This work demonstrated that the Mulga woodland displayed $g_1$ values similar to a C4 grassland in the dry season (despite the absence of C4 grasses at this time with low $g_{1\text{-EC-fluxes}}$, high $eWUE_i$) but exhibited $g_1$ values more typical of an evergreen forest during periods of high water abundance (high $g_{1\text{-EC-fluxes}}$, low $eWUE_i$) in the wet season.

Values of $g_1$ derived from carbon isotopic compositions were consistent across the three study periods (Fig. 4.7). These $g_1$ values ($g_{1\text{-sugars}}$ and $g_{1\text{-bulk-leaf}}$) significantly differed from $g_{1\text{-leaf-gas}}$ in both late wet season and dry seasons. However, I found congruence in the median of $g_1$ isotopic derived values and the median of $g_{1\text{-EC-fluxes}}$ during the wet season (Feb-2016; Fig. 4.7). $g_{1\text{-sugars}}$ and $g_{1\text{-bulk-leaf}}$ were similar during dry period (Oct-2015) and early wet season (Feb-2016). A first potential explanation for differences between $g_{1\text{-leaf-gas}}$ and $g_1$ isotopic derived values may be related to the VPD value used in the derivation. Daily averages of VPD of the sampling days were applied in equation 4.5, rather than the average of the long-term daytime VPD for $g_{1\text{-bulk-leaf}}$. Because bulk-leaf tissue is expected to reflect the long-term isotopic signal during the entire period of C assimilation (Brugnoli and Farquhar, 2000), the use of a single daily average value of VPD may result in significant errors. Second, it is possible that the influence of mesophyll conductance that is partially included in the isotopic discrimination model (Seibt *et al.*, 2008), does not fully account for the effect of carbon diffusion inside the chloroplasts, therefore affecting $C_i/C_a$ and hence $WUE_i$.

During the wet season, $g_1$ increased because C assimilation rates were considerably larger than the dry season (Fig. 4.2). However, during dry seasons stomatal conductance significantly regulates the $C_i/C_a$ ratio and hence isotopic discrimination, implying that changes in $WUE_i$ are due to changes in $g_s$ rather than in changes $A$ (Rumman *et al.*, 2017). In a continental study of $^{13}C$-discrimination and leaf traits, Rumman *et al.* (2017) found that during dry seasons the $C_i/C_a$

ratio derived from bulk-leaf isotopic compositions did not correlate with net carbon assimilation but did correlate with $g_s$. This suggests that low $g_s$ values observed during the dry season (Fig. 4.2) and $G_c$ at the ecosystem-scale (Fig. 4.1) were the principle determining factors controlling the $C_i/C_a$ and thus $g_1$ isotopic derived values. Moreover, Rumman *et al.* (2017) concluded that it may be possible that application of current carbon discrimination theory is more reliable during wet periods.

The fact that $g_{1\text{-EC-fluxes}}$, $g_{1\text{-sugars}}$ and $g_{1\text{-bulk-leaf}}$ were similar during the wet season suggest that this may be related to the favourable conditions maintaining a large $C_i/C_a$ ratio. Additionally, wet conditions increased vegetation cover by increasing leaf area index (see Chapter II of this thesis) and gradually decreased the coupling of the canopy with the atmosphere, thus reducing aerodynamic resistance compared to the dry season. All of these factors affect in different degrees my ability to accurately estimate $g_1$ values during the extremely dry season. Seasonal and annual variation in $g_1$ derived from the three methods in this present study highlights the concern that the generic use of constant values of $g_1$ to describe stomatal functioning is not reliable when parameterizing global climate models (Medlyn *et al.*, 2017; Wolz *et al.*, 2017).

## *4.5 Conclusions*

The scientific community has been paying particular attention to how models parameterize stomatal functioning, with extensive discussion of the lack of consensus among different data sets, and within and across species (Medlyn *et al.*, 2017; Miner *et al.*, 2017; Wolz *et al.*, 2017). Clearly, the work presented here suggests that ecosystems modellers should not use fixed parameters values of $g_1$ when modelling carbon and water fluxes. My work helps to clarify distinctions in stomatal responses among species and across seasons in the field and highlights, the variability in behaviour in response to changes in environmental conditions.

Here, I presented in detail $g_1$ values between species and at an ecosystem-scale with three distinct methods at the same ecosystem. I found that $g_1$ was highly responsive to environmental factors such as water availability, which is highly variable inter and intra-annual at the Mulga woodland. My work represents a key advance in our understanding of the $g_1$ response to soil water content. In conclusion, whether or not optimal stomatal behaviour varies with abiotic (i.e., fluctuations in water availability or incident radiation) or biotic (i.e., endogenous plant hormone concentration, leaf water potential) factors depends on the site and specific vegetation eco-physiological traits to face the constantly changing environment.

Understanding stomatal responses to the changing environment across different plant species and ecosystems is crucial to improve our ability to predict global changes. This advance of knowledge will help to improve regional predictions in global analysis of water and carbon cycles. However, more work is needed to evaluate other plant limitation for gas exchange such as limitations on photosynthesis while modelling stomatal functioning.

# *Chapter V*

## Contrasting regulation of leaf gas exchange of semi-arid tree species under drought

## *5.1 Introduction*

Globally, drought is the most widespread climate extreme affecting the carbon cycle (Frank *et al.*, 2015; Reichstein *et al.*, 2014). Over the last decade (2000-2009), 70 % of the vegetated land area in the Southern hemisphere exhibited decreased net primary production (photosynthesis minus respiration; Chapin *et al.*, 2006) due to drought (Zhao and Running, 2010). However, little is known about how photosynthesis and respiration are being affected from extreme conditions such as drought (Frank *et al.*, 2015), particularly for arid and semi-arid zone species. Therefore, long-term predictions of the water and carbon cycles that incorporate vegetation parameters in biogeochemical models remain uncertain and speculative.

Predicting how plants respond to drought requires an understanding of physiological mechanisms, at species, tissue and organism levels (Choat *et al.*, 2012; Page *et al.*, 2011) of how plants adjust their gas exchange with different strategies to tolerate drought, including the avoidance of drought-induced mortality (Adams *et al.*, 2009; Allen *et al.*, 2010; Peñuelas *et al.*, 2001; Sperry and Love, 2015). Atmospheric $CO_2$ diffuses into leaves through stomata, involving concomitant water loss (transpiration). Transpiration ($E$) is an inherent cost of carbon assimilation ($A$) and links the water and carbon cycles. Stomata respond to both declining soil water availability and increasing atmospheric vapour pressure deficit (Duursma *et al.*, 2014; Sperry and Love, 2015), by reducing transpiration and therefore carbon assimilation rates. Water-use-efficiency (WUE) can be defined as the ratio of $A/E$, alternatively intrinsic water-use-efficiency ($WUE_i$) can be defined as the ratio of net assimilation ($A_n$) to stomatal conductance ($g_s$). This is because stomatal conductance is a measure of the rate of flux of either water vapour or $CO_2$ through stomatal pores (Nobel, 2009). An understanding of responses of WUE and $WUE_i$ to drought is fundamental to developing our understanding of plant responses to drought.

Photosynthetic capacity is a function of the maximum rate of carboxylation ($V_{cmax}$; maximum rate of the Rubisco activity) and the maximum rate of electron transport ($J_{max}$)(Farquhar *et al.*, 1980). Rates of $V_{cmax}$ and $J_{max}$ provide important insights into plant functioning, in which the Rubisco enzyme is responsible for primary carbon assimilation in C3 plants (Cernusak *et al.*, 2011). Under moist conditions $V_{cmax}$ is expected to be higher when to compared to plants that have experienced drought (Zhou *et al.*, 2016). Short-term water stress leads to a decrease of Rubisco activity, therefore $V_{cmax}$ is reduced. However, Zhou *et al.* (2016) has shown that long-term water stress in eucalypt species leads to an acclimation effect by modifying Rubisco activity leading to a higher protein content allocated to Rubisco, especially in drought-tolerant leaves, so that $V_{cmax}$ can be maintained.

Plants under prolonged water stress can also adapt to drought in other ways. One of the adaptive mechanisms is through increased leaf mass *per* area (LMA). LMA is an adaptation to water stress because leaves reduce expansion rates and are more compact and wilt less easily (Poorter *et al.*, 2009). Low LMA is related to alterations in leaf construction, large volume of air spaces may enhance conductivity for both water and $CO_2$, thereby facilitating photosynthesis (Poorter *et al.*, 2009; Wright *et al.*, 2004). In contrast, high LMA is related with leaf and plant survival due to increased leaf toughness (Poorter *et al.,* 2009). $V_{cmax}$ has been correlated with LMA, because nitrogen content is generally higher in leaves with high LMA (Misson *et al.*, 2006). Similarly, the $J_{max}$ and $V_{cmax}$ ratio has been shown to decrease as water stress increases because of the higher sensitivity of water-stressed leaves to regenerating Rubisco than to carboxylation capacity (Misson *et al.*, 2006). Therefore, increasing carbon assimilation is not just a function of $g_s$, but also depends on related rate parameters, including $V_{cmax}$ and $J_{max}$, and LMA.

To-date, there is a consensus that $WUE_i$ responds to (i) stomatal closure and, (ii) non-stomatal limitations to photosynthesis, through changes in $V_{cmax}$ and $J_{max}$ (Flexas *et al.*, 2006; Galmes *et al.*, 2007; Sperry and Love, 2015). Likewise, photosynthetic is correlated with large respiration rates under water deficit (Gauthier *et al.*, 2014). Under drought conditions, reductions in $A$ affect leaf carbon balance, since the respiratory loss of $CO_2$ by plants can account for up to 30-80 % of daily carbon uptake, realised in part as dark respiration ($R_d$) (Gimeno *et al.*, 2010); thus reductions in $A_n$ modify the ratio $R_d/A_n$. Nevertheless, there is a gap in our knowledge regarding drivers of leaf gas exchange for co-occurring species with different eco-hydrological niches. Niche separation theory provides a framework to explain the co-occurrence of competing species (Silvertown *et al.*, 2015). Key questions that remain outstanding include: 1) what are the implications of changes in $A_n$ and $g_s$ on $WUE_i$ and the $R_d/A_n$ ratio during and after multiple droughts? 2) Does gas exchange fully recover after drought? 3) At what stage during

drought does $WUE_i$ increase or decrease? And 4) how do these changes vary among co-occurring species?

Semi-arid Australia is characterized by low mean annual rainfall with high inter-annual variability, high light intensity, nutrient poor soils and low vegetation cover (Eamus *et al.*, 2016; Van Etten, 2009). These conditions limit several physiological functions of semi-arid vegetation to a short period each year. Consequently, plant species have adapted several physiological traits in response to large seasonal changes in water availability (Gleason *et al.*, 2013). Several plant functional traits, including leaf area and LMA, and several plant variables, including pre-dawn and midday leaf water potentials and stomatal conductance, decrease during periods of low water availability (O'Grady *et al.*, 2009; O'Grady *et al.*, 2006; Page *et al.*, 2016). Declining pre-dawn water potential negatively impacts on plant physiological attributes such as rates of carbon and water fluxes (McDowell *et al.*, 2015).

In semi-arid central Australia, four main tree genera occur (*Eucalyptus, Corymbia, Acacia*, and *Hakea).* These genera have evergreen sclerophyllous foliage and, due to different hydraulic strategies, are able to co-occur (Nolan *et al.*, 2017b; O'Grady *et al.*, 2009; Santini *et al.*, 2015). Sclerophyllous foliage is a plant adaptive response to low water availability by allowing species to store more water in their leaves (Lamont *et al.*, 2002). Woody native species are members of the family *Myrtaceae,* including *Eucalyptus spp.,* and *Corymbia spp.* These are both tall, deep-rooted trees known to access groundwater (O'Grady *et al.*, 2006; Rumman *et al.*, 2018). This means they may rarely experience extremes of low soil moisture content characteristic of semi-arid environments, due to reliable access to groundwater, thus differences between wet and dry seasons in in $A_n$, $g_s$ and $WUE_i$ has not been observed in species members of the *Myrtaceae* family that inhabit central Australia (O'Grady *et al.*, 2009; 2006; Rumman *et al.*, 2018). In contrast, *Acacia* spp*.,* especially those from the Mulga complex, are known for being highly tolerant to very low soil moisture contents (Page *et al.*, 2011) and dominate ~20-25% of the semi-arid Australian continent (Cleverly *et al.*, 2016c; Eamus *et al.*, 2013). Both *Acacia spp.*, and *Hakea spp.*, have shallow root systems, possessing specific features to withstand high light and low water availability such as the capacity to adjust the turgor loss point to survive drought (Groom *et al.*, 1994; Lamont, 1993; Nolan *et al.*, 2017c; Page *et al.*, 2011). In particular, it has been commonly observed that *Hakea* spp. can produce root clusters, which are beneficial to plant water relation by increasing the surface area for water uptake (Lamont, 2003).

From remote sensing studies, we know that Australian semi-arid regions accounted for 60 % of the additional net C uptake during that occurred during the global land sink anomaly of 2010 (Poulter *et al.,* 2014). Poulter *et al.* (2014) showed that additions of 100 mm of rainfall

above the long-term average during the growing season led to a four-fold increase in net C uptake. This demonstrates the resilience and large capacity of such species to respond rapidly and positively to larger-than-average rainfall. Likewise, Haverd *et al.* (2017) found that 74 % of the Australian land surface had a positive response of gross primary productivity (total photosynthesis by the ecosystem) to annual anomalies of high inputs of rainfall.

The aim of this study was to compare the responses of leaf gas exchange as water stress increased in four co-occurring species of central Australia during experimentally imposed repeated droughts. Different responses of $A$, $g_s$ and $WUE_i$ under drought conditions are expected across species due to differences in eco-physiological strategies among species. Specifically, species that have physiological adaptations to access groundwater may be less effective in their adjustments of leaf gas exchange compared to species that do not access groundwater and repeatedly experience soil water deficits in the upper soil levels (O'Grady *et al.*, 2009) during the dry season. The hypotheses tested in this study are based on differences in hydrological traits within the four dominant species of the Ti-Tree basin in central Australia. My hypotheses are outlined below:

1. Because of the necessity for developing deep root system to facilitate access to groundwater; I hypothesise that species of the *Myrtaceae* family will have faster rates of growth to facilitate access to deeper water stores than to Mulga and *Hakea* spp.
2. Under field conditions, *Corymbia sp.* and *Eucalyptus sp.* (*Myrtaceae* family) rarely experience extremely low levels of soil moisture content. Therefore I hypothesise that these species will exhibit larger declines in $A_n$ and $g_s$ for a given leaf water potential during the development of drought, than Mulga and *Hakea* sp.
3. Within species, plants that have experienced drought previously will be less sensitive to subsequent droughts; this will be observed as smaller reductions of $A_n$ and $g_s$ as leaf water potential declines during repeated droughts.
4. I hypothesised that the degree of recovery in leaf-scale gas exchange variables after repeated droughts will be larger in the Mulga and *Hakea* species than the *Eucalyptus* and *Corymbia* species because of the extreme drought resistance exhibited in the former species but not the latter two species.
5. Drought resistance is largest in species having highly sclerophyllous foliage; this may contribute to a rapid recovery of leaf gas exchange variables (i.e., $A$ and $g_s$, $V_{cmax}$, $J_{max}$ and $WUE_i$) in all species.

## *5.2 Methods*

### 5.2.1 Plant taxa and plant growth conditions

Seedlings of *Acacia aptaneura*, *Corymbia opaca*, *Eucalyptus camaldulensis var. obtusa* and *Hakea macrocarpa* were germinated from seeds in the winter of 2015 in a glasshouse at the University of Technology Sydney, in Sydney, Australia. These species were selected due to their dominance in semi-arid central Australia (Cleverly *et al.*, 2016c; Eamus *et al.*, 2013) and because of their contrasting hydrological traits (Table 5.1). A pre-treatment with boiling water was applied to *A. aptaneura* seeds, to break seed dormancy, and then seeds were left to soak overnight. The other three species did not need a pre-treatment (www.anbg.gov.au). Around 20 seeds *per* species were placed in each of several petri dishes with 4-8 % agar and located in a glasshouse at ~25 $^{O}$C until germination in *ca.* 3 - 30 days. The seeds were germinated within a glass cabinet with a sunlit polythene-covered lid that transmitted 70 % of sunlight. Seedlings were transplanted from the agar plates to seedling trays (20 x 30 cm) with the same reduced sunlight until they were > 5 cm tall. The seedling-trays were filled with sterilized soil to prevent contamination from microbes / fungi. The prepared mixed soil consisted of 50 % of native mix containing low-phosphorous (Greenlife® Native Mix) and 50 % river sand (www.anlscape.com.au). The seedlings were planted into 16 pots *per* species in 18 L pots, once plants were > 10 cm tall. These pots were filled with the same prepared mixed soil. Seedling grew for an additional 12 months in the glasshouse, naturally illuminated, with a light-diffusing curtain. High soil water content conditions were maintained until initiation of the drought treatments (see below). An automated drip water system was installed to irrigate pots every two days. During the growing period, daily air temperature ranged from 13 to 38 $^{\circ}$C, and daytime of vapour pressure deficit (*D*) was on average 1.9 kPa (Nolan *et al.,* 2017c).

Table 5.1 Plant species description from the literature. Note *Acacia aptaneura* was previously named *A. aneura* (Maslin and Reid, 2012). *Plant functional type (PFT).

| Family / Species | PFT* | Life form | Leaf morphology | Xylem attributes | Rooting attributes | Reference |
|---|---|---|---|---|---|---|
| *Myrtaceae / Eucalyptus camaldulensis* | Riparian evergreen, sclerophyll angiosperm tree | Tall tree >15 m | Broad leaves, sapwood having high density xylem vessels | Low wood density | Deep-rooted | Santini *et al.* (2015) O'Grady *et al.* (2009) |
| *Myrtaceae / Corymbia opaca* | Savanna, evergreen angiosperm tree | Tall tree >15 m | Broad leaves, sapwood with high density xylem vessels | Large hydraulic conductivity, relatively low wood density | Deep-rooted | Santini *et al.* (2015) O'Grady *et al.* (2006 & 2009) |
| *Proteaceae / Hakea macrocarpa* | Evergreen angiosperm tree | Tall shrub 1-3 m | Broad and terete leaves | Low wood density | Strongly dimorphic | Groom *et al.* (1994) |
| *Fabaceae / Acacia aptaneura* | Evergreen, angiosperm tree | As shrub <2 m As tree < 15 m | Evergreen with phyllodes and high leaf density and thickness | Complex xylem vessel network with small vessels size<br>Large wood density with low hydraulic conductivity | Shallow root system with taproot and feeder roots<br>$N_2$-fixing species | Page *et al.* (2011) Santini *et al.* (2015) O'Grady *et al.* (2009) |

### 5.2.2 Experimental design

The experimental design of this study consisted of 3 repeated droughts to test the effect of pre-exposure to drought (Nolan *et al.*, 2017c). The drought-imposed experiment had eight replicates *per* treatment (well-watered: WW; and water-stressed: WS) *per* species (n= 16). Plants were assigned to either WS or WW treatments such that there were no differences in mean plant height across treatments. Prior to the imposition of the three experimental droughts, a pre-treatment water stress was imposed to all species and all individuals (i.e., both WW and WS plants were exposed to a pre-treatment drought) during July-August-2016 (Fig. 5.1). This pre-treatment helps to increase seedling survival (Nolan *et al.*, 2017c) and was applied a year after germination (seedling were >20 cm tall) and served to imitate natural conditions experienced during the end of the wet season in central Australia.

Drought was imposed by completely ceasing irrigation. Glasshouse natural settings allowed the pots to dry slowly while $g_s$ (n= 5 plants *per* treatment *per* species) was monitored *ca.* every 4 days under natural light conditions using a porometer (AP4 Leaf Porometer, Delta-T-Devices, Cambridge, UK). Soil moisture was measured gravimetrically, at the same time as the measurements of $g_s$. During this, pre-treatment $g_s$ dropped by ~30 % of maximal $g_s$ and was

followed with a recovery period where plants were watered to field capacity (FC). Following the start of rewatering all plants recovered fully in the following *ca.* 2 weeks. Note that the length of the dry-down during this pre-treatment differed across the four species, and was determined by the length of time it took for $g_s$ to decline by approximately 30 %.

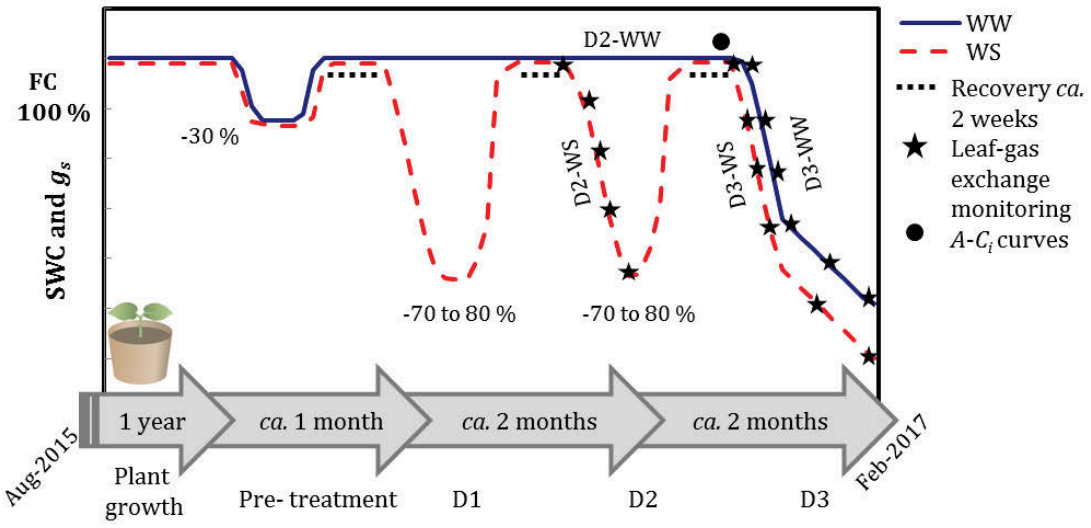


Figure 5.1 Drought experiment design for well-watered (WW) and water-stressed (WS) treatments. Stomatal conductance ($g_s$) and soil water content (SWC) were repeatedly monitored during the experiment after the first year of plant growth. Percentages indicate the decline in $g_s$ of the maximum. Experimental droughts are indicated by D1, D2 and D3.

Following the pre-treatment drought, three sequential experimental droughts (D1, D2 and D3) were applied between September 2016 and February 2017 (Figs. 5.1 and 5.2). SWC and $g_s$ were monitored repeatedly for all plants. The imposition of water stress after the pre-treatment drought was stopped when $g_s$ was approximately 70-80 % of control values of $g_s$ (Fig. 5.1). The first drought was initiated in mid-September for WS treatments in all species (duration of *ca.* 20-30 days). The second drought (D2) was initiated for *E. camaldulensis* on the 21st October in 2016 (for 21 days), continued by *A. aptaneura* and *H. macrocarpa* on the 26th (both for 30 days) and *C. opaca* on the 13th of Nov for WS treatment (for 37 days). The third drought (D3) was initiated for *E. camaldulensis* (for 22 days), *A. aptaneura* (for 26 days) and *H. macrocarpa* (for 31 days) on the 18th December but for *C. opaca* this final drought was initiated on the 30th December (for 38 days). During the entire experimental-drought period, pots were repeatedly moved every 3 weeks across bench tops to reduce the impact of any variation in micro-climate across benches within the glasshouse.

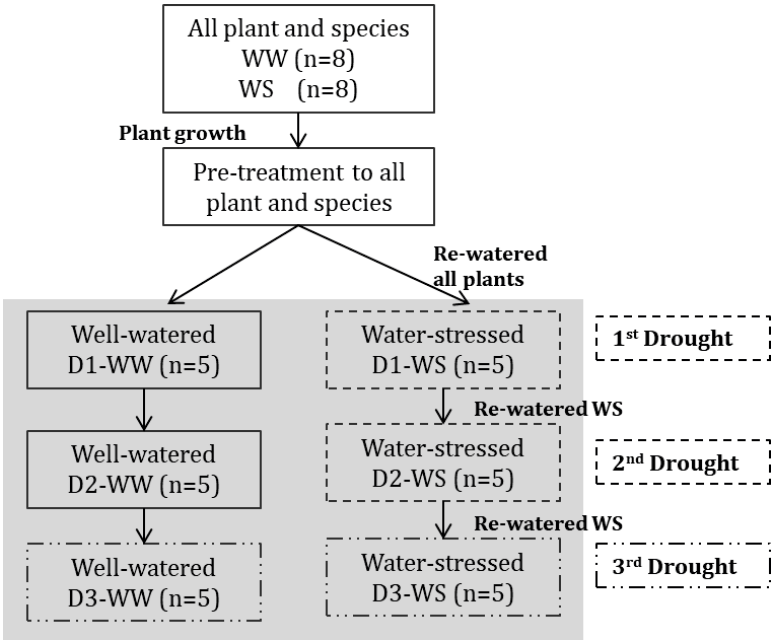


Figure 5.2 Pre-treatment and experimental drought diagram for well-watered (WW) and water-stressed (WS) plants. The gray box indicates when all leaf-gas exchange measurements were conducted. Experimental droughts are indicated by D1, D2 and D3.

### 5.2.3 Leaf gas exchange

Leaf gas exchange measurements were made with an infrared gas analyser (IRGA) system (Li-6400XT, Li-Cor Inc., Lincoln, NE, USA) coupled to a 2 x 3 cm broadleaf chamber (6400-02B LED Light Source; Li-Cor Inc.). Two leaves *per* individual were measured on 5 replicate plants *per* treatment *per* species during the second and third experimental droughts. Leaf dark respiration ($R_d$) was measured during drought 3 on one leaf *per* plant (n= 4) *per* treatment. Leaves for $R_d$ were wrapped in aluminium foil prior to sunrise. Gas exchange measurements, including $R_{d,}$ were made between 09:00 h and 11:00 h, each measurement took between 5 to 10 minutes, until stomatal conductance approached steady-state conditions. Temperature was maintained on average at 33 ± 2.5 $^{O}$C during measurements. $CO_2$ concentration was set at 400 ppm inside of the leaf chamber and photosynthetic photon flux density (PPFD) was 1500 μmol $m^{-2}$ $s^{-1}$ and 0 μmol $m^{-2}$ $s^{-1}$ when measuring $R_d$. Projected leaf area was measured using an image analysis system (WinDIAS 3, Delta-T Devices, Cambridge UK), and leaf gas exchange values were area-corrected.

Photosynthetic responses to sub-stomatal $CO_2$ concentrations ($A$-$C_i$ curves) measurements were made before the start of drought 3, once plants had recovered from the previous drought (D2), (recovery was assessed through measurements of $g_s$; Fig. 5.1). $CO_2$ concentrations in the

leaf cuvette were set at 400, 200, 100, 50, 40, 400, 400, 1000, 1200, 1400 and 1700 ppm (n=4 *per* species, *per* treatment) using 3 min time step between measurements. The plantecophys R package (Duursma, 2015) was used in R 3.2.1 (R Development Core Team, 2016) to estimate $J_{max}$ and $V_{cmax}$ from the fitted $A$-$C_i$ curves using the Farquhar *et al.* (1980) model. Leaf temperature was corrected to 25 °C and $D$ was held as constant as possible during the measurements at 2.3 ± 0.8 kPa.

### 5.2.4 Plant water status

Pre-dawn leaf water potential ($\Psi_{pd}$) was measured on the same days as leaf gas exchange measurements. Leaves / phyllodes were selected randomly before sunrise between 05:00 h and 06:00 h (n= 4 *per* species *per* treatment). Excised leaves were immediately placed in Ziploc bags and sealed and transported to the laboratory in an insulated cooler and their water potential was measured within the following hour in a Scholander-type pressure chamber (PMS Instruments, Albany, OR, USA).

### 5.2.5 Gas exchange sensitivity to water stress

To estimate the sensitivity of $A_n$ and $g_s$ rates to drought, the value of SWC at 50 % loss of leaf gas exchange was calculated following the method of Domec and Gartner (2001). $A_n$ and $g_s$ were normalized to 100 % using maximum values. To fit the leaf gas exchange curves as SWC declined, the following Weibull function was used:

$$y\ (\%\ \text{of max}\ g_s \text{ or } A_n) = 100 - (100\ /\ (1 + e^{(a*(SWC-b))}) \qquad \text{(eq. 5.1)}$$

where $y$ is either $A_n$ or $g_s$ (normalized values), $a$ describes the slope of the curve and $b$ is the SWC at 50 % of $A_n$ or $g_s$ ($A_{n50}$ and $g_{s50}$, respectively).

### 5.2.6 Metrics of leaf growth and LMA

Leaf mass *per* area (LMA) was calculated using ~10 leaves (g $m^{-2}$) *per* species. Leaf areas of fresh leaves were measured in a leaf area scanner (WinDIAS 3, Delta-T Devices, Cambridge UK). The same leaves were then oven-dried at 65 °C and dry weights were obtained after 72 hours. Additionally, plant growth was monitored at the start of each experimental drought (from D1 to D3) by measuring number of leaves, stem diameter and plant height.

### 5.2.7 Statistical analyses

To test for differences within and among species and between treatments, statistical analyses were undertaken using the R 3.1.1 Project software® (R Development Core Team 2016). The normality of the data was verified with the Shapiro-Wilk test. When necessary, logarithmic transformations were applied to the data to meet test assumptions. Linear mixed models with observations as random factor were applied to plant growth to evaluate differences across species. A Tukey's honest significant difference test was used to determine significant differences between species to test hypotheses 1. Linear regressions were applied *per* species to determine the relationship between: $\Psi_{pd}$ *versus* $A_n$ and $g_s$. Differences in slopes were tested with two approaches separately: 1) for every treatment between species and 2) within species between treatments. The first approach allowed me to differentiate rates in declining leaf gas exchange variables as drought progressed between species within the same treatment either WW or WS across droughts (to test hypothesis 2). The second approach allowed me to differentiate changes in rates with repeated droughts, for example to compare plants from D2 *versus* plants from D3 within species (to test hypothesis 3). Slope differences were tested using a standardized major axis method in the SMATR package in R and multiple comparison pair-wise test comparisons among species (Warton *et al.*, 2012). Additionally, LMA was regressed against $J_{max}$ and $V_{cmax}$ and the ratio $J_{max}$ and $V_{cmax}$. A nonlinear least squares "nls" function in R was used to evaluate the response of $g_s$ and $A_n$ to soil water content. Additionally, to test plant recovery, differences in leaf gas exchange variable between species and treatments and the interaction term species × treatment were statistically tested using two-way analysis of variance (ANOVA). Pair-wise student's t-test was used for *post hoc* comparisons of species with Bonferroni correction to discriminate specific differences among species and treatments.

## *5.3 Results*

### 5.3.1 Plant height and diameter differences during drought

Plant height ranged between 30 and > 100 cm (Fig. 5.3). Throughout the experiment *E. camaldulensis* was the tallest species, followed by *A. aptaneura* (Fig. 5.3a; *p*-value<0.05; supplementary Table S.5.1), whilst *C. opaca* was the smallest (30 to 60 cm) species after one year of growth. Within species, there were no significant differences between treatments in height and diameter values (*p*-value>0.05, supplementary Table S.5.1).

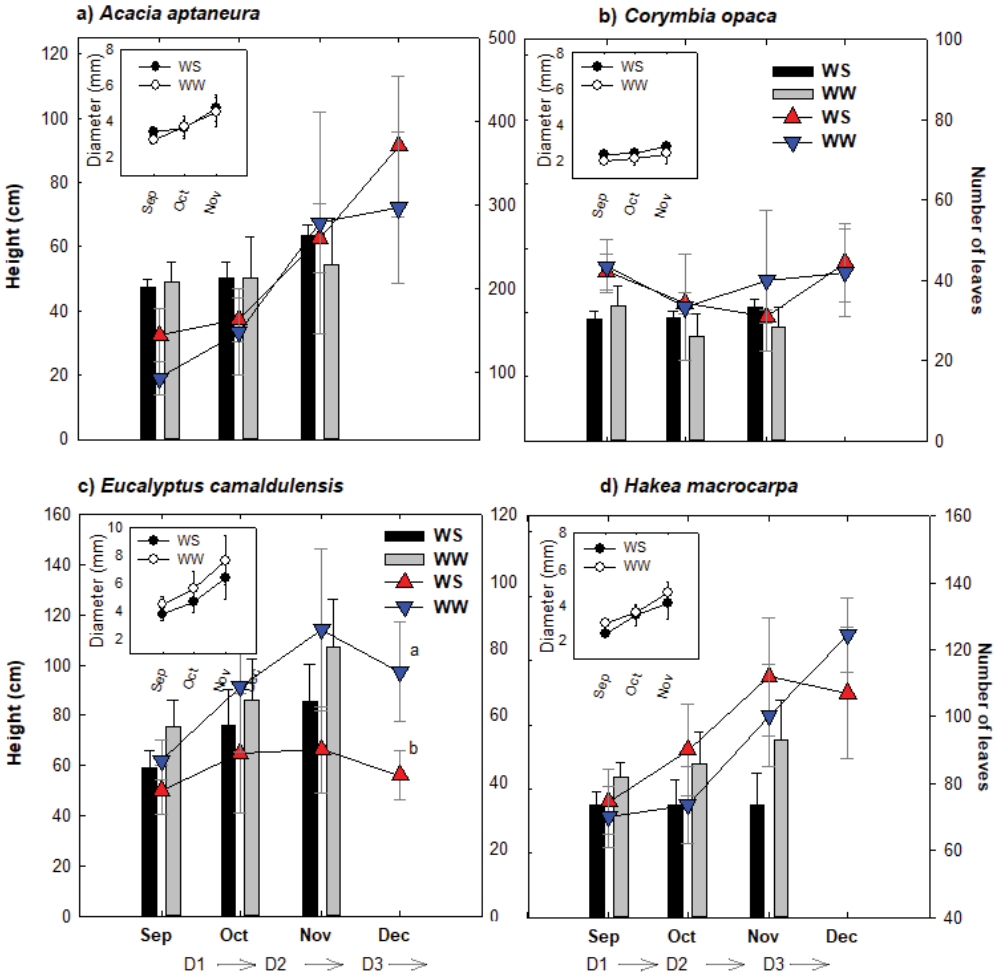


Figure 5.3 Plant height (bars), number of leaves (triangles) and stem diameter (circles) changes for well-watered (WW) and water-stressed (WS) treatments during Sep-Dec-2016 after one year of growth. *X*-axes also indicate estimated starts of each experimental drought (D1, D2, D3; dates vary for each species). Note that scales of *Y*-axes for both middle and right side change at each species. The middle *Y*-axis only represents numbers of leaves for (a) and (b). Error bars represent ± 1SE (n= 4).

There was a considerable reduction in the numbers of leaves for the WS and WW in *E. camaldulensis* during D3 ($p$-value<0.05). Stem diameter was considerably large in *E. camaldulensis* during the entire experiment (4-8 mm), but was similar within the remaining three species (2-5 mm). Moist conditions in the WW treatment were favourable for plant height in *E. camaldulensis* and this species was significantly taller than the remaining three species in the interaction across species ($p$-value<0.05).

### 5.3.2 Temporal trends in leaf gas exchange

In all species $g_s$ and $A_n$ decreased significantly when SWC declined below *ca.* 0.20 $m^3 m^{-3}$ (Fig. 5.4). Leaf gas exchange parameters ($g_s$ and $A_n$) displayed a sigmoidal function with SWC ($y = a / (1 + e^{[-(x-c)/b]})$; $p$-value<0.05). A large range of $g_s$ (0.02-.3 mol $m^{-2}$ $s^{-2}$; Fig. 5.4a-d), $A_n$ (0.84-35 μmol $m^{-2}$ $s^{-1}$; Fig. 5.4e-h) and, $WUE_i$ (8-336 μmol $mol^{-1}$) were observed across the full range of SWC experienced during the drought experiments across species.

The largest rates of $g_s$ were observed in *E. camaldulensis* (0.67-1.07 mol $m^{-2}$ $s^{-1}$) and *C. opaca* (0.59-1.26 mol $m^{-2}$ $s^{-1}$) across the two treatments when SWC > 0.20 $m^3 m^{-3}$. This is in comparison to *H. macrocarpa* and *A. aptaneura* where $g_s$ ranged from 0.02-0.44 and 0.04-0.63 mol $m^{-2}s^{-1}$, respectively. In contrast, the largest $A_n$ was observed in *A. aptaneura* (32.8 μmol $m^{-2}$ $s^{-1}$) with minimal differences across the remaining three species ($A_n$= 28.2, 26.6, and 22.5 μmol $m^{-2}$ $s^{-1}$ for *H. macrocarpa*, *C. opaca* and *E. camaldulensis,* respectively). When SWC was large (> *ca* 0.2 $m^3$ $m^{-3}$) both $g_s$ and $A_n$ were independent of SWC and ranged between *ca.* 0.2 – 0.6 mol $m^{-2}$ $s^{-1}$ for $g_s$ and *ca.* 15 – 30 μmol $m^{-2}$ $s^{-1}$ for $A_n$.

Generally, across all four species $WUE_i$ was independent of SWC for moderate-to-large values of SWC (*ca.* > 0.1 $m^3$ $m^{-3}$). However, for low values of SWC (*ca.* < 0.08 $m^3$ $m^{-3}$) $WUE_i$ increased in some, but not all treatments and this was most pronounced in *A. aptaneura* and *E. camaldulensis* (Fig. 5.4i, l). In *C. opaca* and *E. camaldulensis*, moderate reductions in SWC, from 0.2 to 0.1 $m^3$ $m^{-3}$, resulted in increased $WUE_i$ but further reductions in SWC decreased $WUE_i$ (Fig. 5.4k, l).

To compare leaf gas exchange among species following recovery and under moist conditions (during the last recovery period after D2; see Fig. 5.1), averages of $g_s$, $A_n$ and $WUE_i$ were calculated separately for the four species *per* treatment (Table 5.2). The most water-use-efficient plants were *H. macrocarpa* (88.8 ± 9.0 μmol $mol^{-1}$), *A. aptaneura* (82.9 ± 4.6 μmol $mol^{-1}$) and *C. opaca* (80.7±7.8 μmol $mol^{-1}$) all of them in the WS treatment. However, *A. aptaneura* had low $WUE_i$ in the WW treatment (64.1 ± 4.6 μmol $mol^{-1}$) and was not significantly different from

the $WUE_i$ of *C. opaca* WW (63.5 ± 6.3 μmol $mol^{-1}$). The lowest $WUE_i$ was for *E. camaldulensis* (27.9 ± 3.9 μmol $mol^{-1}$) in both WW and WS treatments and, *C. opaca* (27.9 ± 3.9 μmol $mol^{-1}$) for WW treatment.

After the second drought, $R_d/A_n$ was largest in *H. macrocarpa* (WS= 0.83 ± 0.22 and WW= 0.52 ± 0.14) and significantly different from the remaining three species (Table 5.2). The smallest ratio was observed in *A. aptaneura* (WS= 0.10 ± 0.04 and WW= 0.10 ± 0.3) and *E. camaldulensis* (WS= 0.07 ± 0.01 and WW= 0.12 ± 0.03). For WW treatment, *H. macrocarpa* also had the largest $R_d/A_n$ value, but this was, statically different from *E. camaldulensis*, *C. opaca* and *A. aptaneura*.

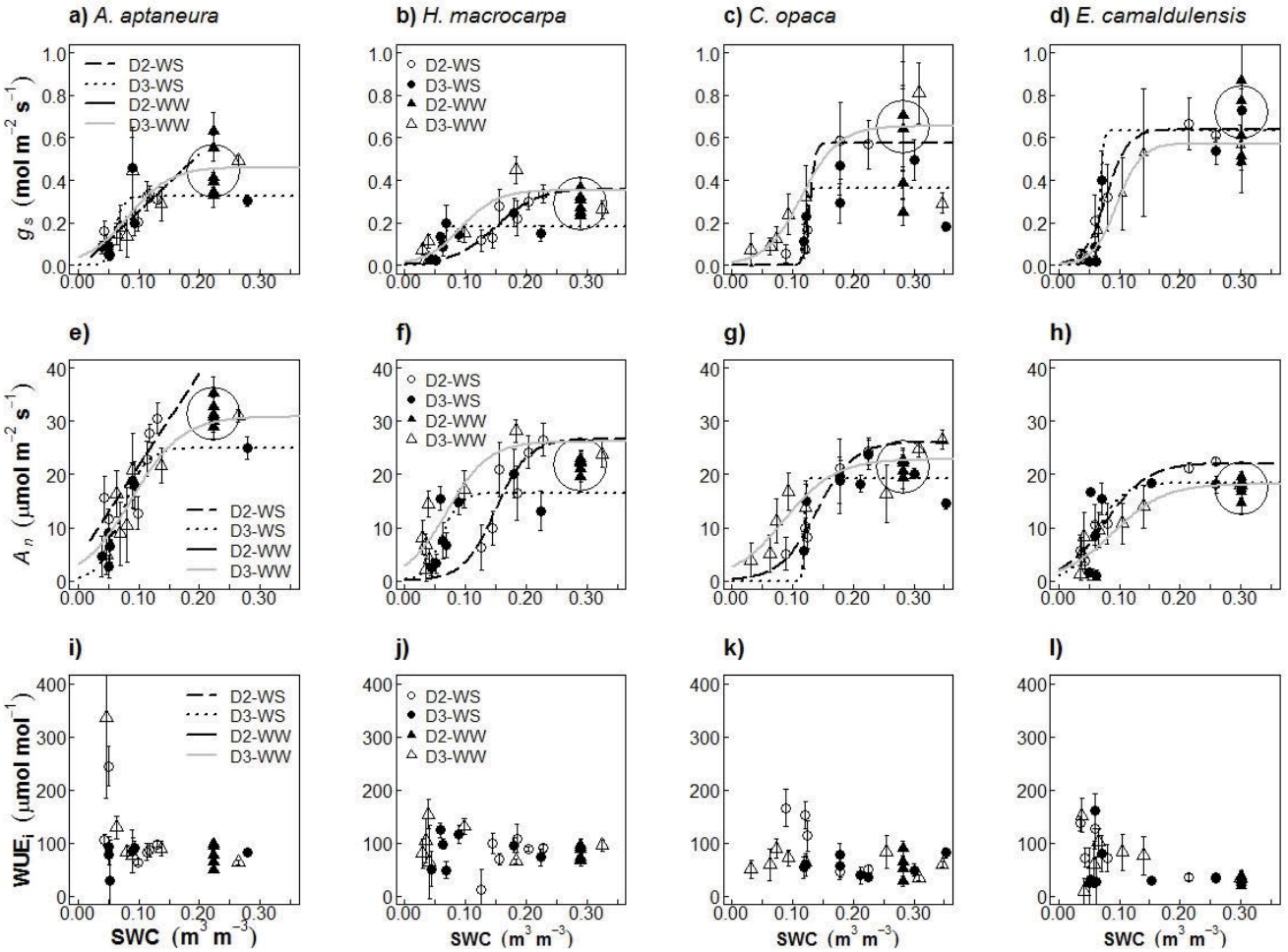


Figure 5.4 Effect of drought on leaf gas exchange: net assimilation ($A_n$), stomatal conductance ($g_s$) and intrinsic water-use-efficiency ($WUE_i$). Treatments are well-watered (WW) and water-stress (WS) for 2nd and 3rd drought (D2 and D3; see fig. 5.1). Big circles indicate D2-WW treatment at 100 % field capacity during D2. Error bars represent ± 1SE. Each curve is a non-linear fit for the watering regimes. A three-parameter sigmoid function was used for the treatments. Data points are the means of measurements within each treatment (n= 5). Only regressions with significant *p*-values <0.05 are shown.

Table 5.2 Summary of plant species comparisons of mean values of leaf mass *per* area (LMA; g $m^{-2}$), net assimilation ($A_n$; μmol $m^{-2}$ $s^{-1}$), stomatal conductance ($g_s$; mol $m^{-2}$ $s^{-1}$), intrinsic water-use-efficiency ($WUE_i$; μmol $mol^{-1}$), the ratio of night-time respiration to daytime net assimilation ($R_d/A_n$), velocities of carboxylase ($V_{cmax}$; maximum rate of the Rubisco activity; μmol $m^{-2}$ $s^{-1}$) and the maximum rate of electron transport ($J_{max}$; μmol $m^{-2}$ $s^{-1}$) for each treatment: well-watered (WW) and water-stressed (WS). Parameters such as $A_n$, $g_s$, $WUE_i$, LMA, $V_{cmax}$ and $J_{max}$ correspond to the last recovery period of the experiment. $R_d/A_n$ ratio values were averaged from different point measurements during the third drought *per* treatment (WS and WS). Errors represent ± 1SE (n= 5 and 4 for $V_{cmax}$ and $J_{max}$). Within columns, different letters indicate that means were significantly different at *p*-value < 0.05 among species and treatments assessed with two-way ANOVAs and pair-wise t-test with Bonferroni correction to compare among species and treatments.

| Species* | Treatment | LMA | $A_n$ | $R_d/A_n$ | $g_s$ | $WUE_i$ | $V_{cmax}$ | $J_{max}$ |
|---|---|---|---|---|---|---|---|---|
| ***ACA*** | WS | 543±38.6 a | 25.0±2.1 ac | 0.10±0.04 ab | 0.30±0.03 ab | 82.9±4.6 a | 85±14.7ab | 287±53.4 a |
| | WW | 385±93.3 abc | 31.0±1.2 a | 0.10±0.3 ab | 0.49±0.03 abd | 64.1±4.6 a | 95±7.8 ab | 283.4±31.7 abc |
| ***COR*** | WS | 286±34.1 bd | 14.5±1.0 b | 0.18±0.07 a | 0.18±0.01 a | 80.7±7.8 a | 110±3.4 a | 771.6±77.6 d |
| | WW | 220±53.2 cd | 16.5±2.4 bc | 0.21±0.07 ab | 0.28±0.06 ab | 63.5±6.3 ac | 91±6.5 ab | 294±14a c |
| ***EUC*** | WS | 135±16.7 d | 18.3±0.4 bc | 0.07±0.01 a | 0.73±0.06 cd | 27.9±3.9 b | 68±2.4 bc | 137±13.7 b |
| | WW | 130±10.6 d | 18.1±1.2 bc | 0.12±0.03 ab | 0.57±0.10 bc | 34.7±5.0 bc | 60±7.5 c | 119±8.5 b |
| ***HAK*** | WS | 498±54.2 ab | 16.7±4.3 bc | 0.83±0.22 c | 0.18±0.03 a | 88.0±8.5 a | 76±5.7 ac | 180±29.5 ab |
| | WW | 285±52.5 bcd | 19.8±2.8 bc | 0.52±0.14 bc | 0.23±0.03 a | 88.9±9.0 a | 86±5.7 ac | 254±23.2 ab |

*Species ID are *Acacia aptaneura* (ACA), *Corymbia opaca* (COR), *Eucalyptus camaldulensis* (EUC); *Hakea macrocarpa* (HAK).

### 5.3.3 Soil water content values associated with a 50 % loss in gas exchange

With the normalized values of $g_s$ and $A_n$ (normalized to 100 % using maximum values of $g_s$ and $A_n$ at high soil water content; supplementary material Figs. S.5.1 and S.5.2) SWC values associated with a 50 % loss in $g_s$ and $A_n$ were calculated (Table 5.3). During D2, values of SWC associated with a 50 % of loss in $g_s$ ($g_{s50}$) and $A_n$ ($A_{n50}$) were larger in *H. macrocarpa* (0.15 $m^3$ $m^{-3}$) and *C. opaca* (0.13 $m^3$ $m^{-3}$) than *E. camaldulensis* (0.08 $m^3$ $m^{-3}$) and *A. aptaneura* (0.07 $m^3$ $m^{-3}$). In *H. macrocarpa* $g_{s50}$ and $A_{n50}$ were twice as large for the D2-WS (0.15 $m^3$ $m^{-3}$) as for D3-WS (0.07 $m^3$ $m^{-3}$). For *E. camaldulensis* plants subject to repeated water stress, there was a 10 % decline in the value of SWC associated with a 50 % decline in $g_{s50}$ and $A_{n50}$ between the second and third droughts (from 0.08 to 0.07 $m^3$ $m^{-3}$). In contrast, for *C. opaca* plants subject to repeated water stress there was an increase in the value of SWC associated with a 50 % decline in $g_{s50}$ and $A_{n50}$, from 0.13 to 0.18 $m^3$ $m^{-3}$. *A. aptaneura* did not show changes in either $g_{s50}$ and $A_{n50}$. (*ca.* 0.07 $m^3$ $m^{-3}$).

During D3, that was applied to both treatments WS (D3-WS) and WW treatment (D3-WW), larger SWC values at the 50 % loss in $g_{s50}$ were observed in D3-WW than D3-WS in three of four species examined, with *C. opaca* being the exception. The largest difference of $g_{s50}$ between D3-WW (0.12 $m^3$ $m^{-3}$) and D3-WS (0.07 $m^3$ $m^{-3}$) was observed in *E. camaldulensis,* followed for *H. macrocarpa* and *A. aptaneura*, with no changes in *C. opaca* (0.18 $m^3$ $m^{-3}$).

Table 5.3 Values of SWC ($m^3$ $m^{-3}$) associated with a 50 % decline in $g_s$ and $A_n$ across treatments and species. Second and third experimental droughts are indicated by D2 and D3 respectively. Note that D3 is actually the first experimental drought experienced by the WW plants.

| Species | Treatment | D2 | | D3 | |
|---|---|---|---|---|---|
| | | $g_{s50}$ | $A_{n50}$ | $g_{s50}$ | $A_{n50}$ |
| ***Acacia aptaneura*** | WS | 0.07 | 0.06 | 0.08 | 0.07 |
| | WW | -- | -- | 0.09 | 0.07 |
| ***Hakea macrocarpa*** | WS | 0.15 | 0.15 | 0.07 | 0.07 |
| | WW | -- | -- | 0.10 | 0.08 |
| ***Corymbia opaca*** | WS | 0.13 | 0.13 | 0.18 | 0.13 |
| | WW | -- | -- | 0.18 | 0.12 |
| ***Eucalyptus camaldulensis*** | WS | 0.08 | 0.08 | 0.07 | 0.06 |
| | WW | -- | -- | 0.12 | 0.09 |

### 5.3.4 Plant sensitivity to leaf pre-dawn water potentials

Variations in $g_s$ and $A_n$ (log10 transformed) were linearly correlated with $\Psi_{pd}$ in all four species (Figs. 5.5 and 5.6 for $g_s$ and $A_n$ respectively). In D2 imposed on the WS treatment plants (D2-WS), *E. camaldulensis* showed the largest slope (m) in $g_s$ (m= 0.50, Fig. 5.5c and Table 5.4) and $A_n$ (m= 0.40, Fig. 5.6c), followed by *C. opaca* for $g_s$ (m= 0.39, Fig. 5.5b) and *H. macrocarpa* for $A_n$ (m= 0.26, Fig. 5.6b). *H. macrocarpa* had the smallest slopes for $g_s$ (m= 0.16; Fig. 5.5d) in D2-WS and *A. aptaneura* for $A_n$ (m= 0.15; Fig. 5.6a) in D2-WS.

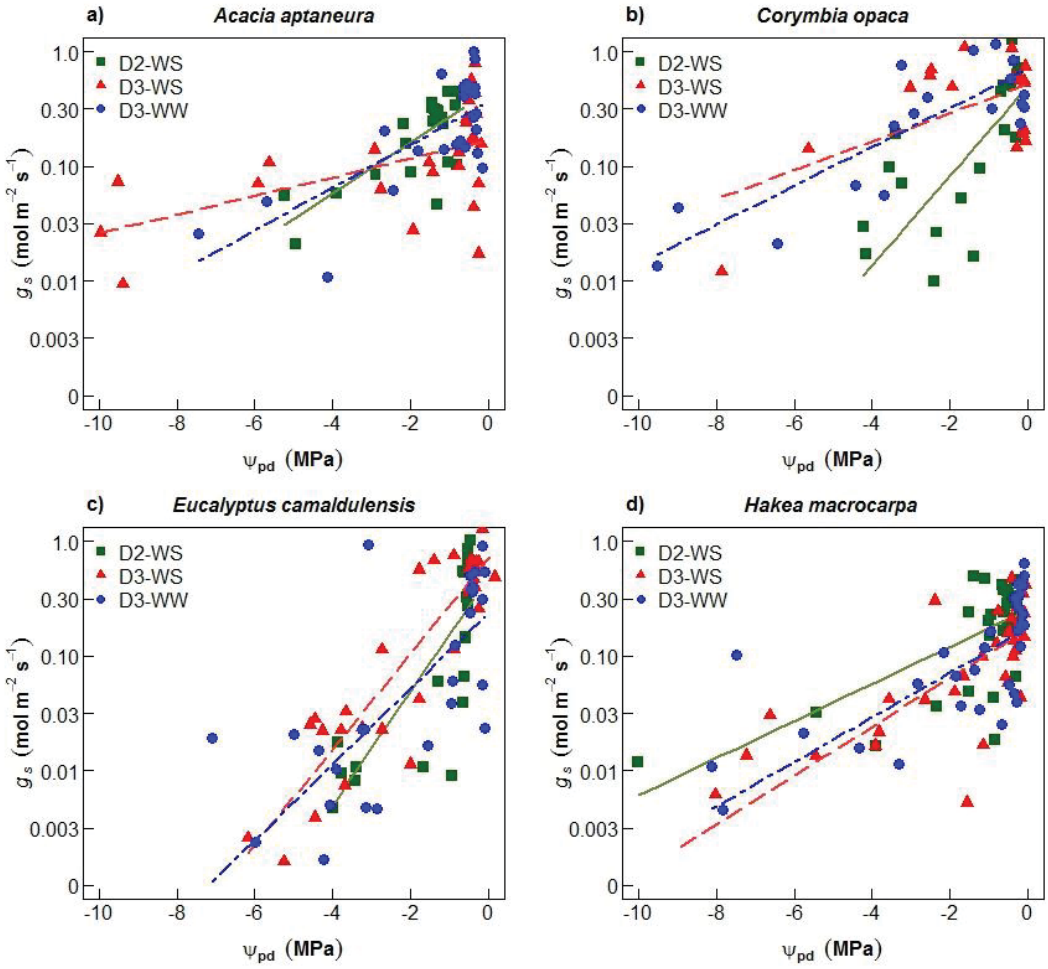


Figure 5.5 Stomatal conductance (log10($g_s$) scale; mol $m^{-2}$ $s^{-1}$) *versus* leaf pre-dawn water potentials ($\Psi_{pd}$). Symbols indicate treatments as: squares for 2nd drought (D2-WS; water-stressed treatment), triangles for 3rd drought (D3-WS) and circles for D3-WW (well-watered treatment). Regression line colour corresponds to treatment symbol colour. Regression coefficients are shown in Table 5.4.

Table 5.4 Coefficients (± 1SE) of the linear regressions between pre-dawn water potentials ($\Psi_{pd}$; MPa) and stomatal conductance (Fig. 5.5, log10($g_s$) scale; mol $m^{-2}$ $s^{-1}$) and $\Psi_p$ *versus* net assimilation (Fig. 5.6, log10($A_n$) scale; μmol $m^{-2}$ $s^{-1}$), for each species and treatment. Within columns, capital letters indicate that slopes were significantly different ($p$-value<0.05) between treatments within same species and lower case letters within species and the same treatment (either WS or WW) as tested separately using a standardized major axis method.

| | | $g_s$ *vs.* $\Psi_{pd}$ ; Fig. 5.5 | | | $A_n$ *vs.* $\Psi_{pd}$; Fig. 5.6 | | |
|---|---|---|---|---|---|---|---|
| **Species*** | **Treatment** | **Slope** | $r^2$ | ***p*-value** | **Slope** | $r^2$ | ***p*-value** |
| *Acacia aptaneura* | D2-WS | 0.22±0.04 aA | 0.55 | <0.001 | 0.15±0.02 aA | 0.63 | <0.001 |
| | D3-WS | 0.08±0.02 aB | 0.27 | <0.001 | 0.09±0.02 aB | 0.51 | <0.001 |
| | D3-WW | 0.19±0.04 aA | 0.51 | <0.001 | 0.14±0.02 aA | 0.68 | <0.001 |
| *Corymbia opaca* | D2-WS | 0.39±0.09 bA | 0.45 | <0.001 | 0.24±0.07 bA | 0.35 | 0.003 |
| | D3-WS | 0.12±0.04 acB | 0.31 | 0.01 | 0.08±0.02 aB | 0.49 | <0.001 |
| | D3-WW | 0.17±0.02 acB | 0.67 | <0.001 | 0.11±0.01 bB | 0.76 | <0.001 |
| *Eucalyptus camaldulensis* | D2-WS | 0.50±0.08 bA | 0.63 | <0.001 | 0.40±0.06 bA | 0.65 | <0.001 |
| | D3-WS | 0.41±0.03 bB | 0.81 | <0.001 | 0.22±0.03 bB | 0.61 | <0.001 |
| | D3-WW | 0.33±0.06 bB | 0.51 | <0.001 | 0.32±0.04 cA | 0.68 | <0.001 |
| *Hakea macrocarpa* | D2-WS | 0.16±0.03 aA | 0.43 | <0.001 | 0.26±0.07 bA | 0.32 | <0.001 |
| | D3-WS | 0.21±0.03 cA | 0.62 | <0.001 | 0.25±0.03 bA | 0.7 | <0.001 |
| | D3-WW | 0.19±0.03 cA | 0.53 | <0.001 | 0.23±0.05 aA | 0.41 | <0.001 |

There was a decrease in the slopes of the response of $g_s$ to $\Psi_{pd}$ of 18, 64 and 68 % for *E. camaldulensis, A. aptaneura* and *C. opaca* respectively, from D2-WS to D3-WS (Table 5.4). In contrast, an increase was observed in the slope (of $g_s$ to $\Psi_{pd}$) of 31 % in *H. macrocarpa* (Fig. 5.5d). There were significant differences in slopes only in *A. aptaneura* for the plants that experienced three droughts (D3-WS) and plants that experienced only the final drought (D3-WW; Table 5.4). In *A. aptaneura* the slope of D3-WS (m= 0.08) was 58 % smaller than D3-WW (m= 0.19).

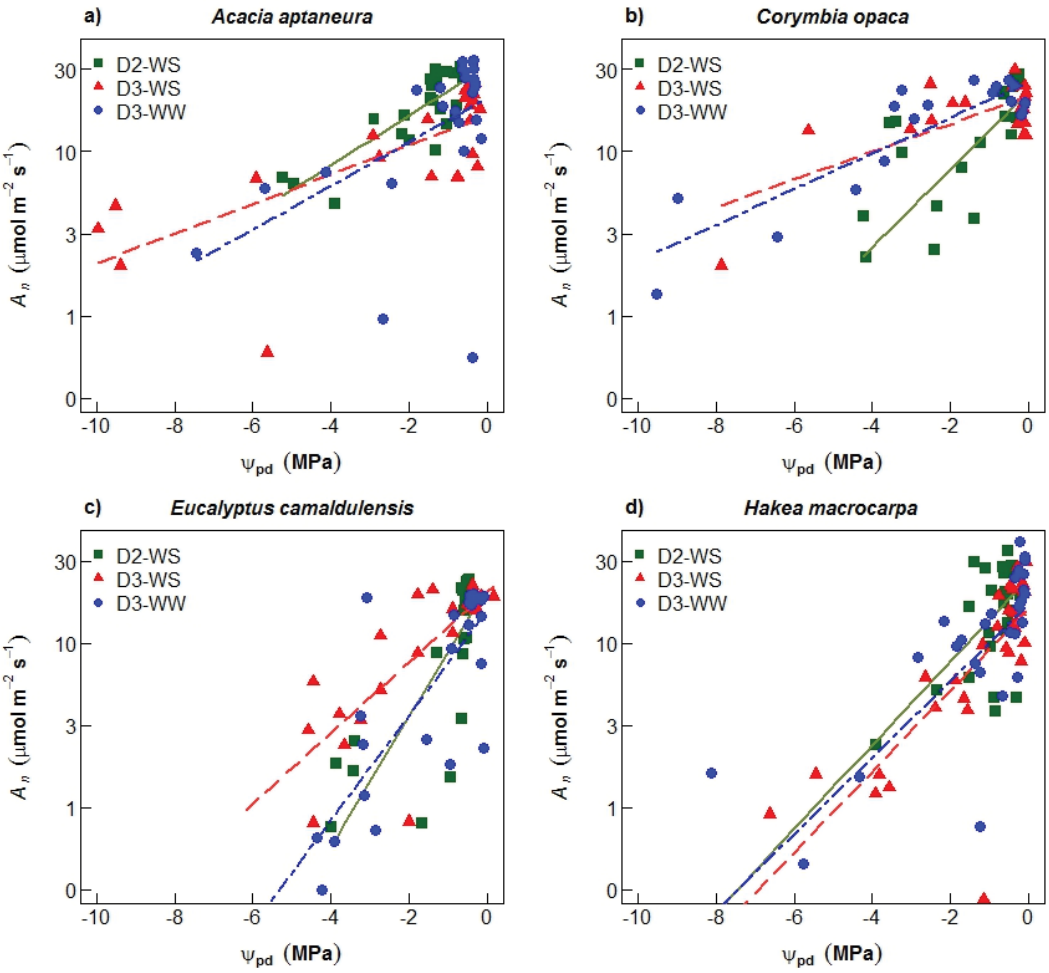


Figure 5.6 Net assimilation (log10($A_n$) scale; µmol m$^{-2}$ s$^{-1}$), *versus* leaf pre-dawn water potentials ($\Psi_{pd}$). Symbols indicate treatments as: squares for 2$^{nd}$ drought (D2-WS; water-stressed treatment), triangles for 3$^{rd}$ drought (D3-WS) and, circles for D3-WW (well-watered treatment). Regression line colour corresponds to treatment symbol colour. Regression coefficients are shown in Table 5.4.

The slope of the regression of $A_n$ *versus* $\Psi_{pd}$ plotted on a semi-log plot significantly decreased between D2-WS and D3-WS treatment for all species except *H. macrocarpa* (m= 0.26 and m= 0.25, D2-WS and D3-WS respectively; Table 5.4). Differences between the treatments (D3-WS and D3-WW) during the final drought were observed in *A. aptaneura* and *E. camaldulensis*. The slope ($A_n$ *versus* $\Psi_{pd}$) in *A. aptaneura* of D3-WS (m= 0.09; repeated drought) was 36 % smaller than D3-WW (m= 0.14), whereas in *E. camaldulensis* the difference was of 31 % smaller in D3-WS (m= 0.22) compared with D3-WW (0.32) treatment (Table 5.4). *C. opaca* did not show significant differences between slopes (D3.-WS and D3-WW).

### 5.3.5 $A$-$C_i$ curves and responses of $V_{cmax}$ and $J_{max}$ to drought

As $C_i$ increased, $A_n$ increased curvilinearly, with an initial linear increase in $A_n$ for small values of $C_i$ ($ca$ < 300 ppm), approaching an asymptote at large values of $C_i$ ($ca$ > 1000 ppm) (Fig. 5.7). There were no significant differences in the $A$-$C_i$ curves for *A. aptaneura* and *E. camaldulensis* between WW and WS treatments (Fig. 5.7a, c). For all species**,** the initial slope of the regression for low values of $C_i$ ($C_i$ < 300 ppm) did not differ between treatments. In contrast, $A_n$ for large values of $C_i$ were smaller in well-watered plants than WS plants for *C. opaca* but the opposite was true for *H. macrocarpa* (Fig. 5.7b, d).

Mean values for rates of carboxylation ($V_{cmax}$; maximum rate of the Rubisco activity; μmol $m^{-2}$ $s^{-1}$) and the maximum rate of electron transport ($J_{max}$; μmol $m^{-2}$ $s^{-1}$) estimated from $A$-$C_i$ curves are presented in Table 5.2. There were no differences between treatments within the same species for $V_{cmax}$ values. In contrast, $J_{max}$ was significantly different between WS and WW treatments in *C. opaca* (771 ± 77.6 and 294 ± 14.0 μmol $m^{-2}$ $s^{-1}$; WS and WW respectively).

*A. aptaneura* and *E. camaldulensis* had the smallest differences in $J_{max}$ between treatments. The largest difference between treatment was in *H. macrocarpa* (180 ± 29.5 and 254 ± 23.2 μmol $m^{-2}$ $s^{-1}$; WS and WW respectively; Table 5.2), but differences were not statistically significant. *C. opaca* had the highest $V_{cmax}$ values (110 ± 3.4 μmol $m^{-2}$ $s^{-1}$) in WS treatment, whilst *A. aptaneura* had the highest $V_{cmax}$ value (95 ± 7.8 μmol $m^{-2}$ $s^{-1}$) in WW treatment (Table 5.2). Minimum $V_{cmax}$ values for both WS and WW were observed in *E. camaldulensis*, but these were not statistically different from *H. macrocarpa* in both treatments, WW for *C. opaca* and both treatments for *A. aptaneura.*

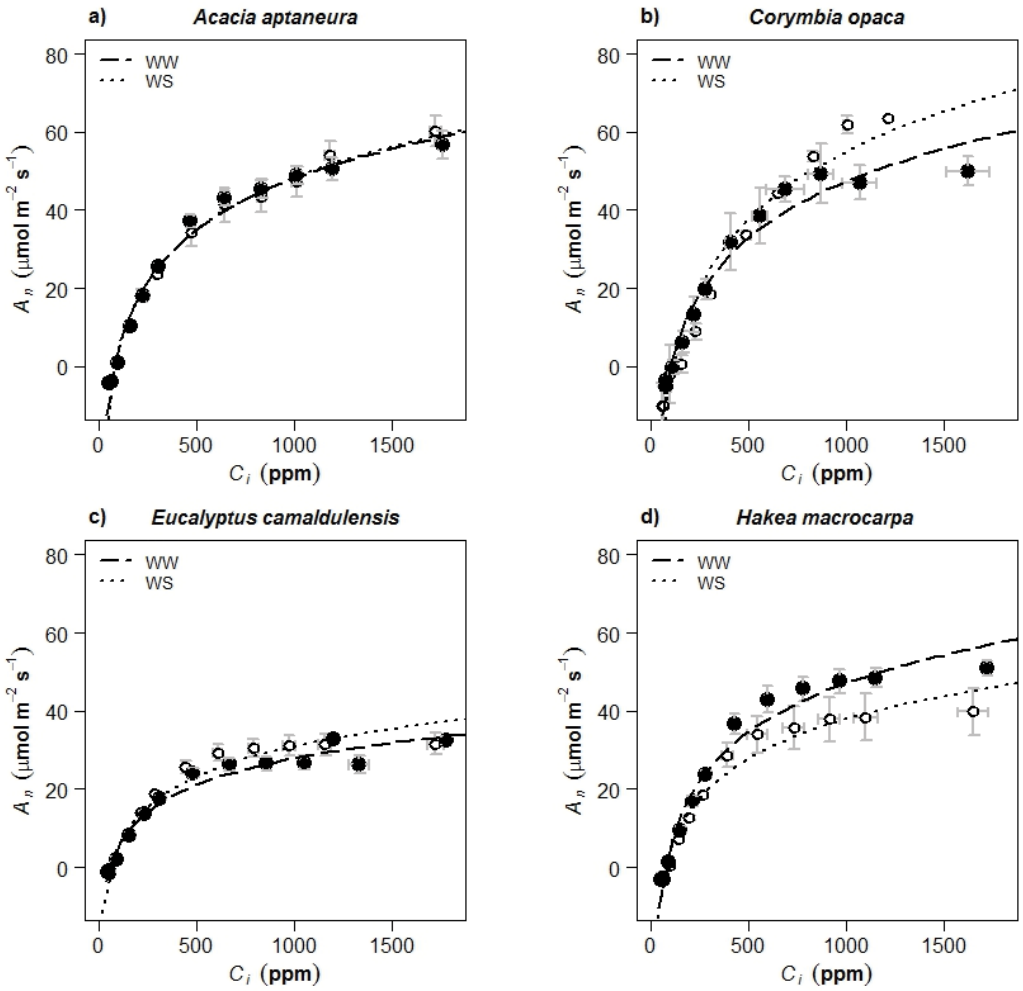


Figure 5.7 The response of net assimilation ($A_n$) to intercellular $CO_2$ ($C_i$). Open circles corresponds to WW treatment and closed symbols to WS treatment. Error bars represent ± 1SE (n= 4).

The estimated $V_{cmax}$ and $J_{max}$ parameters were positively correlated among species and treatments (Fig. 5.8a). *E. camaldulensis* consistently exhibited the smallest values of $V_{cmax}$ and $J_{max}$ for both WW and WS treatments. The WS treatment had the steepest slope (m) in the correlation $J_{max}$ and $V_{cmax}$ (m= 4.1, $r^2$= 0.51; $p$=0.019), compared with the WW treatment (m= 3.0, $r^2$= 0.69; $p$-value< 0.001) but there were no statistically significant differences among the slopes between treatments ($p$-value > 0.05).

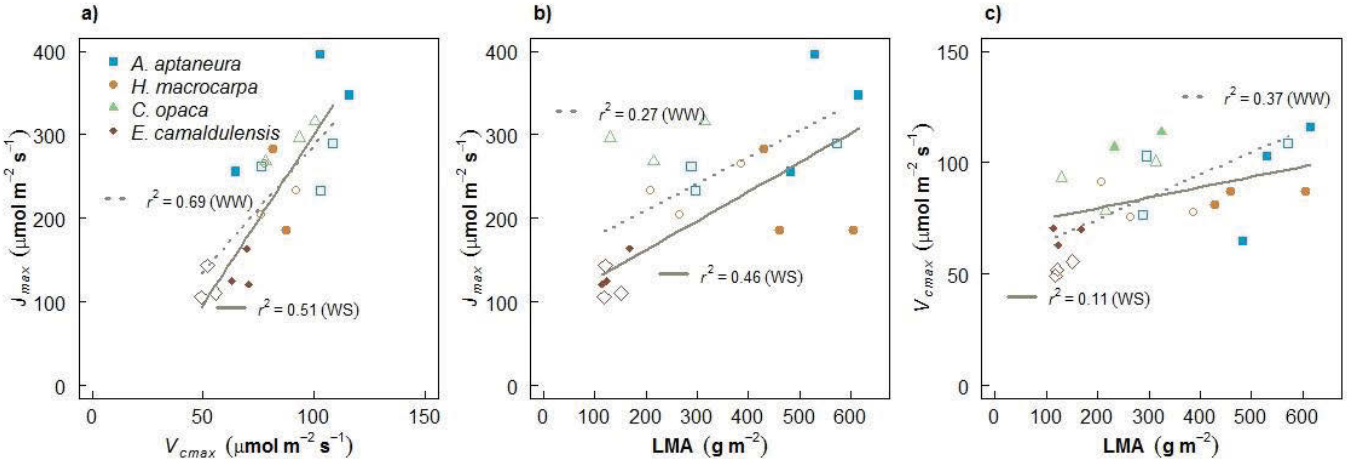


Figure 5.8 (a) Relationships between velocities of carboxylase ($V_{cmax}$; maximum rate of the Rubisco activity) and the maximum rate of electron transport ($J_{max}$). (b) Relationship between $J_{max}$ and leaf mass *per* area (LMA) and (c) $V_{cmax}$ *versus* LMA. Open circles corresponds to WW treatment and closed symbols to WS treatment. Lines indicated regression as dotted lines for WW and solid lines for WS treatment.

$V_{cmax}$ and $J_{max}$ were positively correlated with LMA (Fig. 5.8b, c). Similar to the regression of $J_{max}$ *versus* $V_{cmax}$, *E. camaldulensis* had the smallest values of LMA with smallest $V_{cmax}$ and $J_{max}$ for both WW and WS treatments. There was a significant increase in the vertical displacement to larger $J_{max}$ values for a given value of LMA in the WW treatment ($r^2$= 0.27, $p$-value= 0.05) compared with WS treatment ($r^2$= 0.46, $p$-value= 0.02). $V_{cmax}$ had a significant positive correlation with LMA in the WW treatment ($r^2$= 0.37, $p$-value= 0.02), but not in the WS ($r^2$=0.11, $p$-value= 0.168). Smaller $V_{cmax}$ values were observed in the WS only in *A. aptaneura* (85 ± 23.2 μmol m$^{-2}$ s$^{-1}$) and *H. macrocarpa* (76 ± 5.7 μmol m$^{-2}$ s$^{-1}$) but not different from the WW treatment (Table 5.2).

## 5.4 Discussion

This study evaluated the response of leaf gas exchange, plant growth and recovery during and following drought, of contrasting co-occurring tree species within the Ti-Tree basin of central Australia. The four species selected for this experiment occupy different eco-hydrological niches and have exhibited contrasting physiological strategies in field conditions (Nolan *et al.*, 2017a; O'Grady *et al.*, 2009; Rumman *et al.*, 2018; Santini *et al.*, 2015). Therefore, contrasting responses of leaf gas exchange parameters such as $A_n$ and $g_s$ and plant growth were expected to be observed across species.

In agreement with my first hypothesis, *E. camaldulensis* was the tallest species, and thus had the fastest growth rate; and had the largest declines in $A_n$ and $g_s$ during the three droughts, but *C. opaca* behaved differently to my hypothesis (discussed in the next section). In support of my second hypothesis, *A. aptaneura* and *H. macrocarpa* had the smallest declines in $A_n$ and $g_s$ as soil water content decreased whereas *E. camaldulensis* had the largest declines. Leaf gas exchange (both $A_n$ and $g_s$) declines with increasing water stress ware smaller for plants that experienced three droughts than for plants that experienced only the final drought, but this was not apparent in all species (hypothesis 3). Likewise, a rapid recovery from imposed-drought was observed in leaf gas exchange parameters when re-watering to field capacity was applied in all species, across all treatments (hypothesis 4 and 5). I will now discuss these results in detail.

### 5.4.1 Plant growth responses to water deficit

*E. camaldulensis* was the tallest species and had the widest stem diameter during the entire experiment, even in the water-stressed (WS) treatment (Fig. 5.3c). Surprisingly, my first hypothesis was not supported for *C. opaca*. Hypothesis 1 stated that species of the *Myrtaceae* family (*E. camaldulensis* and *C. opaca*) will have faster rates of growth, due to the necessity for developing a deep root system to facilitate access to groundwater. In central Australia *E. camaldulensis* and *C. opaca* are tall, deep-rooted trees, that access groundwater (Cleverly *et al.*, 2016c; O'Grady *et al.*, 2009). Therefore, it was expected that seedling of *E. camaldulensis* and *C. opaca* would rapidly develop biomass to get a taproot down to ground water.

Growing taller requires plants species to have strategies to improve water-transport because of the increased path length that water travels from the roots to the canopy (Zeppel and Eamus, 2008). In the present study *E. camaldulensis* had the widest stem diameter (and hence sapwood area) and was the tallest of all four species examined (Fig. 5.3c). O'Grady *et al.* (2009) observed high sap flow values in *E. camaldulensis*, up to 1642.5 $m^3$ $m^{-2}$ sapwood $y^{-1}$ (Rumman *et al.*, 2018),

and this was considerably larger than the water use for *A. aptaneura* that O'Grady *et al.,* (2009) examined, reflecting the high water usage of *E. camaldulensis* (note that *A. aptaneura* was previously named *A. aneura*; see Table 5.1). Other hydraulic strategies observed in *Eucalyptus* species are high hydraulic conductivity, wide xylem vessels (Santini *et al.*, 2015) and large Huber values (the ratio of sapwood to leaf area; Zeppel and Eamus, 2008). These physiological traits in *E. camaldulensis* increase the efficiency of water transport from roots to leaves. The efficiency of water supply and transport ultimately determines plant growth and survival (Brodribb and Jordan, 2011), especially in arid and semi-arid regions.

Although, the two species from the *Myrtaceae* family (*E. camaldulensis* and *C. opaca*) have access to groundwater under field conditions (O'Grady *et al.*, 2009; Rumman *et al.*, 2018); *C. opaca* didn't grow tall as *E. camaldulensis* the present glasshouse study. Differences in hydraulic traits identified between the two species by Santini *et al.* (2015, 2017) may explain this difference in plant growth. For example, *C. opaca* has higher woody density, lower root hydraulic conductance and smaller vessel diameter than those observed in *E. camaldulensis* (Santini *et al.*, 2015; Santini *et al.*, 2017). Investing in high wood density often occurs at the expense of plant height and diameter growth (Enquist *et al.*, 1999; O'Grady *et al.*, 2009), whilst low wood density can lead to high growth rate (Roderick, 2000) as was observed in *E. camaldulensis*.

Plant growth has a dependence on roots to provide nutrients and water to leaves, while roots depend on the carbohydrates from leaves (Poorter *et al.*, 2012). Investing carbohydrates in plant maintenance and hydraulic architecture such as deep roots and high venation density (to enhance water transport) is often made at expense of leaf traits such as thickness or toughness (Brodribb and Jordan, 2011; Poorter *et al.*, 2012; Yin *et al.*, 2018). Thus, during these imposed droughts, it was observed in the final drought that *E. camaldulensis* reduced its numbers of leaves in the water-stressed (WS) treatment and many others turned brown half way through the drought (data not shown), but this was not observed in *C. opaca* (Fig. 5.3c). This suggests that allocation of assimilated carbon was preferably given to anchorage and a tall structure, rather than maintaining leaves while droughts were imposed. In contrast, at high soil water content (> 0.20 $m^3 m^{-3}$; Fig. 5.4) which existed in the well-watered (WW) treatment, both species showed large values of carbon assimilation ($A_n$) and stomatal conductance ($g_s$). Therefore, there was a coordination between water transport and leaf gas exchange (Katul *et al.*, 2003; Sperry and Love, 2015) that I will now discuss further.

### 5.4.2 Coordination among leaf gas exchange and foliar water potential (species comparison)

The response to progressive water stress observed in the four study species was in agreement with studies that have sought to understand the response of leaf gas exchange to drought in C3 plants (Cano *et al.*, 2014; Flexas *et al.*, 2004; Galmes *et al.*, 2007). In the present study, when SWC decreased below *ca.* < 0.1 $m^3\ m^{-3}$ (considered dry soil) declines in both $g_s$ and $A_n$ occurred across the four species during drought 2 and 3 (Fig. 5.4). $WUE_i$ was maintained at more or less constant values in the early stage of droughts and only increased when SWC declined to 0.10 $m^3\ m^{-3}$. However, below a certain threshold (< 0.10 $m^3\ m^{-3}$ for *E. camaldulensis* and *C. opaca;* < 0.05 $m^3\ m^{-3}$ for *A. aptaneura* and *H. macrocarpa*), $WUE_i$ declined for all species (Fig. 5.4i-l). This biphasic pattern, an increase in $WUE_i$ as soil water stress increases, but consistent decline in $WUE_i$ under extreme water stress has been observed across multiple plant species (Limousin *et al.*, 2013; Limousin *et al.*, 2015; Manzoni *et al.*, 2011).

As SWC declines, water tension increases within plants, causing leaf water potential and leaf gas exchange to decline, leading to correlations among these variables: $A_n$ *vs* $\Psi_{pd}$ and $g_s$ *vs* $\Psi_{pd}$ (McDowell *et al.*, 2008). The effect of declining pre-dawn water potential ($\Psi_{pd}$) on stomatal conductance and regulation of carbon and water balance has been commonly observed across different plant functional types (Martinez-Vilalta *et al.*, 2014; McDowell *et al.*, 2015; Meinzer *et al.*, 2009). In this study, I aimed to test the hypothesis that larger declines in $A_n$ and $g_s$ occur in *C. opaca* and *E. camaldulensis* than *A. aptaneura* and *H. macrocarpa* because the two former species rarely experience low levels of soil moisture in the field and their hydrological traits are close to those of species adapted to more mesic environments, in contrast to the traits exhibited by the latter two species (hypothesis 2).

The four co-occurring species showed a long-linear decline of $A_n$ and $g_s$ as $\Psi_{pd}$ declined as the soil dried during when a drought was applied (i.e., drought 2 and 3; Figs. 5.5 and 5.6). Results from repeated droughts (D2 and D3) showed contrasting rates of decline among species within the same treatment WW or WS (Table 5.4). For example, *E. camaldulensis* had large declines across all droughts in both relationships: $A_n$ *vs* $\Psi_{pd}$ and $g_s$ *vs* $\Psi_{pd}$, while *C. opaca* exhibited large declines, but only in the water stress treatment during the second drought (D2-WS). *A. aptaneura* exhibited small declines in both relationships ($A_n$ *vs* $\Psi_{pd}$ and $g_s$ *vs* $\Psi_{pd}$), in both treatments, during both droughts, with the smallest slopes in the plants previously subject to water stress (i.e., D3-WS). In contrast to expectations, *H. macrocarpa* did not exhibit behaviour consistent with hypothesis 3 in the relation $A_n$ *vs* $\Psi_{pd}$, there were larger declines in $A_n$ in plants previously subject to water stress. Two extreme strategies have been described to characterize

stomatal regulation of leaf water potential, namely isohydric and anisohydric (Klein, 2014). This is now discussed in further detail.

*E. camaldulensis* showed the largest slopes in the regression of $g_s$ (during D2-WS: m= 0.50) and $A_n$ (m=0 .40) *versus* $\Psi_{pd}$ (Fig. 5.5c and Fig. 5.6c, respectively). Similarly, in drought 2, *C. opaca* had large declines in $g_s$ as $\Psi_{pd}$ declined (m= 0.39; Fig. 5.5b). This behaviour of tight regulation $g_s$ for a given decline in $\Psi_{pd}$ corresponds to an isohydric behaviour. Isohydric species use rapid and early declines in $g_s$ to tightly regulate leaf water potentials in the early stages of drought, resulting in decreasing $A_n$ (Limousin *et al.*, 2013; Meinzer *et al.*, 2009; Nolan *et al.*, 2017a). However, *C. opaca* did not show such an isohydric behaviour in the third drought for both treatments, and slope values for the WW treatment were in the same range as *A. aptaneura* (table 5.4; see D3-WW). Therefore, my results agree with previous studies that have observed that the coordination between water potentials and leaf gas exchange under drought and field conditions demonstrated the isohydric behaviour for *E. camaldulensis* and *C. opaca* (Nolan *et al.*, 2017a; Nolan *et al.*, 2017c; O'Grady *et al.*, 2009). Hydrological strategies explained by Santini *et al.* (2017 and 2015) contribute to understanding the isohydric behaviour observed in *E. camaldulensis* and *C. opaca*. For example, Santini *et al.* (2017 and 2015) studied different sets of hydraulic traits in branches and roots, and found that the *Myrtaceae* species (*C. opaca* and *E. camaldulensis*) have larger xylem vessel diameter with lower wood density and larger hydraulic conductivity than *Acacia* species (*A. aneura* and *A. aptaneura*) studied. These strategies confer on *C. opaca* and *E. camaldulensis* a large whole-tree hydraulic conductance. Large hydraulic conductance and wide vessel size makes the xylem more sensitive to embolism, however, stomatal closure can prevent hydraulic failure when water availability declines and therefore drought-induced mortality (Eamus *et al.*, 2000; McDowell *et al.*, 2008).

*Acacia aptaneura* showed the smallest slopes in the regression of $g_s$ and $A_n$ *versus* $\Psi_{pd}$ during the last drought (Table 5.4). In support of the second hypothesis, this species exhibited moderate declines (slopes) for a wider range of water potential values (Fig. 5.5 and 5.6). To a smaller degree *H. macrocarpa* had also small declines in $g_s$ *versus* $\Psi_{pd}$ during drought. Smaller declines in the relationship of $g_s$ *versus* $\Psi_{pd}$ compared with *C. opaca* and *E. camaldulensis*, implies that *A. aptaneura and H. macrocarpa* had more risky stomatal regulation for a wider range of leaf water stress. Previous studies have identified *A. aptaneura* as an anisohydric species (Nolan *et al.*, 2017a; Page *et al.*, 2016). Anisohydric species tolerate a larger decline of leaf water potentials, thereby allowing the maintenance of $g_s$ and $A_n$ further into drought (Martinez-Vilalta *et al.*, 2014). *A. aptaneura and H. macrocarpa* continued to photosynthesize at much lower $\Psi_{pd}$ (Fig. 5.6a and d). These two species are known for being highly tolerant to drought and high

temperatures (Table 5.1). For example, higher wood density was observed within the two species (*A. aptaneura and H. macrocarpa*) than species from the *Myrtaceae* family (Santini *et al.*, 2015). High wood density protects against xylem implosion, leading to a superior resistance to cell wall collapse, thereby allowing species with high wood density to tolerate low water potentials (Santiago *et al.*, 2004). Although *A. aptaneura* and *H. macrocarpa* maintained photosynthetic rates at low $\Psi_{pd}$, they have major risk of hydraulic failure and embolism and therefore drought-induced mortality (Meinzer *et al.*, 2009), although this is offset to some extent by the previously mentioned anatomical traits. Results of this study are also in the range of extremely negative pre-dawn and leaf gas exchange values observed in *Acacia* spp. (O'Grady *et al.*, 2009; Page *et al.*, 2016).

I will now discuss and compare the effect of repeated drought on leaf gas exchange and water potentials in the following section.

### 5.4.3 The effect of repeated droughts and plant recovery

During this experiment of repeated droughts, three re-watering cycles were applied to all species (Fig. 5.1). I aimed to determine i) whether or not plants that experienced repeated drought would be less sensitive to subsequent droughts and ii) whether or not plants would fully recover during re-watering cycles.

Plants initially showed a considerable reduction in the slope of $g_s$ *versus* $\Psi_{pd}$ from drought 2 and 3 in the water-stressed treatment, this was by 18, 64 and 68 % in *E. camaldulensis, A. aptaneura* and *C. opaca* respectively (excepting *H. macrocarpa*; Table 5.4); there were however, only significant differences in the slope of $g_s$ *versus* $\Psi_{pd}$ of *A. aptaneura* from plants that experienced three droughts (D3-WS). In D3-WS, the slope of $g_s$ *versus* $\Psi_{pd}$ for *A. aptaneura* was smaller than plants that experienced only the final drought (D3-WW; Fig. 5.5a). This stomatal sensitivity to a repeated drought is in agreement with hypothesis 3, but this effect was not observed in the remaining three species. I hypothesised that plants that experienced drought previously would be less sensitive to subsequent droughts and that, smaller reductions of $A_n$ and $g_s$ would be observed as leaf water potential declined during a repeat drought. This implies that *A. aptaneura* plants from D3-WS were more anisohydric than plants from D3-WW. An increase in exogenous hormones (i.e. ABA) may explain this behaviour, since the accumulation of ABA that is expected to occur during previous droughts enhances stomatal sensitivity to a low water potential levels in repeated droughts (Eamus and Narayan, 1989; Nolan *et al.*, 2017c; Thomas *et al.*, 2000). Another explanation is the possible accumulation of osmotically active

solutes as the soil dries which allows species to adjust the turgor loss point at which leaf cells lose turgor and close stomatal (Bartlett *et al.*, 2014; Nolan *et al.*, 2017c).

While *H. macrocarpa* did not show significant differences between treatments during the final drought (Table 5.4), the point at which both $g_s$ and $A_n$ were reduced by > 50 % differed from 0.15 (during the second drought) to 0.07 $m^3$ $m^{-3}$ (Table 5.3; during the final drought). It may be possible that root clusters which are common across *Hakea* spp. (Lamont, 2003) benefited plant water relations. Root clusters can increase the soil volume explored by a factor of up to 300; and release deeply sourced water at night for subsequent uptake the following day through the process of hydraulic lift (Lamont, 2003). This may explain why there were not changes in rate declines of $g_s$ and $A_n$ when regressed with $\Psi_{pd}$. Similarly, *E. camaldulensis* and *C. opaca* plants from the final drought did not show differences between treatments, with plants from both treatment exhibiting large photosynthetic rates and stomatal conductance values (Fig. 5.4). It has been observed in field conditions across different rainfall gradients, that eucalyptus have shown little or no variation in leaf water potentials wet and dry seasons due to the access to groundwater (Eamus *et al.*, 2000; Mitchell *et al.*, 2014; Nolan *et al.*, 2017a). Thus, the anisohydric behaviour and hydrological traits discussed above explain why *C. opaca* and *E. camaldulensis* were less sensitive to repeated droughts than the *Acacia* species examined in the present study.

Plant responses to drought have been extensively examined in relation to limitations in leaf gas exchange, the response of mesophyll conductance and biogeochemical limitations occurring at different time-scales during periods of drought (Flexas *et al.*, 2004; Flexas *et al.*, 2006; Limousin *et al.*, 2013; Zhou *et al.*, 2016). Thus, plant recovery from droughts depends on species ability to diminish these limitations when water subsequently becomes available (Galmes *et al.*, 2007). In the present study, my results showed full recovery in $A_n$ and $g_s$ during the last re-watering cycle (between the second and final droughts) within the first 3 days after soil water content was increased to field capacity for all species (Table 5.2). Thus, there were no significant differences in leaf gas exchange between WW and WS treatments, indicating a complete recovery is support of hypothesis 4, in which a rapid plant recovery following drought was hypothesized for all species due to the sclerophyllous foliage. Full plant recovery following alleviation of drought has been observed in other C3 plants, in which the period of recovery varied from 1 to 3 days (Cano *et al.*, 2014; Flexas *et al.*, 2006; Resco *et al.*, 2009). As observed in Flexas *et al.* (2006), usually photosynthesis recovers in one day at mild water stress, but photosynthesis can have a slower recovery if the biochemical or hydraulic pathway was damaged (Resco *et al.*, 2009).

The photosynthetic response to drought that occurs independent of stomatal responses can be assessed by evaluating changes in the capacities of carboxylation ($V_{cmax}$) and electron transport ($J_{max}$) (Vogan and Maherali, 2014). Photosynthesis depends on the biogeochemical capacity of $V_{cmax}$ and $J_{max}$ which provide information about plant performance and critical factors for carbon and water fluxes (Quebbeman and Ramirez, 2016). In the present study, it was observed that $V_{cmax}$ increased for some of the WS treatments and in a few species $J_{max}$ also showed an increase, but there were no significant differences between treatments in all species except for *C. opaca* in $J_{max}$ (Table 5.2). Maintenance of $V_{cmax}$ and $J_{max}$ may indicate that plant species examined in this study have large resistance to drought in support of my hypothesis 5$^{th}$. The lack of changes between treatments in $V_{cmax}$ and $J_{max}$ (thus, $J_{max}$ /$V_{cmax}$ ratio) can be attributed to photosynthetic acclimation, as has been observed in pines trees and eucalyptus trees (Lin *et al.*, 2013; Medlyn *et al.*, 2002; Zhou *et al.*, 2016). However, mesophyll conductance controls photosynthetic capacity, and can be the main limiting factor for plant recovery (Galmes *et al.*, 2007). Therefore, further studies are needed to fully understand the relative importance of different limitations including mesophyll conductance that occur during drought and recovery from drought.

Photosynthetic velocities ($V_{cmax}$ and $J_{max}$) were positively correlated with LMA (Fig. 5.8). *C. opaca* and *E. camaldulensis* had the smallest LMA compared with remaining two species. *A. aptaneura* and *H. macrocarpa* had the largest differences (in LMA) but differences were not statistically significant between treatments (Table 5.2). Large LMA is a common leaf trait in species having sclerophyllous foliage in semi-arid habitats, contributing to the resistance to fast desiccation and, a large LMA increases leaf resistance and contributes to plant survival (Lamont *et al.*, 2002; Poorter *et al.*, 2009; Wright and Westoby, 2002). In contrast, there were differences in LMA across species (Table 5.2). $N_2$-fixing species have large foliar N contents and, foliar N is positively correlated with LMA (Poorter *et al.*, 2009). For example, *A. aptaneura* has the ability to fix atmospheric $N_2$ (Cook and Dawes-Gromadzki, 2005; Page *et al.*, 2011) and my results showed that *A. aptaneura* had the largest LMA values for both treatments (Table 5.2). Although, I did not measure foliar N content during the drought experiment, differences in leaf N content among species can be explained by expected variations in leaf nitrogen derived from field assessments of foliar N (Chapter III) explained with variations in leaf nitrogen content as it has been observed in C3 plant species (Lin *et al.*, 2013).

## 5.5 Conclusions

The aim of this chapter was to evaluate the responses of leaf gas exchange, to repeated experimental droughts and plant recovery of four co-occurring species of central Australia. Results of this study showed that *E. camaldulensis* and *C. opaca* maintained large photosynthetic and stomatal conductance rates under well-watered conditions. Large photosynthetic rates allowed *E. camaldulensis* to rapidly develop biomass and therefore grow taller than the remaining species. However, *E. camaldulensis* and *C. opaca* showed large declines in stomatal conductance in order to tightly regulate leaf water potential as each drought progressed, which is a common hydrological strategy of isohydric species. This isohydric strategy was not observed in *H. macrocarpa* and *A. aptaneura* which have specific physiological traits to withstand high light and low water availability and exhibited an anisohydric behaviour. This led to lower (more negative) water potentials than the *Myrtaceae* family species. *H. macrocarpa* maintained high photosynthetic rates across the three repeated droughts due to the beneficial effect of root clusters which are common across *Hakea* spp. (Lamont, 2003). In contrast, *A. aptaneura* had the smallest declines in values of both $A_n$ and $g_s$ during repeated droughts, and a smaller stomatal sensitivity during the third, and final, drought (D3-WS). Finally, the four species in this study showed a rapid recovery from imposed-drought and this was evidenced by comparing leaf gas exchange parameters and limitations imposed by changes in $V_{cmax}$ and $J_{max}$ across treatments.

# *Chapter VI*

## Synthesis and Conclusions

## 4.1 *Introduction*

At the time of writing this thesis, a new post-industrial record of atmospheric $CO_2$ concentration of 411.35 ppm was reached (April 2018, www.esrl.noaa.gov), a level not experienced over the last 800,000 years (Augustin *et al.*, 2004). There are many impacts on climate, vegetation and biogeochemical cycling associated with increasing atmospheric $CO_2$ concentration. Increased atmospheric $CO_2$ levels induce changes in global and regional climate, affecting carbon and water cycles (Cubasch *et al.*, 2013). These effects manifest as rising temperatures, increasing water vapour concentration in the atmosphere, increased variability in precipitation patterns, and changes in the energy budgets of land surfaces; these effects were summarised in Chapter I. Primary producers from terrestrial and marine ecosystems are the only organisms able to remove atmospheric $CO_2$ to convert inorganic carbon to organic carbon through photosynthesis. Therefore, there is enormous interest in improving our understanding of the global and regional carbon and water cycles, climate, and ecosystem functioning.

Worldwide, semi-arid and arid ecosystems occupy 45 % of the Earth's land surface and their productivity is constrained by water availability (Eamus *et al.*, 2016; Huxman *et al.*, 2004b; Schwinning and Sala, 2004). Semi-arid regions dominate the inter-annual variability of the global land carbon (C) sink (Ahlström *et al.*, 2015). Thus, the study of ecosystem functioning in semi-arid regions is a key a component for improved understanding of inter-annual C variability in the global C cycle. In particular, Australian arid and semi-arid ecosystems can have a large role in contributing to this variability. For example, during the 2011 global land carbon sink anomaly (GLSA), which saw an increase in the terrestrial carbon sink from the historical average of 2.6 Pg C $y^{-1}$ to 4.1 Pg C $y^{-1}$, Australian semi-arid and arid regions were estimated to account for 60 % of this anomaly (Poulter *et al.*, 2014). Despite the importance of these Australian arid and semi-arid environments, mechanisms that explain C variability and trends are not well understood, and these ecosystems remain poorly studied.

### 6.1.1 Thesis aim

The aim of this thesis was to investigate ecosystem functioning of two semi-arid woodlands of central Australia to improve our understanding of the interactions of C and water fluxes with the atmosphere. To accomplish this general objective, C and water fluxes were evaluated at different temporal-scales (i.e., diurnal, seasonal, annual and inter-annual) and different spatial-scales, from plot - to leaf-scales, in two dominant ecosystems: a Mulga woodland and a *Corymbia* savanna. I employed three different approaches to evaluate C and water fluxes: i) eddy covariance data (at plot-scale); ii) a range of *in situ* eco-physiological investigations (at leaf-scale); and iii) glasshouse experimentation (at leaf- and whole-plant- scale).

The research conducted in this doctoral project sought:

**i)** to compare and contrast C and water fluxes of two semi-arid woodland ecosystems and to identify the relative importance of several climatic drivers influencing ecosystem productivity and evapotranspiration (**Chapter II**);

**ii)** to evaluate seasonal water-use-efficiencies (WUE) and resource-use-efficiencies (RUEs) to assess different rates of C gain of co-occurring species within the two woodland ecosystems (**Chapter III**);

**iii)** to acquire a better understanding of different estimations of intrinsic WUE ($WUE_i$) and their relationships with soil water content seasonally and annually, through the application of the normalized proxy of $WUE_i$: the $g_1$ parameter (**Chapter IV**), and lastly;

**iv)** to evaluate eco-physiological traits and adjustments in leaf gas exchange of several dominant plant species of the two semi-arid woodland under repeatedly imposed experimental droughts (**Chapter V**).

Within this final chapter, I will synthetize and highlight the main findings from my research, and identify the limitations of this thesis and prospects for future research.

### 6.1.2 The over-arching influence of rainfall on productivity in semi-arid woodlands

The growing season in semi-arid ecosystems is triggered by the arrival of the wet season which promotes water availability in the soil profile (Eamus *et al.*, 2013). Path analysis showed that during the entire wet season of each year examined (from 2010-2016), soil water content (SWC) was a major determining factor by negatively affecting NEP. However, when sub-periods within wet seasons were examined, that is, the early part of the wet season and mid-to-late wet season, the effects of SWC on NEP fluctuated between positive and negative coefficients in both ecosystems (Fig. 2.10e, i). Several explanations were addressed during the discussion section in Chapter II, which I will now summarise and explain, whilst drawing upon relevant results found within different data chapters of this thesis.

Although the two semi-arid woodlands are dominated by evergreen species, the primary growing season occurs during the wet season (as observed with increased EVI, mainly, but solely, attributed to the understory vegetation; Fig. 2.2d and 2.3d). Thus, ecosystem respiration increased and the effect of SWC on NEP was negative during this period (Fig. 2.10). Another possible explanation for the negative effect of SWC on NEP may be related to the occurrence of a degassing of the soil profile. This was evident throughout the entire wet season, thus, there was a decline in NEP following large rainfall pulses (i.e., Fig. 2.4 and 2.5). Large rainfall events positively stimulate soil effluxes ($CO_2$ released from the soil to the atmosphere; Vargas *et al.,* 2012), and thus NEP was negative. More detailed and hence conclusive studies are needed in order to quantify different effluxes that may be playing an important role in the overall net ecosystem C exchange in semi-arid central Australia.

Additionally, NEP did not diminish immediately after the last rainfall events of late April or May of each year. Rather, NEP remained positive for up to 4 months in the Mulga woodland (e.g. 2011-2012) and 2 months at the *Corymbia* savanna (e.g. 2014–2015). Thus, ecosystem productivity was maintained for a significant fraction of each dry season. Therefore, when water was available it triggered carbon assimilation, but different eco-physiological strategies in co-occurring and dominant plant species allow some species to maintain photosynthetic rates at a low SWC, hence positive NEP within the two ecosystems. These different eco-physiological strategies among co-occurring species will be discussed below in section 6.1.5.

### 6.1.3 Inter-annual variability in productivity

Large differences in C and water budgets were observed between the two ecosystems: the tall, open *Corymbia* savanna and closed Mulga woodland, despite these two ecosystems experiencing similar climatic conditions (Table 6.1). Annual NEP at the Mulga woodland ranged from 217 to -47 gC $m^{-2}$ $y^{-1}$ (from 2010 to 2017), with the second largest positive NEP observed

during the global C sink anomaly (2010-2011; Poulter *et al.*, 2014). This indicates that the Mulga woodland has the capacity to dramatically increase C uptake during wetter-than-average years. This was further demonstrated during the last hydrological year observed at the Mulga woodland (2016-2017) which closed with an NEP of 217 gC $m^{-2}$ $y^{-1}$ following the largest annual rainfall recorded during my monitoring of ecosystem fluxes (713 mm); this exceeded the 565 mm annual rainfall of 2010-2011. In contrast, at the *Corymbia* savanna, annual NEP ranged from 115 to -190 gC $m^{-2}$ $y^{-1}$, with a frequent occurrence of negative NEP values.

Negative NEP at the *Corymbia* savanna site may potentially be attributed to the occurrence of large rates of photo-and thermal-degradation of leaf litter, particularly of spinifex (a dominant grass species) leaves (Austin and Vivanco, 2006; Cleverly *et al.*, 2016c; Rutledge *et al.*, 2009) and other accumulated biomass following the extremely wet- year of 2010-2011. If the *Corymbia* savanna was as productive (hence, it had a large positive NEP) during the anomalous year of 2010-2011 as the neighbouring Mulga woodland, as suggested with remote sensing observations (Ma *et al.*, 2016b), then high biomass produced during 2010-2011 was the fuel for photo-degradation in subsequent years (hence negative NEP budgets were observed). This pattern of negative NEP following the GLSA was similarly observed in Mulga woodland, when mean annual precipitation (MAP) was below the long-term mean (324 mm; www.bom.gov.au) in the following two consecutive years (2011-2012 and 2012-2013).

Table 6.1 Annual rainfall and carbon and water budgets at the a) Mulga woodland and b) *Corymbia* savanna. Each hydrological year is defined from August to July. Annual budgets for net ecosystem production (NEP), rainfall (PPT), evapotranspiration (ET) and the ratio ET:PPT.

| Hydrological year | PPT (mm $y^{-1}$) | ET | ET:PPT | NEP (gC $m^{-2}$ $y^{-1}$) | | PPT (mm $y^{-1}$) | ET | ET:PPT | NEP (gC $m^{-2}$ $y^{-1}$) | |
|---|---|---|---|---|---|---|---|---|---|---|
| | **a) Mulga woodland** | | | | | **b) *Corymbia* savanna** | | | | |
| 2010-2011 | 565 | 512 | 0.91 | 131 | (sink) | | | | | |
| 2011-2012 | 239 | 207 | 0.87 | -47 | (source) | | | | | |
| 2012-2013 | 193 | 153 | 0.79 | -14 | (source) | 103 | 96 | 0.93 | -85 | (source) |
| 2013-2014 | 295 | 249 | 0.84 | 23 | (sink) | 180 | 151 | 0.84 | -191 | (source) |
| 2014-2015 | 301 | 251 | 0.83 | 45 | (sink) | 371 | 323 | 0.87 | -116 | (source) |
| 2015-2016 | 336 | 247 | 0.74 | 22 | (sink) | 366 | 299 | 0.82 | -37 | (source) |
| 2016-2017 | 713 | 530 | 0.74 | 217 | (sink) | 728 | 487 | 0.67 | 115 | (sink) |

Pivot-points are defined by the *y*-intercept between annual total rainfall *versus* annual NEP, and this identifies when a given ecosystem switches from being a C source to a C sink (Chen *et*

*al.*, 2013; Scott *et al.*, 2015). Multiple years of continuous observation of C fluxes at both ecosystems with the EC systems allowed me to estimate, for the first time, precipitation thresholds (i.e., pivot-points) for the two semi-arid woodlands. This occurred when the Mulga woodland received 262 mm $y^{-1}$ and with a larger pivot-point of 506 mm $y^{-1}$ at the *Corymbia* savanna (Fig. 2.6). Pivot-points identified for the *Corymbia* savanna and Mulga woodland were in the same range as other pivot-points identified for semi-arid ecosystems worldwide (Chen *et al.*, 2013; Scott *et al.*, 2015). However, it is possible that the pivot-point identified for the *Corymbia* savanna is highly influenced by the negative NEP following the above-than average year in 2010-2011.

Extreme wetter-than average years seem to occur every 10 years in central Australia (Fig. 1.4; see total annual precipitation record from 1962 to 2011). It is clear that semi-arid Australian ecosystems can be significantly productive and exhibit an increasing C sink during wetter-than-average-years, as observed in 2010-2011 and more recently 2016-2017. Similarly, wet-years occurred in the 1970s, but past record reconstructions of the C cycle remain challenging, even though it is likely that during those wet-years in the 70s the Mulga woodland and *Corymbia* savanna were significantly productive with large and positive NEP. In the same way, it would be valuable to evaluate to what extent this last hydrological year (2016-2017) may have increased the total land C sink in Australia and how this may have affected the global land C sink, compared to what was observed in 2010-2011 when the GLSA occurred (Poulter *et al.*, 2014).

An above-average rainfall year increased ecosystem productivity, biomass and understory vegetation. When above-average rainfall years are followed by periods of low MAP, the risk of fire increases (O'Donnell *et al.*, 2011; Turner *et al.*, 2008). Fires depend on antecedents of climatic conditions, with above-average rainfall being the most important factor to produce sufficient fuel loads (Turner *et al.*, 2011). In central Australia, fires have occurred for millennia of years not only as natural extreme phenomena, but also as a cultural significance for Aboriginal communities to maintain balance within ecosystems (Turner *et al.*, 2008). Silcock *et al.* (2016) has demonstrated that historically fires in Mulga woodlands in eastern Australia arrived with irregular unusual weather events when above-average rainfall year occurred followed by dry periods. Thus, the trend of wet-years with large NEP (2010-2011) followed by dry-years with negative NEP (2011-2012) is likely to have major implications in the long-term C balance for semi-arid ecosystems.

The occurrence, in parallel, of different C processes such as photo-degradation and fire (when they occur), can drive large rates of ecosystem $CO_2$ efflux, ultimately affecting C balances of ecosystems. These processes would mask different sources of $CO_2$ that contribute to the

overall net ecosystem exchange. Further investigation of these effluxes processes are required to quantify the fate of biomass produced during exceptional rainfall years. These lagged effects should be taken into careful consideration when modelling regional and global C cycles.

### 6.1.4 Climatic drivers of C and water fluxes within semi-arid woodlands

While rainfall is clearly a strong driving force for sustaining large rates of C uptake and water fluxes in these semi-arid woodlands, my research also demonstrates that other climatic drivers are also important (Chapter II). I will now discuss the role of other climatic drivers on C and water fluxes in the two semi-arid woodlands.

There was a negative effect of increasing air temperature ($T_{air}$) on NEP at the Mulga woodland (-0.30 standardized coefficient) and the *Corymbia* savanna (-0.36 standardized coefficient), which was observed across the entire wet season (Fig. 2.9). Temperature and vapour pressure deficit (VPD) exert strong influences on photosynthesis through the temperature dependency of carboxylation and electron transport (Farquhar *et al.,* 1980) and through effects on stomatal conductance (Duursma *et al.*, 2014). Here, I observed that VPD and air temperature limited ET and rates of NEP during the wet and dry season and at ecosystem and at a leaf-scales (Fig. 2.8, Fig. 3.3). High temperature generally caused negative effects on NEP during the wet season in both ecosystems (Fig. 2.9a, c). The feed-forward response of stomatal conductance to transpiration due to high VPD, ultimately may have caused a decline in stomatal conductance to avoid an increase in plant water stress (Duursma *et al.*, 2014). Thus, a negative effect of increased $T_{air}$ over NEP was observed across the entire wet season at both ecosystems. This suggests that there may be major implications for NEP as climate progressively warms, with a smaller ecosystem C sink occurring because of a shortening of the growing season. Potential implications of climate change for these ecosystems are discussed further in section 6.1.8.

Increasing air temperatures, as forecast by climate change models, will have consequences for the energy balance of ecosystems. In the present study, ET accounted for >70 % of annual rainfall at the Mulga woodland and up to 106 % at the *Corymbia* savanna (Table 2.2). Runoff from the EC sites was unlikely to be significant, and the excess of rainwater presumably contributed to groundwater recharge. Path analysis results showed a positive relationship between ET and NEP, and patterns in ET were mainly driven by changes in SWC at both ecosystems. Changes in ET influence the total ecosystem energy balance by affecting the Bowen ratio (the ratio of sensible to latent heat) (Richardson *et al.*, 2013). The *Corymbia* savanna tended to have larger rates of ET than Mulga the woodland, due to the open grassland in the former. Owing to the relationship of ET with canopy conductance and solar radiation, these are

also factors affecting ecosystem productivity (Running *et al.*, 2000; Yang *et al.*, 2015). As ET increases during the wet months - generating more clouds, and the arrival of monsoonal clouds from the north – this reduces solar radiation and thus NEP. Large ET also reduces water availability in the upper soil profile, therefore limiting those species that cannot access groundwater to a narrow period for water availability. From an eco-hydrological point of view, there is a need to understand the interaction and linkages among ecosystem productivity, atmosphere and, water availability among semi-arid ecosystems.

### 6.1.5 Differences in eco-physiological strategies between species

Different rates of C and water fluxes from leaf-scale measurements among species revealed insights to explain the divergences in C and water fluxes between the Mulga woodland and *Corymbia* savanna (Fig. 6.1). At a leaf-scale, field observations in a range of *in situ* eco-physiological investigations were conducted during three contrasting periods (late wet season, dry season and mid wet season during the hydrological year of 2015-2016), in addition to a glasshouse experimentation drought in dominant plant species of semi-arid Australia to understand differences in C assimilation.

The *Corymbia* savanna exhibited larger rates of water-use (i.e., large rates of ET, Table 2.2), and this is presumably because of the behaviour of the species present. Thus, *Corymbia opaca* is a tall, deep-rooted tree, *Triodia schinzii* is a C4 grass and, *Hakea macrocarpa* is a shrub that produces cluster roots (Lamont, 2003). These three species usually maintained the largest photosynthetic rates ($A_n$) and stomatal conductance ($g_s$) in favourable wet conditions (Fig. 3.5). However, all-year round access to groundwater by *C. opaca* (O'Grady *et al.*, 2009) and the presumed development of cluster-roots in *H. macrocarpa*, which increase the soil volume explored by a factor of up to 300 (Lamont, 2003) are likely to explain the large rates of gas exchange observed across seasons in these species under field conditions. Because of larger rates of ET, the *Corymbia* savanna maintained a smaller $WUE_i$ (Fig. 6.1b), than the Mulga (Fig. 6.1a).

Although *E. camaldulensis* is not found within the footprint of the EC sites, *Eucalypts* is one of the most iconic and widespread genus in Australia. *Eucalyptus camaldulensis* (river red gum) forest occurs along ephemeral rivers in alluvial zones within the Ti-Tree basin, where the Mulga woodland and *Corymbia* savanna are located (Fig. 1.8). During a drought experiment, *Corymbia opaca* and *Eucalyptus camaldulensis* (both deep-rooted trees from the family *Myrtaceae*) maintained the largest values in $A_n$ and $g_s$ in the well-watered treatment, but significantly reduced values of $A_n$ and $g_s$, as plant water stress increased. Closure of stomata was apparent in

both species early in the drought and this served to tightly regulate foliar water potential and minimise declines in foliar water potential. The regulation of water potentials to reduce plant water stress by declining $g_s$ defined an isohydric behaviour in *C. opaca* and *E. camaldulensis.* Early stomatal closure in *E. camaldulensis* and *C. opaca* to avoid the loss of whole-tree hydraulic conductivity may push these species to the potential for C starvation during periods of water deficit (Adams *et al.*, 2017; McDowell *et al.*, 2008).

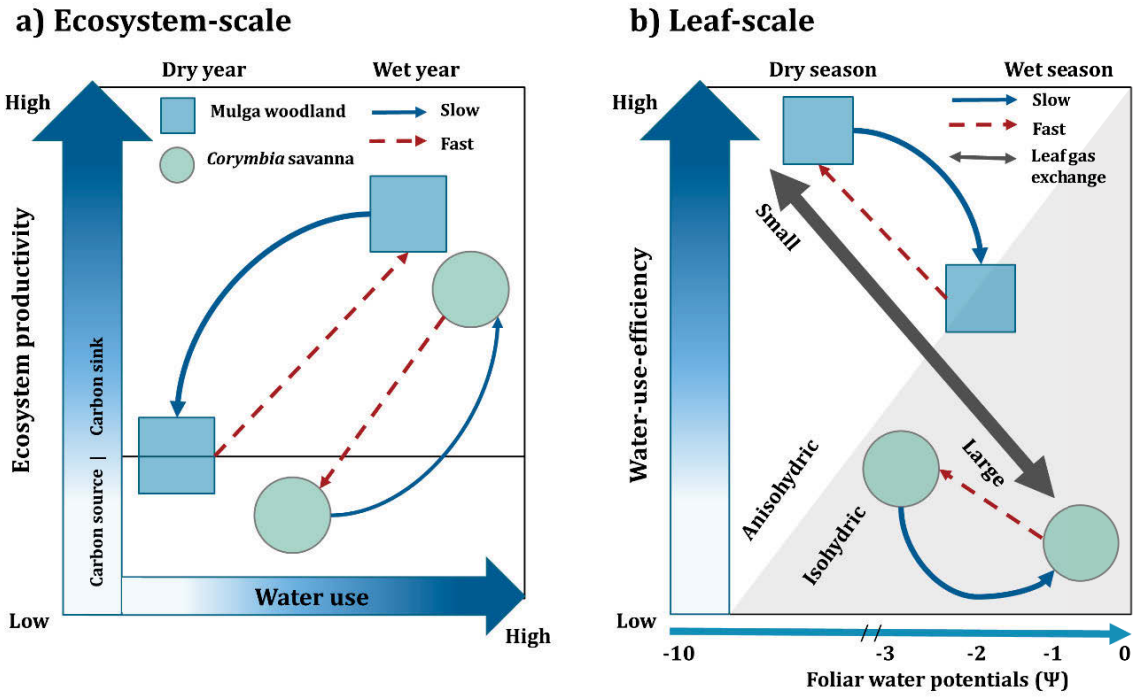


Figure 6.1 Water and carbon relations at a) ecosystem-scale and b) leaf-scale for the Mulga woodland and *Corymbia* savanna. The leaf-scale diagram represents species for the Mulga woodland such as *Acacia aptaneura* and *A. aneura*; whereas *Corymbia* savanna represents species such as *Corymbia* opaca and *Hakea macrocarpa*, although *Eucalyptus camaldulensis* can be included. Spinifex grass should be excluded of the leaf-scale diagram because represents an outlier due to its C4 photosynthetic pathway. Single arrows indicate transition periods, whilst double arrow (in panel b) indicates leaf gas exchange (carbon assimilation and stomatal conductance).

Dominant species at the Mulga woodland are: *Acacia aneura* and *Acacia aptaneura* (shallow rooted, $N_2$-fixing trees, both from the Mulga complex of species) (Maslin and Reid, 2012; O'Grady *et al.*, 2009). Mulga species are well adapted to long periods of low values in SWC and rely on shallow SWC supply above the hardpan (<1.2. m; Cleverly *et al.*, 2016b). Consequently, foliar water potential in the Mulga spp. was significantly lower during the dry season than the

wet season and significantly lower than values observed in *E. camaldulensis* and *C. opaca* (Table 3.2). But, how does the Mulga woodland maintain positive NEP into the dry season? Several studies have identified that *Acacia* spp. have an anisohydric behaviour, allowing these species to maintain C assimilation rates at more negative soil and foliar water potentials, as experienced in the dry season (Klein, 2014; Nolan *et al.*, 2017a). This anisohydric behaviour was observed in this study when I regressed $g_s$ *versus* foliar water potential and $A_n$ *versus* foliar-water potential (Figs. 3.5, 3.6) and during the glasshouse experiment (Fig. 5.5).

Slow declines by *Acacia aptaneura* in gas exchange as an imposed drought progressed (Chapter VI), was similarly observed at an ecosystem-scale when transitioning from a wet season to a dry season (Fig. 6.1a). This was evidenced when applying the $g_1$ parameter (a proxy of intrinsic water-use-efficiency; Medlyn *et al.*, 2011) to continuous monitoring of ecosystem-scale gas exchange at the Mulga woodland. In Fig. 4.4, which shows the years where the leaf gas exchange observations were conducted, in *A. aptaneura* and *A. aneura*, $g_1$ values slowly declined from the end of the wet season until the end of August (meaning a slow increase in $WUE_i$). This indicated that Mulga species gradually reduced stomatal conductance while maintaining productivity as the dry seasons progressed. At the end of the dry season (Oct-2015) large $WUE_i$ was observed at ecosystem-and leaf-scale in the Mulga.

Semi-arid Australia is not only characterized by low mean annual rainfall with high inter-annual variability, but also with high light intensity, nutrient-poor soils and low vegetation cover. These conditions limit several physiological functions of semi-arid vegetation to a short period year-to-year and increases competition among co-occurring species. Partitioning of limited resources by niche separation across species allows species to co-occur within the same ecosystem (Silvertown *et al.*, 2015). Results in this thesis (Chapter III) suggested that despite differences in plant physiological traits and different eco-hydrological niches among species, all species tended to converge to similar light-use-efficiency (LUE) and carbon-use-efficiency (CUE) with relatively few, and only small, differences among species in LUE and CUE, but notable differences in WUE (Tables 3.5, 3.6).

Mulga showed lower photosynthetic-$N_2$-use-efficiency (PNUE) than *C. opaca* (Table 3.5). This is because Mulga are not limited by foliar $N_2$ content, whereas PNUE was large in *C. opaca* because of its low leaf N content and large photosynthetic rates, even during dry season field conditions. *C. opaca* also showed a large CUE. When CUE is large, this indicates that more C is allocated to growth *per* unit C acquired than is lost as respiration (Bradford and Crowther, 2013). *C. opaca* has a large investment in biomass accumulation to grow a tall structure and develop a deep taproot to access groundwater. In consequence of the large CUE of *C. opaca* was

associated with the smallest dark respiration of all the species examined in the present study (Tables 3.3, 3.5). Access to groundwater, large PNUE and CUE is likely to explain how *C. opaca,* despite its high water-use demand, survive in the semi-arid regions of Australia.

To summarize, observations at a leaf-scale were consistent with observations at an ecosystem-scale when comparing eco-physiological strategies among common species that co-occur within the Mulga woodland and *Corymbia* savanna (Fig. 6.1). These eco-physiological mechanisms provided new insights for the characterization and understanding of key plant species, which play an important role in ecosystem functioning of these two semi-arid woodlands. Ecosystem productivity was less limited in the Mulga woodland following the GLSA than in the *Corymbia* savanna. Anisohydric behaviour and large $WUE_i$ can explain the dominance of Mulga species in semi-arid Australia, where water is limited and to some extent, this also explain the large mean ecosystem WUE observed in Australia when compared with North American ecosystems during the drier and warmer conditions in the early 21$^{st}$ century (Ponce-Campos *et al.*, 2013).

### 6.1.6 The large WUE at the Mulga woodland

The $g_1$ parameter is a useful proxy of $WUE_i$ ($g_1$ is inversely related to $WUE_i$), but normalized for VPD and atmospheric $CO_2$, which simplifies comparisons among different ecosystems, plant functional types and studies from ecosystem-scale to leaf-scale (Lin *et al.*, 2015; Medlyn *et al.*, 2017). The application of the $g_1$ parameter based on optimization theory of stomatal behaviour (Cowan and Farquhar, 1977; Medlyn *et al.*, 2011) clearly illustrates that the Mulga woodland has the capacity to support large rates of water consumption in wet periods and the plasticity to become highly water-use-efficient during dry periods (low $g_1$ values; Chapter IV).

In this study, I demonstrated the fast response from the Mulga woodland to increasing soil water, thus increasing productivity when water was available, and exhibiting a significant decrease in $WUE_i$ at the ecosystem-scale ($eWUE_i$, low $g_1$ values; Fig. 4.5). Moreover, $g_1$ showed a tight relationship with soil water availability by increasing in a concave function as volumetric water content (VWC) increased (Fig. 4.6). Low $eWUE_i$ due to the high productivity and large water consumption during favourably wet periods contribute to explaining the large NEP observed during wetter-than-average years such as 2010-2011 and most recently 2016-2017. The application of the $g_1$ model in the Mulga woodland for the first time can contribute also to explaining the observed behavior during the drought period early in the 21$^{st}$ century with large WUE in semi-arid Australia (Ponce-Campos *et al.*, 2013).

One of the most novel aspects of this thesis, contained in Chapter IV, was to combine three different data sets for the estimation of the $g_1$ parameter within the same ecosystem, by applying different approaches for estimating C and water fluxes (i.e., eddy covariance, leaf gas exchange, and carbon stable isotopes). All three methods converged to similar values during the wet season (Feb-2016; Fig. 4.7). This agreement among the three methods during favourably wet conditions may be associated with the large ratio of intercellular to ambient $CO_2$ concentrations ($C_i/C_a$) in which both leaf gas exchange and stable isotopes theories are founded. Another possible explanation for the convergence between leaf-scale $g_1$ values and ecosystem-scale $g_1$ values ($g_{1\text{-EC-fluxes}}$) can be attributed to a decrease in the coupling of the canopy with the atmosphere that is likely to occur during the wet season. This reduces the aerodynamic resistance, which influences the canopy conductance derivation within the Penman-Monteith (PM) inverted equation (eq. 4.3).

Discrepancies were observed between $g_1$ values derived from leaf gas exchange and eddy covariance ($g_{1\text{-leaf-gas}}$ and $g_{1\text{-EC-fluxes}}$, respectively) with $g_1$ values derived from carbon isotope signatures (total sugars ($g_{1\text{-sugars}}$) and bulk-leaf ($g_{1\text{-bulk-leaf}}$)) in all periods, except for the wet season (Feb-2016; Fig. 4.7.). At a leaf-scale, differences between methods may be associated with limitations behind the isotopic theory, for example the partial inclusion of mesophyll conductance in the isotopic discrimination model (Seibt *et al.*, 2008). Another assumption when applying the isotopic model relates to the value of vapour pressure deficit at the leaf surface (D) used in eq. 4.5 obtained from leaf gas exchange measurements. This value may not be representative of the mean of the entire time-period during which the C assimilation occurred (i.e., long term D for bulk-leaf isotopic compositions). In a continental study of $^{13}C$-discrimination and leaf traits, Rumman *et al.* (2017) found that during dry seasons the $C_i/C_a$ ratio derived from bulk-leaf isotopic compositions did not correlate with net carbon assimilation but did correlate with $g_s$. Thus, there is a need to evaluate limitations in the isotopic $g_1$ derived values to conclusively elucidate the cause(s) of divergence among methods, especially during dry seasons. It is likely that application of current carbon discrimination theory is more reliable during wet periods.

### 6.1.7 Management implications

Arid and semiarid zones receive less than 500 mm of rainfall per year and are represented in ~45 % of terrestrial ecosystems. Approximately 40 % of the global population live in arid and semi-arid regions (Chapin *et al.,* 2002), where groundwater is the major source of water for human consumption and irrigation. Although central Australia has a low population density, many Aboriginal communities and economic activities such as mining and farming rely on

groundwater. Thus, in semi-arid Australia groundwater is often extracted for agriculture, stock watering, mining and settlements. Harrington *et al.* (2002) has demonstrated that at the Ti-Tree basin, groundwater recharge occurs only after intense rainfall of at least 150 to 200 mm/month. This has important implications for water management in the region for, social, economic and environmental roles, if water extraction surpasses the safe yield of the aquifer. For example, the two iconic Australian tall trees within the Ti-Tree basin *E. camaldulensis* and *C. opaca,* which exhibit large rates of water-use and dependency on groundwater (O'Grady *et al.*, 2009) may be threatened if access to groundwater is significantly reduced.

An improved understanding of current and future possible eco-physiological behaviours is a central component to progress in the development of programs for ecosystem adaptation and mitigation in face of a changing environment, especially global hydrological change. A better understanding of ecosystem productivity at a regional-scale will also improve ecosystems assessments of fire risk when evaluating fuel load based on available and detailed data within specific ecosystems. Findings in this research will help to improve the accuracy of coupled climate models (by including more representative values when parameterizing models) to provide advances in our knowledge that is central for decision makers in the management and understanding of landscape function.

### 6.1.8 Potential implications of climate change

With the high inter-annual variability in rainfall observed in semi-arid Australia (Van Etten, 2009), it is expected that both ecosystems will continue switching between C sinks and C sources in future years. Although pivot-points have now been identified for both ecosystems, questions remain regarding ecosystem functioning due to i) an increase in atmospheric $CO_2$ that can induce a $CO_2$ fertilization effect of photosynthesis, thereby increasing NEP (Cernusak *et al.*, 2013b; Xu *et al.*, 2014); or ii) changes in regional climate, especially in precipitation regimes and increasing temperatures (Cubasch *et al.*, 2013). For example, current scenarios of climate are predicting drier -dry periods and wetter-wet periods (IPCC, 2014). High temperatures increase the atmospheric demand for water, affecting photosynthetic rates by inducing stomata closure which supresses cooling at the leaf's surface, leading to hotter and drier conditions (Frank *et al.*, 2015). In contrast, wetter-wet periods can be highly productive, as already observed in the two woodland ecosystems (i.e., 2010-2011, 2016-2017). Long-term legacy effects remain uncertain due to the different C processes occurring across different spatial-temporal-scales (i.e., decomposition, photo-degradation), that cannot be easily quantified with eddy covariance measurements alone. Therefore, long-term C monitoring in different C pools and a better understanding of driving factors (i.e., climate variables, eco-physiological

responses) of all the different component C processes (i.e., photosynthesis, respiration and photo and thermal degradation) are vital components to improve our understanding in the C cycle at regional and global-scales.

Current projections of climate predict that droughts will increase in frequency, intensity and duration, especially in semi-arid regions (IPCC, 2012). Drought is a climate extreme that most affects the C cycle (Frank *et al.*, 2015). However, there is a gap in knowledge regarding plant functional strategies (i.e., hydraulic traits) and their relation with drought. In addition, limited knowledge exists about rates of leaf gas exchange in response to drought across different plant species (Bartlett *et al.*, 2014).

During the experimental drought study (Chapter VI), a wider tolerance to low SWC values was observed in *A. apataneura* that experienced three droughts than in plants that experienced one drought. Drought resistance is related to complex physiological traits (i.e., high resistance to vessel implosion to avoid xylem embolism, high wood density; Santini *et al.,* 2015; Eamus *et al.,* 2016). It is possible that an accumulation of osmotically active solutes during the prior droughts allowed *A. aptaneura* to modify the turgor loss point, the point at which leaf cells lose turgor and close stomata, and thus maintain stomatal conductance at lower values of leaf water potential (Nolan *et al.*, 2017c). It would be valuable to advance our understanding of underlying processes (i.e., the increase of solute concentration within the guard cells and the signalling of hormones, such as abscisic acid) that allow species to further increase their plasticity and tolerance to drought. All these physiological factors possessed by Mulga species (drought resistance, plasticity, large WUE, anisohydric behavior) are great factors to survive the extreme conditions of semi-arid Australia. Nevertheless, maintenance of photosynthetic rates at low $g_s$ and extreme negative foliar-water potentials, increases to some extent the risk of hydraulic failure and embolism and possible die-back (Meinzer *et al.*, 2009) while WUE is increased. Declines in water availability during drought events compromise plant survival, particularly through hydraulic failure, which is a major factor resulting in plant mortality following drought (Adams *et al.*, 2017; Allen *et al.*, 2010; McDowell *et al.*, 2008).

### 6.1.9 Implications for vegetation modelling

Terrestrial vegetation C models that can calculate GPP at regional and mesoscales are based on photosynthetic capacity parameters such as the maximum rate of carboxylation ($V_{cmax}$; Farquhar *et al.,* 1980). Fixed parameters of values for $V_{cmax}$ in terrestrial models can produce unrealistic GPP values (Piao *et al.*, 2013; Xia *et al.*, 2015). Therefore, $V_{cmax}$ values obtained for dominant co-occurring species (Table 5.2) are valuable information that can contribute to an

improved ability to produce better estimates of global photosynthesis and to possible benchmark model performance on simulating regional GPP (Xia *et al.*, 2015).

Previous studies in Australia have shown that light-use-efficiency varies across seasons (Shi *et al.*, 2014) and among different vegetation types (Ma *et al.*, 2014). However, these studies rely on remote sensing observations, which ultimately derive GPP, and hence LUE, based on a plant functional type classification approach for algorithm parameterization. It is likely that ecosystem-scale observations via remote sensing vary significantly from species-specific observations. Thus, my results derived from light response curves for individual species (Chapter III), including quantum yield, may contribute to parameterization of remote sensing algorithms that can reduce uncertainties in estimations of GPP at ecosystem-scales (Running *et al.*, 2004).

In Chapter IV, I provided an understanding of the significant relationship between soil water availability and stomatal optimization behaviour, and to my knowledge this has not been previously tested with the $g_1$ parameter at an ecosystem-scale. First, it was observed that normalized $g_1$ values gradually decreased in the wettest-than-average years (i.e., 2010-2011 and 2016-2017) but $g_1$ values abruptly declined at a very low VWC values during drier-than-average years (i.e., 2011-2012; 2014-2015; Fig. 4.6). This outcome is a critical process within water and C cycles and my results highlight the importance of including such stomatal response to different levels of soil water availability when modelling ecosystem function. Second, my results evaluated, for the first time, the three different methods for estimated $g_1$ values (from ecosystem- to leaf-scale) within the same ecosystem, emphasised the bias that can occur when applying different methods in earth system models (Miner *et al.*, 2017). Consequently, there is now an opportunity to evaluate the inclusion of *in situ* observations and account for variations on stomatal functioning to improve our understanding of the optimal stomatal theory in a changing environment.

## 6.2 *Concluding remarks*

Different climatic drivers vary in the degree to which they exert limitation on NEP in both ecosystems. Temperature and its effect on VPD, and SWC were strong drivers of NEP at the Mulga woodland and *Corymbia* savanna. High temperatures can affect plant water status (through foliar water potentials) via both drier SWC and by increasing atmospheric water demand (high VPD) which induces stomatal closure and associated declines in C assimilation at a leaf-scale. Identifying to what extent SWC controls C and water fluxes within the two ecosystems is an important insight into ecosystem C and water interactions, which ultimately determines the intra-annual variability of ecosystem and leaf C exchange. However, variation in C and water fluxes cannot be explained with climatological approaches alone (Reichstein *et al.*, 2014) and plant eco-physiological studies provide broad insights for mechanisms that explain C and water variability within ecosystems.

My research at a leaf-scale highlights the importance of species-specific attributes in driving C fluxes in semi-arid Australia. Integrating plant eco-physiological responses of dominant species is an essential component for improving our understanding of C variability within a Mulga woodland and *Corymbia* savanna. By assessing contrasting eco-physiological behaviours in dominant plant species of central Australia under field condition and in an experimental drought study, I was able to contribute to an improved understanding of ecosystem-scale C and water fluxes, which in turn assists to gain information for the understanding of global C variability.

Finally, my research presented a significant and important detailed study on ecosystem and leaf water-use-efficiency, which is crucial for the understanding of ecosystem functioning for successful management of land and water resources in semi-arid Australia. Moreover, understanding functional attributes in the face of climate change and changes in land use will contribute to refining water management for the central Australian region.

# *References*


Abramowitz, G., Gupta, H., Pitman, A., Wang, Y., Leuning, R., Cleugh, H.A. (2006). Neural Error Regression Diagnosis (NERD): A tool for model bias identification and prognostic data assimilation. *Journal of Hydrometeorology* 7, 160-177.

Adair, C.E., Reich, P.B., Trost, J.J., Hobbie, S.E. (2011). Elevated $CO_2$ stimulates grassland soil respiration by increasing carbon inputs rather than by enhancing soil moisture. *Global Change Biology* 17, 3546-3563.

Adams, H.D., Guardiola-Claramonte, M., Barron-Gafford, G.A., Villegas, J.C., Breshears, D.D., Zou, C.B., Troch, P.A., Huxman, T.E. (2009). Temperature sensitivity of drought-induced tree mortality portends increased regional die-off under global-change-type drought. *Proceedings of the National Academy of Sciences of the United States of America (PNAS)* 106, 7063-7066.

Adams, H.D., Zeppel, M.J.B., Anderegg, W.R.L., Hartmann, H., Landhausser, S.M., Tissue, D.T., Huxman, T.E., Hudson, P.J., Franz, T.E., Allen, C.D., Anderegg, L.D.L., Barron-Gafford, G.A., Beerling, D.J., Breshears, D.D., Brodribb, T.J., Bugmann, H., Cobb, R.C., Collins, A.D., Dickman, L.T., Duan, H., Ewers, B.E., Galiano, L., Galvez, D.A., Garcia-Forner, N., Gaylord, M.L., Germino, M.J., Gessler, A., Hacke, U.G., Hakamada, R., Hector, A., Jenkins, M.W., Kane, J.M., Kolb, T.E., Law, D.J., Lewis, J.D., Limousin, J.M., Love, D.M., Macalady, A.K., Martinez-Vilalta, J., Mencuccini, M., Mitchell, P.J., Muss, J.D., O'Brien, M.J., O'Grady, A.P., Pangle, R.E., Pinkard, E.A., Piper, F.I., Plaut, J.A., Pockman, W.T., Quirk, J., Reinhardt, K., Ripullone, F., Ryan, M.G., Sala, A., Sevanto, S., Sperry, J.S., Vargas, R., Vennetier, M., Way, D.A., Xu, C., Yepez, E.A., McDowell, N.G. (2017). A multi-species synthesis of physiological mechanisms in drought-induced tree mortality. *Nature Ecology & Evolution* 1, 1285-1291.

Ahlström, A., Raupach, M.R., Schurgers, G., Smith, B., Arneth, A., Jung, M., Canadell, J.G., Friedlingstein, P., Jain, A.K., Kato, E., Poulter, B., Sitch, S., Stocker, B.D., Viovy, N., Wang, Y.P., Wiltshire, A., Zaehle, S., Zeng, N. (2015). The dominant role of semi-arid ecosystems in the trend and variability of the land $CO_2$ sink. *Science* 348, 895-899.

Allen, C.D., Macalady, A.K., Chenchouni, H., Bachelet, D., McDowell, N., Vennetier, M., Kitzberger, T., Rigling, A., Breshears, D.D., Hogg, E.H., Gonzalez, P., Fensham, R., Zhang, Z., Castro, J., Demidova, N., Lim, J.-H., Allard, G., Running, S.W., Semerci, A., Cobb, N. (2010). A global overview of drought and heat-induced tree mortality reveals emerging climate change risks for forests. *Forest Ecology and Management* 259, 660-684.

Allen, R.G., Pereira, L.S., Raes, D., Smith, M. (1998). Crop evapotranspiration: Guidelines for computing crop water requirements. *FAO Irrigation and Drainage Paper* 56.

Alvarez-Yepiz, J.C., Burquez, A., Martinez-Yrizar, A., Teece, M., Yepez, E.A., Dovciak, M. (2017). Resource partitioning by evergreen and deciduous species in a tropical dry forest. *Oecologia* 183, 607-618.

Atkin, O. (2003). Thermal acclimation and the dynamic response of plant respiration to temperature. *Trends in Plant Science* 8, 343-351.

Augustin, L., Barbante, C., Barnes, P.R.F., Barnola, J.M., Bigler, M., Castellano, E., Cattani, O., Chappellaz, J., Dahl-Jensen, D., Delmonte, B., Dreyfus, G., Durand, G., Falourd, S., Fischer, H., Flückiger, J., Hansson, M.E., Huybrechts, P., Jugie, G., Johnsen, J.S., Jouzel, J., Kaufmann, P., Kiptstuhl, J., Lamgert, F., Lipenkov, V.Y., Littot, G.C., Longinelli, A., Lorrain, R., Maggie, V., Masson-Delmonte, V., Miller, H., Mulvaney, R., Oerlemans, J., Oerter, H., Orombelli, G., Parrenin, F., Peel, D.A., Petit, J.-R., Raynaud, D., Ritz, C., Ruth, U., Schwander, J., Siegenthaler, U., Spuchez, R., Stauffer, B., Steffensen, J.P., Stenni, B., Stocker, T.F., Tabacco, I.E., Udisti, R., van de Wal, R.S.W., van den Broeke, M., Weiss, J., Wilhelms, F., J.-G., W., Wolff, E.W., Zucchelli, M. (2004). Eight glacial cycles from an Antarctic ice core. *Nature* 429, 623-628.

Austin, A.T., Vivanco, L. (2006). Plant litter decomposition in a semi-arid ecosystem controlled by photodegradation. *Nature* 442, 555-558.

Austin, A.T., Yahdjian, L., Stark, J.M., Belnap, J., Porporato, A., Norton, U., Ravetta, D.A., Schaeffer, S.M. (2004). Water pulses and biogeochemical cycles in arid and semiarid ecosystems. *Oecologia* 141, 221-235.

Baldocchi, D. (2003). Assessing the eddy covariance technique for evaluating carbon dioxide exchange rates of ecosystems: past, present and future. *Global Change Biology* 9, 479-492.

Baldocchi, D. (2014). Measuring fluxes of trace gases and energy between ecosystems and the atmosphere - the state and future of the eddy covariance method. *Global Change Biology* 20, 3600-3609.

Baldocchi, D., Falge, E., Gu, L., Olrson R., Hollinger, D.Y., Running, S., Anthoni, P., Bernhofer, C., Davis, K.J., Evans, R., Fuentes, J., A.H., G., Katul, G., Law, B.E., Lee, X., Malhi, Y., Meyer, T., Munger, W., Oechel, W.C., Paw U, K.T., Pilegaard, K., Schmid, H.P., Valentini, R., Verma, S., Vesala, T., Wilson, K., Wofsy, S. (2001). FLUXNET: A new tool to study the temporal and spatial variability of ecosystem–scale carbon dioxide, water vapor, and energy flux densities. *Bulletin of the American Meteorological Society* 82, 2415-2434.

Ball, J.T., Berry, J.A., (1987). A model predicting stomatal conductance and its contribution to the control of photosynthesis under different environmental conditions, in: Publishers, M.-N. (Ed.), In: Progress in Photosynthesis Research (ed. Biggins J), Dordrecht, the Netherlands, pp. 221-224.

Bartlett, M.K., Zhang, Y., Kreidler, N., Sun, S., Ardy, R., Cao, K., Sack, L. (2014). Global analysis of plasticity in turgor loss point, a key drought tolerance trait. *Ecology Letters* 17, 1580-1590.

Beer, C., Ciais, P., Reichstein, M., Baldocchi, D., Law, B.E., Papale, D., Soussana, J.F., Ammann, C., Buchmann, N., Frank, D., Gianelle, D., Janssens, I.A., Knohl, A., Köstner, B., Moors, E., Roupsard, O., Verbeeck, H., Vesala, T., Williams, C.A., Wohlfahrt, G. (2009). Temporal and among-site variability of inherent water use efficiency at the ecosystem level. *Global Biogeochemical Cycles* 23, n/a-n/a.

Berry, G., Reeder, M.J., Jakob, C. (2011). Physical mechanisms regulating summertime rainfall over northwestern Australia. *Journal of Climate* 24, 3705-3717.

Berry, J.A., Beerling, D.J., Franks, P.J. (2010). Stomata: key players in the earth system, past and present. *Current Opinion in Plant Biology* 13, 233-240.

Biederman, J.A., Scott, R.L., Bell, T.W., Bowling, D.R., Dore, S., Garatuza-Payan, J., Kolb, T.E., Krishnan, P., Krofcheck, D.J., Litvak, M.E., Maurer, G.E., Meyers, T.P., Oechel, W.C., Papuga, S.A., Ponce-Campos, G.E., Rodriguez, J.C., Smith, W.K., Vargas, R., Watts, C.J., Yepez, E.A., Goulden, M.L. (2017). $CO_2$ exchange and evapotranspiration across dryland ecosystems of southwestern North America. *Global Change Biology* 23, 4204–4221.

Biederman, J.A., Scott, R.L., Goulden, M.L., Vargas, R., Litvak, M.E., Kolb, T.E., Yepez, E.A., Oechel, W.C., Blanken, P.D., Bell, T.W., Garatuza-Payan, J., Maurer, G.E., Dore, S., Burns, S.P. (2016). Terrestrial carbon balance in a drier world: the effects of water availability in southwestern North America. *Global Change Biology* 22, 1867-1879.

Bloom, A.J., Chapin, F.S., Mooney, H.A. (1985). Resource limitation in plants- An economic analogy. *Annual Review of Ecology and Systematics* 16, 363-392.

Bowling, D.R., Bethers-Marchetti, S., Lunch, C.K., Grote, E.E., Belnap, J. (2010). Carbon, water, and energy fluxes in a semiarid cold desert grassland during and following multiyear drought. *Journal of Geophysical Research* 115.

Bowling, D.R., Pataki, D.E., Randerson, J.T. (2008). Carbon isotopes in terrestrial ecosystem pools and $CO_2$ fluxes. *New Phytologist* 178, 24-40.

Bowman, D., Boggs, G., Prior, L., Krull, E. (2007). Dynamics of *Acacia aneura*-*Triodia* boundaries using carbon ($^{14}C$ and $\delta^{13}C$) and nitrogen ($\delta^{15}N$) signatures in soil organic matter in central Australia. *Holocene* 17, 311-318.

Bowman, D.M.J.S., Boggs, G.S., Prior, L.D. (2008). Fire maintains an *Acacia aneura* shrubland—*Triodia* grassland mosaic in central Australia. *Journal of Arid Environments* 72, 34-47.

Bradford, M.A., Crowther, T.W. (2013). Carbon use efficiency and storage in terrestrial ecosystems. *New Phytologist* 199, 7-9.

Brandes, E., Kodama, N., Whittaker, K., Weston, C., Rennenberg, H., Keitel, C., Adams, M.A., Gessler, A. (2006). Short-term variation in the isotopic composition of organic matter allocated from the leaves to the stem of *Pinus sylvestris*: effects of photosynthetic and postphotosynthetic carbon isotope fractionation. *Global Change Biology* 12, 1922-1939.

Breshears, D.D., Adams, H.D., Eamus, D., McDowell, N.G., Law, D.J., Will, R.E., Williams, A.P., Zou, C.B. (2013). The critical amplifying role of increasing atmospheric moisture demand on tree mortality and associated regional die-off. *Frontiers in Plant Science* 4, 266.

Brienen, R.J.W., Gloor, E., Clerici, S., Newton, R., Arppe, L., Boom, A., Bottrell, S., Callaghan, M., Heaton, T., Helama, S., Helle, G., Leng, M.J., Mielikainen, K., Oinonen, M., Timonen, M.

(2017). Tree height strongly affects estimates of water-use efficiency responses to climate and $CO_2$ using isotopes. *Nature Communications* 8, 288.

Brodribb, T.J., Feild, T.S., Jordan, G.J. (2007). Leaf maximum photosynthetic rate and venation are linked by hydraulics. *Plant Physiology* 144, 1890-1898.

Brodribb, T.J., Jordan, G.J. (2011). Water supply and demand remain balanced during leaf acclimation of *Nothofagus cunninghamii* trees. *New Phytologist* 192, 437-448.

Brugnoli, E., Farquhar, G.D., (2000). Photosynthetic fractionation of carbon isotopes. In: Leegood RC, Sharkey TD, von Caemmerer S, eds., Photosynthesis: physiology and metabolism. Kluwer, Dordrecht, the Netherlands, pp. 399-434.

Brugnoli, E., Hubick, K.T., von Caemmerer, S., Wong, S.C., Farquhar, G.D. (1988). Correlation between the carbon isotope discrimination in leaf starch and sugars of C3 plants and the ratio of intercellular and atmospheric partial pressures of carbon dioxide. *Plant Physiology* 88, 1418-1424.

Caemmerer, S., Farquhar, G.D. (1981). Some relationships between the biochemistry of photosynthesis and the gas exchange of leaves. *Planta* 153, 376-387.

Cai, W., Zheng, X.-T., Weller, E., Collins, M., Cowan, T., Lengaigne, M., Yu, W., Yamagata, T. (2013). Projected response of the Indian Ocean Dipole to greenhouse warming. *Nature Geoscience* 6, 999-1007.

Cano, F.J., Lopez, R., Warren, C.R. (2014). Implications of the mesophyll conductance to $CO_2$ for photosynthesis and water-use efficiency during long-term water stress and recovery in two contrasting *Eucalyptus* species. *Plant, Cell and Environment* 37, 2470-2490.

Cernusak, L.A., Farquhar, G.D., Pate, J.S. (2005). Environmental and physiological controls over oxygen and carbon isotope composition of Tasmanian blue gum, *Eucalyptus globulus*. *Tree Physiology* 25, 129-146.

Cernusak, L.A., Hutley, L.B., Beringer, J., Holtum, J.A.M., Turner, B.L. (2011). Photosynthetic physiology of eucalypts along a sub-continental rainfall gradient in northern Australia. *Agricultural and Forest Meteorology* 151, 1462-1470.

Cernusak, L.A., Ubierna, N., Winter, K., Holtum, J.A., Marshall, J.D., Farquhar, G.D. (2013a). Environmental and physiological determinants of carbon isotope discrimination in terrestrial plants. *New Phytologist* 200, 950-965.

Cernusak, L.A., Winter, K., Dalling, J.W., Holtum, J.A.M., Jaramillo, C., Körner, C., Leakey, A.D.B., Norby, R.J., Poulter, B., Turner, B.L., Wright, S.J. (2013b). Tropical forest responses to increasing atmospheric $CO_2$: current knowledge and opportunities for future research. *Functional Plant Biology* 40, 531-551.

Chapin, F.S. (2002). Principles in terrestrial ecosystem ecology / F. Stuart Chapin III, Pamela A. Matson, Harold A. Mooney. Springer-Verlag New York, Inc., United States of America.

Chapin, F.S., Woodwell, G.M., Randerson, J.T., Rastetter, E.B., Lovett, G.M., Baldocchi, D.D., Clark, D.A., Harmon, M.E., Schimel, D.S., Valentini, R., Wirth, C., Aber, J.D., Cole, J.J., Goulden, M.L., Harden, J.W., Heimann, M., Howarth, R.W., Matson, P.A., McGuire, A.D., Melillo, J.M., Mooney, H.A., Neff, J.C., Houghton, R.A., Pace, M.L., Ryan, M.G., Running, S.W., Sala, O.E., Schlesinger, W.H., Schulze, E.D. (2006). Reconciling carbon-cycle concepts, terminology, and methods. *Ecosystems* 9, 1041-1050.

Chen, B., Ge, Q., Fu, D., Yu, G., Sun, X., Wang, S., Wang, H. (2010). A data-model fusion approach for upscaling gross ecosystem productivity to the landscape scale based on remote sensing and flux footprint modelling. *Biogeosciences* 7, 2943-2958.

Chen, C., Cleverly, J., Zhang, L., Yu, Q., Eamus, D. (2016). Modelling seasonal and inter-annual variations in carbon and water fluxes in an arid-zone *Acacia* savanna woodland, 1981–2012. *Ecosystems* 19, 625-644.

Chen, Z., Yu, G., Ge, J., Sun, X., Hirano, T., Saigusa, N., Wang, Q., Zhu, X., Zhang, Y., Zhang, J., Yan, J., Wang, H., Zhao, L., Wang, Y., Shi, P., Zhao, F. (2013). Temperature and precipitation control of the spatial variation of terrestrial ecosystem carbon exchange in the Asian region. *Agricultural and Forest Meteorology* 182-183, 266-276.

Chen, Z., Yu, G., Zhu, X., Wang, Q., Niu, S., Hu, Z. (2015). Covariation between gross primary production and ecosystem respiration across space and the underlying mechanisms: A global synthesis. *Agricultural and Forest Meteorology* 203, 180-190.

Choat, B., Jansen, S., Brodribb, T.J., Cochard, H., Delzon, S., Bhaskar, R., Bucci, S.J., Feild, T.S., Gleason, S.M., Hacke, U.G., Jacobsen, A.L., Lens, F., Maherali, H., Martinez-Vilalta, J., Mayr, S., Mencuccini, M., Mitchell, P.J., Nardini, A., Pittermann, J., Pratt, R.B., Sperry, J.S., Westoby, M., Wright, I.J., Zanne, A.E. (2012). Global convergence in the vulnerability of forests to drought. *Nature* 491, 752-755.

Chu, C., Bartlett, M., Wang, Y., He, F., Weiner, J., Chave, J., Sack, L. (2016). Does climate directly influence NPP globally? *Global Change Biology* 22, 12-24.

Cleverly, J., Boulain, N., Villalobos-Vega, R., Grant, N., Faux, R., Wood, C., Cook, P.G., Yu, Q., Leigh, A., Eamus, D. (2013a). Dynamics of component carbon fluxes in a semi-arid *Acacia* woodland, central Australia. *Journal of Geophysical Research: Biogeosciences* 118, 1168-1185.

Cleverly, J., Chen, C., Boulain, N., Villalobos-Vega, R., Faux, R., Grant, N., Yu, Q., Eamus, D. (2013b). Aerodynamic resistance and Penman–Monteith evapotranspiration over a seasonally two-layered canopy in semiarid central Australia. *Journal of Hydrometeorology* 14, 1562-1570.

Cleverly, J., Eamus, D., Luo, Q., Restrepo Coupe, N., Kljun, N., Ma, X., Ewenz, C., Li, L., Yu, Q., Huete, A. (2016a). The importance of interacting climate modes on Australia's contribution to global carbon cycle extremes. *Scientific Reports* 6, 23113.

Cleverly, J., Eamus, D., Restrepo Coupe, N., Chen, C., Maes, W., Li, L., Faux, R., Santini, N.S., Rumman, R., Yu, Q., Huete, A. (2016b). Soil moisture controls on phenology and

productivity in a semi-arid critical zone. *Science of the Total Environment* 568, 1227-1237.

Cleverly, J., Eamus, D., Van Gorsel, E., Chen, C., Rumman, R., Luo, Q., Coupe, N.R., Li, L., Kljun, N., Faux, R., Yu, Q., Huete, A. (2016c). Productivity and evapotranspiration of two contrasting semiarid ecosystems following the 2011 global carbon land sink anomaly. *Agricultural and Forest Meteorology* 220, 151-159.

Condon, A.G., Richards, R.A., Rebetzke, G.J., Farquhar, G.D. (2004). Breeding for high water-use efficiency. *Journal of Experimental Botany* 55, 2447-2460.

Cook, G.D., Dawes-Gromadzki, T.Z. (2005). Stable isotope signatures and landscape functioning in banded vegetation in arid-central Australia. *Landscape Ecology* 20, 649-660.

Cowan, I., Farquhar, G.D., (1977). Stomatal function in relation to leaf metabolism and environment: Stomatal function in the regulation of gas exchange, Symposium of the Society for Experimental Botany (ed. D.H. Jennings). Cambridge University Press, Cambridge, pp. 471-505.

Cubasch, U., Wuebbles, D., Chen, D., Facchini, M.C., Frame, D., Mahowald, N., Winther, J.G. (2013). The physical science basis. Contribution of working group I to the Fifth Assessment Report of the Intergovernmental Panel on Climate Change. Cambridge University Press, Cambridge, United Kingdom and New York, NY, USA. 119-158.

Cueva, A., Bahn, M., Litvak, M., Pumpanen, J., Vargas, R. (2015). A multisite analysis of temporal random errors in soil $CO_2$ efflux. *Journal of Geophysical Research: Biogeosciences* 120, 737-751.

Damour, G., Simonneau, T., Cochard, H., Urban, L. (2010). An overview of models of stomatal conductance at the leaf level. *Plant, Cell and Environment* 33, 1419-1438.

DeLucia, E.H., Drake, J.E., Thomas, R.B., Gonzalez-Meler, M. (2007). Forest carbon use efficiency: is respiration a constant fraction of gross primary production? *Global Change Biology* 13, 1157-1167.

Domec, J.-C., Gartner, B.L. (2001). Cavitation and water storage capacity in bole xylem segments of mature and young Douglas-fir trees. *Trees* 15, 204-214.

Dominguez, F., Kumar, P., Vivoni, E.R. (2008). Precipitation recycling variability and ecoclimatological stability—A study using NARR Data. Part II: North American monsoon region. *Journal of Climate* 21, 5187-5203.

Dominguez, F., Villegas, J.C., Breshears, D.D. (2009). Spatial extent of the North American monsoon: increased cross-regional linkages via atmospheric pathways. *Geophysical Research Letters* 36, L07401.

Drake, J.E., Power, S.A., Duursma, R.A., Medlyn, B.E., Aspinwall, M.J., Choat, B., Creek, D., Eamus, D., Maier, C., Pfautsch, S., Smith, R.A., Tjoelker, M.G., Tissue, D.T. (2017). Stomatal and

non-stomatal limitations of photosynthesis for four tree species under drought: A comparison of model formulations. *Agricultural and Forest Meteorology* 247, 454-466.

Duursma, R.A. (2015). Plantecophys--An R Package for Analysing and Modelling Leaf Gas Exchange Data. *PLoS One* 10, e0143346.

Duursma, R.A., Barton, C.V.M., Lin, Y.-S., Medlyn, B.E., Eamus, D., Tissue, D.T., Ellsworth, D.S., McMurtrie, R.E. (2014). The peaked response of transpiration rate to vapour pressure deficit in field conditions can be explained by the temperature optimum of photosynthesis. *Agricultural and Forest Meteorology* 189-190, 2-10.

Eamus, D. (1991). The interaction of rising $CO_2$ and temperatures with water use efficiency. *Plant, Cell and Environment* 14, 843-852.

Eamus, D., Cleverly, J., Boulain, N., Grant, N., Faux, R., Villalobos-Vega, R. (2013). Carbon and water fluxes in an arid-zone *Acacia* savanna woodland: An analyses of seasonal patterns and responses to rainfall events. *Agricultural and Forest Meteorology* 182-183, 225-238.

Eamus, D., Hatton, T.J., Colvin, C. (2006). Ecohydrology: vegetation function, water and resource management. CSIRO Publishing, Collingwood VIC. Australia, 348.

Eamus, D., Huete, A., Cleverly, J., Nolan, R.H., Ma, X., Tarin, T., Santini, N.S. (2016). Mulga, a major tropical dry open forest of Australia: recent insights to carbon and water fluxes. *Environmental Research Letters* 11, 125011.

Eamus, D., Narayan, A.D. (1989). The influence of prior water stress and abscisic acid foliar spraying on stomatal responses to $CO_2$, IAA, ABA, and calcium in leaves of *Solanum melongena*. *Journal of Experimental Botany* 40, 573-579.

Eamus, D., O'Grady, A.P., Hutley, L.B. (2000). Dry season conditions determine wet season water use in the wet-dry tropical savannas of northern Australia. *Tree Physiology* 20, 1219-1226.

Eamus, D., Taylor, D.T., Macinnis-Ng, C.M., Shanahan, S., De Silva, L. (2008). Comparing model predictions and experimental data for the response of stomatal conductance and guard cell turgor to manipulations of cuticular conductance, leaf-to-air vapour pressure difference and temperature: feedback mechanisms are able to account for all observations. *Plant, Cell and Environment* 31, 269-277.

Ehrenfeld, J.G. (2003). Effects of exotic plant invasions on soil nutrient cycling processes. *Ecosystems* 6, 503-523.

Enquist, B., West, G.B., Charnov, E.L., Brown, J.H. (1999). Allometric scaling of production and life-history variation in vascular plants. 401, 907-911.

Epskamp, S. (2017). Path diagrams and visual analysis of various SEM packages' output. *URL: https://github.com/SachaEpskamp/semPlot*.

Evans, J.R. (1989). Photosynthesis and nitrogen relationships in leaves of $C_3$ plants. *Oecologia* 78, 9-19.

Farquhar, G.D., Ehleringer, J.R., Hubick, K.T. (1989). Carbon isotope discrimination and photosynthesis. *Annual Review of Plant Physiology* 40, 503-537.

Farquhar, G.D., Richard, R.A. (1984). Isotopic composition of plant carbon correlates with water-use-efficiency of wheat genotypes. *Australian Journal Plant Physiology* 11, 539-552.

Farquhar, G.D., S., v.C., Berry, J.A. (1980). A biochemical model of photosynthetic $CO_2$ assimilation in leaves of C3 species. *Planta* 149, 78-90.

Fei, X., Jin, Y., Zhang, Y., Sha, L., Liu, Y., Song, Q., Zhou, W., Liang, N., Yu, G., Zhang, L., Zhou, R., Li, J., Zhang, S., Li, P. (2017). Eddy covariance and biometric measurements show that a savanna ecosystem in Southwest China is a carbon sink. *Scientific Reports* 7, 41025.

Fernández-Martínez, M., Vicca, S., Janssens, I.A., Luyssaert, S., Campioli, M., Sardans, J., Estiarte, M., Peñuelas, J. (2014). Spatial variability and controls over biomass stocks, carbon fluxes, and resource-use efficiencies across forest ecosystems. *Trees* 28, 597-611.

Flanagan, L.B., Adkinson, A.C. (2011). Interacting controls on productivity in a northern Great Plains grassland and implications for response to ENSO events. *Global Change Biology* 17, 3293-3311.

Flexas, J., Bota, J., Loreto, F., Cornic, G., Sharkey, T.D. (2004). Diffusive and metabolic limitations to photosynthesis under drought and salinity in C3 plants. *Plant Biology* 6, 269-279.

Flexas, J., Ribas-Carbo, M., Bota, J., Galmes, J., Henkle, M., Martinez-Canellas, S., Medrano, H. (2006). Decreased Rubisco activity during water stress is not induced by decreased relative water content but related to conditions of low stomatal conductance and chloroplast $CO_2$ concentration. *New Phytologist* 172, 73-82.

Fox, J., Weisberg, S. (2011). An R companion to applied regression. Second edition. Sage, Thousand Oaks, CA. *URL: http://socserv.socsci.mcmaster.ca/jfox/Books/Companion*.

Frank, D., Reichstein, M., Bahn, M., Thonicke, K., Frank, D., Mahecha, M.D., Smith, P., van der Velde, M., Vicca, S., Babst, F., Beer, C., Buchmann, N., Canadell, J.G., Ciais, P., Cramer, W., Ibrom, A., Miglietta, F., Poulter, B., Rammig, A., Seneviratne, S.I., Walz, A., Wattenbach, M., Zavala, M.A., Zscheischler, J. (2015). Effects of climate extremes on the terrestrial carbon cycle: concepts, processes and potential future impacts. *Global Change Biology* 21, 2861-2880.

Frantz, M.J., Bugbee, B. (2005). Acclimation of plant population to shade: photosynthesis, respiration, and carbon use efficiency. *Journal of American Society for Horticultural Science* 130, 918-927.

Fry, B. (2006). Stable Isotope Ecology. Springer, New York, USA. 308.

Funk, J.L., Vitousek, P.M. (2007). Resource-use efficiency and plant invasion in low-resource systems. *Nature* 446, 1079-1081.

Galmes, J., Medrano, H., Flexas, J. (2007). Photosynthetic limitations in response to water stress and recovery in Mediterranean plants with different growth forms. *New Phytologist* 175, 81-93.

Gao, Y., Zhu, X., Yu, G., He, N., Wang, Q., Tian, J. (2014). Water use efficiency threshold for terrestrial ecosystem carbon sequestration in China under afforestation. *Agricultural and Forest Meteorology* 195-196, 32-37.

Garbulsky, M.F., Peñuelas, J., Papale, D., Ardö, J., Goulden, M.L., Kiely, G., Richardson, A.D., Rotenberg, E., Veenendaal, E.M., Filella, I. (2010). Patterns and controls of the variability of radiation use efficiency and primary productivity across terrestrial ecosystems. *Global Ecology and Biogeography* 19, 253-267.

Gauthier, P.P., Crous, K.Y., Ayub, G., Duan, H., Weerasinghe, L.K., Ellsworth, D.S., Tjoelker, M.G., Evans, J.R., Tissue, D.T., Atkin, O.K. (2014). Drought increases heat tolerance of leaf respiration in *Eucalyptus globulus* saplings grown under both ambient and elevated atmospheric [$CO_2$] and temperature. *Journal of Experimental Botany* 65, 6471-6485.

Gimeno, T.E., Sommerville, K.E., Valladares, F., Owen, K.A. (2010). Homeostasis of respiration under drought and its important consequences for foliar carbon balance in a drier climate: insights from two contrasting *Acacia* species. *Functional Plant Biology* 37, 323-333.

Gleason, S.M., Butler, D.W., Waryszak, P. (2013). Shifts in leaf and stem hydraulic traits across aridity gradients in eastern Australia. *International Journal of Plant Sciences* 174, 1292-1301.

Gou, S., Gonzales, S., Miller, G.R. (2015). Mapping potential groundwater-dependent ecosystems for sustainable management. *Ground Water* 53, 99-110.

Grant, R.F., Baldocchi, D.D., Ma, S. (2012). Ecological controls on net ecosystem productivity of a seasonally dry annual grassland under current and future climates: Modelling with ecosys. *Agricultural and Forest Meteorology* 152, 189-200.

Grigg, A.M., Veneklaas, E.J., Lambers, H. (2008). Water relations and mineral nutrition of closely related woody plant species on desert dunes and interdunes. *Australian Journal of Botany* 56, 27-43.

Groom, P.K., Lamont, B.B., Kupsky, L. (1994). Contrasting morphology and mcophysiology of co-occurring broad and terete leaves in *Hakea trifurcata* (Proteaceae). *Australian Journal of Botany* 42, 307-320.

Han, J., Chen, J., Miao, Y., Wan, S. (2016). Multiple resource use efficiency (mRUE): A new concept for ecosystem production. *Scientific Reports* 6, 37453.

Harrington, G.A., Cook, P.G., Herezeg, A.L. (2002). Spatial and temporal variability of ground water recharge in central Australia: A tracer approach. *Ground Water* 40, 518-528.

Haverd, V., Ahlstrom, A., Smith, B., Canadell, J.G. (2017). Carbon cycle responses of semi-arid ecosystems to positive asymmetry in rainfall. *Global Change Biology* 23, 793-800.

Heberling, J.M., Fridley, J.D. (2013). Resource-use strategies of native and invasive plants in Eastern North American forests. *New Phytologist* 200, 523-533.

Heroult, A., Lin, Y.S., Bourne, A., Medlyn, B.E., Ellsworth, D.S. (2013). Optimal stomatal conductance in relation to photosynthesis in climatically contrasting *Eucalyptus* species under drought. *Plant, Cell and Environment* 36, 262-274.

Hsu, K.-l., Gupta, H.V., Gao, X., Sorooshian, S., Imam, B. (2002). Self-organizing linear output map (SOLO): An artificial neural network suitable for hydrologic modeling and analysis. *Water Resources Research* 38, 38-31-38-17.

Hu, Z., Yu, G., Fu, Y., Sun, X., Li, Y., Shi, P., Wang, Y., Zheng, Z. (2008). Effects of vegetation control on ecosystem water use efficiency within and among four grassland ecosystems in China. *Global Change Biology* 14, 1609-1619.

Huang, M., Piao, S., Sun, Y., Ciais, P., Cheng, L., Mao, J., Poulter, B., Shi, X., Zeng, Z., Wang, Y. (2015). Change in terrestrial ecosystem water-use efficiency over the last three decades. *Global Change Biology* 21, 2366-2378.

Huang, X., Hao, Y., Wang, Y., Wang, Y., Cui, X., Mo, X., Zhou, X. (2010). Partitioning of evapotranspiration and its relation to carbon dioxide fluxes in Inner Mongolia steppe. *Journal of Arid Environments* 74, 1616-1623.

Huete, A., Didan, K., Miura, T., Rodriguez, E.P., Gao, X., Ferreira, L.G. (2002). Overview of the radiometric and biophysical performance of the MODIS vegetation indices. *Remote Sensing of Environment* 83, 195-2013.

Huxman, T.E., Smith, M.D., Fay, P.A., Knapp, A.K., Shaw, M.R., Weltzin, J.F., Pockman, W.T., Sala, O.E., Haddad, B.M., Harte, J., Koch, G.W., Schwinning, S., Small, E.E., Williams, D.G. (2004a). Convergence across biomes to a common rain-use-efficiency. *Nature* 429, 651-654.

Huxman, T.E., Snyder, K.A., Tissue, D., Leffler, A.J., Ogle, K., Pockman, W.T., Sandquist, D.R., Potts, D.L., Schwinning, S. (2004b). Precipitation pulses and carbon fluxes in semiarid and arid ecosystems. *Oecologia* 141, 254-268.

Huxman, T.E., Turnipseed, A.A., Sparks, J.P., Harley, P.C., Monson, R.K. (2003). Temperature as a control over ecosystem $CO_2$ fluxes in a high-elevation, subalpine forest. *Oecologia* 134, 537-546.

Huxman, T.E., Wilcox, B.P., Breshears, D.D., Scott, R.L., Snyder, K.A., Small, E.E., Hultine, K., Pockman, W.T., Jackson, R.B. (2005). Ecohydrological implications of woody plant encroachment *Journal of Ecology* 86, 308-319.

IPCC, (2012). Managing the risks of extreme events and disasters to advance climate change adaptation. Special report of working groups I and II of the Intergovernmental Panel on Climate Change. [Field, C.B., V. Barros, T.F. Stocker, D. Qin, D.J. Dokken, K.L. Ebi, M.D. Mastrandrea, K.J. Mach, G.-K. Plattner, S.K. Allen, M. Tignor, and P.M. Midgley (eds.)]. Cambridge, UK, and New York, NY, USA, p. 585.

IPCC, (2014). Climate change 2014: synthesis report. Contribution of working groups I, II and III to the Fifth Assessment Report of the Intergovernmental Panel on Climate Change [Core Writing Team, R.K. Pachauri and L.A. Meyer (eds.). IPCC, Geneva, Switzerland, p. 151.

Isaac, P., Cleverly, J., McHugh, I., van Gorsel, E., Ewenz, C., Beringer, J. (2017). OzFlux data: network integration from collection to curation. *Biogeosciences* 14, 2903-2928.

Janssens, I.A., Lankreijer, H., Matteucci, G. (2001). Productivity overshadows temperature in determining soil and ecosystem respiration across European forests. *Global Change Biology* 7, 269-278.

Jasechko, S., Sharp, Z.D., Gibson, J.J., Birks, S.J., Yi, Y., Fawcett, P.J. (2013). Terrestrial water fluxes dominated by transpiration. *Nature* 496, 347-350.

Jia, X., Zha, T., Gong, J., Wang, B., Zhang, Y., Wu, B., Qin, S., Peltola, H. (2016). Carbon and water exchange over a temperate semi-arid shrubland during three years of contrasting precipitation and soil moisture patterns. *Agricultural and Forest Meteorology* 228-229, 120-129.

Jung, M., Reichstein, M., Ciais, P., Seneviratne, S.I., Sheffield, J., Goulden, M.L., Bonan, G., Cescatti, A., Chen, J., de Jeu, R., Dolman, A.J., Eugster, W., Gerten, D., Gianelle, D., Gobron, N., Heinke, J., Kimball, J., Law, B.E., Montagnani, L., Mu, Q., Mueller, B., Oleson, K., Papale, D., Richardson, A.D., Roupsard, O., Running, S., Tomelleri, E., Viovy, N., Weber, U., Williams, C., Wood, E., Zaehle, S., Zhang, K. (2010). Recent decline in the global land evapotranspiration trend due to limited moisture supply. *Nature* 467, 951-954.

Katul, G., Leuning, R., Oren, R. (2003). Relationship between plant hydraulic and biochemical properties derived from a steady-state coupled water and carbon transport model. *Plant, Cell and Environment* 26, 339-350.

Keenan, T.F., Gray, J., Friedl, M.A., Toomey, M., Bohrer, G., Hollinger, D.Y., Munger, J.W., O'Keefe, J., Schmid, H.P., Wing, I.S., Yang, B., Richardson, A.D. (2014). Net carbon uptake has increased through warming-induced changes in temperate forest phenology. *Nature Climate Change* 4, 598-604.

Keenan, T.F., Hollinger, D.Y., Bohrer, G., Dragoni, D., Munger, J.W., Schmid, H.P., Richardson, A.D. (2013). Increase in forest water-use efficiency as atmospheric carbon dioxide concentrations rise. *Nature* 499, 324-327.

Kelley, G., O'Grady, A.P., Hutley, L.B., Eamus, D. (2007). A comparison of tree water use in two contiguous vegetation communities of the seasonally dry tropics of northern Australia: the importance of site water budget to tree hydraulics. *Australian Journal of Botany* 55, 700-708.

Klein, T. (2014). The variability of stomatal sensitivity to leaf water potential across tree species indicates a continuum between isohydric and anisohydric behaviours. *Functional Ecology* 28, 1313-1320.

Kljun, N., Calanca, P., Rotach, M.W., Schmid, H.P. (2004). A simple parameterisation for flux footprint predictions. *Boundary-Layer Meteorology* 112, 503-523.

Knauer, J., Zaehle, S., Medlyn, B.E., Reichstein, M., Williams, C.A., Migliavacca, M., De Kauwe, M.G., Werner, C., Keitel, C., Kolari, P., Limousin, J.M., Linderson, M.L. (2018). Towards physiologically meaningful water-use efficiency estimates from eddy covariance data. *Global Change Biology* 24, 694-710.

Kuzyakov, Y., Gavrichkova, O. (2010). REVIEW: Time lag between photosynthesis and carbon dioxide efflux from soil: a review of mechanisms and controls. *Global Change Biology* 16, 3386-3406.

Lamont, B.B. (1993). Why are hairy root clusters so abundant in the most nutrient-impoverished soils of Australia? *Plant and Soil* 155, 269-272.

Lamont, B.B. (2003). Structure, ecology and physiology of root clusters - a review. *Plant and Soil* 248, 1-19.

Lamont, B.B., Groom, P.K., Cowling, R.M. (2002). High leaf mass per area of related species assemblages may reflect low rainfall and carbon isotope discrimination rather than low phosphorus and nitrogen concentrations. *Functional Ecology* 16, 403-412.

Le Quéré, C., Andrew, R.M., Friedlingstein, P., Sitch, S., Pongratz, J., Manning, A.C., Korsbakken, J.I., Peters, G.P., Canadell, J.G., Jackson, R.B., Boden, T.A., Tans, P.P., Andrews, O.D., Arora, V.K., Bakker, D.C.E., Barbero, L., Becker, M., Betts, R.A., Bopp, L., Chevallier, F., Chini, L.P., Ciais, P., Cosca, C.E., Cross, J., Currie, K., Gasser, T., Harris, I., Hauck, J., Haverd, V., Houghton, R.A., Hunt, C.W., Hurtt, G., Ilyina, T., Jain, A.K., Kato, E., Kautz, M., Keeling, R.F., Klein Goldewijk, K., Körtzinger, A., Landschützer, P., Lefèvre, N., Lenton, A., Lienert, S., Lima, I., Lombardozzi, D., Metzl, N., Millero, F., Monteiro, P.M.S., Munro, D.R., Nabel, J.E.M.S., Nakaoka, S.-i., Nojiri, Y., Padín, X.A., Peregon, A., Pfeil, B., Pierrot, D., Poulter, B., Rehder, G., Reimer, J., Rödenbeck, C., Schwinger, J., Séférian, R., Skjelvan, I., Stocker, B.D., Tian, H., Tilbrook, B., van der Laan-Luijkx, I.T., van der Werf, G.R., van Heuven, S., Viovy, N., Vuichard, N., Walker, A.P., Watson, A.J., Wiltshire, A.J., Zaehle, S., Zhu, D. (2017). Global Carbon Budget 2017. *Earth System Science Data Discussions*, 1-79.

Lieth, H. (1973). Primary production: terrestrial ecosystems. *Human Ecology* 1, 303-332.

Limousin, J.-M., Bickford, C.P., Dickman, L.T., Pangle, R.E., Hudson, P.J., Boutz, A.L., Gehres, N., Osuna, J.L., Pockman, W.T., McDowell, N.G. (2013). Regulation and acclimation of leaf gas exchange in a piñon-juniper woodland exposed to three different precipitation regimes. *Plant, Cell and Environment* 36, 1812-1825.

Limousin, J.-M., Yepez, E.A., McDowell, N.G., Pockman, W.T., Tjoelker, M. (2015). Convergence in resource use efficiency across trees with differing hydraulic strategies in response to ecosystem precipitation manipulation. *Functional Ecology* 29, 1125-1136.

Lin, Y.-S., Medlyn, B.E., Duursma, R.A., Prentice, I.C., Wang, H., Baig, S., Eamus, D., de Dios, Victor R., Mitchell, P., Ellsworth, D.S., de Beeck, M.O., Wallin, G., Uddling, J., Tarvainen, L., Linderson, M.-L., Cernusak, L.A., Nippert, J.B., Ocheltree, T.W., Tissue, D.T., Martin-StPaul, N.K., Rogers, A., Warren, J.M., De Angelis, P., Hikosaka, K., Han, Q., Onoda, Y., Gimeno, T.E., Barton, C.V.M., Bennie, J., Bonal, D., Bosc, A., Löw, M., Macinins-Ng, C., Rey, A., Rowland, L., Setterfield, S.A., Tausz-Posch, S., Zaragoza-Castells, J., Broadmeadow, M.S.J., Drake, J.E., Freeman, M., Ghannoum, O., Hutley, Lindsay B., Kelly, J.W., Kikuzawa, K., Kolari, P., Koyama, K., Limousin, J.-M., Meir, P., Lola da Costa, A.C., Mikkelsen, T.N., Salinas, N., Sun, W., Wingate, L. (2015). Optimal stomatal behaviour around the world. *Nature Climate Change* 5, 459-464.

Lin, Y.S., Medlyn, B.E., De Kauwe, M.G., Ellsworth, D.S. (2013). Biochemical photosynthetic responses to temperature: how do interspecific differences compare with seasonal shifts? *Tree Physiology* 33, 793-806.

Loik, M.E., Breshears, D.D., Lauenroth, W.K., Belnap, J. (2004). A multi-scale perspective of water pulses in dryland ecosystems: climatology and ecohydrology of the western USA. *Oecologia* 141, 269-281.

Lu, Y., Duursma, R.A., Medlyn, B.E. (2016). Optimal stomatal behaviour under stochastic rainfall. *Journal of Theoretical Biology* 394, 160-171.

Ma, S., Baldocchi, D., Wolf, S., Verfaillie, J. (2016a). Slow ecosystem responses conditionally regulate annual carbon balance over 15 years in Californian oak-grass savanna. *Agricultural and Forest Meteorology* 228-229, 252-264.

Ma, X., Huete, A., Cleverly, J., Eamus, D., Chevallier, F., Joiner, J., Poulter, B., Zhang, Y., Guanter, L., Meyer, W., Xie, Z., Ponce-Campos, G. (2016b). Drought rapidly diminishes the large net $CO_2$ uptake in 2011 over semi-arid Australia. *Scientific Reports* 6, 37747.

Ma, X., Huete, A., Yu, Q., Coupe, N.R., Davies, K., Broich, M., Ratana, P., Beringer, J., Hutley, L.B., Cleverly, J., Boulain, N., Eamus, D. (2013). Spatial patterns and temporal dynamics in savanna vegetation phenology across the North Australian Tropical Transect. *Remote Sensing of Environment* 139, 97-115.

Ma, X., Huete, A., Yu, Q., Restrepo-Coupe, N., Beringer, J., Hutley, L.B., Kanniah, K.D., Cleverly, J., Eamus, D. (2014). Parameterization of an ecosystem light-use-efficiency model for predicting savanna GPP using MODIS EVI. *Remote Sensing of Environment* 154, 253-271.

Malek, E. (1993). Rapid changes of the surface soil heat flux and its effects on the estimation of evapotranspiration. *Journal of Hydrology* 142, 89-97.

Manzoni, S., Vico, G., Katul, G., Fay, P.A., Polley, W., Palmroth, S., Porporato, A. (2011). Optimizing stomatal conductance for maximum carbon gain under water stress: a meta-analysis across plant functional types and climates. *Functional Ecology* 25, 456-467.

Martinez-Vilalta, J., Poyatos, R., Aguade, D., Retana, J., Mencuccini, M. (2014). A new look at water transport regulation in plants. *New Phytologist* 204, 105-115.

Mascaro, G., Vivoni, E.R. (2016). On the observed hysteresis in field-scale soil moisture variability and its physical controls. *Environmental Research Letters* 11, 084008.

Maslin, B.R., Reid, J.E. (2012). A taxonomic revision of Mulga (*Acacia aneura* and its close relatives: Fabaceae) in Western Australia. *The journal of the Western Australian Herbarium* 22, 129-267.

Massman, W., Clement, R., (2004). Uncertainty in eddy covariance flux estimates resulting from spectral attenuation, in: Lee, X., Massman, W., Law, B.E. (Eds.), Handbook of Micrometeorology: A guide for Surface Flux Measurement and Analysis. Kluwer Academic Publishers, Dordrecht/Boston/Longon, pp. 67-100.

McDowell, N., Bond, B.J., Dickman, L.T., Ryan, M.G., Whitehead, D., (2011). In size-and age-Related Changes in Tree Structure and Function, in: Springer (Ed.), pp. 255-286.

McDowell, N., Pockman, W.T., Allen, C.D., Breshears, D.D., Cobb, N., Kolb, T., Plaut, J., Sperry, J., West, A., Williams, D.G., Yepez, E.A. (2008). Mechanisms of plant survival and mortality during drought: why do some plants survive while others succumb to drought? *New Phytologist* 178, 719-739.

McDowell, N.G., Bowling, D.R., Schauer, A., Irvine, J., Bond, B.J., Law, B.E., Ehleringer, J.R. (2004). Associations between carbon isotope ratios of ecosystem respiration, water availability and canopy conductance. *Global Change Biology* 10, 1767-1784.

McDowell, N.G., Williams, A.P., Xu, C., Pockman, W.T., Dickman, L.T., Sevanto, S., Pangle, R., Limousin, J., Plaut, J., Mackay, D.S., Ogee, J., Domec, J.C., Allen, C.D., Fisher, R.A., Jiang, X., Muss, J.D., Breshears, D.D., Rauscher, S.A., Koven, C. (2015). Multi-scale predictions of massive conifer mortality due to chronic temperature rise. *Nature Climate Change* 6, 295-300.

MEA, (2005). Millennium Ecosystem Assessment: Ecosystems and human well-being: synthesis, in: Press, I. (Ed.), Washington, DC. 137.

Medlyn, B.E., De Kauwe, M.G., Lin, Y.S., Knauer, J., Duursma, R.A., Williams, C.A., Arneth, A., Clement, R., Isaac, P., Limousin, J.M., Linderson, M.L., Meir, P., Martin-StPaul, N., Wingate, L. (2017). How do leaf and ecosystem measures of water-use efficiency compare? *New Phytologist* 216, 758-770.

Medlyn, B.E., Dreyer, E., Ellsworth, D.S., Forstreuter, M., Harley, P.C., Kirschbaum, M.U.F., Le Roux, X., Montpied, P., Strassemeyer, J., Walcroft, A., Wang, K., Loustau, D. (2002). Temperature response of parameters of a biochemically based model of photosynthesis. II. A review of experimental data. *Plant, Cell and Environment* 25, 1167-1179.

Medlyn, B.E., Duursma, R.A., Eamus, D., Ellsworth, D.S., Prentice, I.C., Barton, C.V.M., Crous, K.Y., De Angelis, P., Freeman, M., Wingate, L. (2011). Reconciling the optimal and empirical approaches to modelling stomatal conductance. *Global Change Biology* 17, 2134-2144.

Meinzer, F.C., Johnson, D.M., Lachenbruch, B., McCulloh, K.A., Woodruff, D.R. (2009). Xylem hydraulic safety margins in woody plants: coordination of stomatal control of xylem tension with hydraulic capacitance. *Functional Ecology* 23, 922-930.

Méndez-Barroso, L.A., Vivoni, E.R., Robles-Morua, A., Giuseppe Mascaro, Yepez, E.A., Rodriguez, J.C., Watts, C., Garatuza-Payan, J., Saiz-Hernández, J.A. (2014). A modeling approach reveals differences in evapotranspiration and its partitioning in two semiarid ecosystems in Northwest. *Water Resources Research* 50, 3229-3252.

Michaletz, S.T., Cheng, D., Kerkhoff, A.J., Enquist, B.J. (2014). Convergence of terrestrial plant production across global climate gradients. *Nature* 512, 39-43.

Miller, J.M., Williams, R.J., Farquhar, G.D. (2001). Carbon isotope discrimination by a sequence of *Eucalyptus* species along a subcontinental rainfall gradient in Australia. *Functional Ecology* 15, 222-232.

Miner, G.L., Bauerle, W.L., Baldocchi, D.D. (2017). Estimating the sensitivity of stomatal conductance to photosynthesis: a review. *Plant, Cell and Environment* 40, 1214-1238.

Misson, L., Tu, K.P., Boniello, R.A., Goldstein, A.H. (2006). Seasonality of photosynthetic parameters in a multi-specific and vertically complex forest ecosystem in the Sierra Nevada of California. *Tree Physiology* 26, 729-741.

Mitchell, P.J., O'Grady, A.P., Tissue, D.T., Worledge, D., Pinkard, E.A. (2014). Co-ordination of growth, gas exchange and hydraulics define the carbon safety margin in tree species with contrasting drought strategies. *Tree Physiology* 34, 443-458.

Mitchell, P.J., Veneklaas, E.J., Lambers, H., Burgess, S.S. (2008). Using multiple trait associations to define hydraulic functional types in plant communities of south-western Australia. *Oecologia* 158, 385-397.

Moreno-Gutierrez, C., Dawson, T.E., Nicolas, E., Querejeta, J.I. (2012). Isotopes reveal contrasting water use strategies among coexisting plant species in a Mediterranean ecosystem. *New Phytologist* 196, 489-496.

Newman, B.D., Wilcox, B.P., Archer, S.R., Breshears, D.D., Dahm, C.N., Duffy, C.J., McDowell, N.G., Phillips, F.M., Scanlon, B.R., Vivoni, E.R. (2006). Ecohydrology of water-limited environments: A scientific vision. *Water Resources Research* 42, W06302.

Nobel, P.S. (2009). Physicochemical and Environmental Plant Physiology, 4 ed. Academic Press / Elsevier Inc. 568.

Nolan, R.H., Fairweather, K.A., Tarin, T., Santini, N.S., Cleverly, J., Faux, R., Eamus, D. (2017a). Divergence in plant water-use strategies in semiarid woody species. *Functional Plant Biology* 44, 1134-1146.

Nolan, R.H., Tarin, T., Fairweather, K.A., Cleverly, J., Eamus, D. (2017b). Variation in photosynthetic traits related to access to water in semiarid Australian woody species. *Functional Plant Biology* 44, 1087-1097.

Nolan, R.H., Tarin, T., Santini, N.S., McAdam, S.A.M., Ruman, R., Eamus, D. (2017c). Differences in osmotic adjustment, foliar abscisic acid dynamics, and stomatal regulation between an isohydric and anisohydric woody angiosperm during drought. *Plant, Cell and Environment* 40, 3122-3134.

Novick, K.A., Ficklin, D.L., Stoy, P.C., Williams, C.A., Bohrer, G., Oishi, A.C., Papuga, S.A., Blanken, P.D., Noormets, A., Sulman, B.N., Scott, R.L., Wang, L., Phillips, R.P. (2016). The increasing importance of atmospheric demand for ecosystem water and carbon fluxes. *Nature Climate Change* 6, 1023-1027.

O'Grady, A.P., Cook, P.G., Eamus, D., Duguid, A., Wischusen, J.D., Fass, T., Worldege, D. (2009). Convergence of tree water use within an arid-zone woodland. *Oecologia* 160, 643-655.

O'Grady, A.P., Eamus, D., Cook, P.G., Lamontagne, S. (2006). Groundwater use by riparian vegetation in the wet–dry tropics of northern Australia. *Australian Journal of Botany* 54, 145-154.

O'Leary, M.H. (1981). Carbon isotope fractionation in plants. *Phytochemestry* 20, 553-567.

O'Donnell, A.J., Boer, M.M., McCaw, W.L., Grierson, P.F. (2011). Vegetation and landscape connectivity control wildfire intervals in unmanaged semi-arid shrublands and woodlands in Australia. *Journal of Biogeography* 38, 112-124.

Owens, M.K., Lyons, R.K., Alejandro, C.L. (2006). Rainfall partitioning within semiarid juniper communities: effects of event size and canopy cover. *Hydrological Processes* 20, 3179-3189.

Page, G.F., Liu, J., Grierson, P.F. (2011). Three-dimensional xylem networks and phyllode properties of co-occurring *Acacia*. *Plant, Cell and Environment* 34, 2149-2158.

Page, G.F.M., Merchant, A., Grierson, P.F. (2016). Inter-specific differences in the dynamics of water use and pulse-response of co-dominant canopy species in a dryland woodland. *Journal of Arid Environments* 124, 332-340.

Pataki, D.E., Ehleringer, J.R., Flanagan, L.B., Yakir, D., Bowling, D.R., Still, C.J., Buchmann, N., Kaplan, J.O., Berry, J.A. (2003). The application and interpretation of Keeling plots in terrestrial carbon cycle research. *Global Biogeochemical Cycles* 17, 1022.

Peng, D., Zhang, B., Wu, C., Huete, A.R., Gonsamo, A., Lei, L., Ponce-Campos, G.E., Liu, X., Wu, Y. (2017). Country-level net primary production distribution and response to drought and land cover change. *Science of the Total Environment* 574, 65-77.

Peñuelas, J., Lloret, F., Montoya, R. (2001). Severe drought effects on Mediterranean woody flora in Spain. *Forest Science* 47, 214-218.

Perez-Ruiz, E.R., Garatuza-Payan, J., Watts, C.J., Rodriguez, J.C., Yepez, E.A., Scott, R.L. (2010). Carbon dioxide and water vapour exchange in a tropical dry forest as influenced by the North American Monsoon System (NAMS). *Journal of Arid Environments* 74, 556-563.

Piao, S., Sitch, S., Ciais, P., Friedlingstein, P., Peylin, P., Wang, X., Ahlstrom, A., Anav, A., Canadell, J.G., Cong, N., Huntingford, C., Jung, M., Levis, S., Levy, P.E., Li, J., Lin, X., Lomas, M.R., Lu, M., Luo, Y., Ma, Y., Myneni, R.B., Poulter, B., Sun, Z., Wang, T., Viovy, N., Zaehle, S., Zeng, N. (2013). Evaluation of terrestrial carbon cycle models for their response to climate variability and to $CO_2$ trends. *Global Change Biology* 19, 2117-2132.

Ponce-Campos, G.E., Moran, M.S., Huete, A., Zhang, Y., Bresloff, C., Huxman, T.E., Eamus, D., Bosch, D.D., Buda, A.R., Gunter, S.A., Scalley, T.H., Kitchen, S.G., McClaran, M.P., McNab, W.H., Montoya, D.S., Morgan, J.A., Peters, D.P., Sadler, E.J., Seyfried, M.S., Starks, P.J. (2013). Ecosystem resilience despite large-scale altered hydroclimatic conditions. *Nature* 494, 349-352.

Ponton, S., Flanagan, L.B., Alstad, K.P., Johnson, B.G., Morgenstern, K.A.I., Kljun, N., Black, T.A., Barr, A.G. (2006). Comparison of ecosystem water-use efficiency among Douglas-fir forest, aspen forest and grassland using eddy covariance and carbon isotope techniques. *Global Change Biology* 12, 294-310.

Poorter, H., Niinemets, Ü., Poorter, L., Wright, I.J., Villar, R. (2009). Causes and consequences of variation in leaf mass *per* area (LMA): a meta-analysis. *New Phytologist* 182, 565-588.

Poorter, H., Niklas, K.J., Reich, P.B., Oleksyn, J., Poot, P., Mommer, L. (2012). Biomass allocation to leaves, stems and roots: meta-analyses of interspecific variation and environmental control. *New Phytologist* 193, 30-50.

Poulter, B., Frank, D., Ciais, P., Myneni, R.B., Andela, N., Bi, J., Broquet, G., Canadell, J.G., Chevallier, F., Liu, Y.Y., Running, S.W., Sitch, S., van der Werf, G.R. (2014). Contribution of semi-arid ecosystems to interannual variability of the global carbon cycle. *Nature* 509, 600-603.

Pressland, A.J. (1973). Rainfall partitioning by an arid woodland (*Acacia aneura* F. Muell.) in south-western Queensland *Australian Journal of Botany* 21, 235-245.

Prior, L.D., Bowman, D.M.J.S., Eamus, D. (2005). Intra-specific variation in leaf attributes of four savanna tree species across a rainfall gradient in tropical Australia. *Australian Journal of Botany* 53, 323-335.

Prueger, J.H., Hipps, L.E., Cooper, D.I. (1996). Evaporation and the development of the local boundary layer over an irrigated surface in an arid region. *Agricultural and Forest Meteorology* 78, 223-237.

Quebbeman, J.A., Ramirez, J.A. (2016). Optimal allocation of leaf-level nitrogen: Implications for covariation of $V_{cmax}$ and $J_{max}$ and photosynthetic downregulation. *Journal of Geophysical Research: Biogeosciences* 121, 2464-2475.

Reichstein, M., Bahn, M., Ciais, P., Frank, D., Mahecha, M.D., Seneviratne, S.I., Zscheischler, J., Beer, C., Buchmann, N., Frank, D.C., Papale, D., Rammig, A., Smith, P., Thonicke, K., van der Velde, M., Vicca, S., Walz, A., Wattenbach, M. (2013). Climate extremes and the carbon cycle. *Nature* 500, 287-295.

Reichstein, M., Bahn, M., Mahecha, M.D., Kattge, J., Baldocchi, D.D. (2014). Linking plant and ecosystem functional biogeography. *Proceedings of the National Academy of Sciences of the United States of America (PNAS)* 111, 13697-13702.

Reichstein, M., Falge, E., Baldocchi, D., Papale, D., Aubinet, M., Berbigier, P., Bernhofer, C., Buchmann, N., Gilmanov, T., Granier, A., Grunwald, T., Havrankova, K., Ilvesniemi, H., Janous, D., Knohl, A., Laurila, T., Lohila, A., Loustau, D., Matteucci, G., Meyers, T., Miglietta, F., Ourcival, J.-M., Pumpanen, J., Rambal, S., Rotenberg, E., Sanz, M., Tenhunen, J., Seufert, G., Vaccari, F., Vesala, T., Yakir, D., Valentini, R. (2005). On the separation of net ecosystem exchange into assimilation and ecosystem respiration: review and improved algorithm. *Global Change Biology* 11, 1424-1439.

Resco, V., Ewers, B.E., Sun, W., Huxman, T.E., Weltzin, J.F., Williams, D.G. (2009). Drought-induced hydraulic limitations constrain leaf gas exchange recovery after precipitation pulses in the C3 woody legume, Prosopis velutina. *New Phytologist* 181, 672-682.

Restrepo-Coupe, N., Huete, A., Davies, K., Cleverly, J., Beringer, J., Eamus, D., van Gorsel, E., Hutley, L.B., Meyer, W.S. (2016). MODIS vegetation products as proxies of photosynthetic potential along a gradient of meteorologically and biologically driven ecosystem productivity. *Biogeosciences* 13, 5587-5608.

Reynolds, J.F., Kemp, R.F., Tenhunen, J.D. (2000). Effects of long-term rainfall variability on evapotranspiration and soil water distribution in the Chihuahuan Desert: A modeling analysis. *Plant Ecology* 150, 145-159.

Richardson, A.D., Keenan, T.F., Migliavacca, M., Ryu, Y., Sonnentag, O., Toomey, M. (2013). Climate change, phenology, and phenological control of vegetation feedbacks to the climate system. *Agricultural and Forest Meteorology* 169, 156-173.

Roderick, M.L. (2000). On the measurement of growth with applications to the modelling and analysis of plant growth. *Functional Ecology* 14, 244-251.

Rumman, R., Atkin, O.K., Bloomfield, K.J., Eamus, D. (2017). Variation in bulk-leaf $^{13}C$ discrimination, leaf traits and water-use efficiency-trait relationships along a continental-scale climate gradient in Australia. *Global Change Biology* 24, 1186-1200.

Rumman, R., Cleverly, J., Nolan, R.H., Tarin, T., Eamus, D. (2018). Speculations on the application of foliar $^{13}C$ discrimination to reveal groundwater dependency of vegetation, provide estimates of root depth and rates of groundwater use. *Hydrology and Earth System Sciences Discussions*, 1-25.

Running, S.W., Nemani, R.R., Heinsch, F.A., Zhao, M., Reeves, M., Hashimoto, H. (2004). A continuous satellite-derived measure of global terrestrial primary production. *Bioscience* 54, 547-560.

Running, S.W., Thornton, P.E., Nemani, R., Glassy, J.M. (2000). Global terrestrial gross and net primary productivity from the earth observing system. *Bioscience* 54, 547-560.

Rutledge, S., Campbell, D.I., Baldocchi, D., Schipper, L.A. (2009). Photodegradation leads to increased carbon dioxide losses from terrestrial organic matter. *Global Change Biology* 16, 3065-3074.

Ryu, Y., Baldocchi, D.D., Ma, S., Hehn, T. (2008). Interannual variability of evapotranspiration and energy exchange over an annual grassland in California. *Journal of Geophysical Research* 113, D09104.

Santiago, L.S., Goldstein, G., Meinzer, F.C., Fisher, J.B., Machado, K., Woodruff, D., Jones, T. (2004). Leaf photosynthetic traits scale with hydraulic conductivity and wood density in Panamanian forest canopy trees. *Oecologia* 140, 543-550.

Santini, N.S., Cleverly, J., Faux, R., Lestrange, C., Rumman, R., Eamus, D. (2015). Xylem traits and water-use efficiency of woody species co-occurring in the Ti Tree Basin arid zone. *Trees* 30, 295-303.

Santini, N.S., Cleverly, J., Faux, R., McBean, K., Nolan, R., Eamus, D. (2017). Root xylem characteristics and hydraulic strategies of species co-occurring in semi-arid Australia. *International Association of Wood Anatomists, Journal* 39, 43-62.

Scanlon, T.M., Kustas, W.P. (2010). Partitioning carbon dioxide and water vapor fluxes using correlation analysis. *Agricultural and Forest Meteorology* 150, 89-99.

Scartazza, A., Mata, C., Matteucci, G., Yakir, D., Moscatello, S., Brugnoli, E. (2004). Comparisons of delta $^{13}C$ of photosynthetic products and ecosystem respiratory $CO_2$ and their responses to seasonal climate variability. *Oecologia* 140, 340-351.

Scartazza, A., Moscatello, S., Matteucci, G., Battistelli, A., Brugnoli, E. (2013). Seasonal and inter-annual dynamics of growth, non-structural carbohydrates and C stable isotopes in a Mediterranean beech forest. *Tree Physiology* 33, 730-742.

Schlesinger, W.H. (2017). An evaluation of abiotic carbon sinks in deserts. *Global Change Biology* 23, 25-27.

Schlesinger, W.H., Jasechko, S. (2014). Transpiration in the global water cycle. *Agricultural and Forest Meteorology* 189-190, 115-117.

Schotanus, P., Nieuwstadt, F., Debruin, H. (1983). Temperature-measurement with a sonic anemometer and its application to heat and moisture fluxes. *Boundary-Layer Meteorology* 26, 81-93.

Schwinning, S., Sala, O.E. (2004). Hierarchy of responses to resource pulses in arid and semi-arid ecosystems. *Oecologia* 141, 211-220.

Scott, R.L., Biederman, J.A., Hamerlynck, E.P., Barron-Gafford, G.A. (2015). The carbon balance pivot point of southwestern U.S. semiarid ecosystems: Insights from the 21st century drought. *Journal of Geophysical Research: Biogeosciences* 120, 2612-2624.

Scott, R.L., Huxman, T.E., Cable, W.L., Emmerich, W.E. (2006). Partitioning of evapotranspiration and its relation to carbon dioxide exchange in a Chihuahuan Desert shrubland. *Hydrological Processes* 20, 3227-3243.

Seibt, U., Rajabi, A., Griffiths, H., Berry, J.A. (2008). Carbon isotopes and water use efficiency: sense and sensitivity. *Oecologia* 155, 441-454.

Seneviratne, S.I., Luthi, D., Litschi, M., Schar, C. (2006). Land-atmosphere coupling and climate change in Europe. *Nature* 443, 205-209.

Shanafield, M., Cook, P.G., Gutiérrez-Jurado, H.A., Faux, R., Cleverly, J., Eamus, D. (2015). Field comparison of methods for estimating groundwater discharge by evaporation and evapotranspiration in an arid-zone playa. *Journal of Hydrology* 527, 1073-1083.

Shen, F., Gao, R., Liu, W., Zhang, W. (2002). Physical analysis of the process of cavitation in xylem sap. *Tree Physiology* 22, 655–659.

Shen, W., Jenerette, G.D., Hui, D., Scott, R.L. (2016). Precipitation legacy effects on dryland ecosystem carbon fluxes: direction, magnitude and biogeochemical carryovers. *Biogeosciences* 13, 425-439.

Shi, H., Li, L., Eamus, D., Cleverly, J., Huete, A., Beringer, J., Yu, Q., van Gorsel, E., Hutley, L. (2014). Intrinsic climate dependency of ecosystem light and water-use-efficiencies across Australian biomes. *Environmental Research Letters* 9, 104002.

Shi, H., Li, L., Eamus, D., Huete, A., Cleverly, J., Tian, X., Yu, Q., Wang, S., Montagnani, L., Magliulo, V., Rotenberg, E., Pavelka, M., Carrara, A. (2017). Assessing the ability of MODIS EVI to estimate terrestrial ecosystem gross primary production of multiple land cover types. *Ecological Indicators* 72, 153-164.

Shipley, B. (2000). Cause and correlation in biology: a user's guide to path analysis, structural equations and causal inference. Cambridge University, Press Cambridge, UK. 317.

Shipley, B., De Bello, F., Cornelissen, J.H., Laliberte, E., Laughlin, D.C., Reich, P.B. (2016). Reinforcing loose foundation stones in trait-based plant ecology. *Oecologia* 180, 923-931.

Silcock, J.L., Witt, G.B., Fensham, R.J. (2016). A 150-year fire history of mulga (*Acacia aneura* F. Muell. ex Benth.) dominated vegetation in semiarid Queensland, Australia. *The Rangeland Journal* 38, 391–415.

Silvertown, J., Araya, Y., Gowing, D., Cornwell, W. (2015). Hydrological niches in terrestrial plant communities: a review. *Journal of Ecology* 103, 93-108.

Smith, N.G., Rodgers, V.L., Brzostek, E.R., Kulmatiski, A., Avolio, M.L., Hoover, D.L., Koerner, S.E., Grant, K., Jentsch, A., Fatichi, S., Niyogi, D. (2014). Toward a better integration of biological data from precipitation manipulation experiments into Earth system models. *Reviews of Geophysics* 52, 412-434.

Sperry, J.S., Love, D.M. (2015). What plant hydraulics can tell us about responses to climate-change droughts. *New Phytologist* 207, 14-27.

Tang, X., Li, H., Desai, A.R., Nagy, Z., Luo, J., Kolb, T.E., Olioso, A., Xu, X., Yao, L., Kutsch, W., Pilegaard, K., Kostner, B., Ammann, C. (2014). How is water-use efficiency of terrestrial ecosystems distributed and changing on Earth? *Scientific Reports* 4, 7483.

Tarvainen, L., Rantfors, M., Wallin, G. (2015). Seasonal and within-canopy variation in shoot-scale resource-use efficiency trade-offs in a Norway spruce stand. *Plant, Cell and Environment* 38, 2487-2496.

Taylor, D.T., Eamus, D. (2007). Coordinating leaf functional traits with branch hydraulic conductivity: resource substitution and implications for carbon gain. *Tree Physiologist* 28, 1169-1177.

Thomas, D.S., Eamus, D., Bell, D. (1999a). Optimization theory of stomatal behaviour I. A critical evaluation of five methods of calculation. *Journal of Experimental Botany* 50, 382-392.

Thomas, D.S., Eamus, D., Bell, D. (1999b). Optimization theory of stomatal behaviour II. Stomatal responses of several tree species of north Australia to changes in light, soil and atmospheric water content and temperature. *Journal of Experimental Botany* 50, 393-400.

Thomas, D.S., Eamus, D., Shanahan, S. (2000). Influence of season, drought and xylem ABA on stomatal responses to leaf-to-air vapour pressure difference of trees of the Australian wet–dry tropics. *Australian Journal of Botany* 48, 143-151.

Thomey, M.L., Collins, S.L., Vargas, R., Johnson, J.E., Brown, R.F., Natvig, D.O., Friggens, M.T. (2011). Effect of precipitation variability on net primary production and soil respiration in a Chihuahuan Desert grassland. *Global Change Biology* 17, 1505-1515.

Troch, P.A., Martinez, G.F., Pauwels, V.R.N., Durcik, M., Sivapalan, M., Harman, C., Brooks, P.D., Gupta, H., Huxman, T. (2009). Climate and vegetation water use efficiency at catchment scales. *Hydrological Processes* 23, 2409-2414.

Turner, D., Lewis, M., Ostendorf, B. (2011). Spatial indicators of fire risk in the arid and semi-arid zone of Australia. *Ecological Indicators* 11, 149-167.

Turner, D., Ostendorf, B., Lewis, M. (2008). An introduction to patterns of fire in arid and semi-arid Australia, 1998-2004. *The Rangeland Journal* 30, 95-107.

Turner, N.C., Schulze, E.D., Nicolle, D., Kuhlmann, I. (2010). Growth in two common gardens reveals species by environment interaction in carbon isotope discrimination of *Eucalyptus*. *Tree Physiologist* 30, 741-747.

Van Etten, E.J.B. (2009). Inter-annual rainfall variability of arid Australia: greater than elsewhere? *Australian Geographer* 40, 109-120.

Vargas, R., Collins, S.L., Thomey, M.L., Johnson, J.E., Brown, R.F., Natvig, D.O., Friggens, M.T. (2012). Precipitation variability and fire influence the temporal dynamics of soil $CO_2$ efflux in an arid grassland. *Global Change Biology* 18, 1401-1411.

Verduzco, V.S., Garatuza-Payán, J., Yépez, E.A., Watts, C.J., Rodríguez, J.C., Robles-Morua, A., Vivoni, E.R. (2015). Variations of net ecosystem production due to seasonal precipitation differences in a tropical dry forest of northwest Mexico. *Journal of Geophysical Research: Biogeosciences* 120, 2081-2094.

Vicente-Serrano, S.M., Beguería, S., López-Moreno, J.I. (2010). A multiscalar drought index sensitive to global warming: The Standardized Precipitation Evapotranspiration Index. *Journal of Climate* 23, 1696-1718.

Vogan, P.J., Maherali, H. (2014). Increased photosynthetic capacity as a mechanism of drought adaptation in C3 Plants. *International Journal of Plant Sciences* 175, 1033-1041.

Wang, S., Zhang, Y., Lu, S., Su, P., Shang, L., Li, Z. (2016). Biophysical regulation of carbon fluxes over an alpine meadow ecosystem in the eastern Tibetan Plateau. *International Journal of Biometeorology* 60, 801-812.

Warren, C.R., Aranda, I., Cano, F.J. (2011). Responses to water stress of gas exchange and metabolites in *Eucalyptus* and *Acacia* spp. *Plant, Cell and Environment* 34, 1609-1629.

Warton, D.I., Duursma, R.A., Falster, D.S., Taskinen, S. (2012). smatr 3- an R package for estimation and inference about allometric lines. *Methods in Ecology and Evolution* 3, 257-259.

Webb, E., Pearman, G., Leuning, R. (1980). Correction of flux measurements for density effects due to heat and water-vapor transfer. *Quarterly Journal of the Royal Meteorological Society* 106, 85-100.

Wesely, M.L., (1970). (Ph.D. dissertation thesis). Eddy Correlation Measurements in the Atmospheric Surface Layer over Agricultural Crops. University of Wisconsin, Madison, p. 102.

West, A.G., Hultine, K.R., Burtch, K.G., Ehleringer, J.R. (2007). Seasonal variations in moisture use in a piñon-juniper woodland. *Oecologia* 153, 787-798.

Whitehead, D., Gower, S.T. (2001). Photosynthesis and light-use efficiency by plants in a Canadian boreal forest ecosystem. *Tree Physiology* 21, 925-929.

Wilson, K.B., Hanson, P.J., Mulholland, P.J., Baldocchi, D., Wullschleger, S.D. (2001). A comparison of methods for determining forest evapotranspiration and its components: sap-flow, soil water budget, eddy covariance and catchment water balance. *Agricultural and Forest Meteorology* 106, 153-168.

Wischusen, J.D.H., Bastrakov, E.N., Magee, J.W., Lewis, S.J., Gow, L.J., Kilgour, P.L., Bell, J.G., Kelly, T., (2012). Hydrogeological Investigation of Deep Groundwater Resources in the Ti-Tree Basin, Northern Territory. Final Technical Report of the Palaeovalley Groundwater

Project for the Ti-Tree Demonstration Site, in: 2012/08., R. (Ed.), Geoscience Australia: Canberra.

Wolf, S., (2010). (Ph.D. dissertation thesis). Carbon dioxide and water vapour fluxes of tropical pasture and afforestation: seasonal variations of net ecosystem exchange and carbon sequestration potentials, Dipl.-Geogr., Dresden University of Technology. Swiss Federal Institute of Technology in Zurich, Zurich, German, p. 140.

Wolz, K.J., Wertin, T.M., Abordo, M., Wang, D., Leakey, A.D.B. (2017). Diversity in stomatal function is integral to modelling plant carbon and water fluxes. *Nature Ecology & Evolution* 1, 1292-1298.

Wright, I.J., Reich, P.B., Westoby, M., Ackerly, D.D., Baruch, Z., Bongers, F., Cavender-Bares, J., Chapin, T., Cornelissen, J.H.C., Matthias, D., Flexas, J., Garnier, E., Groom, P.K., Gulias, J., Hikosaka, K., Lamont, B.B., Lee, T., Lee, W., Lusk, C., Midgley, J.J., Navas, M.-L., Niinemets, Ü., Oleksyn, J., Osada, N., Poorter, H., Poot, P., Prior, L.D., Pyankov, V.I., Roumet, C., Thomas, S.C., Tjoelker, M.G., Veneklaas, E.J., Villar, R. (2004). The worldwide leaf economis spectrum. *Nature* 428, 821-827.

Wright, I.J., Westoby, M. (2002). Leaves at low versus high rainfall: coordination of structure, lifespan and physiology. *New Phytologist* 2002, 403-416.

Wu, L., Zhang, Y., Zhang, J., Downing, A. (2015). Precipitation intensity is the primary driver of moss crust-derived $CO_2$ exchange: Implications for soil C balance in a temperate desert of northwestern China. *European Journal of Soil Biology* 67, 27-34.

Xia, J., Niu, S., Ciais, P., Janssens, I.A., Chen, J., Ammann, C., Arain, A., Blanken, P.D., Cescatti, A., Bonal, D., Buchmann, N., Curtis, P.S., Chen, S., Dong, J., Flanagan, L.B., Frankenberg, C., Georgiadis, T., Gough, C.M., Hui, D., Kiely, G., Li, J., Lund, M., Magliulo, V., Marcolla, B., Merbold, L., Montagnani, L., Moors, E.J., Olesen, J.E., Piao, S., Raschi, A., Roupsard, O., Suyker, A.E., Urbaniak, M., Vaccari, F.P., Varlagin, A., Vesala, T., Wilkinson, M., Weng, E., Wohlfahrt, G., Yan, L., Luo, Y. (2015). Joint control of terrestrial gross primary productivity by plant phenology and physiology. *Proceedings of the National Academy of Sciences of the United States of America (PNAS)* 112, 2788-2793.

Xu, C., Baldocchi, D. (2003). Seasonal trends in photosynthetic parameters and stomatal conductance of blue oak (*Quercus douglasii*) under prolonged summer drought and high temperature. *Tree Physiologist* 23, 865–877.

Xu, X., Medvigy, D., Powers, J.S., Becknell, J.M., Guan, K. (2016). Diversity in plant hydraulic traits explains seasonal and inter-annual variations of vegetation dynamics in seasonally dry tropical forests. *New Phytologist* 212, 80-95.

Xu, Z., Shimizu, H., Ito, S., Yagasaki, Y., Zou, C., Zhou, G., Zheng, Y. (2014). Effects of elevated $CO_2$, warming and precipitation change on plant growth, photosynthesis and peroxidation in dominant species from North China grassland. *Planta* 239, 421-435.

Yang, Y., Donohue, R.J., McVicar, T.R., Roderick, M.L. (2015). An analytical model for relating global terrestrial carbon assimilation with climate and surface conditions using a rate limitation framework. *Geophysical Research Letters* 42, 9825-9835.

Yaseef, N.R., Yakir, D., Rotenberg, E., Schiller, G., Cohen, S. (2010). Ecohydrology of a semi-arid forest: partitioning among water balance components and its implications for predicted precipitation changes. *Ecohydrology* 3, 143-154.

Yepez, E.A., Scott, R.L., Cable, W.L., Williams, D.G. (2007). Intraseasonal variation in water and carbon dioxide flux components in a semiarid riparian woodland. *Ecosystems* 10, 1100-1115.

Yin, Q., Wang, L., Lei, M., Dang, H., Quan, J., Tian, T., Chai, Y., Yue, M. (2018). The relationships between leaf economics and hydraulic traits of woody plants depend on water availability. *Science of the Total Environment* 621, 245-252.

Yves, R. (2012). lavaan: An R Package for Structural Equation Modeling. *Journal of Statistical Software* 48, 1-36.

Zeppel, M., Eamus, D. (2008). Coordination of leaf area, sapwood area and canopy conductance leads to species convergence of tree water use in a remnant evergreen woodland. *Australian Journal of Botany* 56, 97-108.

Zhao, M., Running, S. (2010). Drought-induced reduction in global terrestrial net primary production from 2000 throught 2009. *Science* 329, 940-943.

Zhou, S., Duursma, R.A., Medlyn, B.E., Kelly, J.W.G., Prentice, I.C. (2013). How should we model plant responses to drought? An analysis of stomatal and non-stomatal responses to water stress. *Agricultural and Forest Meteorology* 182-183, 204-214.

Zhou, S., Yu, B., Huang, Y., Wang, G. (2014). The effect of vapor pressure deficit on water use efficiency at the subdaily time scale. *Geophysical Research Letters* 41, 5005-5013.

Zhou, S., Zhang, Y., Ciais, P., Xiao, X., Luo, Y., Caylor, K.K., Huang, Y., Wang, G. (2017). Dominant role of plant physiology in trend and variability of gross primary productivity in North America. *Scientific Reports* 7, 41366.

Zhou, S.X., Medlyn, B.E., Prentice, I.C. (2016). Long-term water stress leads to acclimation of drought sensitivity of photosynthetic capacity in xeric but not riparian *Eucalyptus* species. *Annals of Botany* 117, 133-144.

# *Supplementary information*

## Supplementary tables

Table S.2. 1 Summary of site characteristics and instrumentation.

| Characteristic / instrumentation | Mulga woodland | *Corymbia* savanna |
|---|---|---|
| Canopy height | 6.5 m | 4.85 m |
| Tower height | 13.7 m | 10 m |
| Infrared gas analyser | LI7500 | LI7500A |
| 3D sonic anemometer | CSAT3 | CSAT3 |
| 3D sonic anemometer | CSAT3 (11.6 m height) | CSAT3 (9.8 m height) |
| Net radiation | CNR1 | CNR4 |
| Temperature | HMP45C | HMP45C |
| Relative humidity | HMP45C | HMP45C |
| Rain gauge | CS7000 | CS7000 |
| Atmospheric pressure | CS106 | CS106 |
| Data logged | 30 min resolution (CR3000) | 30 min resolution (CR3000) |
| Soil water reflectometers | CS616 | CS610 |
| Ground heat flux plates | CN3 | CN3 |
| Soil thermocouples | TCAV | TCAV |

Table S.3.1 ANOVA table showing the interactive effects species, dates and methods (if applicable) on different variables with trees considered as replicates (n= 4) with Tukey's HSD *post-hoc* tests for significant differences between species. Two-way ANOVAs was conducted to asses differences between species and dates, whilst three-way ANOVA was used to evaluate the effect species × date × method for different approaches of measuring $WUE_i$. Significant effects are indicated by *p*-values (.) >0.05, (*) <0.05, (**) <0.01, (***) <0.001.

| Variable | Effect | Df | F-value | *p*-value | |
|---|---|---|---|---|---|
| $\Psi_{pd}$ | Species | 5 | 695.2 | <0.0001 | *** |
| | Date | 2 | 520.4 | <0.0001 | *** |
| | Species:Dates | 8 | 164.4 | <0.0001 | *** |
| $\Psi_{md}$ | Species | 5 | 611.03 | <0.0001 | *** |
| | Date | 2 | 233.81 | <0.0001 | *** |
| | Species:Dates | 8 | 63.67 | <0.0001 | *** |
| $A_n$ | Species | 4 | 63.878 | <0.0001 | *** |
| | Date | 1 | 105.542 | <0.0001 | *** |
| | Species:Dates | 3 | 3.544 | 0.0149 | * |
| $g_s$ | Species | 4 | 25.196 | <0.0001 | *** |
| | Date | 1 | 52.44 | <0.0001 | *** |
| | Species:Dates | 3 | 7.768 | <0.0001 | *** |
| $N_a$ | Species | 5 | 31.112 | <0.0001 | *** |
| | Date | 2 | 9.275 | 0.0004 | *** |
| | Species:Dates | 10 | 1.778 | 0.0501 | . |
| **LMA** | Species | 5 | 14.951 | <0.0001 | *** |
| | Date | 2 | 15.44 | <0.0001 | *** |
| | Species:Dates | 10 | 2.116 | 0.0423 | * |
| $WUE_{i(leaf\text{-}gas)}$ | Species | 5 | 7.138 | <0.0001 | *** |
| | Date | 2 | 13.041 | <0.0001 | *** |
| | Species:Dates | 7 | 2.054 | 0.043 | * |
| $WUE_{i(bulk\text{-}leaf)}$ | Species | 4 | 5.182 | 0.0016 | ** |
| | Date | 2 | 3.413 | 0.0417 | * |
| | Species:Dates | 8 | 3.065 | 0.0077 | ** |
| $WUE_{i(total\text{-}sugars)}$ | Species | 4 | 73.35 | <0.0001 | *** |
| | Date | 2 | 17.73 | <0.0001 | *** |
| | Species:Dates | 8 | 4.66 | 0.0004 | *** |
| $WUE_i$ | Species | 5 | 10.542 | <0.0001 | *** |
| | Method | 2 | 68.529 | <0.0001 | *** |
| | Date | 2 | 12.864 | <0.0001 | *** |
| | Species:Method | 8 | 2.35 | <0.05 | * |
| | Species:Method:Date | 27 | 1.085 | 0.3551 | |
| **PNUE** | Species | 5 | 66.997 | <0.0001 | *** |
| | Date | 5 | 1.112 | 0.3397 | |
| | Species:Date | 7 | 3.733 | 0.0034 | ** |
| **CUE** | Species | 5 | 3.997 | 0.0148 | * |
| **LUE** | Species | 5 | 1.716 | 0.185 | |
| **LCP** | Species | 5 | 4.818 | 0.0063 | ** |

| | | | | | |
|---|---|---|---|---|---|
| **LSP** | Species | 5 | 1.357 | 0.289 | |
| $\phi$ | Species | 5 | 1.716 | 0.185 | |
| $R_d$ | Species | 5 | 4.472 | 0.0087 | ** |
| $A_{max}$ | Species | 5 | 6.171 | 0.002 | ** |
| $A_{n2000}$ | Species | 5 | 9.225 | 0.0002 | *** |

Table S.3.2 Plant parameters derived from bulk-leaf isotopic compositions ($\delta^{13}C_{bulk\text{-}leaf}$); carbon isotope discrimination ($\Delta^{13}C$) and the ratio of the intercellular and ambient $CO_2$ concentration ($C_i/C_a$, respectively). (*) *A. aptaneura* corresponds to the *Corymbia* savanna site. Error represent 1SE (n= 4). Within columns, lower case letters indicate that means were significantly different ($p$-value<0.05) as tested with linear mixed models with observations as random factor and, the Tukey's HSD *post-hoc* tests for significant differences across species within the same date. Capital letters indicate that means were significantly different ($p$-value<0.05) within the same species across sampling dates.

| | $\delta^{13}C_{bulk\text{-}leaf}$ (‰) | | $C_i/C_a$ | | $\Delta^{13}C_{bulk\text{-}leaf}$ | |
|---|---|---|---|---|---|---|
| **March, 2015** | **(late wet season)** | | | | | |
| *A. aptaneura* | -27.0 | ±0.13abA | 0.67 | ±0.006abA | 19.5 | ±0.14abA |
| *A. aneura* | -27.4 | ±0.20abA | 0.69 | ±0.009abA | 19.9 | ±0.21abA |
| *C. opaca* | -26.5 | ±0.47bA | 0.65 | ±0.022aA | 19.0 | ±0.49aA |
| *H. macrocarpa* | -27.7 | ±0.18aA | 0.70 | ±0.009bA | 20.2 | ±0.19bA |
| *A. aptaneura** | -27.6 | ±0.25aA | 0.70 | ±0.012bA | 20.1 | ±0.26bA |
| **October, 2015** | **(dry season)** | | | | | |
| *A. aptaneura* | -26.5 | ±0.20aA | 0.65 | ±0.009aA | 19.0 | ±0.20aA |
| *A. aneura* | -26.6 | ±0.11aA | 0.65 | ±0.005aA | 19.1 | ±0.12aA |
| *C. opaca* | -26.2 | ±0.14aB | 0.63 | ±0.006aA | 18.7 | ±0.14aA |
| *H. macrocarpa* | -28.1 | ±0.30bA | 0.72 | ±0.014bA | 20.7 | ±0.32bA |
| *A. aptaneura** | -26.7 | ±0.58aA | 0.66 | ±0.027aA | 19.2 | ±0.61aA |
| **February, 2016** | **(wet season)** | | | | | |
| *A. aptaneura* | -26.5 | ±0.09bA | 0.64 | ±0.004aA | 19.0 | ±0.09aA |
| *A. aneura* | -27.5 | ±0.59abA | 0.69 | ±0.027abA | 20.0 | ±0.62abA |
| *C. opaca* | -28.4 | ±0.20aA | 0.73 | ±0.009bB | 21.0 | ±0.21bB |
| *H. macrocarpa* | -28.1 | ±0.15abA | 0.72 | ±0.007abA | 20.7 | ±0.16abA |
| *A. aptaneura** | -26.7 | ±0.86bA | 0.65 | ±0.04aA | 19.2 | ±0.91aA |

Table S.3.3 Plant parameters derived from leaf soluble sugars ($\delta^{13}C_{sugars}$); carbon isotope discrimination ($\Delta^{13}C$) and the ratio of the intercellular and ambient $CO_2$ concentration ($C_i$/ $C_a$, respectively). (*) *A. aptaneura* corresponds to the *Corymbia* savanna site. Error represent 1SE (n= 4). Within columns, lower case letters indicate that means were significantly different ($p$-value<0.05) as tested with linear mixed models with observations as random factor and, the Tukey's HSD *post-hoc* tests for significant differences across species within the same date. Capital letters indicate that means were significantly different ($p$-value<0.05) within the same species across sampling dates.

| | $\delta^{13}C_{sugars}$ (‰) | | $C_i/C_a$ | | $\Delta^{13}C_{sugars}$ | |
|---|---|---|---|---|---|---|
| **March, 2015** | **(late wet season)** | | | | | |
| *A. aptaneura* | -28.1 | ±0.29abA | 0.72 | ±0.014bcA | 20.7 | ±0.31bcA |
| *A. aneura* | -29.1 | ±0.10aA | 0.77 | ±0.005cA | 21.8 | ±0.11cA |
| *C. opaca* | -24.3 | ±0.58cA | 0.54 | ±0.027aA | 16.7 | ±0.61aA |
| *H. macrocarpa* | -26.7 | ±0.28bA | 0.65 | ±0.013bA | 19.2 | ±0.29bA |
| *A. aptaneura** | -28.3 | ±0.37aA | 0.73 | ±0.017cA | 20.8 | ±0.39cA |
| **October, 2015** | **(dry season)** | | | | | |
| *A. aptaneura* | -27.0 | ±0.17abA | 0.67 | ±0.008bcA | 19.5 | ±0.18bcA |
| *A. aneura* | -28.0 | ±0.13aA | 0.72 | ±0.006cA | 20.6 | ±0.14cA |
| *C. opaca* | -22.5 | ±0.52cB | 0.46 | ±0.024aB | 14.8 | ±0.54aB |
| *H. macrocarpa* | -26.3 | ±0.42bA | 0.63 | ±0.019bA | 18.7 | ±0.44bA |
| *A. aptaneura** | -26.7 | ±0.32abB | 0.66 | ±0.015bcB | 19.2 | ±0.33bcA |
| **February, 2016** | **(wet season)** | | | | | |
| *A. aptaneura* | -27.7 | ±0.26abA | 0.70 | ±0.012bcA | 20.3 | ±0.28bcA |
| *A. aneura* | -27.8 | ±0.10aA | 0.71 | ±0.005cA | 20.3 | ±0.11cA |
| *C. opaca* | -25.7 | ±0.17cA | 0.61 | ±0.008aA | 18.1 | ±0.17aA |
| *H. macrocarpa* | -26.8 | ±0.43bA | 0.66 | ±0.02bA | 19.4 | ±0.45bA |
| *A. aptaneura** | -27.5 | ±0.13abA | 0.69 | ±0.006bcA | 20.0 | ±0.14bcA |

Table S.4.1 ANOVA table showing a) the interactive effects species and dates for data presented in Table 4.2 with pair-wise student's t-test for *post hoc* comparisons of species with Bonferroni correction; and b) the interactive effect methods × date for data presented in figure 4.7, with Tukey's HSD *post-hoc* tests for significant differences between methods × dates. Significant effects are indicated by *p*-values (.) >0.05, (*) <0.05, (**) <0.01, (***) <0.001.

| Variable | Effect | Df | F-value | *p*-value | |
|---|---|---|---|---|---|
| ***a) Variables presented in Table 4.2*** | | | | | |
| $g_{1\text{-leaf gas}}$ | Species | 1 | 3.83 | 0.0553 | . |
| | Dates | 2 | 20.464 | 0.0001 | *** |
| | Species:Dates | 2 | 1.786 | 0.1768 | |
| $g_{1\text{-bulk-leaf}}$ | Species | 1 | 0.004 | 0.9547 | |
| | Dates | 2 | 0.63 | 0.5437 | |
| | Species:Dates | 2 | 5.34 | 0.0151 | * |
| $g_{1\text{-sugars}}$ | Species | 1 | 2.409 | 0.1451 | |
| | Dates | 2 | 17.503 | 0.0001 | *** |
| | Species:Dates | 2 | 3.006 | 0.0534 | * |
| ***b) Variables presented in fig 4.7*** | | | | | |
| $g_1$ | Methods | 3 | 129.53 | <0.0001 | *** |
| | Dates | 2 | 60.39 | <0.0001 | *** |
| | Methods:Dates | 6 | 44.65 | <0.0001 | *** |

Table S.5.1 ANOVA table showing the interactive effect in species × methods for data presented in Figure 5.3 with Tukey's HSD *post-hoc* tests for significant differences in the interaction species × methods.

| Variable | Effect | Df | F-value | *p*-value | |
|---|---|---|---|---|---|
| **height** | Species | 3 | 27.074 | <0.0001 | *** |
| | Treatments | 1 | 5.639 | 0.019 | * |
| | Species:Treatments | 3 | 1.951 | 0.124 | |
| **leaves** | Species | 3 | 27.402 | <0.0001 | *** |
| | Treatments | 1 | 0.007 | 0.935 | |
| | Species:Treatments | 3 | 0.489 | 0.691 | |
| **diameter** | Species | 3 | 26.766 | <0.0001 | *** |
| | Treatments | 1 | 1.007 | 0.317 | |
| | Species:Treatments | 3 | 2.064 | 0.108 | |

## Supplementary figures

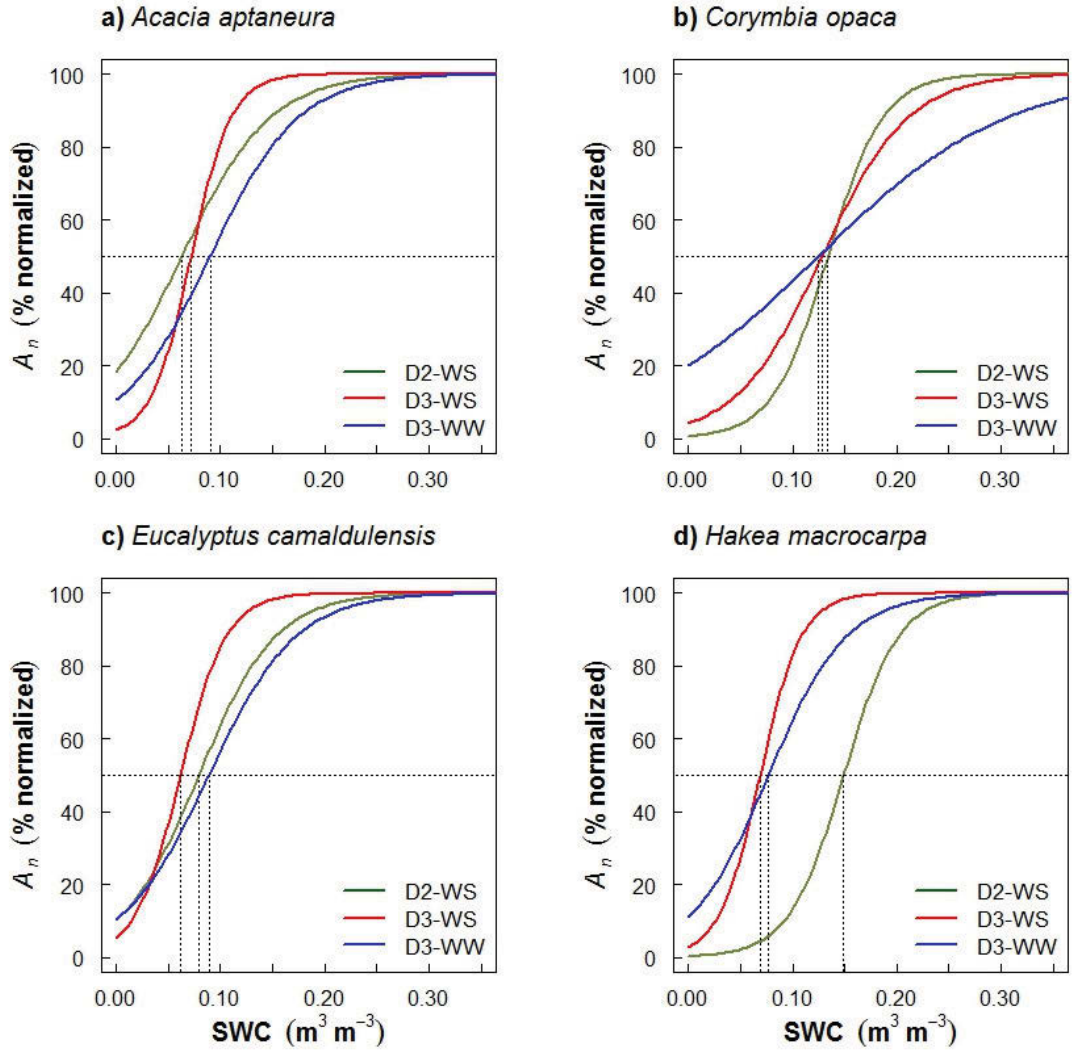


Figure S.5.1 Normalized net assimilation ($A_n$) relative to maximum values of $A_n$ at high soil water content based on values from figure 5.4. Vertical dotted lines indicate the SWC value associated with the 50 % in $A_n$.

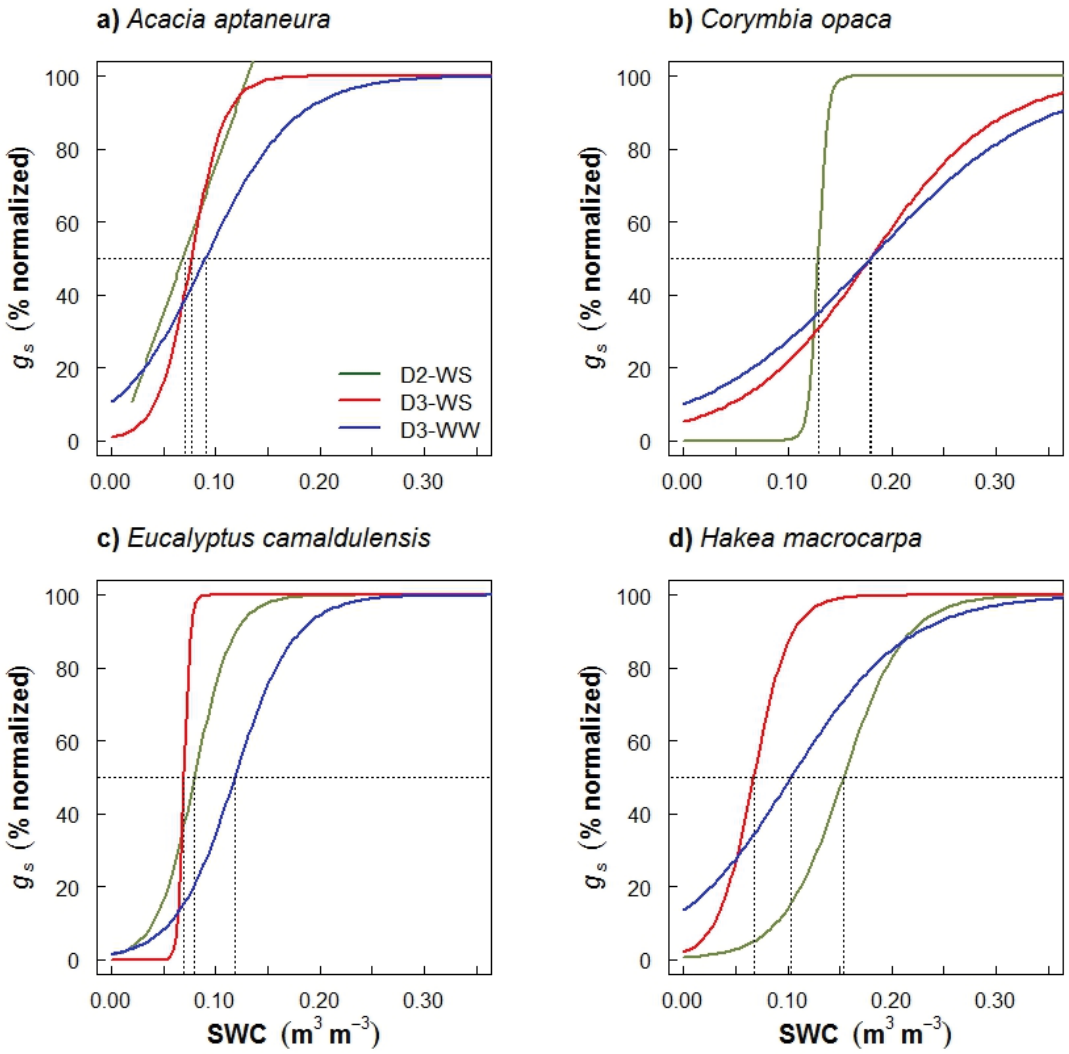


Figure S.5.2 Normalized stomatal conductance ($g_s$) relative to maximum values of $g_s$ at high soil water content based on values from figure 5.4. Vertical dotted lines indicate the SWC value associated with the 50 % in $g_s$.